Positron Hydrogen Molecule Scattering

James Neil Cooper, MSci.

Thesis submitted to The University of Nottingham
for the degree of Doctor of Philosophy

November 2009

Abstract

In this thesis, we present Kohn variational calculations of scattering and annihilation parameters for very low energy interactions of positrons, e^+, with molecular hydrogen, H_2. Our analysis includes the first application of the Kohn method for this system in which the interelectronic potential in the molecular target is treated explicitly. All previous Kohn calculations on $(e^+ - H_2)$ scattering have avoided this complication by the use of the method of models. The advantage of the explicit treatment over the method of models is that it allows approximate target wavefunctions of a very high accuracy to be admitted more easily to the Kohn calculations. We find that the accuracy of the approximate target wavefunction is an extremely important factor in obtaining reliable results from the calculations.

We carry out an extensive investigation of anomalous, nonphysical behaviour in the results of our Kohn calculations. Our explanations of how these anomalies arise and how they may be avoided significantly improves upon the discussions of these phenomena given in earlier accounts of $(e^+ - H_2)$ scattering calculations by other authors.

As with all previous models of $(e^+ - H_2)$ scattering, we find discrepancies between the experimental value of the annihilation parameter, Z_{eff}, and the theoretical value of this quantity as determined from our Kohn calculations. Limitations of the model that could explain these discrepancies are discussed and suggestions for future improvements are proposed.

Publications

J. N. Cooper, E. A. G. Armour and M. Plummer, J. Phys. A: Math. Gen. **42**, 095207 (2009).

J. N. Cooper, E. A. G. Armour and M. Plummer, J. Phys. B: At. Mol. Opt. Phys. **41**, 245201 (2008).

J. N. Cooper and E. A. G. Armour, Nucl. Instr. and Meth. B **266**, 452 (2008).

Acknowledgements

Sincere thanks must go first to my supervisor, Prof. Edward Armour, whose patience, experience and expertise are seemingly inexhaustible. Edward, thank you. I am also indebted to Dr. Jorma Louko, both in his capacity as my *de jure* supervisor since Edward's retirement and for not asking too many difficult questions in my first two annual reviews.

I would like to express my gratitude to Dr. Martin Plummer and Dr. Allan Todd for their invaluable contributions to the computational framework used in the calculations, as well as to Prof. John Humberston and Dr. Mark Gregory for a great many illuminating discussions.

I have been fortunate enough to share office space with a number of gifted pure mathematicians. In no particular order: Dr. Adam Philpotts, Dr. Giedrius Alkauskas, Matthew Morrow, Oliver Braeunling and Alberto Camara are all deserving of greater tributes than can be delivered here. Financial support from EPSRC is gratefully acknowledged, as is assistance from the technical and administrative support staff in the School of Mathematical Sciences: Dave Parkin, Andrea Blackbourn, Krys Glowczewska, Helen Cunliffe and Hilary Lonsdale.

Finally, I would like to thank my family and friends for their unwavering support. Mum, Dad, Nanna, Fen, Garan, Ross, Sarah, Rich, Pete, Jilli and Carmen: you told me I'd get there in the end.

Contents

Chapter 1

Introduction

1.1 The positron

The prediction [1–3] and subsequent discovery [4] of the positron, e^+, the antiparticle of the electron, e^-, represents one of the great triumphs in the development of twentieth century physics. Dirac interpreted the negative energy solutions of his relativistic wave equation [1] for spin-$\frac{1}{2}$ particles, such as electrons, as being physically significant. He supposed that the negative energy states were generally unobservable since they were uniformly and universally occupied with negative energy electrons. The occasional appearance of an unoccupied state, or 'hole', in this so-called 'sea' of electrons would itself be regarded as the appearance of a positively charged particle with positive energy. Subsequent transition of an electron of positive energy into the unoccupied state would lead to the ostensible disappearance of both electron and 'hole', with the energy lost in the de-excitation being emitted as photons.

In the intervening years since Dirac's prediction, understanding of this problem has developed considerably. The interpretation of electron de-excitation into unoccupied negative energy states is now conventionally replaced with the notion of annihilation of colliding electrons and positrons or, more generally, the annihilation of any particle with its corresponding antiparticle. In the case of electrons and positrons, the mass of the constituent particles lost in this annihilation process is converted into energy in the form of photons.

Historically, experimental studies of positron physics have been limited by difficulties in obtaining positrons in sufficiently large numbers for practical application. Advances in this field, however, have now made the use of high intensity positron beams routine. A review of experimental investigations of positron-atom and positron-molecule interactions up until 2005 is given by Surko, Gribakin and Buckman [5].

The scope of antimatter physics and chemistry has grown to encompass bound states of particles with antiparticles, such as positronium [6], a bound state of a positron and an electron, and protonium [7], a bound state of a proton and an antiproton. Bound states composed entirely of antiparticles have also been observed with the recent production [8, 9] of antihydrogen at CERN. Nevertheless, there remain many unanswered questions of fundamental importance concerning our understanding of matter-antimatter processes. It is the intention of this thesis to examine some of these questions.

In the case of positron interactions with simple atoms and molecules, the cross section for positron annihilation with one of the bound electrons is typically very small when compared with other channels. At very low positron energies, for example, elastic scattering is generally a much more dominant process than

annihilation. A great deal of effort has been made to develop accurate theoretical models for such processes. Detailed reviews of the theory of low energy positron collisions with simple atoms and molecules have been given by Armour [10] and by Armour and Humberston [11]. Here, we will concentrate on the particular case of the theory of elastic scattering of positrons by molecular hydrogen, H_2.

Nonrelativistic quantum mechanical descriptions of positron-molecule systems are given by wavefunctions that satisfy the Schrödinger equation. Even for the simplest molecules, this equation cannot be solved analytically and a variety of numerical techniques must be employed to determine approximate solutions. Variational methods have been used with enormous success in calculating approximate wavefunctions for molecular bound states (see, for example, [12]). The power of such methods lies in the existence of a rigorous energy minimisation principle common to all bound states. Although this principle does not apply to scattering states, we will see that variational methods still offer a well established framework in which to perform accurate scattering calculations for simple physical systems.

In our calculations, we will use a generalisation of the Kohn variational method [13] to obtain approximations to wavefunctions and phase shifts for low energy, elastic $(e^+ - H_2)$ scattering. The Kohn method has been applied extensively to scattering of leptons by both atomic hydrogen [14–18] and atomic helium [19, 20]. The application of variational methods to scattering calculations on molecular systems has received less attention than the atomic case, being considerably more difficult to implement due to the increased complexity of the molecular target. The first account of electron scattering by molecular hydrogen using the Kohn variational method, as well as the method due to Hulthèn

[21], was given by Massey and Ridley [22] in 1956. Their treatment was used as the starting point of Armour's work [23] on $(e^+ - H_2)$ scattering. His Kohn calculations were carried out using Drachman's method of models [24]. This method contains a useful simplification as it avoids the need for an explicit consideration of the interelectronic potential in the Hamiltonian describing the scattering state.

In addition to the calculation of scattering parameters, approximate scattering wavefunctions can also be used to estimate values of the electron-positron annihilation parameter, Z_{eff} [6]. This dimensionless quantity is a measure of the extent to which a positron distorts an atomic or molecular electron cloud at close range; it can be regarded as the effective number of electrons, due to this distortion, that are available for annihilation. The value of Z_{eff} is usually significantly larger than the actual number, Z, of electrons in the scattering target, since the correlation of the positron with the target electrons tends to increase the electronic charge density in the region of the positron when it is close to the target. In the case of molecular hydrogen, the accepted experimental value of Z_{eff} for thermal positrons at 297 K is 14.61 ± 0.14 [25].

Early Kohn calculations of scattering and annihilation parameters for H_2 by Armour and coworkers [23, 26, 27] failed to account for the corresponding experimental values. Later treatments [28, 29] used a greatly improved description of the electron-positron correlation and were much more successful. The most sophisticated of those calculations [29] accounted for experimental values of the elastic scattering cross section for incident positron energies up to $\sim$ 5 eV. However, despite significant improvements in the theoretical values of Z_{eff}, discrepancies with experiment still remained. The highest value of Z_{eff} reported in those later treatments, relevant to the calculations presented here,

was $Z_{\text{eff}} = 10.7$ [29]. All Kohn calculations on the $(e^+ - H_2)$ system up to this point made use of the method of models.

Theoretical investigations of positron scattering and annihilation in molecular hydrogen have been carried out using alternatives to the Kohn variational method. The R-matrix method was introduced by Wigner [30] in the theory of nuclear reactions. The first application of this method to electron scattering by diatomic molecules was made by Burke, Mackey and Shimamura [31] and calculations of phase shifts and cross sections for elastic $(e^+ - H_2)$ scattering were carried out by Tennyson [32] and by Danby and Tennyson [33]. The distributed positron model [34] has also been used [35] to calculate low energy $(e^+ - H_2)$ scattering parameters. Good agreement has been obtained between experimental cross sections and those predicted by this method, though it does rely on an explicit model potential. Scattering parameters and values of Z_{eff} for $(e^+ - H_2)$ have been calculated by the Lima group [36, 37] using the Schwinger multichannel method [38]. Despite their theoretical values of total cross sections comparing well with experimental results, their calculations of Z_{eff} were in poor agreement with experiment, the highest reported value being $Z_{\text{eff}} = 7.5$. Higher values of Z_{eff} for H_2 have been obtained by Franz and Gianturco [39] who calculated $Z_{\text{eff}} = 11.6$ at very low positron energies, although this was with the assistance of a semi-empirical 'enhancement factor', evaluated by treating the target molecule as a homogeneous electron gas.

We conclude that existing theoretical models do not correctly describe the interaction between the positron and the hydrogen molecule at low positron energies. In an attempt to address this problem, we will carry out the first accurate Kohn calculations for the $(e^+ - H_2)$ system that do not rely on the method of models. As we shall see, although this introduces a significant complication

into the implementation of the variational method, it allows for a much more accurate description of the hydrogen molecule to be used in the calculations. We will investigate whether or not this improvement in accuracy brings about closer agreement between theoretical and experimental results, particularly in the case of calculations of Z_{eff}.

In chapters 2-5, we will carry out Kohn calculations of elastic scattering phase shifts on the $(e^+ - H_2)$ system, both with and without the assistance of the method of models. We will pay particular attention to avoid well documented problems [40–46] associated with so-called Schwartz singularities [14, 47]. The results of Kohn calculations carried out in the region of these singularities are known to be susceptible to nonphysical anomalies. We will explore in considerable detail methods of handling these anomalies. From chapter 6 onwards, we will present low energy calculations of Z_{eff} for H_2, again both with and without recourse to the method of models. The purpose of the remainder of this chapter is to introduce the general physical and mathematical concepts relevant to our calculations.

1.2 Concepts of elastic scattering

In this section, we will discuss the fundamental principles involved in the theory of elastic scattering, in the context of the $(e^+ - H_2)$ system and following the account given by Armour [10]. In what follows, we will idealise the $(e^+ - H_2)$ system by making the assumption that it is conservative and exists in a stationary state of constant, well-defined energy. As a result, the Hamiltonians that we will consider do not depend explicitly upon time and the mechanics of the scattering problem are described by solutions of the time-independent

Schrödinger equation.

We begin by considering the nuclei in the hydrogen molecule and denote by M_p the mass of the proton. We denote by m_e the mass of the electron and take it to be equal to the mass of the positron. All of our calculations on the $(e^+ - H_2)$ system will involve only internal forces. Under these circumstances, the usual approach is to consider the motion of the centre of mass of the system, which moves with uniform velocity. Here, since $M_p/m_e \simeq 1836$, to a very good approximation the nuclear centre of mass moves with uniform velocity and can be regarded as the origin of the inertial laboratory frame system of coordinates.

All of our calculations on the $(e^+ - H_2)$ system will be carried out in the adiabatic nuclei approximation [48–51], in which the motion of the nuclei is uncoupled from the motion of the leptons. This is an extension of the Born-Oppenheimer approximation [52] used for accurate calculations on molecular bound states which neglect couplings between the electronic and nuclear motion that are usually small. We shall have more to say about these approximations in chapter 9.

We label the nuclei in the molecule A and B. Let $\mathbf{R}$ be the vector from A to B, $\mathbf{r}_1$ and $\mathbf{r}_2$ the position vectors of the two electrons and $\mathbf{r}_3$ the position vector of the positron, with respect to a coordinate system with origin at the nuclear centre of mass and z-axis along the direction of $\mathbf{R}$. This coordinate system will be called the molecule-fixed coordinate system. The labelling of the coordinates of the electrons and positrons in this way introduces a system that will be used throughout this thesis; the electrons will be referred to as particles 1 and 2, with the positron being referred to as particle 3.

We will carry out all of our calculations in the Hartree system of atomic units,

in which $\hbar = m_e = e = 1$, with e being the charge on the positron. In the molecule-fixed coordinate system, the internal motion of the $(e^+ - H_2)$ system is represented in atomic units approximately by the nonrelativistic Hamiltonian

$$\hat{\mathbb{H}} = \hat{\mathbb{H}}_T + V_p - \frac{1}{2}\nabla_3^2. \tag{1.2.1}$$

Here, $-\frac{1}{2}\nabla_3^2$ is the kinetic energy operator for the positron and V_p comprises all terms in the scattering potential which involve the positron. It takes the form

$$V_p = -\frac{1}{r_{13}} - \frac{1}{r_{23}} + \frac{1}{r_{A3}} + \frac{1}{r_{B3}}, \tag{1.2.2}$$

where r_{13} and r_{23} are the distances between the positron and the two electrons, with r_{A3} and r_{B3} being the distances of the positron respectively from the nuclei A and B.

The first term on the right hand side of (1.2.1) is the Hamiltonian for the target H_2 molecule. It takes the form

$$\hat{\mathbb{H}}_T = V_T - \frac{1}{2\mu_N}\nabla_{\mathbf{R}}^2 - \frac{1}{2}\nabla_1^2 - \frac{1}{2}\nabla_2^2, \tag{1.2.3}$$

where μ_N is the reduced nuclear mass and $-\frac{1}{2\mu_N}\nabla_{\mathbf{R}}^2$ is the kinetic energy operator representing nuclear motion. The kinetic energy operators of the two electrons are given by $-\frac{1}{2}\nabla_1^2$ and $-\frac{1}{2}\nabla_2^2$. The target potential is given by V_T and takes the form

$$V_T = \frac{1}{r_{12}} + \frac{1}{R} - \frac{1}{r_{A1}} - \frac{1}{r_{B1}} - \frac{1}{r_{A2}} - \frac{1}{r_{B2}}, \tag{1.2.4}$$

in which r_{Ai} and r_{Bi} are the distances of the i^{th} electron respectively from A and B and r_{12} is the interelectronic distance. The internuclear separation is given by R.

Armour [10] notes that, although the rotation of the nuclei about their centre of mass makes the molecule-fixed coordinate system non-inertial, these effects can be neglected owing to the large difference between the nuclear and leptonic masses.

Since (1.2.1) does not contain any terms involving spin, we will generally avoid explicit reference to spin in our approximations to both the scattering and target eigenfunctions, except when required by the Pauli exclusion principle.

In the Born-Oppenheimer approximation [52], eigenfunctions of $\hat{\mathbb{H}}_{\text{T}}$ are given approximately by

$$\phi_{\nu\bar{\nu}}\left(\mathbf{r}_1, \mathbf{r}_2, \mathbf{R}\right) \sim \Pi_{\nu\bar{\nu}}\left(\mathbf{R}\right) \psi_{\nu}\left(\mathbf{r}_1, \mathbf{r}_2; \mathbf{R}\right). \tag{1.2.5}$$

The function, $\psi_{\nu}\left(\mathbf{r}_1, \mathbf{r}_2; \mathbf{R}\right)$, is an electronic wavefunction, in which ν represents all quantities required to specify uniquely a given electronic state. This subscript is independent of the subscript, $\bar{\nu}$, used in the specification of the nuclear wavefunction, $\Pi_{\nu\bar{\nu}}\left(\mathbf{R}\right)$.

The electronic wavefunctions are eigenfunctions of the electronic Hamiltonian

$$\hat{H}_{\text{T}} = V_{\text{T}} - \frac{1}{2}\nabla_1^2 - \frac{1}{2}\nabla_2^2 = \hat{\mathbb{H}}_{\text{T}} + \frac{1}{2\mu_{\text{N}}}\nabla_{\mathbf{R}}^2, \tag{1.2.6}$$

so that

$$\hat{H}_{\mathrm{T}}\psi_{\nu}\left(\mathbf{r}_1,\mathbf{r}_2;\mathbf{R}\right)=\epsilon_{\nu}\left(R\right)\psi_{\nu}\left(\mathbf{r}_1,\mathbf{r}_2;\mathbf{R}\right). \tag{1.2.7}$$

Here, $\psi_{\nu}\left(\mathbf{r}_1,\mathbf{r}_2;\mathbf{R}\right)$ depends parametrically on $\mathbf{R}$ and the eigenvalue, $\epsilon_{\nu}\left(R\right)$, depends parametrically on R.

The nuclear wavefunctions, $\Pi_{\nu\bar{\nu}}\left(\mathbf{R}\right)$, are eigenfunctions of

$$\hat{H}_{\mathrm{N}}=-\frac{1}{2\mu_{\mathrm{N}}}\nabla^2_{\mathbf{R}}+\epsilon_{\nu}\left(R\right), \tag{1.2.8}$$

in which $\epsilon_{\nu}\left(R\right)$ plays the role of a potential.

Eigenfunctions of $\hat{\mathbb{H}}$ satisfy the time-independent Schrödinger equation

$$\hat{\mathbb{H}}\Phi_{\nu_i\bar{\nu}_i}\left(\mathbf{r}_1,\mathbf{r}_2,\mathbf{r}_3,\mathbf{R}\right)=\mathbb{E}\Phi_{\nu_i\bar{\nu}_i}\left(\mathbf{r}_1,\mathbf{r}_2,\mathbf{r}_3,\mathbf{R}\right) \tag{1.2.9}$$

and, in the adiabatic nuclei approximation [48–51], are given approximately by

$$\Phi_{\nu_i\bar{\nu}_i}\left(\mathbf{r}_1,\mathbf{r}_2,\mathbf{r}_3,\mathbf{R}\right)\sim\Pi_{\nu_i\bar{\nu}_i}\left(\mathbf{R}\right)\Psi_{\nu_i}\left(\mathbf{r}_1,\mathbf{r}_2,\mathbf{r}_3;\mathbf{R}\right), \tag{1.2.10}$$

in which ν_i characterises $\Psi_{\nu_i}\left(\mathbf{r}_1,\mathbf{r}_2,\mathbf{r}_3;\mathbf{R}\right)$, the leptonic wavefunction for the scattering problem, with $\bar{\nu}_i$ specifying the unperturbed initial nuclear wavefunction, $\Pi_{\nu_i\bar{\nu}_i}\left(\mathbf{R}\right)$, of the target. The function, $\Psi_{\nu_i}\left(\mathbf{r}_1,\mathbf{r}_2,\mathbf{r}_3;\mathbf{R}\right)$, is an eigenfunction of the leptonic Hamiltonian

$$\hat{H}=\hat{H}_{\mathrm{T}}+V_{\mathrm{p}}-\frac{1}{2}\nabla^2_3, \tag{1.2.11}$$

so that

$$\hat{H}\Psi_{\nu_i}\left(\mathbf{r}_1,\mathbf{r}_2,\mathbf{r}_3;\mathbf{R}\right)=\left(\epsilon_{\nu_i}+\frac{1}{2}k_i^2\right)\Psi_{\nu_i}\left(\mathbf{r}_1,\mathbf{r}_2,\mathbf{r}_3;\mathbf{R}\right), \tag{1.2.12}$$

where ϵ_{ν_i} is the eigenvalue of $\hat{H}_{\mathrm{T}}$ corresponding to the initial electronic wavefunction of the target and the wavenumber, k_i, is the magnitude of the vector, $\mathbf{k}_i$, the initial wave vector of the positron. In atomic units, $\mathbf{k}_i$ is equal to the initial momentum of the positron. For brevity, henceforth we will usually refer to the wavenumber of the positron simply as its momentum, rather than the magnitude of its momentum in atomic units. We note also that the energy of the positron in atomic units is proportional to k_i^2.

The leptonic function, $\Psi_{\nu_i}\left(\mathbf{r}_1,\mathbf{r}_2,\mathbf{r}_3;\mathbf{R}\right)$, depends only parametrically on $\mathbf{R}$. A standard approach is to examine the eigenvalue problem (1.2.12) separately at different fixed values of $\mathbf{R}$. This technique is known as the fixed-nuclei approximation [53–55].

Let the initial and final electronic wavefunctions of the target respectively be $\psi_{\nu_i}\left(\mathbf{r}_1,\mathbf{r}_2;\mathbf{R}\right)$ and $\psi_{\nu_j}\left(\mathbf{r}_1,\mathbf{r}_2;\mathbf{R}\right)$. Then, in the fixed-nuclei approximation, Armour [10] notes that $\Psi_{\nu_i}\left(\mathbf{r}_1,\mathbf{r}_2,\mathbf{r}_3;\mathbf{R}\right)$ has the asymptotic form

$$\begin{aligned}\Psi_{\nu_i}\left(\mathbf{r}_1,\mathbf{r}_2,\mathbf{r}_3;\mathbf{R}\right)\underset{r_3\to\infty}{\sim} \quad & B \quad \Bigg[\exp\left(\mathrm{i}\mathbf{k}_i.\mathbf{r}_3\right)\psi_{\nu_i}\left(\mathbf{r}_1,\mathbf{r}_2;\mathbf{R}\right) \\ & + \quad \sum_j \frac{\exp\left(\mathrm{i}\bar{k}_j r_3\right)}{r_3} f_{\nu_i\nu_j}\left(\mathbf{k}_i,\bar{\mathbf{k}}_j;\mathbf{R}\right)\psi_{\nu_j}\left(\mathbf{r}_1,\mathbf{r}_2;\mathbf{R}\right)\Bigg],\end{aligned} \tag{1.2.13}$$

where $r_3 = |\mathbf{r}_3|$, $\bar{\mathbf{k}}_j$ is the final wave vector of the scattered positron and the summation is over all energetically accessible states. B is a normalisation constant. The incident positron is represented asymptotically by the plane wave,

$\exp\left(\mathrm{i}\mathbf{k}_i.\mathbf{r}_3\right)$. The scattered positron is represented asymptotically by the outgoing spherical wave, $\exp\left(\mathrm{i}\bar{k}_j r_3\right)/r_3$, with $f_{\nu_i\nu_j}\left(\mathbf{k}_i, \bar{\mathbf{k}}_j; \mathbf{R}\right)$ being the scattering amplitude.

At the very low energies with which our calculations will be concerned, the only significant energetically accessible channel, other than positron annihilation, is elastic scattering. In principle, dissociation of the hydrogen molecule can occur at or above 4.48 eV, but this channel does not become significant until the region around the positronium formation threshold at 8.63 eV is reached. As discussed by Armour [10], this is due to the Franck-Condon principle.

Thus, at very low energies, we need consider only the final state in which $\bar{k}_j = k_i$ and where $\psi_{\nu_j}\left(\mathbf{r}_1, \mathbf{r}_2; \mathbf{R}\right) = \psi_{\nu_i}\left(\mathbf{r}_1, \mathbf{r}_2; \mathbf{R}\right)$. Moreover, as pointed out by Armour [10], in practice it is necessary to consider $\Psi_{\nu_i}\left(\mathbf{r}_1, \mathbf{r}_2, \mathbf{r}_3; \mathbf{R}\right)$, $\psi\left(\mathbf{r}_1, \mathbf{r}_2; \mathbf{R}\right)$ and $f_{\nu_i\nu_j}\left(\mathbf{k}_i, \bar{\mathbf{k}}_j; \mathbf{R}\right)$ as parametric functions only of R rather than $\mathbf{R}$ [53, 54]. Hence, in the case of elastic scattering we can write

$$\Psi\left(\mathbf{r}_1, \mathbf{r}_2, \mathbf{r}_3; R\right) \underset{r_3\to\infty}{\sim} B\left[\exp\left(\mathrm{i}\mathbf{k}.\mathbf{r}_3\right) + \frac{\exp\left(\mathrm{i}kr_3\right)}{r_3} f\left(\mathbf{k}, \bar{\mathbf{k}}; R\right)\right] \psi\left(\mathbf{r}_1, \mathbf{r}_2; R\right), \tag{1.2.14}$$

where we have dropped the subscripts, i, j, ν_i and ν_j.

All of the calculations discussed in the following chapters will be carried out in the fixed-nuclei approximation. Prior to chapter 9, these calculations will be carried out at a fixed internuclear separation, R, equal to the H_2 equilibrium internuclear separation in atomic units, $R_0 = 1.4$ (see, for example, [12]). Under these circumstances, in addressing the scattering problem we will endeavour to find accurate approximations to the leptonic scattering function, $\Psi\left(\mathbf{r}_1, \mathbf{r}_2, \mathbf{r}_3; R\right)$, at this fixed value of R, effectively ignoring the nuclear wavefunction, $\Pi\left(\mathbf{R}\right)$. In

chapter 9, we will carry out fixed-nuclei calculations at several different choices of R, for which it will then be necessary to calculate approximations to $\Pi(\mathbf{R})$ in order to account for nuclear motion.

In this section, we have discussed the basic ideas involved in $(e^+ - H_2)$ elastic scattering. We will reserve until chapter 6 a detailed discussion of the concepts involved in positron annihilation with the electrons in the molecular target.

1.3 Prolate spheroidal coordinates

When carrying out theoretical calculations on a physical system, it is often desirable to adopt coordinates which reflect, wherever possible, symmetry properties of that system. Spherical polar coordinates, for example, are very well suited to problems involving atomic systems. In the case of diatomic molecules, which have a symmetry about the fixed internuclear axis, it is helpful to use a coordinate system which exploits this symmetry.

The system of prolate spheroidal coordinates is a three-dimensional orthogonal coordinate system convenient for studies of diatomic molecules. It is obtained by rotating the two-dimensional system of elliptic coordinates about its focal axis. The prolate spheroidal coordinates, (λ, μ, ϕ), can be defined implicitly in terms of the molecule-fixed Cartesian coordinates, with origin at the midpoint of the foci and z-axis along the internuclear axis, viz.

$$x = \frac{1}{2}R\left[\left(\lambda^2-1\right)\left(1-\mu^2\right)\right]^{\frac{1}{2}}\cos\left(\phi\right), \tag{1.3.1}$$

$$y = \frac{1}{2}R\left[\left(\lambda^2-1\right)\left(1-\mu^2\right)\right]^{\frac{1}{2}}\sin\left(\phi\right), \tag{1.3.2}$$

$$z = \frac{1}{2}R\lambda\mu, \tag{1.3.3}$$

where $\lambda \in [1,\infty)$, $\mu \in [-1,1]$ and $\phi \in [0,2\pi)$, R is the distance between the foci and ϕ is the azimuthal angle of spherical polar coordinates. Alternatively, if r_{A} and r_{B} are the distances of a point, P, respectively from the foci labelled A and B, then the prolate spheroidal coordinates, λ and μ, of P are defined explicitly by

$$\lambda = \frac{1}{R}\left(r_{\mathrm{A}}+r_{\mathrm{B}}\right), \tag{1.3.4}$$

$$\mu = \frac{1}{R}\left(r_{\mathrm{A}}-r_{\mathrm{B}}\right). \tag{1.3.5}$$

Surfaces of constant λ are ellipsoids and surfaces of constant μ are hyperboloids of two sheets. Prolate spheroidal coordinates are particularly useful for studying the electronic wavefunction of the ground state of the hydrogen molecule. Being a Σ_{g}^{+} state, the ground state wavefunction is symmetric about the internuclear axis. Moreover, by choosing the interfocal length to coincide with the internuclear separation in the fixed-nuclei approximation, the two protons naturally coincide with the foci of the coordinate system.

We note the following standard properties regarding the coordinate system. The Jacobian determinant is given by

$$\frac{\partial\left(x,y,z\right)}{\partial\left(\lambda,\mu,\phi\right)} = \frac{1}{8}R^3\left(\lambda^2-\mu^2\right) \tag{1.3.6}$$

and the Laplacian takes the form

$$\nabla^2 = \frac{4}{R^2}\left(\frac{1}{\lambda^2-\mu^2}\right)\left(\frac{\partial}{\partial\lambda}\left[\left(\lambda^2-1\right)\frac{\partial}{\partial\lambda}\right]+\frac{\partial}{\partial\mu}\left[\left(1-\mu^2\right)\frac{\partial}{\partial\mu}\right]\right.$$
$$\left.+\frac{\lambda^2-\mu^2}{\left(\lambda^2-1\right)\left(1-\mu^2\right)}\frac{\partial^2}{\partial\phi^2}\right). \qquad (1.3.7)$$

We note further that

$$\lim_{r\to\infty}\left(r-\frac{1}{2}R\lambda\right)=0 \qquad (1.3.8)$$

and

$$\lim_{r\to\infty}\mu=\cos\left(\theta\right), \qquad (1.3.9)$$

r and θ being the usual spherical polar coordinates.

In the case of positron scattering by molecular hydrogen, we can rewrite (1.2.2) and (1.2.4) in prolate spheroidal coordinates as

$$\begin{aligned} V_{\mathrm{P}} &= -\frac{1}{r_{13}}-\frac{1}{r_{23}}+\frac{1}{r_{A3}}+\frac{1}{r_{B3}} \\ &= \frac{2}{R}\left[\frac{2\lambda_3}{\lambda_3^2-\mu_3^2}-\frac{1}{\rho_{13}}-\frac{1}{\rho_{23}}\right] \end{aligned} \qquad (1.3.10)$$

and

$$\begin{aligned} V_{\mathrm{T}} &= \frac{1}{r_{12}} + \frac{1}{R} - \frac{1}{r_{A1}} - \frac{1}{r_{B1}} - \frac{1}{r_{A2}} - \frac{1}{r_{B2}} \\ &= \frac{1}{R}\left[1 - \frac{4\lambda_1}{\lambda_1^2 - \mu_1^2} - \frac{4\lambda_2}{\lambda_2^2 - \mu_2^2} + \frac{2}{\rho_{12}}\right], \end{aligned} \tag{1.3.11}$$

where we have maintained the same numbering system for the coordinates of the three leptons as given in section 1.2 and, following James and Coolidge [12], we have defined

$$\rho_{ij} = \frac{2}{R} r_{ij}. \tag{1.3.12}$$

Henceforth, we will use prolate spheroidal coordinates in all of our calculations on the $(e^+ - \mathrm{H}_2)$ system.

1.4 The free particle equation in prolate spheroidal coordinates

We have noted that all of our calculations will be carried out in prolate spheroidal coordinates, since this is a particularly convenient system for describing the ground state of the hydrogen molecule. In the general context of potential scattering, though, there is usually no great advantage in using prolate spheroidal coordinates when solving the one particle Schrödinger equation for the scattering problem. This is because Eisenhart [56] has shown that, in the case of axially symmetric potentials, this equation is separable only for potentials of the form

$$V_s(\mathbf{r}) = \frac{f(\lambda) + g(\mu)}{\lambda^2 - \mu^2}, \tag{1.4.1}$$

for any functions, $f(\lambda)$ and $g(\mu)$.

In the context of the $(e^+ - H_2)$ scattering problem, the hydrogen molecule can be regarded as the source of a scattering potential. This potential decays more quickly than $1/r_3$ as $r_3 \to \infty$. Consequently, as noted for example by Bransden and Joachain [57], the part of the leptonic scattering wavefunction describing the positron must satisfy the time-independent, free particle Schrödinger equation when the positron is asymptotically far from the target molecule. Solutions to the free particle equation are separable in prolate spheroidal coordinates and it is important to investigate such solutions.

In atomic units, the free particle equation takes the form

$$\left[\nabla^2 + k^2\right] F(\mathbf{r}) = 0, \tag{1.4.2}$$

where k is the magnitude of the momentum of the particle.

We will summarise the relevant details of the solutions of the free particle equation in prolate spheroidal coordinates given by Flammer [58] and discussed later by Armour and Humberston [11]. Flammer [58] notes that, in prolate spheroidal coordinates where ∇^2 is given by (1.3.7), separable solutions of (1.4.2) exist and are of the form

$$F^{(1)}_{mn}(\lambda, \mu, \phi) = S_{mn}(c, \mu) R^{(1)}_{mn}(c, \lambda) \cos(m\phi), \tag{1.4.3}$$

$$F^{(2)}_{mn}(\lambda, \mu, \phi) = S_{mn}(c, \mu) R^{(2)}_{mn}(c, \lambda) \cos(m\phi), \tag{1.4.4}$$

for integers, $0 \leq m \leq n$, where we have defined

$$c = \frac{1}{2}kR. \tag{1.4.5}$$

The function, $S_{mn}(c, \mu)$, satisfies the differential equation

$$\frac{\mathrm{d}}{\mathrm{d}\mu}\left[\left(1-\mu^2\right)\frac{\mathrm{d}}{\mathrm{d}\mu}S_{mn}(c,\mu)\right] + \left[\sigma_{mn}(c) - c^2\mu^2 - \frac{m^2}{1-\mu^2}\right]S_{mn}(c,\mu) = 0. \tag{1.4.6}$$

The functions, $R^{(1)}_{mn}(c, \lambda)$ and $R^{(2)}_{mn}(c, \lambda)$, each satisfy the differential equation

$$\frac{\mathrm{d}}{\mathrm{d}\lambda}\left[\left(\lambda^2-1\right)\frac{\mathrm{d}}{\mathrm{d}\lambda}R_{mn}(c,\lambda)\right] - \left[\sigma_{mn}(c) - c^2\lambda^2 + \frac{m^2}{\lambda^2-1}\right]R_{mn}(c,\lambda) = 0 \tag{1.4.7}$$

and are respectively regular and irregular at $\lambda = 1$.

Solutions of (1.4.6) that are defined $\forall \mu \in [-1, 1]$ exist only for a discrete set of values of the separation constant, $\sigma_{mn}(c)$. As pointed out by Flammer [58], these solutions take the form

$$S_{mn}(c,\mu) = \overline{\sum_{r=0,1}^{\infty}} d_r^{mn}(c)\, P^m_{m+r}(\mu), \tag{1.4.8}$$

where, henceforth, the bar on the summation sign indicates that it is performed over only even values of r when $(n - m)$ is even and over only odd values of r when $(n - m)$ is odd. $P^m_{m+r}(\mu)$ is the associated Legendre function of the first kind [59]. The coefficients, $d_r^{mn}(c)$, are defined up to a normalisation factor. Here, we will use the normalisation chosen by Flammer [58], such that

$$S_{mn}(0,\mu) = P_n^m(\mu) \tag{1.4.9}$$

and, for sufficiently small $c = kR/2$,

$$S_{mn}(c,\mu) \simeq P_n^m(\mu). \tag{1.4.10}$$

As pointed out by Armour [10], the functions, $R_{mn}^{(1)}(c,\lambda)$ and $R_{mn}^{(2)}(c,\lambda)$, can be normalised so that they have the asymptotic forms

$$R_{mn}^{(1)}(c,\lambda) \underset{\lambda\to\infty}{\sim} \frac{\sin\left(c\lambda - \frac{1}{2}n\pi\right)}{c\lambda} \underset{\lambda\to\infty}{\sim} \frac{\sin\left(kr - \frac{1}{2}n\pi\right)}{kr} \tag{1.4.11}$$

and

$$R_{mn}^{(2)}(c,\lambda) \underset{\lambda\to\infty}{\sim} -\frac{\cos\left(c\lambda - \frac{1}{2}n\pi\right)}{c\lambda} \underset{\lambda\to\infty}{\sim} -\frac{\cos\left(kr - \frac{1}{2}n\pi\right)}{kr}, \tag{1.4.12}$$

where we have used (1.3.8) and (1.4.5). Thus, $R_{mn}^{(1)}(c,\lambda)$ and $R_{mn}^{(2)}(c,\lambda)$ respectively have the same asymptotic forms as the spherical Bessel and Neumann functions [59], $j_n(kr)$ and $n_n(kr)$.

Now, consider the case $m = n = 0$. Using (1.4.3), (1.4.4), (1.4.10), (1.4.11) and (1.4.12), for small values of $c = kR/2$ we can write

$$F_{00}^{(1)}(\lambda,\mu,\phi) \underset{\lambda\to\infty}{\sim} \frac{\sin(c\lambda)}{c\lambda} \underset{\lambda\to\infty}{\sim} \frac{\sin(kr)}{kr} \tag{1.4.13}$$

and

$$F_{00}^{(2)}(\lambda,\mu,\phi) \underset{\lambda\to\infty}{\sim} -\frac{\cos(c\lambda)}{c\lambda} \underset{\lambda\to\infty}{\sim} -\frac{\cos(kr)}{kr}. \tag{1.4.14}$$

We will return to this result later.

1.5 Partial wave analysis

As noted by Armour and Humberston [11], the plane wave, $\exp(\mathrm{i}\mathbf{k}.\mathbf{r})$, can be expanded in prolate spheroidal coordinates as a series of partial waves, according to

$$\exp(\mathrm{i}\mathbf{k}.\mathbf{r}) = 2\sum_{n=0}^{\infty}\sum_{m=0}^{n} \mathrm{i}^n \frac{(2-\delta_{0m})}{N_{mn}(c)} S_{mn}(c,\cos(\theta_0))\, S_{mn}(c,\mu) \times R_{mn}^{(1)}(c,\lambda)\cos[m(\phi-\phi_0)], \tag{1.5.1}$$

where the functions, $S_{mn}(c,\mu)$ and $R_{mn}^{(1)}(c,\lambda)$, are as in section 1.4. The spherical polar angles of $\mathbf{k}$ are θ_0 and ϕ_0. The functions, $N_{mn}(c)$, are defined to be

$$N_{mn}(c) = \sqrt{2\sum_{r=0,1}^{\infty} \frac{(r+2m)!\,(d_r^{mn}(c))^2}{(2r+2m+1)\,r!}}, \tag{1.5.2}$$

where the $d_r^{mn}(c)$ are as in section 1.4 and the bar on the summation sign carries the same meaning as in (1.4.8).

Consider the case $m = n = 0$. Flammer [58] has tabulated values of $d_r^{00}(c)$. For sufficiently small values of c, $d_0^{00}(c) \simeq 1$ and $d_r^{00}(c) \simeq 0$ for $r \in \{2,4,6,\dots\}$. To a good approximation, using (1.5.2) we can thus take $N_{00}(c) \simeq 2$ for small values of c. Armour and Humberston [11] point out that, at low energies, only

partial waves corresponding to low n values will contribute to the scattering process. As explained, for example, by Bransden and Joachain [57], this is due to the presence of the so-called centrifugal barrier which, at a given incident energy, prevents partial waves above a particular value of n from interacting with the scattering potential. The magnitude of the centrifugal barrier increases with n and, for very small values of c, only the first term in the expansion (1.5.1) is significant. Hence, to a good approximation, we need consider only the lowest partial wave having $m = n = 0$ in the expansion (1.5.1). This partial wave is of Σ_g^+ symmetry. Under these circumstances, using (1.4.10) and (1.5.1), at small values of c we have

$$\exp\left(\mathrm{i}\mathbf{k}.\mathbf{r}\right) \simeq R_{00}^{(1)}\left(c,\lambda\right). \tag{1.5.3}$$

Now, from (1.4.11), the asymptotic form of $R_{00}^{(1)}\left(c,\lambda\right)$ is

$$R_{00}^{(1)}\left(c,\lambda\right) \underset{\lambda\to\infty}{\sim} \frac{\sin\left(c\lambda\right)}{c\lambda} \underset{r\to\infty}{\sim} \frac{\sin\left(kr\right)}{kr}, \tag{1.5.4}$$

so that, at small values of c, we can write

$$\exp\left(\mathrm{i}\mathbf{k}.\mathbf{r}\right) \underset{r\to\infty}{\sim} \frac{\sin\left(kr\right)}{kr}. \tag{1.5.5}$$

We conclude that, at very low positron energies, the plane wave appearing in (1.2.14) has no preferred direction in space asymptotically far from the target molecule. This is equivalent to saying that, at low energies, the scattering problem is effectively independent of the orientation of the nuclear axis. Calculations of scattering phase shifts, for example, should then be essentially isotropic.

Henceforth, in all of our calculations, we will consider only the lowest partial wave of Σ_g^+ symmetry.

1.6 The hydrogen molecule

1.6.1 The Rayleigh-Ritz variational method

The time-independent, electronic Schrödinger equation (1.2.7) for the hydrogen molecule cannot be solved exactly. However, very accurate approximate solutions can be found using a variational method.

The Rayleigh-Ritz variational method has been used with great success on a wide variety of bound state problems. It was first applied to calculations on the hydrogen molecule in a celebrated paper by James and Coolidge [12]. Here, we briefly recount the essential aspects of the derivation, closely following Bransden and Joachain [57].

Consider the time-independent Hamiltonian, $\hat{\mathcal{H}}$, having eigenvalues, $\{\mathcal{E}_i\}$, at least one of which is discrete, together with corresponding orthonormal eigenfunctions, $\{\psi_i\}$. Suppose that ξ is an arbitrary square-integrable function within the domain of $\hat{\mathcal{H}}$ and define the functional, $\mathcal{E}[\xi]$, to be

$$\mathcal{E}[\xi] = \frac{\langle \xi | \hat{\mathcal{H}} | \xi \rangle}{\langle \xi | \xi \rangle}, \tag{1.6.1}$$

where the Dirac integral notation is understood and the integration is carried out over the configuration space of the coordinates of the system. Expanding ξ in the complete set of orthonormal eigenfunctions of $\hat{\mathcal{H}}$, so that

$$\xi = \sum_i a_i \psi_i, \tag{1.6.2}$$

then subtracting from (1.6.1) the smallest eigenvalue, $\mathcal{E}_0$, of $\hat{\mathcal{H}}$, we have

$$\mathcal{E}[\xi] - \mathcal{E}_0 = \frac{\sum_i |a_i|^2 (\mathcal{E}_i - \mathcal{E}_0)}{\sum_i |a_i|^2}, \tag{1.6.3}$$

where we have made use of the orthonormality of the eigenfunctions. Since $\mathcal{E}_i \geq \mathcal{E}_0$, we can conclude from (1.6.3) that

$$\mathcal{E}_0 \leq \mathcal{E}[\xi], \tag{1.6.4}$$

so that $\mathcal{E}[\xi]$ gives a minimum principle for the ground state energy associated with $\hat{\mathcal{H}}$; this is the basis of the Rayleigh-Ritz variational method.

In the Rayleigh-Ritz method, approximations to the ground state eigenfunction and eigenvalue of $\hat{\mathcal{H}}$ are achieved in the following way. Consider a trial function, ξ_t, formed from a linear combination of L linearly independent functions, $\{\varphi_1, \varphi_2, \ldots, \varphi_L\}$,

$$\xi_t = \sum_{j=1}^{L} c_j \varphi_j, \tag{1.6.5}$$

where the coefficients in the expansion are parameters to be determined so that they minimise $\mathcal{E}[\xi_t]$, thus finding the best approximation to $\mathcal{E}_0$ for the set, $\{\varphi_1, \varphi_2, \ldots, \varphi_L\}$. To obtain this minimisation, we first require of each c_j that $\partial\mathcal{E}/\partial c_j = 0$. It is then straightforward to show that this requirement leads to the system of linear equations,

$$\sum_{j=1}^{L} c_j \left(\langle \varphi_i | \hat{\mathcal{H}} | \varphi_j \rangle - \mathcal{E} \langle \varphi_i | \varphi_j \rangle \right) = 0 \qquad (i = 1, \ldots, L) \,. \tag{1.6.6}$$

This system has a nontrivial solution if and only if

$$\det \left(H_{ij} - \mathcal{E} S_{ij} \right) = 0, \tag{1.6.7}$$

where H_{ij} is the $(L \times L)$ matrix whose element in the i^{th} row and j^{th} column is equal to $\langle \varphi_i | \hat{\mathcal{H}} | \varphi_j \rangle$ and S_{ij} is the $(L \times L)$ matrix whose element in the i^{th} row and j^{th} column is equal to $\langle \varphi_i | \varphi_j \rangle$. The smallest value of $\mathcal{E}$ satisfying (1.6.7) is then the optimised upper bound of $\mathcal{E}_0$. Substituting this value into (1.6.6) allows $\{c_1, c_2, \ldots, c_L\}$ to be found up to an arbitrary normalisation constant, thus optimising ξ_t. It is usual to take the normalisation constant to be such that

$$\langle \xi_t | \xi_t \rangle = 1. \tag{1.6.8}$$

1.6.2 The ground state wavefunction of the hydrogen molecule

The first application of the Rayleigh-Ritz method to determine accurate approximations to the ground state wavefunction of the hydrogen molecule was carried out by James and Coolidge [12]. In our fixed-nuclei calculations, we will consider the electronic Hamiltonian (1.2.6), together with a trial wavefunction, ψ_G, having a general form equivalent to the one used by those authors, namely

$$\psi_G = \sum_{v=1}^{L} c_v \varphi_v, \tag{1.6.9}$$

where

$$\begin{aligned}\varphi_v &= \frac{1}{2\pi}\left(\lambda_1^{m_v}\lambda_2^{n_v}\mu_1^{j_v}\mu_2^{k_v} + \lambda_1^{n_v}\lambda_2^{m_v}\mu_1^{k_v}\mu_2^{j_v}\right) \\ &\times \; s_{12}(\omega_v)\exp\left[-\delta\left(\lambda_1+\lambda_2\right)\right], \end{aligned} \tag{1.6.10}$$

for prescribed basis states, $\{m_v, n_v, j_v, k_v, \omega_v\}$, comprising non-negative integers and where $(j_v + k_v)$ must be even, with

$$s_{12}(\omega_v) = \begin{cases} \rho_{12} = \frac{2}{R}r_{12} & (\omega_v = 1) \\ M_{12}\cos(\phi_1 - \phi_2) & (\omega_v = 2) \\ 1 & (\text{otherwise}) \end{cases} \tag{1.6.11}$$

and

$$M_{12} = \left[(\lambda_1^2 - 1)(1-\mu_1^2)(\lambda_2^2-1)(1-\mu_2^2)\right]^{\frac{1}{2}}. \tag{1.6.12}$$

The role of functions in (1.6.11) having $\omega_v = 2$ can be shown to be equivalent to that of terms quadratic in the interelectronic distance, r_{12}. The importance of including in ψ_{G} basis functions linear in r_{12}, having $\omega_v = 1$, was first pointed out by Hylleraas [60]. They allow for very accurate approximations to the exact target wavefunction, ψ, to be found. In our calculations, we will henceforth describe any term that is linear in an interleptonic distance as being of Hylleraas-type.

For Rayleigh-Ritz calculations involving ψ_{G}, (1.6.6) becomes

$$\sum_{v=1}^{L} c_v \left(\langle \varphi_u | \hat{H}_{\mathrm{T}} | \varphi_v \rangle - \mathcal{E} \langle \varphi_u | \varphi_v \rangle \right) = 0 \qquad (u = 1, \ldots, L) \,. \tag{1.6.13}$$

The positive nonlinear parameter, δ, in (1.6.10) characterises the rate of exponential decline of the trial function. It is not determined from the solution of (1.6.13) but must instead be chosen at the beginning of the variational calculation. A preferred value for δ can be obtained by repeated application of the Rayleigh-Ritz method over a range of appropriate trial values of δ. The candidate giving rise to the smallest value of $\mathcal{E}$ then approximately optimises δ, provided that sufficiently many different candidates are considered.

The key difficulty in implementing the Rayleigh-Ritz method for the hydrogen molecule is the evaluation of the integrals comprising the elements of H_{ij} and S_{ij} in (1.6.7) when $\hat{\mathcal{H}} = \hat{H}_{\mathrm{T}}$. Methods of evaluation are described in extensive detail by James and Coolidge [12].

The accuracy of the approximate target wavefunction is typically measured in terms of the correlation energy of the molecule. This is the amount of the ground state energy, due to electronic correlation, beyond that which is taken into account in a Hartree-Fock calculation [57]. The percentage, P_{c}, of the correlation energy accounted for by an approximate target wavefunction with ground state energy expectation, ϵ_{G}, is

$$P_{\mathrm{c}} = \left(\frac{\epsilon_{\mathrm{G}} - E_{\mathrm{HF}}}{\epsilon - E_{\mathrm{HF}}} \right) \times 100, \tag{1.6.14}$$

where ϵ is the exact, nonrelativistic ground state energy in the Born-Oppenheimer approximation [52] at a fixed internuclear separation and E_{HF} is the Hartree-Fock energy. In our calculations, we will determine values of P_{c} by taking the

values of E_{HF} and ϵ respectively from Jensen [61] and Wolniewicz [62], regarding them to be essentially exact for our purposes.

In the fixed-nuclei Kohn variational calculations we will carry out in the following chapters, we will consider two different approximate target wavefunctions which we shall denote by $\psi_{\mathrm{G}}^{(\mathrm{A})}$ and $\psi_{\mathrm{G}}^{(\mathrm{B})}$. Both functions have the general form described by (1.6.9)-(1.6.12). The function, $\psi_{\mathrm{G}}^{(\mathrm{A})}$, comprises a basis set of $L = 6$ terms having $\omega_v = 0$. It is identical to the 6-term function used by Armour [23], but for the fact that the value of $\delta = 1.1$ in $\psi_{\mathrm{G}}^{(\mathrm{A})}$ at $R = R_0$ has here been chosen to minimise its ground state energy expectation value, which accounts for 57.1% of the correlation energy of H_2. The function, $\psi_{\mathrm{G}}^{(\mathrm{B})}$, has $L = 144$, with a basis set comprising 72 terms having $\omega_v = 0$ and 72 terms having $\omega_v = 2$. A value of $\delta = 1.14$ at $R = R_0$ has been chosen for $\psi_{\mathrm{G}}^{(\mathrm{B})}$ to minimise its ground state energy expectation value, which accounts for 96.8% of the correlation energy of H_2. Further details regarding the basis sets comprising $\psi_{\mathrm{G}}^{(\mathrm{A})}$ and $\psi_{\mathrm{G}}^{(\mathrm{B})}$ can be found in appendix A.

The need to consider both $\psi_{\mathrm{G}}^{(\mathrm{A})}$ and $\psi_{\mathrm{G}}^{(\mathrm{B})}$ in our calculations will soon become clear. It should be noted that neither $\psi_{\mathrm{G}}^{(\mathrm{A})}$ nor $\psi_{\mathrm{G}}^{(\mathrm{B})}$ contains basis functions including Hylleraas-type terms in ρ_{12}, even though these have long been known [12] greatly to improve the speed at which the description of the electronic correlation converges. Although they can readily be incorporated into a Rayleigh-Ritz calculation using the integral framework developed by James and Coolidge [12], we will see in section 1.8 that they can present practical difficulties in the wider context of a Kohn variational calculation. In chapter 8, we address these problems and consider a function, $\psi_{\mathrm{G}}^{(\mathrm{C})}$, having $L = 145$. This function is identical to $\psi_{\mathrm{G}}^{(\mathrm{B})}$ but for the inclusion of a basis function containing a Hylleraas-type term in ρ_{12}; $\psi_{\mathrm{G}}^{(\mathrm{C})}$ accounts for 99.6% of the correlation energy of H_2.

1.7 The Kohn variational method

In this section, we will discuss the application of the Kohn variational method [13] to our calculations of phase shift for low energy elastic $(e^+ - H_2)$ scattering. The general mechanics of this method are well established and have been discussed in detail by many authors (see, for example, [57, 63, 64]). Here, we review the relevant aspects of the method in the context of the $(e^+ - H_2)$ system. We will restrict our calculations to very low positron energies so that only the lowest partial wave of Σ_g^+ symmetry in the expansion (1.5.1) need be considered.

1.7.1 The Kohn trial function

Using (1.4.13) and (1.4.14), at low energies the general solution of the free particle equation in prolate spheroidal coordinates has the asymptotic form

$$F_{00} \underset{\lambda_3 \to \infty}{\sim} D \frac{\sin(kr_3 + \eta)}{r_3}, \tag{1.7.1}$$

for a particle with position vector, $\mathbf{r}_3$, where D is a constant and η represents a phase shift due to a scattering potential. If the source of this potential is the hydrogen molecule, at low energies the asymptotic form of the leptonic scattering wavefunction, Ψ, is then

$$\Psi \underset{\lambda_3 \to \infty}{\sim} D \frac{\sin(kr_3 + \eta)}{r_3} \psi, \tag{1.7.2}$$

where ψ is the exact, unperturbed electronic ground state wavefunction of the hydrogen molecule.

The Kohn variational method [13] allows accurate approximations to exact scattering wavefunctions and phase shifts to be determined. To implement the method, it is necessary to prescribe an initial trial function, Ψ_t, having the same general asymptotic form as the exact scattering wavefunction, Ψ. The trial function depends linearly on a number of unknown parameters. The Kohn method exploits a stationary principle to determine optimal values for these parameters and determine the trial function completely.

For our Kohn calculations on $(e^+ - H_2)$ scattering, we consider first the trial function

$$\Psi_t = (\bar{S} + a_t\bar{C} + p_0\chi_0)\,\psi_G + \sum_{i=1}^{M} p_i\chi_i, \tag{1.7.3}$$

where

$$\begin{bmatrix} \bar{S} \\ \bar{C} \end{bmatrix} = \begin{bmatrix} \cos(\tau) & \sin(\tau) \\ -\sin(\tau) & \cos(\tau) \end{bmatrix} \begin{bmatrix} S \\ C \end{bmatrix}, \tag{1.7.4}$$

for some choice of $\tau \in [0, \pi)$, and

$$S = \frac{N}{\lambda_3 - 1} \sin\left[c\,(\lambda_3 - 1)\right], \tag{1.7.5}$$

$$C = \frac{N}{\lambda_3 - 1} \cos\left[c\,(\lambda_3 - 1)\right] \left(1 - \exp\left[-\gamma\,(\lambda_3 - 1)\right]\right), \tag{1.7.6}$$

where N is a normalisation constant. The unknowns, $\{a_t, p_0, \ldots, p_M\}$, are the parameters to be determined by the variational method.

The functions, S and C, form a basis that represents incident and scattered positrons asymptotically far from the target molecule. They were introduced by

Massey and Ridley [22] in their calculations on $(e^- - H_2)$ scattering. They were later used by Armour and coworkers in their Kohn calculations on $(e^+ - H_2)$ scattering [10, 29]. We will sometimes refer to S, C, $\bar{S}$ and $\bar{C}$ as open-channel functions.

The parameter, τ, represents an additive phase constant in the description of incident and scattered positron waves asymptotically far from the target molecule. For a sufficiently accurate trial function, we would not expect the choice of τ to be of particular physical importance in the calculation of scattering phase shifts. However, in the following chapters we will find that τ plays an important role in avoiding well known mathematical difficulties in the results of Kohn calculations.

The shielding parameter, γ, preserves the regularity of C at the origin. In all of our Kohn calculations, we follow Massey and Ridley [22] and take $\gamma = 0.75$.

The function, ψ_G, is a unit-normalised approximate wavefunction for the ground state of the hydrogen molecule. It has the same general form as described by (1.6.9)-(1.6.12) and is determined, prior to the implementation of the Kohn method on Ψ_t, by the use of the Rayleigh-Ritz variational method. The functions, $\{\chi_0, \ldots, \chi_M\}$, are short-range correlation functions. They are used to describe interactions between the positron and the target electrons when they are close together. These functions take the form

$$\begin{aligned} \chi_0 &= \frac{N}{\lambda_3 - 1} \cos\left[c\left(\lambda_3 - 1\right)\right]\left(1 - \exp\left[-\gamma\left(\lambda_3 - 1\right)\right]\right) \\ &\times \exp\left[-\gamma\left(\lambda_3 - 1\right)\right] \end{aligned} \tag{1.7.7}$$

and

$$\begin{aligned}\chi_i &= N\left[\lambda_1^{a_i}\lambda_2^{b_i}\mu_1^{c_i}\mu_2^{d_i}s_{13}(\theta_i)+\lambda_1^{b_i}\lambda_2^{a_i}\mu_1^{d_i}\mu_2^{c_i}s_{23}(\theta_i)\right]\\ &\times\ \lambda_3^{r_i}\mu_3^{s_i}s_{12}(\theta_i)\exp\left[-\beta\left(\lambda_1+\lambda_2\right)-\alpha\lambda_3\right],\end{aligned} \tag{1.7.8}$$

for prescribed basis states, $\{a_i, b_i, c_i, d_i, r_i, s_i, \theta_i\}$, comprising non-negative integers and where $(c_i + d_i + s_i)$ must be even. The interparticle functions, $s_{pq}(\theta_i)$, have the form

$$s_{12}(\theta_i) = \begin{cases} \rho_{12} = \frac{2}{R}r_{12} & (\theta_i = 1) \\ M_{12}\cos(\phi_1 - \phi_2) & (\theta_i = 2) \\ 1 & (\text{otherwise}) \end{cases} \tag{1.7.9}$$

and

$$s_{j3}(\theta_i) = \begin{cases} \rho_{j3} = \frac{2}{R}r_{j3} & (\theta_i = 3) \\ M_{j3}\cos(\phi_j - \phi_3) & (\theta_i = 4) \\ 1 & (\text{otherwise}), \end{cases} \tag{1.7.10}$$

for $j \in \{1, 2\}$. The inclusion of terms of the form $M_{pq}\cos(\phi_p - \phi_q)$, where

$$M_{pq} = \left[(\lambda_p^2 - 1)(1 - \mu_p^2)(\lambda_q^2 - 1)(1 - \mu_q^2)\right]^{\frac{1}{2}}, \tag{1.7.11}$$

is equivalent to considering terms in r_{pq}^2. The nonlinear parameters, α and β, characterise the rate of exponential decline of the correlation functions. We will sometimes refer to the correlation functions, $\{\chi_1, \ldots, \chi_M\}$, as closed-channel functions. All of the correlation functions used in our calculations will be of overall Σ_g^+ symmetry; taking $(c_i + d_i + s_i)$ to be even in (1.7.8) ensures this symmetry.

The correlation function, χ_0, was introduced by Massey and Ridley [22]. It is included here for largely historical reasons and does not contribute significantly to the description of the leptonic correlations, since it involves only the positron coordinate, λ_3. Owing to its similarity to C (1.7.6), we will sometimes find it convenient to refer to χ_0 as an open-channel function. However, this is something of a misnomer as it is a square-integrable function and, thus, more closely related in essence to the closed-channel functions, $\{\chi_1, \ldots, \chi_M\}$.

The general form of the remaining correlation functions, $\{\chi_1, \ldots, \chi_M\}$, is essentially the same as those described by Armour [10]. As explained in that account, functions having $s_{12}(\theta_i) = s_{j3}(\theta_i) = 1$ comprise products of electron and positron functions which are either both of Σ_g^+ or both of Σ_u^+ symmetry. These correlation functions thus have the overall Σ_g^+ symmetry of the partial wave under consideration in our scattering calculations. The electronic functions of Σ_u^+ symmetry are used to describe molecular polarisation parallel to the internuclear axis. Correlation functions of this type were first used in $(e^+ - H_2)$ Kohn calculations by Armour [23].

As noted by Armour [10], those correlation functions having $\theta_i = 4$ contain electron and positron functions which are either both of Π_u or both of Π_g symmetry, combined in such a way that the correlation function again has the overall Σ_g^+ symmetry required. The electronic functions of Π_u symmetry are used to describe molecular polarisation perpendicular to the nuclear axis. Correlation functions of this type were first used in $(e^+ - H_2)$ Kohn calculations by Armour [26].

Armour [10] also notes the importance of including Hylleraas-type correlation functions in the electron-positron coordinates, ρ_{j3}, having $\theta_i = 3$. As with the

description of correlations in the H_2 molecule, these functions are well known greatly to improve the speed at which the description of the leptonic correlations converges. Correlation functions of this type were first used in $(e^+ - H_2)$ Kohn calculations by Armour and Baker [28, 65].

For completeness, we have here included in Ψ_t correlation functions having $\theta_i = 1$ and $\theta_i = 2$, though we do not expect these to affect the results of our calculations dramatically, since they do not address the key difficulty of describing explicitly the electron-positron correlation. We will investigate this claim in greater detail in chapter 8.

Now, if we define a value, η_t, satisfying

$$\tan(\eta_t - \tau + c) = a_t, \tag{1.7.12}$$

then, using (1.3.8), it is straightforward to show that Ψ_t has the asymptotic form

$$\Psi_t \underset{\lambda_3 \to \infty}{\sim} D \frac{\sin(kr_3 + \eta_t)}{r_3} \psi_G, \tag{1.7.13}$$

where

$$D = \frac{NR}{2\cos(\xi_t)} \tag{1.7.14}$$

and we have defined

$$\xi_t = \eta_t - \tau + c. \tag{1.7.15}$$

Hence, Ψ_t has the same general asymptotic form as (1.7.2). The value of η_t is a

trial phase shift. If the exact phase shift is given by η, the error in $\tan(\eta_t - \tau + c)$ from $\tan(\eta - \tau + c)$ is first order in the error of Ψ_t from Ψ. We will refer to η_t as the first order approximation to the phase shift.

Using (1.2.14) we note that, at low positron energies where we have argued that the elastic scattering problem is effectively isotropic, a consistent trial function should satisfy

$$\Psi_t(\mathbf{r}_1, \mathbf{r}_2, \mathbf{r}_3; R) \underset{r_3 \to \infty}{\sim} B\left[\exp(i\mathbf{k}.\mathbf{r}_3) + \frac{\exp(ikr_3)}{r_3} f(k, R)\right] \psi_G(\mathbf{r}_1, \mathbf{r}_2; R), \quad (1.7.16)$$

for some normalisation constant, B, and where, at low energies, anisotropic contributions from the expansion (1.5.1) of $\exp(i\mathbf{k}.\mathbf{r}_3)$ are negligible. Relationships between the constants B and N can be derived so that (1.7.16) is indeed satisfied. In chapter 6, we will derive such a relationship explicitly for a trial function of the form (1.7.3).

1.7.2 The variational method

Consider the functional,

$$\mathcal{I}[\Psi_t] = \langle \Psi_t | \hat{H} - E | \Psi_t \rangle, \quad (1.7.17)$$

where Ψ_t is as in (1.7.3), $\hat{H}$ is as in (1.2.11) and

$$E = \epsilon_G + \frac{1}{2}k^2, \quad (1.7.18)$$

ϵ_G being the electronic ground state energy expectation value obtained from the approximate target wavefunction, ψ_G.

The integral in (1.7.17) is evaluated over the configuration space of the positron and the two electrons. For brevity, we henceforth denote by $\langle X, Y\rangle$ any integral of the form $\langle X|\hat{H} - E|Y\rangle$. Hence, we rewrite (1.7.17) as

$$\mathcal{I}\left[\Psi_t\right] = \langle \Psi_t, \Psi_t\rangle. \tag{1.7.19}$$

In section 1.8, we will briefly discuss methods of evaluating the various integrals involved in an application of the Kohn method. Armour and Humberston [11] remark that the integrals

$$\Xi_{SC} = \langle \bar{S}| - \frac{1}{2}\nabla_3^2 - \frac{1}{2}k^2|\bar{C}\rangle, \tag{1.7.20}$$

$$\Xi_{CS} = \langle \bar{C}| - \frac{1}{2}\nabla_3^2 - \frac{1}{2}k^2|\bar{S}\rangle \tag{1.7.21}$$

can be evaluated analytically. We find that

$$\langle \bar{S}\psi_G, \bar{C}\psi_G\rangle - \langle \bar{C}\psi_G, \bar{S}\psi_G\rangle = \Xi_{SC} - \Xi_{CS} = \tilde{k}, \tag{1.7.22}$$

where we have defined

$$\tilde{k} = \frac{\pi N^2 R^2}{2} k. \tag{1.7.23}$$

Moreover, since $\hat{H}$ is Hermitian, $\chi_0\psi_G$ and $\{\chi_i\}$ are all square-integrable and each term in (1.7.3) is real-valued, we note that

$$\langle \bar{S}\psi_G, \chi_0\psi_G\rangle = \langle \chi_0\psi_G, \bar{S}\psi_G\rangle, \tag{1.7.24}$$

$$\langle \bar{C}\psi_G, \chi_0\psi_G\rangle = \langle \chi_0\psi_G, \bar{C}\psi_G\rangle, \tag{1.7.25}$$

$$\langle \bar{S}\psi_G, \chi_i\rangle = \langle \chi_i, \bar{S}\psi_G\rangle \qquad (i = 1, \ldots, M), \tag{1.7.26}$$

$$\langle \bar{C}\psi_G, \chi_i\rangle = \langle \chi_i, \bar{C}\psi_G\rangle \qquad (i = 1, \ldots, M), \tag{1.7.27}$$

$$\langle \chi_0\psi_G, \chi_i\rangle = \langle \chi_i, \chi_0\psi_G\rangle \qquad (i = 1, \ldots, M), \tag{1.7.28}$$

$$\langle \chi_i, \chi_j\rangle = \langle \chi_j, \chi_i\rangle \qquad (i, j = 1, \ldots, M). \tag{1.7.29}$$

Using (1.7.3), (1.7.19) and (1.7.22), together with (1.7.24)-(1.7.29), it is then straightforward to show that

$$\frac{\partial \mathcal{I}[\Psi_t]}{\partial a_t} = \tilde{k} + 2\langle \bar{C}\psi_G, \Psi_t\rangle, \tag{1.7.30}$$

$$\frac{\partial \mathcal{I}[\Psi_t]}{\partial p_0} = 2\langle \chi_0\psi_G, \Psi_t\rangle, \tag{1.7.31}$$

$$\frac{\partial \mathcal{I}[\Psi_t]}{\partial p_i} = 2\langle \chi_i, \Psi_t\rangle \qquad (i = 1, \ldots, M). \tag{1.7.32}$$

Now, if Ψ_t were the exact scattering wavefunction, then each integral on the right hand side of (1.7.30)-(1.7.32) would be equal to zero. In the Kohn variational method, optimal values of the linear parameters, $\{a_t, p_0, \ldots, p_M\}$, are obtained by imposing this condition on the inexact trial function. Hence, we have the Kohn equations,

$$\frac{\partial \mathcal{I}[\Psi_t]}{\partial a_t} = \tilde{k}, \tag{1.7.33}$$

$$\frac{\partial \mathcal{I}[\Psi_t]}{\partial p_i} = 0 \qquad (i = 0, \ldots, M). \tag{1.7.34}$$

Careful inspection of (1.7.30)-(1.7.34) shows that this requirement can also be expressed as a matrix equation,

$$Ax = -b, \tag{1.7.35}$$

where

$$A = \begin{bmatrix} \langle \bar{C}\psi_G, \bar{C}\psi_G \rangle & \langle \bar{C}\psi_G, \chi_0\psi_G \rangle & \cdots & \langle \bar{C}\psi_G, \chi_M \rangle \\ \langle \chi_0\psi_G, \bar{C}\psi_G \rangle & \langle \chi_0\psi_G, \chi_0\psi_G \rangle & \cdots & \langle \chi_0\psi_G, \chi_M \rangle \\ \vdots & \vdots & \ddots & \vdots \\ \langle \chi_M, \bar{C}\psi_G \rangle & \langle \chi_M, \chi_0\psi_G \rangle & \cdots & \langle \chi_M, \chi_M \rangle \end{bmatrix}, \tag{1.7.36}$$

$$b = \begin{bmatrix} \langle \bar{C}\psi_G, \bar{S}\psi_G \rangle \\ \langle \chi_0\psi_G, \bar{S}\psi_G \rangle \\ \vdots \\ \langle \chi_M, \bar{S}\psi_G \rangle \end{bmatrix}, \tag{1.7.37}$$

$$x = \begin{bmatrix} a_t \\ p_0 \\ \vdots \\ p_M \end{bmatrix}. \tag{1.7.38}$$

By the Hermiticity properties (1.7.25) and (1.7.27)-(1.7.29), A is symmetric. For nonsingular A, multiplying both sides of (1.7.35) by A^{-1} determines the optimal values of $\{a_t, p_0, \ldots, p_M\}$. If A is singular, then (1.7.35) either has no solution or infinitely many solutions. Suppose the rank of A is P and the rank of the concatenated matrix, $[A|-b]$, is Q. An inconsistency is avoided if and only if $P = Q$. In practice, for singular A this seems unlikely, given the form of our Kohn equations. That is, we can reasonably expect a singular Kohn matrix, A,

to give rise to an inconsistency rather than an infinity of solutions to (1.7.35).

Take A to be nonsingular. Having found $\{a_t, p_0, \ldots, p_M\}$, $\mathcal{I}[\Psi_t]$ can be evaluated. In fact, when the Kohn equations (1.7.35) are satisfied, various terms in the expansion of (1.7.19) become zero and we may write

$$\mathcal{I}[\Psi_t] = \langle \bar{S}\psi_G, \bar{S}\psi_G \rangle + a_t \langle \bar{S}\psi_G, \bar{C}\psi_G \rangle + p_0 \langle \bar{S}\psi_G, \chi_0 \psi_G \rangle + \sum_{i=1}^{M} p_i \langle \bar{S}\psi_G, \chi_i \rangle. \tag{1.7.39}$$

Next, we consider a functional, $\mathcal{J}[\Psi_t]$, which implicitly defines a quantity, η_v, such that

$$\mathcal{J}[\Psi_t] = \tan(\eta_v - \tau + c) = a_t - \frac{1}{\tilde{k}} \mathcal{I}[\Psi_t]. \tag{1.7.40}$$

This functional is defined in such a way that it is stationary with respect to variations in $\{a_t, p_0, \ldots, p_M\}$ when the Kohn equations (1.7.35) are satisfied. That is,

$$\frac{\partial \mathcal{J}[\Psi_t]}{\partial a_t} = \frac{\partial \mathcal{J}[\Psi_t]}{\partial p_i} = 0 \qquad (i = 0, \ldots, M). \tag{1.7.41}$$

As pointed out by Armour [10], it follows from the Kato identity [66] that the error in $\tan(\eta_v - \tau + c)$ from $\tan(\eta - \tau + c)$ is second order in the error of Ψ_t from Ψ. This is the attraction of the Kohn variational method; if the error in Ψ_t is small, η_v should be an accurate approximation to the scattering phase shift. We will refer to η_v as the second order approximation to the phase shift. The values of both η_t and η_v are independent of the normalisation constant, N.

The main practical difficulty in the implementation of our Kohn variational calculations is the evaluation of the integrals comprising the elements of A and b in (1.7.35). We will discuss this in more detail in section 1.8. For now, we note that in the case where we wish to carry out Kohn calculations for different choices of τ, it is not necessary to recalculate these integrals explicitly at each value of τ. The integrals comprising A and b at any value of τ are available immediately from the integrals calculated at $\tau = 0$, say, via an orthogonal transformation. Specifically, if we define a matrix, B, such that

$$B = \begin{bmatrix} \langle \bar{S}\psi_G, \bar{S}\psi_G \rangle & \langle \bar{S}\psi_G, \bar{C}\psi_G \rangle & \langle \bar{S}\psi_G, \chi_0\psi_G \rangle & \cdots & \langle \bar{S}\psi_G, \chi_M \rangle \\ \langle \bar{C}\psi_G, \bar{S}\psi_G \rangle & \langle \bar{C}\psi_G, \bar{C}\psi_G \rangle & \langle \bar{C}\psi_G, \chi_0\psi_G \rangle & \cdots & \langle \bar{C}\psi_G, \chi_M \rangle \\ \langle \chi_0\psi_G, \bar{S}\psi_G \rangle & \langle \chi_0\psi_G, \bar{C}\psi_G \rangle & \langle \chi_0\psi_G, \chi_0\psi_G \rangle & \cdots & \langle \chi_0\psi_G, \chi_M \rangle \\ \vdots & \vdots & \vdots & \ddots & \vdots \\ \langle \chi_M, \bar{S}\psi_G \rangle & \langle \chi_M, \bar{C}\psi_G \rangle & \langle \chi_M, \chi_0\psi_G \rangle & \cdots & \langle \chi_M, \chi_M \rangle \end{bmatrix} \tag{1.7.42}$$

and, further, an orthogonal matrix, G, such that

$$G = \begin{bmatrix} \cos(\tau) & \sin(\tau) & 0 & 0 & \cdots & 0 \\ -\sin(\tau) & \cos(\tau) & 0 & 0 & \cdots & 0 \\ 0 & 0 & 1 & 0 & \cdots & 0 \\ 0 & 0 & 0 & 1 & \cdots & 0 \\ \vdots & \vdots & \vdots & \vdots & \ddots & \vdots \\ 0 & 0 & 0 & 0 & \cdots & 1 \end{bmatrix}, \tag{1.7.43}$$

then it is easily shown that

$$B = GB_0G^\top, \tag{1.7.44}$$

where B_0 is the matrix obtained by substituting $\tau = 0$ into the right hand side of (1.7.42).

1.7.3 Implementing the variational method

In the following chapters, we will discuss Kohn calculations carried out with a number of different trial functions. Prior to chapter 8, all of our Kohn calculations using a trial function of the form (1.7.3) will be carried out with the same set of short-range correlation functions and the same approximate target wavefunction. Specifically, we will consider the approximate target wavefunction, $\psi_G^{(B)}$, identified in section 1.6.2 and detailed in appendix A. This is a very accurate target wavefunction and accounts for 96.8% of the correlation energy of H_2. We will use a set of $M = 279$ short-range correlation functions that we will denote by $\Omega^{(1)}$. The first 261 of these comprise three sets of 87 correlation functions, corresponding to values of $\theta_i = 0$, $\theta_i = 2$ and $\theta_i = 4$ in (1.7.9) and (1.7.10). Each set of 87 functions consists of all physically distinct permutations of the non-negative integers, $\{a_i, b_i, c_i, d_i, r_i, s_i\}$, such that no integer is larger than 2, with $(c_i + d_i + s_i)$ being even and with $(a_i + b_i + c_i + d_i + r_i + s_i) \leq 5$. Further details of these correlation functions are given in appendix A. The remaining 18 functions in $\Omega^{(1)}$ contain Hylleraas-type terms in the electron-positron coordinates, corresponding to $\theta_i = 3$ in (1.7.10). Details of these functions are given in appendix A.

In a self-evident notation, we will denote by $\Psi_t^{(1,B)}$ the trial function of the form (1.7.3) containing $\Omega^{(1)}$ and $\psi_G^{(B)}$. We will use this notation more generally in the following chapters as a means of distinguishing trial functions containing different approximate target functions and short-range correlation functions.

Regarding the choice of the nonlinear parameters, α and β, in (1.7.8), for $\Psi_t^{(1,B)}$ we will initially take these values to be $\alpha = 0.5$ and $\beta = 1.0$. In chapter 7, we will carry out a systematic investigation into the effects on our calculations of varying these parameters. Regarding the choice of the phase parameter, τ, for convenience we will initially take $\tau = 0$ or $\tau = \pi/2$. As noted by Burke [67], these two choices of τ correspond to the Kohn and inverse Kohn, or Rubinow [68], methods respectively. In chapters 3-5, we will carry out a comprehensive examination of the importance of the choice of τ in our calculations.

In addition to $\Psi_t^{(1,B)}$, at various stages in our calculations we will consider trial functions having a different form to (1.7.3). One such trial function will be introduced in the following section.

1.8 Evaluation of matrix elements

One of the challenges in our implementation of the Kohn method is the evaluation of the integrals required to formulate the matrix equation (1.7.35). It is generally not possible to evaluate these integrals analytically and a variety of computational methods have been developed to allow very accurate numerical approximations to these integrals to be found. These methods have been described in extensive detail by several authors [10, 11, 69–71] and it is not our intention to reproduce those accounts in full here. However, we will find it helpful to conclude this chapter by giving a brief review of a number of points mentioned by those authors.

As discussed by Armour and Humberston [11], in addition to (1.7.20) and (1.7.21), the following integrals:

$$\Xi_{SS} = \langle \bar{S}| - \frac{1}{2}\nabla_3^2 - \frac{1}{2}k^2|\bar{S}\rangle, \tag{1.8.1}$$

$$\Xi_{CC} = \langle \bar{C}| - \frac{1}{2}\nabla_3^2 - \frac{1}{2}k^2|\bar{C}\rangle, \tag{1.8.2}$$

$$\Xi_{\chi_0\chi_0} = \langle \chi_0| - \frac{1}{2}\nabla_3^2 - \frac{1}{2}k^2|\chi_0\rangle, \tag{1.8.3}$$

$$\Xi_{S\chi_0} = \langle \bar{S}| - \frac{1}{2}\nabla_3^2 - \frac{1}{2}k^2|\chi_0\rangle = \langle \chi_0| - \frac{1}{2}\nabla_3^2 - \frac{1}{2}k^2|\bar{S}\rangle, \tag{1.8.4}$$

$$\Xi_{C\chi_0} = \langle \bar{C}| - \frac{1}{2}\nabla_3^2 - \frac{1}{2}k^2|\chi_0\rangle = \langle \chi_0| - \frac{1}{2}\nabla_3^2 - \frac{1}{2}k^2|\bar{C}\rangle \tag{1.8.5}$$

can be evaluated analytically. In our calculations, all of the other integrals involved in the Kohn equations have been evaluated numerically using the C++ framework developed by Todd [70]. This framework is based partly on the original FORTRAN 77 code written by Armour and coworkers and used in all Kohn calculations on the $(e^+ - H_2)$ system up to 1990 [10, 29], as well as including some improvements to this code introduced by Franklin [72]. Both the FORTRAN 77 and C++ frameworks make use of Boys' boundary-derivative reduction method [11, 73, 74] to carry out numerical evaluation of the integrals.

The main difficulty in calculating the matrix elements of (1.7.35) arises due to the presence in (1.3.10), (1.3.11) and the short-range correlation functions (1.7.8) of various combinations of Hylleraas-type terms linear in ρ_{ij}, where i and j each denote either the positron or one of the electrons. The corresponding integrals are not straightforward to evaluate as the ρ_{ij} terms are not separable; that is, they cannot be expressed as a finite expansion of products of single particle functions.

Hylleraas-type functions in ρ_{12} can also appear in the application of the Rayleigh-Ritz method used to determine the approximate ground state wavefunction of the hydrogen molecule, discussed in section 1.6. However, the evaluation of

the integrals required in this case does not present a significant challenge. The operations necessary to determine accurate approximations to the integrals are described in detail by James and Coolidge [12]. Those authors make use of the Neumann expansion,

$$\frac{1}{\rho_{ij}} = \sum_{\tau=0}^{\infty} \sum_{\nu=0}^{\tau} D_\tau^\nu P_\tau^\nu \left(\lambda_<\right) Q_\tau^\nu \left(\lambda_>\right) P_\tau^\nu \left(\mu_i\right) P_\tau^\nu \left(\mu_j\right) \cos\left[\nu\left(\phi_i - \phi_j\right)\right], \tag{1.8.6}$$

with

$$D_\tau^0 = 2\tau + 1, \tag{1.8.7}$$

$$D_\tau^\nu = (-1)^\nu 2\left(2\tau+1\right)\left[\frac{(\tau-\nu)!}{(\tau+\nu)!}\right]^2 \qquad (\nu > 0), \tag{1.8.8}$$

where $\lambda_<$ and $\lambda_>$ are, respectively, the lesser and greater of λ_i and λ_j. P_τ^ν and Q_τ^ν are, respectively, the associated Legendre functions of the first and second kinds [59]. Owing to the high level of recursion involved in the computation, some modifications of the methods developed by James and Coolidge are necessary at high values of τ in (1.8.6).

For the general form of the approximate wavefunctions used in our calculations, it can be shown that only a finite number of terms in the expansion (1.8.6) contribute to the integrals required by the Rayleigh-Ritz and Kohn methods. For our purposes and from the point of view of evaluating these integrals, the Neumann expansion can thus effectively be regarded as a finite series of separable terms. The precise value, $\tau = \tau_{\max}$, beyond which the expansion does not contribute to the integrals, depends on the particular choice of basis functions used in the application of each variational method.

In the case of our implementation of the Rayleigh-Ritz method, integrals involving factors of $1/\rho_{12}$, arising from the presence of this term in (1.3.11), are handled immediately via the Neumann expansion. Integrals involving factors of ρ_{12}, arising from basis functions having $\omega_v = 1$ in (1.6.11), can also be handled via the expansion by noting first that we can write

$$\rho_{12} = \rho_{12}^2 \times \frac{1}{\rho_{12}} \tag{1.8.9}$$

and secondly that ρ_{12}^2 is separable, since it is easily shown that

$$\rho_{12}^2 = \lambda_1^2 + \lambda_2^2 + \mu_1^2 + \mu_2^2 - 2 - 2\lambda_1\lambda_2\mu_1\mu_2 - 2M_{12}\cos(\phi_1 - \phi_2), \tag{1.8.10}$$

with M_{12} as in (1.6.12).

In the case of our implementation of the Kohn variational method, the evaluation of integrals containing Hylleraas-type functions is significantly more complicated. The reason for this is that, in addition to consideration of terms linear in ρ_{12}, terms linear in ρ_{13} and ρ_{23} must also be accounted for. Inspection of (1.3.10), (1.3.11) and (1.7.8) shows that, depending on the choice of the short-range correlation functions, it may be necessary to evaluate integrals containing factors of the form

$$\rho_{ij}\rho_{ik} = \rho_{ij}^2\rho_{ik}^2 \times \frac{1}{\rho_{ij}} \times \frac{1}{\rho_{ik}}, \tag{1.8.11}$$

$$\frac{\rho_{ij}}{\rho_{jk}} = \rho_{ij}^2 \times \frac{1}{\rho_{ij}} \times \frac{1}{\rho_{jk}} \tag{1.8.12}$$

and

$$\frac{\rho_{ij}\rho_{ik}}{\rho_{jk}} = \rho_{ij}^2\rho_{ik}^2 \times \frac{1}{\rho_{ij}} \times \frac{1}{\rho_{ik}} \times \frac{1}{\rho_{jk}}, \tag{1.8.13}$$

where $\{i, j, k\}$ is some permutation of $\{1, 2, 3\}$.

In principle, each of the above cases can be addressed by a method analogous to that described by James and Coolidge using (1.8.6). However, the presence in (1.8.11), (1.8.12) and (1.8.13) of combinations of $1/\rho_{ij}$, $1/\rho_{ik}$ and $1/\rho_{jk}$, necessitates the multiplication of several different Neumann expansions; this considerably complicates the operations required to evaluate the corresponding integrals. For the treatment of (1.8.11) and (1.8.12), it is necessary to use a double Neumann expansion. When considering (1.8.13), a triple Neumann expansion is required.

Previous Kohn calculations [10, 23, 29] on $(e^+ - H_2)$ scattering have made use of the method of models [24], the mechanics of which we will describe shortly. The use of the method of models in the Kohn calculations is very helpful because, as we shall see, it avoids the need to calculate integrals requiring a triple Neumann expansion. This significantly reduces the computational expense of the calculation. In fact, although a small number of integrals involving factors of the form (1.8.13) were calculated by Clary [75], it is only recently that a more general framework [69, 71] has been developed to make the evaluation of a wider class of integrals of this type tractable.

1.8.1 The method of models

All previous Kohn calculations [10, 29] on the $(e^+ - H_2)$ system have made use of the method of models [24]. This approach requires a trial function in which

the approximate target wavefunction is included as a factor. Thus, we consider a trial wavefunction having a slightly different form to (1.7.3), viz.

$$\Psi_{\mathrm{t}} = \left(\bar{S} + a_{\mathrm{t}} \bar{C} + \sum_{i=0}^{M} p_i \chi_i \right) \psi_{\mathrm{G}}, \tag{1.8.14}$$

where, for a given set of short-range correlation functions, the optimal values of $\{a_{\mathrm{t}}, p_0, \ldots, p_M\}$ determined by the Kohn method will be different in (1.7.3) and (1.8.14).

The trial function (1.8.14) has the asymptotic form of (1.7.13), so is suitable for use in our Kohn calculations. To implement the method of models, we replace the target electronic Hamiltonian, $\hat{H}_{\mathrm{T}}$, in (1.2.11) with a model Hamiltonian, $\hat{H}_{\mathrm{M}}$, having the form

$$\hat{H}_{\mathrm{M}} = V_{\mathrm{M}} - \frac{1}{2}\nabla_1^2 - \frac{1}{2}\nabla_2^2, \tag{1.8.15}$$

where V_{M} is an unspecified model potential making the approximate target wavefunction, ψ_{G}, an exact eigenfunction of $\hat{H}_{\mathrm{M}}$. That is,

$$\hat{H}_{\mathrm{M}} \psi_{\mathrm{G}} = E_{\mathrm{M}} \psi_{\mathrm{G}}. \tag{1.8.16}$$

Next, we redefine E (1.7.18) as

$$E = E_{\mathrm{M}} + \frac{1}{2}k^2, \tag{1.8.17}$$

so that, for trial functions of the form (1.8.14), it is straightforward to show using (1.8.15), (1.8.16), (1.8.17) and the standard result

$$\nabla^2 (XY) = X\nabla^2 Y + 2\nabla X.\nabla Y + Y\nabla^2 X, \tag{1.8.18}$$

that

$$\begin{aligned} (\hat{H} - E)\,\Psi_{\rm t} &= \left(-\frac{1}{2}\nabla_1^2 - \frac{1}{2}\nabla_2^2 - \frac{1}{2}\nabla_3^2 + V_{\rm p} + V_{\rm M} - E_{\rm M} - \frac{1}{2}k^2\right)(P\psi_{\rm G}) \\ &= \psi_{\rm G}\left(-\frac{1}{2}\nabla_1^2 - \frac{1}{2}\nabla_2^2 - \frac{1}{2}\nabla_3^2 + V_{\rm p} - \frac{1}{2}k^2\right)P \\ &- (\nabla_1\psi_{\rm G}.\nabla_1 P + \nabla_2\psi_{\rm G}.\nabla_2 P)\,, \end{aligned} \tag{1.8.19}$$

where we have defined

$$P = \bar{S} + a_{\rm t}\bar{C} + \sum_{i=0}^{M} p_i\chi_i. \tag{1.8.20}$$

Hence, in Kohn calculations using the method of models and trial functions of the form (1.8.14), explicit knowledge of $V_{\rm M}$ and $E_{\rm M}$ is not required to evaluate the matrix elements comprising the Kohn equations.

Suppose that we carry out Kohn calculations using a trial function of the form (1.8.14) and with the set of 279 correlation functions, $\Omega^{(1)}$, introduced in section 1.7.3 and detailed in appendix A. We recall that this set of functions contains the very important Hylleraas-type terms in ρ_{13} and ρ_{23} but not those in ρ_{12}. Under these circumstances, provided that the target wavefunction, $\psi_{\rm G}$, appearing in (1.8.14) contains no Hylleraas-type terms in ρ_{12}, we see that the method of models avoids the need to calculate the most troublesome integrals involved in our Kohn calculations, namely those of the form (1.8.13) requiring a triple Neumann expansion. The reason for this is that explicit knowledge of $V_{\rm M}$ is not required to formulate the Kohn equations.

The implementation of the Kohn method for trial functions of the form (1.8.14) is analogous to that described in section 1.7. In particular, we can derive Kohn equations of the form (1.7.35), in which

$$A = \begin{bmatrix} \langle \bar{C}\psi_G, \bar{C}\psi_G \rangle & \langle \bar{C}\psi_G, \chi_0\psi_G \rangle & \cdots & \langle \bar{C}\psi_G, \chi_M\psi_G \rangle \\ \langle \chi_0\psi_G, \bar{C}\psi_G \rangle & \langle \chi_0\psi_G, \chi_0\psi_G \rangle & \cdots & \langle \chi_0\psi_G, \chi_M\psi_G \rangle \\ \vdots & \vdots & \ddots & \vdots \\ \langle \chi_M\psi_G, \bar{C}\psi_G \rangle & \langle \chi_M\psi_G, \chi_0\psi_G \rangle & \cdots & \langle \chi_M\psi_G, \chi_M\psi_G \rangle \end{bmatrix} \quad (1.8.21)$$

$$b = \begin{bmatrix} \langle \bar{C}\psi_G, \bar{S}\psi_G \rangle \\ \langle \chi_0\psi_G, \bar{S}\psi_G \rangle \\ \vdots \\ \langle \chi_M\psi_G, \bar{S}\psi_G \rangle \end{bmatrix} \quad (1.8.22)$$

and where matrix elements of the form $\langle X, Y \rangle$ denote

$$\langle X, Y \rangle = \langle X | \hat{H} - E | Y \rangle = \langle X | \hat{H}_M + V_p - \frac{1}{2}\nabla_3^2 - E_M - \frac{1}{2}k^2 | Y \rangle. \quad (1.8.23)$$

Moreover, (1.7.39) and (1.7.42) respectively become

$$\mathcal{I}[\Psi_t] = \langle \bar{S}\psi_G, \bar{S}\psi_G \rangle + a_t \langle \bar{S}\psi_G, \bar{C}\psi_G \rangle + \sum_{i=0}^{M} p_i \langle \bar{S}\psi_G, \chi_i\psi_G \rangle \quad (1.8.24)$$

and

$$B = \begin{bmatrix} \langle \bar{S}\psi_G, \bar{S}\psi_G \rangle & \langle \bar{S}\psi_G, \bar{C}\psi_G \rangle & \langle \bar{S}\psi_G, \chi_0\psi_G \rangle & \cdots & \langle \bar{S}\psi_G, \chi_M\psi_G \rangle \\ \langle \bar{C}\psi_G, \bar{S}\psi_G \rangle & \langle \bar{C}\psi_G, \bar{C}\psi_G \rangle & \langle \bar{C}\psi_G, \chi_0\psi_G \rangle & \cdots & \langle \bar{C}\psi_G, \chi_M\psi_G \rangle \\ \langle \chi_0\psi_G, \bar{S}\psi_G \rangle & \langle \chi_0\psi_G, \bar{C}\psi_G \rangle & \langle \chi_0\psi_G, \chi_0\psi_G \rangle & \cdots & \langle \chi_0\psi_G, \chi_M\psi_G \rangle \\ \vdots & \vdots & \vdots & \ddots & \vdots \\ \langle \chi_M\psi_G, \bar{S}\psi_G \rangle & \langle \chi_M\psi_G, \bar{C}\psi_G \rangle & \langle \chi_M\psi_G, \chi_0\psi_G \rangle & \cdots & \langle \chi_M\psi_G, \chi_M\psi_G \rangle \end{bmatrix}. \tag{1.8.25}$$

By (1.7.25) and Hermiticity properties analogous to (1.7.27)-(1.7.29), A is again symmetric. As before, by solving the Kohn equations (1.7.35) with A and b as in (1.8.21) and (1.8.22), values of η_v can then be obtained directly from (1.7.40) with $\mathcal{I}[\Psi_t]$ as in (1.8.24).

We have already noted that, in order to avoid integrals necessitating a triple Neumann expansion, the approximate target wavefunction appearing in (1.8.14) cannot contain any Hylleraas-type terms in ρ_{12} if the set of short-range correlation functions, $\Omega^{(1)}$, is used. In fact, owing to the restrictions of the present computational framework, Kohn calculations of this type are tractable only when the expansion of ψ_G comprises terms having $s_{12}(\omega_v) = 1$ in (1.6.11). This is a consequence of including ψ_G as a factor in Ψ_t. Currently, therefore, use of the method of models severely restricts the accuracy of the target wavefunction that can be used in (1.8.14).

In the following chapters, we will carry out Kohn calculations using the method of models and with a trial function of the form (1.8.14). Prior to chapter 8, all of these calculations will be carried out with the set of correlation functions, $\Omega^{(1)}$, together with the 6-term approximate target wavefunction, $\psi_G^{(A)}$, identified in section 1.6.2 and detailed in appendix A. This is a much less accurate target wavefunction than $\psi_G^{(B)}$; it accounts for only 57.1% of the correlation energy of

H_2. We will denote by $\Psi_t^{(1,A)}$ the trial function of the form (1.8.14) containing $\Omega^{(1)}$ and $\psi_G^{(A)}$.

Regarding the choice of the nonlinear parameters, α and β, contained in (1.7.8), for $\Psi_t^{(1,A)}$ we will initially take these values to be $\alpha = 0.5$ and $\beta = -0.1$. A negative value of β can legitimately be chosen here, since the presence of $\psi_G^{(A)}$ as a product in $\Psi_t^{(1,A)}$ ensures that the coefficient of exponential decline of the closed-channel part of the trial function is equal to $(\beta + \delta) = 1.0$. In chapter 7, we will carry out a systematic investigation into the effects on our calculations of varying α and β. Regarding the choice of the phase parameter, τ, as in the case of $\Psi_t^{(1,B)}$ we will initially take $\tau = 0$ or $\tau = \pi/2$.

1.8.2 Removal of the method of models

In our Kohn calculations carried out with $\Psi_t^{(1,B)}$, in which the method of models is not used and where the target potential (1.3.11) must explicitly be taken into account, it is necessary to evaluate integrals of the form (1.8.13) involving a triple Neumann expansion. This has recently become possible by adapting code developed for helium-antihydrogen scattering calculations [69]. The operations required to evaluate such integrals were determined originally by Armour before being optimised by Plummer; a detailed account of the computations is given by Plummer, Armour and coworkers [71]. These operations have been incorporated into a C++ framework by Todd [70].

We carry out our Kohn calculations using Todd's C++ framework. As detailed in [70], this framework allows for numerical evaluation of integrals of the form,

$$
\begin{aligned}
&\Upsilon_{\varepsilon} \quad [a,b,c,p,q,r,u_{12},u_{13},u_{23},w_{12},w_{13},w_{23},f_1,f_2,f_3,\alpha_1,\alpha_2,\alpha_3] \\
&= \frac{1}{8\pi^3}\int_0^{2\pi}\int_0^{2\pi}\int_0^{2\pi}\int_{-1}^{1}\int_{-1}^{1}\int_{-1}^{1}\int_{1}^{\infty}\int_{1}^{\infty}\int_{1}^{\infty} J(\varepsilon)\,\lambda_1^a\lambda_2^b\lambda_3^c\mu_1^p\mu_2^q\mu_3^r \\
&\times \left[M_{12}\cos(\phi_1-\phi_2)\right]^{u_{12}}\left[M_{13}\cos(\phi_1-\phi_3)\right]^{u_{13}}\left[M_{23}\cos(\phi_2-\phi_3)\right]^{u_{23}} \\
&\times \rho_{12}^{w_{12}}\rho_{13}^{w_{13}}\rho_{23}^{w_{23}} \\
&\times \exp\left(-\alpha_1\lambda_1-\alpha_2\lambda_2-\alpha_3\lambda_3\right) \\
&\times f_1(\lambda_1)\,f_2(\lambda_2)\,f_3(\lambda_3)\,\mathrm{d}\lambda_1\mathrm{d}\lambda_2\mathrm{d}\lambda_3\mathrm{d}\mu_1\mathrm{d}\mu_2\mathrm{d}\mu_3\mathrm{d}\phi_1\mathrm{d}\phi_2\mathrm{d}\phi_3, \qquad (1.8.26)
\end{aligned}
$$

where $\varepsilon \in \{0,1,2,3\}$, with

$$
\begin{aligned}
J(0) &= \left(\lambda_1^2-\mu_1^2\right)\left(\lambda_2^2-\mu_2^2\right)\left(\lambda_3^2-\mu_3^2\right), \qquad (1.8.27)\\
J(i) &= \left(\lambda_j^2-\mu_j^2\right)\left(\lambda_k^2-\mu_k^2\right), \qquad (1.8.28)
\end{aligned}
$$

where $\{i,j,k\}$ is some permutation of $\{1,2,3\}$, as well as

$$
\begin{aligned}
&\mathcal{V} \quad [\sigma_1,\sigma_2,\sigma_3,\zeta_1,\zeta_2,\zeta_3,\alpha_1,\alpha_2,\alpha_3] \\
&= \frac{1}{8\pi^3}\int_0^{2\pi}\int_0^{2\pi}\int_0^{2\pi}\int_{-1}^{1}\int_{-1}^{1}\int_{-1}^{1}\int_{1}^{\infty}\int_{1}^{\infty}\int_{1}^{\infty} \lambda_1^{\sigma_1}\lambda_2^{\sigma_2}\lambda_3^{\sigma_3}\mu_1^{\zeta_1}\mu_2^{\zeta_2}\mu_3^{\zeta_3} \\
&\times \frac{\rho_{ij}\rho_{ik}}{\rho_{jk}}\exp\left(-\alpha_1\lambda_1-\alpha_2\lambda_2-\alpha_3\lambda_3\right) \\
&\times \left(\lambda_1^2-\mu_1^2\right)\left(\lambda_2^2-\mu_2^2\right)\left(\lambda_3^2-\mu_3^2\right) \\
&\times \mathrm{d}\lambda_1\mathrm{d}\lambda_2\mathrm{d}\lambda_3\mathrm{d}\mu_1\mathrm{d}\mu_2\mathrm{d}\mu_3\mathrm{d}\phi_1\mathrm{d}\phi_2\mathrm{d}\phi_3. \qquad (1.8.29)
\end{aligned}
$$

In (1.8.26), $\{a,b,c,p,q,r,u_{12},u_{13},u_{23},w_{12},w_{13},w_{23}\}$ are all integers, $\{\alpha_1,\alpha_2,\alpha_3\}$ are each non-negative constants and $\{f_1(\lambda_1), f_2(\lambda_2), f_3(\lambda_3)\}$ can be any functions of their respective arguments, such that the integral exists. In (1.8.29),

$\{\sigma_1, \sigma_2, \sigma_3, \zeta_1, \zeta_2, \zeta_3\}$ are non-negative integers, $\{\alpha_1, \alpha_2, \alpha_3\}$ are as in (1.8.26) and $\{i, j, k\}$ can be any permutation of $\{1, 2, 3\}$.

In the C++ framework developed by Todd, it is not possible to evaluate the integral (1.8.26) for arbitrary choices of $\{u_{12}, u_{13}, u_{23}, w_{12}, w_{13}, w_{23}\}$. However, it can be shown with the help of (1.3.6), (1.3.7), (1.3.10) and (1.3.11) that all of the integrals required in Kohn calculations using $\Psi_t^{(1,A)}$ that cannot be evaluated analytically, can be evaluated numerically in terms of Y integrals (1.8.26) using this framework. Further, in the same way it can be shown that all of the integrals required in Kohn calculations using $\Psi_t^{(1,B)}$ that cannot be evaluated analytically, can be evaluated numerically in terms of Y integrals (1.8.26) and $\mathcal{V}$ integrals (1.8.29) using this framework.

Neither $\psi_G^{(A)}$ nor $\psi_G^{(B)}$ contain Hylleraas-type terms in ρ_{12}. Although terms of this kind greatly improve the speed at which the description of interelectronic correlations converges, their inclusion in scattering trial functions containing $\Omega^{(1)}$ introduces a difficulty into the Kohn calculations. Specifically, in the case of trial functions of the form (1.7.3), it would be necessary to evaluate integrals between open and closed-channel parts of the trial function of a similar form to (1.8.29), but for the inclusion in the integrand of an additional function in λ_3, equal to one of the open-channel functions: S, C or χ_0. Determining integrals of this form would necessitate an extension to the computational framework used in the calculations. In chapter 8, we will discuss this problem in more detail.

Chapter 2

Calculation of Scattering Parameters

2.1 Introduction

In this chapter, we will present preliminary Kohn calculations of scattering parameters using the two trial functions, $\Psi_t^{(1,A)}$ and $\Psi_t^{(1,B)}$, introduced in the previous chapter. We will compare the results obtained with each trial function and briefly discuss the reliability of the calculations with respect to the accuracy of the approximate target wavefunction used in each case.

In an attempt to avoid the problem of Schwartz-type anomalies [14, 47], we will carry out calculations for the choices $\tau = 0$ and $\tau = \pi/2$ in both $\Psi_t^{(1,A)}$ and $\Psi_t^{(1,B)}$. As we have already mentioned, these choices correspond respectively to the Kohn and inverse Kohn methods. For a given value of k, Nesbet [40] and Burke [67] note that, if results obtained using one of these choices of τ are anomalous, in general the results obtained using the other choice will be free of anomalies.

2.2 Calculations of η_v

In figures 2.1 and 2.2, we have plotted values of the Kohn variational phase shift approximation, $\eta_v \in (-\pi/2, \pi/2]$, in radians and as a function of positron momentum, k, obtained respectively with $\Psi_t^{(1,A)}$ and $\Psi_t^{(1,B)}$. In each figure, we have included results for the cases $\tau = 0$ and $\tau = \pi/2$, together with results taken from table 2(e) and table 2(h) of the account given by Armour and Baker [28]. These earlier calculations were, hitherto, the most accurate $(e^+ - H_2)$ Kohn calculations to consider open-channel functions of the form (1.7.5) and (1.7.6), correlation functions of the form (1.7.8) and only the lowest partial wave of Σ_g^+ symmetry. They were carried out using the method of models and were the first Kohn calculations on the $(e^+ - H_2)$ system to include Hylleraas-type correlation functions in the electron-positron distance. The authors used a generalisation of the Kohn variational method to avoid the difficulties associated with Schwartz singularities, which we will discuss in more detail in the following chapter.

In the figures, we consider 40 values of the positron momentum equidistant in the range $k = 0.01\ a_0^{-1}$ to $k = 0.4\ a_0^{-1}$, where a_0 is the Bohr radius. The value of $k = 0.4\ a_0^{-1}$ corresponds to a positron energy of ~ 2 eV. Above this energy, Armour and coworkers [29] found that contributions from higher partial waves become significant in describing scattering processes. In general, we will henceforth omit explicit reference to a_0^{-1} as the unit of measurement for k since, by definition, it is equal to unity in Hartree atomic units.

Figures 2.1 and 2.2 illustrate a number of important features. Firstly, in both figures there is generally broad agreement between the values of η_v obtained at $\tau = 0$ and those obtained at $\tau = \pi/2$. However, we do observe a number of

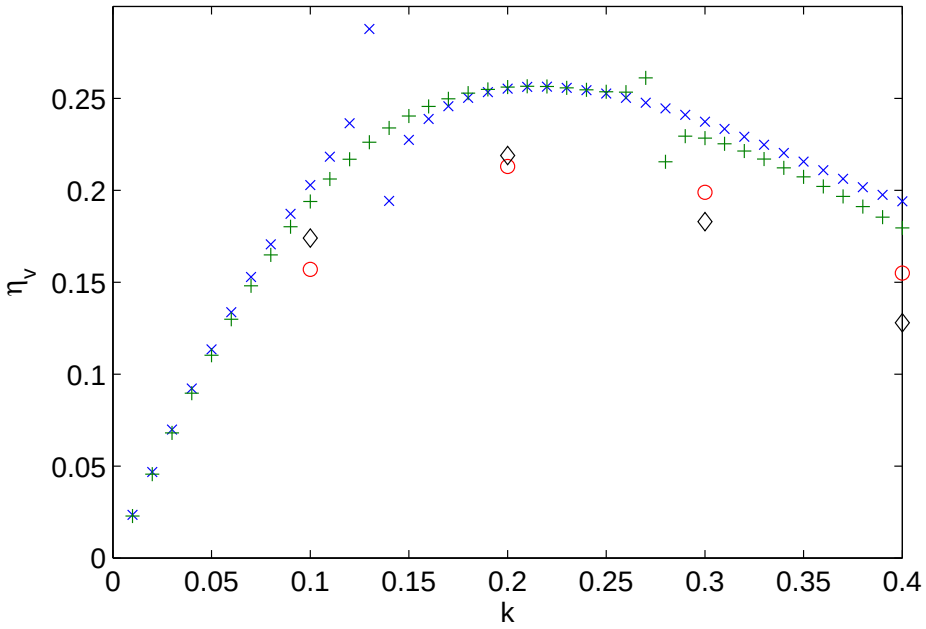

Figure 2.1: Values of [×] $\eta_v\,(k;\tau=0)$ and [+] $\eta_v\,(k;\tau=\pi/2)$ for $\Psi_t^{(1,A)}$, with results from [○] table 2(e) and [◇] table 2(h) in [28].

anomalies in the results. In figure 2.1, calculations carried out at $\tau = 0$ diverge from those carried out at $\tau = \pi/2$ in the region around $k \simeq 0.13$. Calculations carried out at $\tau = \pi/2$ diverge from those carried out at $\tau = 0$ in the region around $k \simeq 0.28$. Analogous effects are observed in figure 2.2, respectively in the regions around $k \simeq 0.14$ and $k \simeq 0.28$. In both figures, at each value of k at least one of the choices of τ appears to give a result which is free of anomalous behaviour.

Away from the anomalous results, inspection of the figures shows that the values of η_v obtained with $\Psi_t^{(1,A)}$ are, in general, appreciably higher than those obtained with $\Psi_t^{(1,B)}$. Moreover, the values of η_v calculated by Armour and Baker [28] typically lie somewhere between the values obtained with $\Psi_t^{(1,A)}$ and those obtained with $\Psi_t^{(1,B)}$. The likely cause of the discrepancies in the results

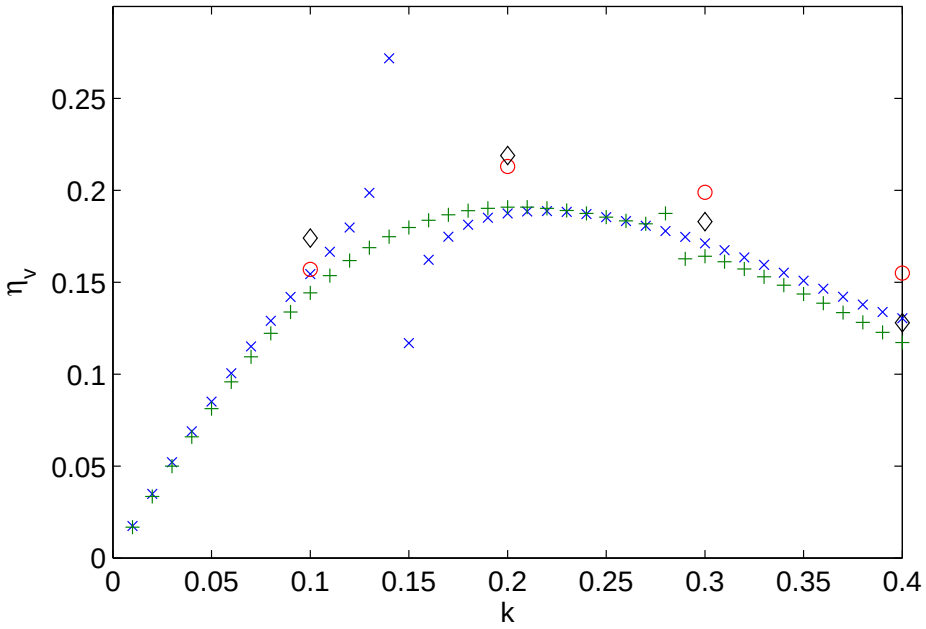

Figure 2.2: Values of [×] $\eta_v\,(k;\tau=0)$ and [+] $\eta_v\,(k;\tau=\pi/2)$ for $\Psi_t^{(1,B)}$, with results from [○] table 2(e) and [◇] table 2(h) in [28].

for $\Psi_t^{(1,A)}$ and $\Psi_t^{(1,B)}$ is the difference in the accuracy of the target wavefunction used in each case. As we have discussed, the calculations carried out with $\Psi_t^{(1,A)}$ use the method of models and a relatively inaccurate target wavefunction. The calculations carried out with $\Psi_t^{(1,B)}$ treat the target potential (1.3.11) explicitly and make use of a much more accurate target wavefunction. The results shown in figures 2.1 and 2.2 give an early indication that the relative accuracy of the target wavefunction has a significant effect on the calculations and, further, that the values of η_v obtained using the method of models may be artificially large because of these effects. We will discuss this possibility further in chapter 8.

We remark in passing that the anomalies appearing in figures 2.1 and 2.2 occur in roughly the same regions of k in each case. Though we do not have a

definitive explanation for this behaviour, it is not entirely unexpected since the two trial functions share a common set of short-range correlation functions and their dependence on τ is the same. The major difference between the two trial functions is the approximate target wavefunction used in each case; thus, the figures offer some evidence that the target wavefunction does not have a very significant role to play in determining the appearance of anomalous behaviour.

2.3 Calculations of σ_v

In terms of practical application, theoretical calculations of scattering cross sections are more immediately useful than calculations of scattering phase shifts, since they can readily be compared with experimental data. At low energies, Armour [23] points out that approximate values, σ_v, of the total scattering cross section can be obtained from

$$\sigma_v = \frac{4\pi}{k^2} \sin^2(\eta_v) . \tag{2.3.1}$$

However, in our calculations we are most interested in very low positron energies, typically having $k < 0.1$. At these energies, there is a paucity of experimental cross section data for $(e^+ - H_2)$ scattering, making a meaningful comparison with our results very difficult.

Nevertheless, for completeness, in figures 2.3 and 2.4 we have plotted values of $\sigma_v(k)$ for $0.01 \leq k \leq 0.4$, obtained using (2.3.1) respectively for Kohn calculations involving $\Psi_t^{(1,A)}$ and $\Psi_t^{(1,B)}$. Values of σ_v are here measured in units of πa_0^2. We have again included results for the choices $\tau = 0$ and $\tau = \pi/2$, as well

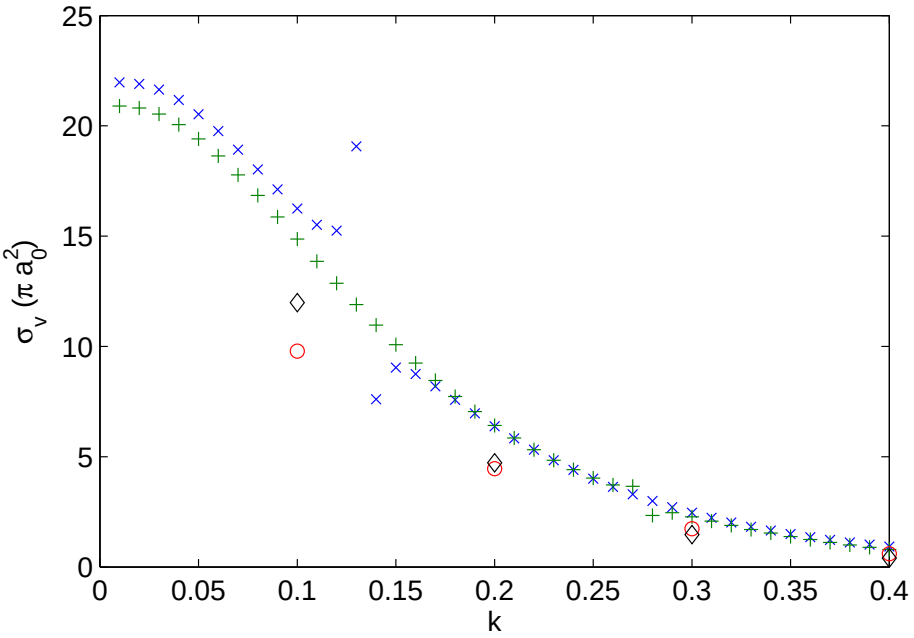

Figure 2.3: Values of [×] $\sigma_v\,(k;\tau=0)$ and [+] $\sigma_v\,(k;\tau=\pi/2)$ for $\Psi_t^{(1,A)}$, with results corresponding to [○] table 2(e) and [◇] table 2(h) in [28].

as the results corresponding to table 2(e) and table 2(h) of the account given by Armour and Baker [28]. Those authors note that their results are broadly in agreement with the experimental results of Hoffman *et al.* [76] and Charlton *et al.* [77] for the range of k we have considered here, although we again point out the lack of experimental data available for $k < 0.1$.

The anomalous results present in figures 2.1 and 2.2 appear also in figures 2.3 and 2.4. Moreover, as in the earlier figures, the results obtained with $\Psi_t^{(1,A)}$ are generally higher than those obtained with $\Psi_t^{(1,B)}$; this effect is particularly striking towards the lower end of the range of k under consideration. The values determined from the calculations of Armour and Baker [28] lie between the results for our two trial functions.

The results shown in figures 2.3 and 2.4 reinforce the need for further investiga-

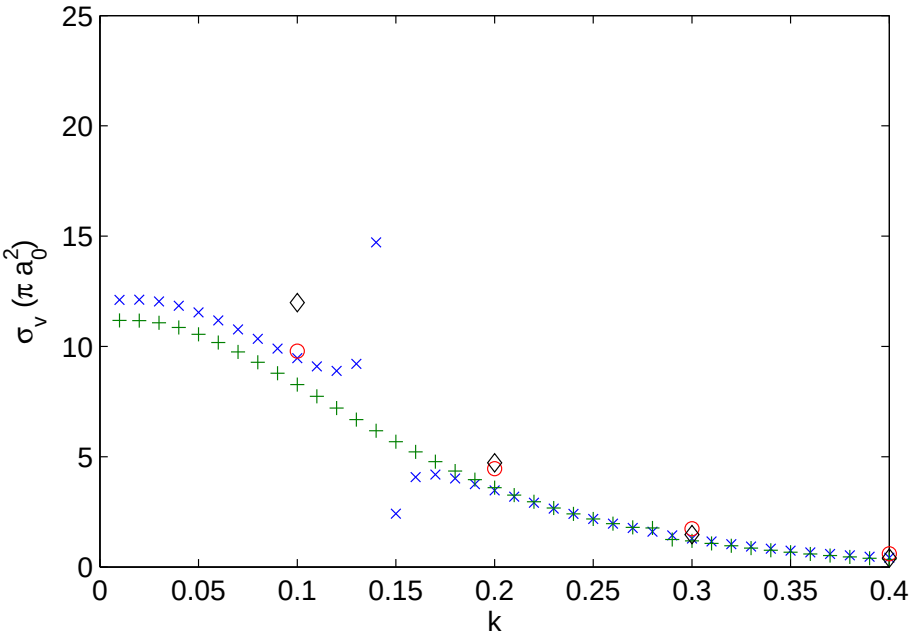

Figure 2.4: Values of [×] $\sigma_{\rm v}\,(k;\tau=0)$ and [+] $\sigma_{\rm v}\,(k;\tau=\pi/2)$ for $\Psi_{\rm t}^{(1,{\rm B})}$, with results corresponding to [○] table 2(e) and [◇] table 2(h) in [28].

tion of two aspects of our Kohn variational calculations. Firstly, it is important to establish a framework in which the anomalous results we have observed here can be formally examined. Secondly, we should consider in more detail the effects of varying the accuracy of the target wavefunction. We will address both of these points in the following chapters.

2.4 Conclusions

We have carried out the first Kohn calculations for the $(e^+ - {\rm H}_2)$ system in which the interelectronic potential in the H_2 target is considered explicitly. This has allowed for the inclusion of a much more accurate target wavefunction than is presently possible in our Kohn calculations using the method of models. We

have found evidence to suggest that this improvement in target accuracy has a significant effect on the calculations of η_v and σ_v.

We have found that anomalies appear in the results of Kohn calculations carried out with $\Psi_t^{(1,A)}$ and with $\Psi_t^{(1,B)}$, but that these anomalies are apparently avoidable with an appropriate choice of τ. We will begin a more detailed investigation of this problem in the next chapter.

We have presented calculations of total scattering cross sections, σ_v, although there is a lack of experimental data with which to compare these results at the very low positron energies in which we are most interested. In the following chapters, we will avoid further calculations of σ_v and focus on methods of developing consistently reliable calculations of η_v. In chapter 6, we will begin to carry out calculations of the Z_{eff} parameter, for which comparisons with experiment at very low energies can be made more easily.

Chapter 3

The Generalised Kohn Method

3.1 Introduction

In this chapter, we will extend our application of the Kohn variational method to consider more general variations of the parameter, τ. As we have already noted, this parameter is of only minor physical significance, playing the role of an additive phase constant in the part of the trial wavefunction representing incident and scattered positrons asymptotically far from the target. From a purely physical point of view, for a sufficiently accurate trial wavefunction we would not expect the value of τ to have a significant effect on calculations of scattering parameters such as the phase shift approximation, η_v. Nevertheless, as we saw in the previous chapter, the choice of τ can be an important factor in obtaining consistent results from Kohn calculations. We shall now investigate this phenomenon in more detail.

It has been widely documented that the matrix equations derived from the

Kohn variational principle are inherently susceptible to spurious singularities. The singularities arise when the coefficient matrix, A, of the Kohn equations (1.7.35) is singular. These singularities were discussed first by Schwartz [14, 47] and have subsequently attracted considerable attention [40–46]. In the region of the spurious singularities, results of Kohn calculations can be anomalous.

Although sharing characteristics similar to those exhibited by scattering resonances [42], Schwartz singularities are nonphysical and arise only because the Kohn trial wavefunction is inexact [78]. For projectiles of a given energy, anomalous results are confined to particular formulations of the trial wavefunction and can, in principle, be avoided by a small change in boundary conditions or some other parameter. For example, we will find that an appropriate choice of $\tau \in [0, \pi)$ in (1.7.3) can usually be made to minimise the effects of Schwartz singularities at a given positron energy.

It is the purpose of this chapter to demonstrate that Schwartz singularities are a general feature of our calculations on $(e^+ - H_2)$ scattering and to discuss mechanisms by which the associated anomalies can be avoided. In the course of our analysis, we will encounter a number of results that cannot be explained without further, more detailed investigation. Consequently, this chapter will act as a preliminary to a more rigorous analysis of Schwartz singularities, to be given in chapters 4 and 5.

We have carried out Kohn calculations involving explicit consideration of the target potential and using the trial wavefunction, $\Psi_t^{(1,B)}$. An equivalent investigation for our method of models calculations using $\Psi_t^{(1,A)}$ could be carried out without additional difficulty, although we have not done so here. The reason for this is that, since $\Psi_t^{(1,A)}$ and $\Psi_t^{(1,B)}$ have the same dependence on τ, we

would not expect such an analysis to provide any new insight.

We will investigate, with some success, methods of choosing τ to avoid Schwartz-type anomalies, although we will also give examples of anomalous behaviour which cannot satisfactorily be addressed by any choice of τ. The origin of these persistent anomalies, along with those of several other results obtained in this chapter, will be explained in chapter 4.

Throughout this chapter, we have chosen values of $\alpha = 0.6$ and $\beta = 1.0$ for the nonlinear parameters found in the short-range correlation functions (1.7.8). This choice of the nonlinear parameters has been made only to highlight the interesting aspects of Schwartz-type anomalies more clearly. For the same reason, we have also found it instructive to carry out Kohn calculations at higher values of k than were considered in chapter 2. It is not our intention to compare these results with experimental data, since higher partial waves than the one considered here will make a significant contribution to scattering processes above $k \simeq 0.4$ [29]. In fact, we will avoid any comparison with experimental results for the following three chapters, concentrating instead on developing an understanding of Schwartz-type behaviour abstracted away from the physical considerations of the $(e^+ - H_2)$ system.

3.2 Schwartz singularities

For Kohn calculations carried out with trial wavefunctions of the form (1.7.3), singularities arise from zeros of $\det(A)$, the determinant of (1.7.36). Under these circumstances, as discussed in chapter 1, the linear system (1.7.35) either has no unique solution or, more probably, no solution at all. For nonsingular

A, anomalies in the evaluation of η_v can appear when the value of a prescribed parameter in the Kohn trial function is close to a value making A singular. The precise cause, or causes, of these anomalies are not immediately obvious and we will not speculate upon them in this chapter. A detailed investigation of the underlying conditions giving rise to the anomalous behaviour will be made in the next chapter.

For $\Psi_t^{(1,B)}$, we have obtained values of $\eta_v \in (-\pi/2, \pi/2]$ using (1.7.35) and (1.7.40), for positron momenta in the range $0.01 \leq k \leq 1$. At each k, the value of $\det(A)$ is a function of τ, so that variations in this parameter can be made to avoid zeros of $\det(A)$. Hence, the effects of Schwartz singularities can conceivably be accounted for by performing calculations over p different values of τ equidistant in the range $\tau \in [0, \pi)$. For the results presented here, we have taken $p = 1001$. Calculations for a large number of τ values can be carried out with minimal additional computational effort as the matrix elements of A (1.7.36) and b (1.7.37) for any τ are readily available from the elements of $A(\tau = 0)$ and $b(\tau = 0)$ via the orthogonal transformation (1.7.44). It is useful to carry out calculations for large p such as this as it allows a detailed examination of the behaviour of η_v very close to Schwartz singularities to be made.

In the account given by Shimamura [42], it is noted that phase shifts passing through a Schwartz singularity can be regarded as changing rapidly by nearly π. This behaviour is also characteristic of a physical resonance; indeed, Shimamura refers to Schwartz-type anomalies as 'pseudoresonances'. In our calculations, we have imposed the restriction $\eta_v \in (-\pi/2, \pi/2]$, where $\eta_v(\tau)$ is periodic in τ with period π. A rapid increase in phase shift by nearly π, in the formalism used by Shimamura, is here equivalent to the following: In the region of a Schwartz singularity, the value of $\eta_v(\tau)$ increases rapidly towards

$+\pi/2$ with increasing τ. In the limit as $\eta_v \to +\pi/2$, there is a discontinuity, beyond which the value of $\eta_v(\tau)$ increases rapidly away from $-\pi/2$, tending towards $\eta_v(\tau = 0)$ as $\tau \to \pi$. The discontinuity in $\eta_v(\tau)$ occurs at a value, τ_d, so that

$$\lim_{\tau \to \tau_d -} [\eta_v(\tau)] = -\lim_{\tau \to \tau_d +} [\eta_v(\tau)] = \frac{\pi}{2}. \tag{3.2.1}$$

Alternatively, a rapid *decrease* in phase shift by nearly π, in the formalism used by Shimamura, would correspond here to values of $\eta_v(\tau)$ decreasing rapidly towards $-\pi/2$ as the discontinuity was approached from below, before decreasing rapidly away from $+\pi/2$ beyond it. However, we have found no behaviour of this second kind in any of our Kohn calculations. The reason for this will be given in the following chapter.

In chapter 4, we will derive a direct correspondence between singularities and the zeros of the function, $\cot(\eta_v - \tau + c)$. Given this relationship, the values, τ_s, making A singular will satisfy

$$\lim_{\tau \to \tau_s} [\eta_v(\tau)] = \left(n + \frac{1}{2}\right)\pi + \tau_s - c, \tag{3.2.2}$$

for some integer, n, chosen to keep $\eta_v \in (-\pi/2, \pi/2]$ in the limit. Inspection of (3.2.1) and (3.2.2) suggests that the values of τ_s and τ_d will not, in general, coincide. However, because η_v generally changes rapidly with τ as it passes through a Schwartz singularity, there typically exists a value of τ_s close to a value of τ_d. Hence, from a graphical point of view, the discontinuities serve as useful landmarks in locating regions of τ containing Schwartz singularities.

To illustrate these ideas more clearly, the calculated values of η_v for $\Psi_t^{(1,B)}$ over

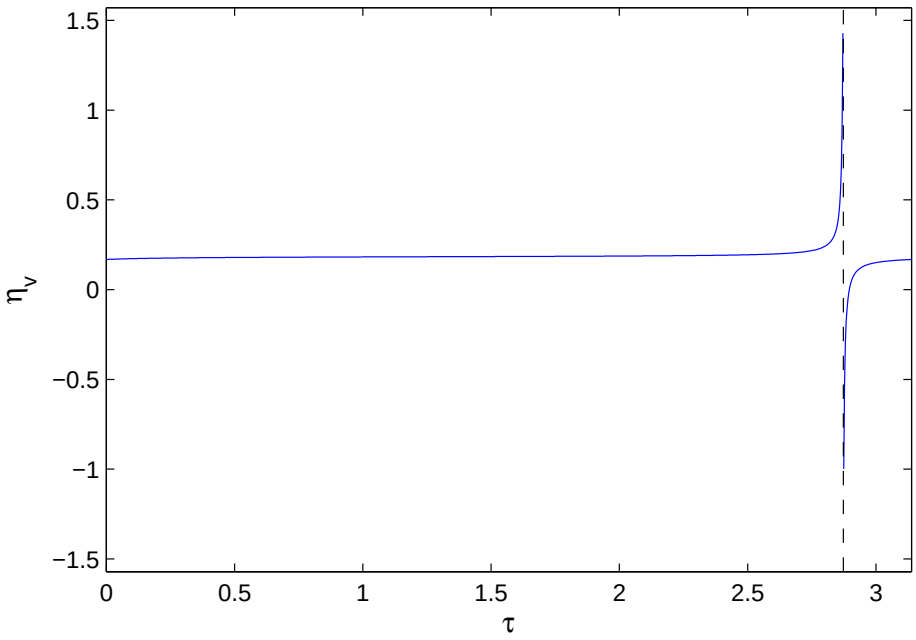

Figure 3.1: Values of $\eta_v(\tau)$ for $\Psi_t^{(1,B)}$ at $k = 0.2$.

the p values of τ at $k = 0.2$ are given in figure 3.1. The existence of a singularity is confirmed by figure 3.2, which shows the behaviour of $\det(A)$ in the region of the anomalies observed in figure 3.1. The scale on the vertical axis in this second figure is unimportant, since the value of $\det(A)$ at each k can be made arbitrarily large or small by a choice of the normalisation constant, N, in $\Psi_t^{(1,B)}$. The feature of interest in the figure is that it shows $\det(A)$ passing through zero at $\tau \simeq 2.87$, corresponding to the anomalous region in figure 3.1, in which we have indicated the value of τ giving rise to the singularity by a dashed line. Away from this value of τ, figure 3.1 shows only small variations in η_v over τ.

We have investigated the behaviour of $\eta_v(\tau)$ at different values of k. To illustrate the observed anomalies in η_v, it is convenient to define the function,

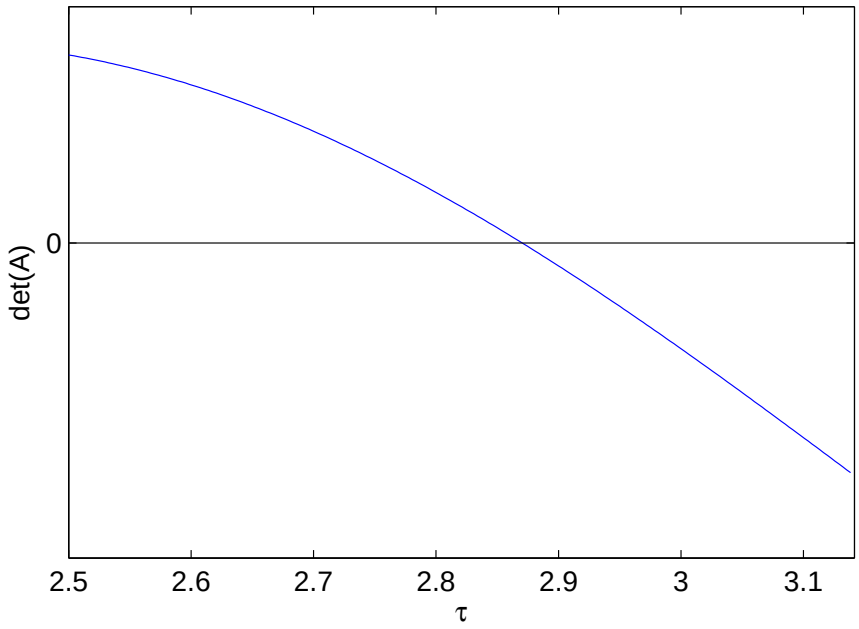

Figure 3.2: The dependence of det (A) on τ near a Schwartz singularity, for $\Psi_t^{(1,B)}$ at $k = 0.2$.

$$\Delta(k,\tau) = |\eta_v(k,\tau) - \langle\eta_v\rangle(k)|, \tag{3.2.3}$$

where, at each k, $\langle\eta_v\rangle$ is the median value of $\eta_v(\tau)$ evaluated over the p values of τ. $\Delta(k,\tau)$ measures the degree to which a given $\eta_v(k,\tau)$ can be considered anomalous. The values of $\Delta(k,\tau)$ for $\Psi_t^{(1,B)}$ are shown in figure 3.3 for 50 values of k equidistant in the range $0.02 \leq k \leq 1$.

It is clear from the figure that Schwartz-type anomalies are distributed about a family of four well-defined paths in the (k,τ) plane. Further, there are regions along these paths where anomalous results are apparently suppressed, so that there exist values of k for which no noticeable anomalies are observed for any of the p values of τ considered here. This effect can be investigated further in the following way. At each k, we consider the distribution of $\eta_v(\tau)$ over the

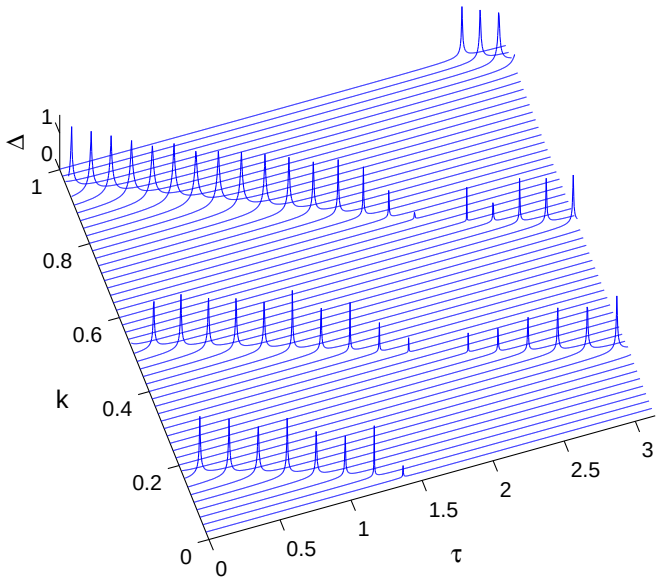

Figure 3.3: Values of $\Delta(k, \tau)$ for $\Psi_t^{(1,B)}$, in the range $0.02 \leq k \leq 1$.

p values of τ. We define $\Pi_1^{99}(k)$ to be the interpercentile range between the first and the 99^{th} percentile of the distribution. $\Pi_1^{99}(k)$ is then an alternative to $\Delta(k, \tau)$ for measuring the magnitude of the anomalies in η_v. We have deliberately chosen to examine an interpercentile range in preference to the full range, $\Pi(k)$, of the distribution of $\eta_v(\tau)$ at a given k. It is more helpful to consider the former case as we have found that $\Pi_1^{99}(k)$ generally varies more smoothly than $\Pi(k)$. The qualitative behaviour of the two functions over k, however, is the same.

A plot of $\Pi_1^{99}(k)$ for $\Psi_t^{(1,B)}$ is given in figure 3.4 for $0.01 \leq k \leq 1$. The minima in this figure, where $\Pi_1^{99}(k)$ is apparently very close to zero, correspond precisely to the regions of figure 3.3 where there are no obvious anomalies at any of the p values of τ. It is also evident from the figure that $\Pi_1^{99}(k)$ oscillates smoothly over k, with the exception of the unexpectedly large value appearing

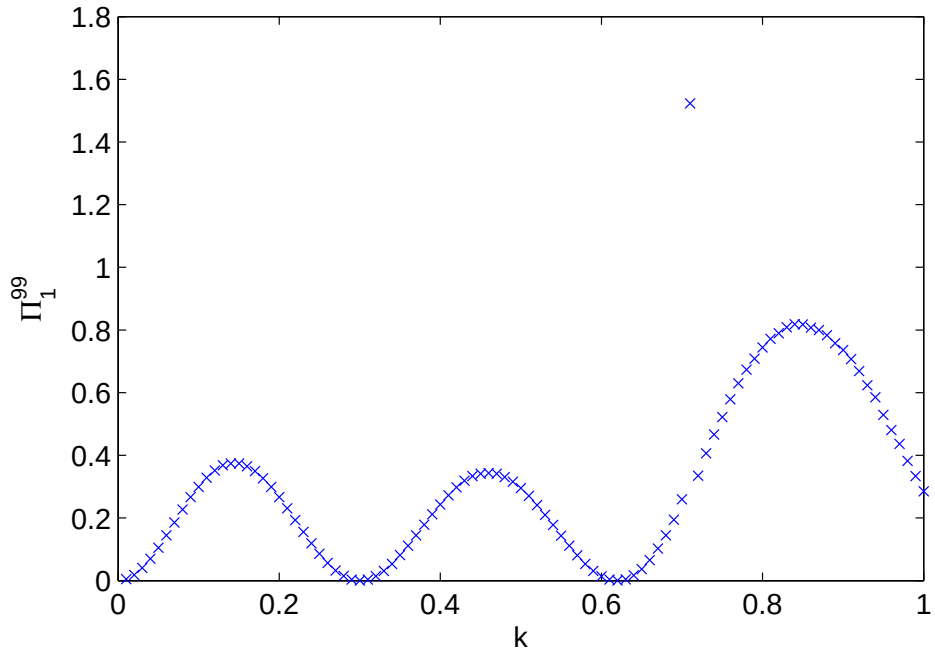

Figure 3.4: Values of $\Pi_1^{99}(k)$ for $\Psi_t^{(1,B)}$, in the range $0.01 \leq k \leq 1$.

at $k = 0.71$. This value of k was not considered in figure 3.3, so this unusual behaviour is absent from those results. In section 3.3 and in the next two chapters, we will discuss the results of Kohn calculations at $k = 0.71$ in greater detail.

We will reserve until chapter 4 a detailed explanation of the general behaviour exhibited in figures 3.3 and 3.4. For now, we note that if k is such that a Schwartz singularity exists for some $\tau \in [0, \pi)$, then (3.2.1) implies

$$\lim_{p \to \infty} [\Pi(k)] = \pi. \tag{3.2.4}$$

Hence, figure 3.4 introduces the notion of the relative width of an anomalous region, measuring the range of τ near a singularity where the associated anomalies in η_v are significant. This width is small if anomalies are confined to a rela-

tively narrow range of τ near the singularity, so that (3.2.4) converges relatively slowly with increasing p. Conversely, the width is large if (3.2.4) converges relatively quickly. For a fixed p, the oscillations shown in figure 3.4 describe qualitatively how the widths of the anomalous regions of τ vary over k.

3.3 Optimisation schemes for τ

Figure 3.3 indicates that there is no single value of τ that avoids anomalies at all values of k. Hence, for our implementation of the generalised Kohn method to be made free of anomalies across the entire energy range under consideration, it is necessary in general to select a different value of τ appropriate to each value of k. This highlights the need for a consistent method of choosing an optimal value of τ from the p available candidates at each k, so as to minimise anomalous behaviour.

In seeking a systematic optimisation scheme for τ that mitigates the effects of Schwartz singularities, it is necessary to clarify the criteria that a successful scheme should satisfy. An obvious requirement is that the peaks in figure 3.3 should be avoided. In addition, though, considerations of physical consistency should be taken into account. The exact phase shift, η, is a continuous function of k and we can reasonably demand that this behaviour be reflected in optimised values of η_{v} over k, in the sense that they should vary as smoothly as possible. At each k, the great majority of the values of τ shown in figure 3.3 correspond to results which are ostensibly free of anomalies. Within these regions of stability, though, small variations in η_{v} over τ still occur. Depending on the characteristics of a given optimisation method, the values of τ chosen to optimise η_{v} at two different values of k may be very different, even if the values

of k are close together. Consequently, for a given scheme, the smoothness of the optimised values of η_v over k is not automatically guaranteed.

In this section, we will propose three different optimisation schemes for τ and evaluate the effectiveness of each. The first scheme we will consider consists of choosing, from the p available candidates, the value of τ giving the maximum value of $|\det(A)|$. This approach is very similar to the method first used in $(e^+ - H_2)$ scattering calculations by Armour [23], who obtained average values of η_v over a range of $(p-r)$ values of τ, after having discarded the $(r < p)$ lowest values of $|\det(A)|$. The usual justification for treatments of this kind is the notion that Schwartz-type anomalies will appear when $\det(A)$ is, in some sense, close to zero. Statements of this type can be misleading; $\det(A)$ can be made arbitrarily close to zero by an appropriate choice of the normalisation constant, N, in the trial wavefunction, without altering the solution of the Kohn equations. That is, there is no well-defined value below which individual values of $|\det(A)|$ can be considered to be close to zero. In practice, however, we have found that choosing τ to maximise $|\det(A)|$ successfully avoids Schwartz-type anomalies at most values of k. The reason for this is that comparing relative values of $|\det(A)|$ at different τ and for a given N, rather than considering values of $|\det(A)|$ in isolation, can be helpful in identifying and avoiding values of τ close to those where singularities occur. Despite this, as we will see, the use of $|\det(A)|$ as an optimisation metric still contains weaknesses.

An alternative method for optimising τ is obtained by considering the functional, $\mathcal{I}[\Psi_t]$ (1.7.19). If the trial wavefunction, Ψ_t, were equal to the exact scattering wavefunction, Ψ, then

$$\mathcal{I}[\Psi_t] = \mathcal{I}[\Psi] = \langle \Psi, \Psi \rangle = 0. \tag{3.3.1}$$

In fact, in the variational method due to Hulthén [21], the equation

$$\langle \Psi_t, \Psi_t \rangle = 0, \tag{3.3.2}$$

is imposed as a requirement for any Ψ_t. The Kohn method does not explicitly demand that this condition be met, as it would lead to a system of $(M+2)$ equations in $(M+1)$ unknowns, from which a consistent solution could not ordinarily be obtained. This problem is avoided in the Hulthén method by omitting the Kohn equation (1.7.33). It seems plausible that Schwartz-type anomalies might best be avoided here by carrying out Kohn calculations over a range of p values of τ before choosing the result giving the smallest value of $|\mathcal{I}[\Psi_t]|$.

In figure 3.5, for $\Psi_t^{(1,B)}$ we compare the optimised values of η_v calculated for $0.01 \leq k \leq 1$ using the two schemes that we have outlined. A number of comments can be made about the results. Firstly, both methods successfully avoid Schwartz-type behaviour in η_v at most values of k. The exception in both cases is the result at $k = 0.71$, where there is an obvious anomaly. This corresponds to the anomaly already observed in figure 3.4 at this value of k. Secondly, away from $k = 0.71$, there are a number of small discontinuities in η_v over k in both sets of results. This demonstrates the relevance of the second criterion described at the beginning of this section, regarding the smoothness of optimised values of η_v over k. The appearance of the discontinuities in figure 3.5 means that neither of our optimisation schemes can be considered wholly satisfactory.

The cause of the discontinuities found in figure 3.5 will be discussed in chapter

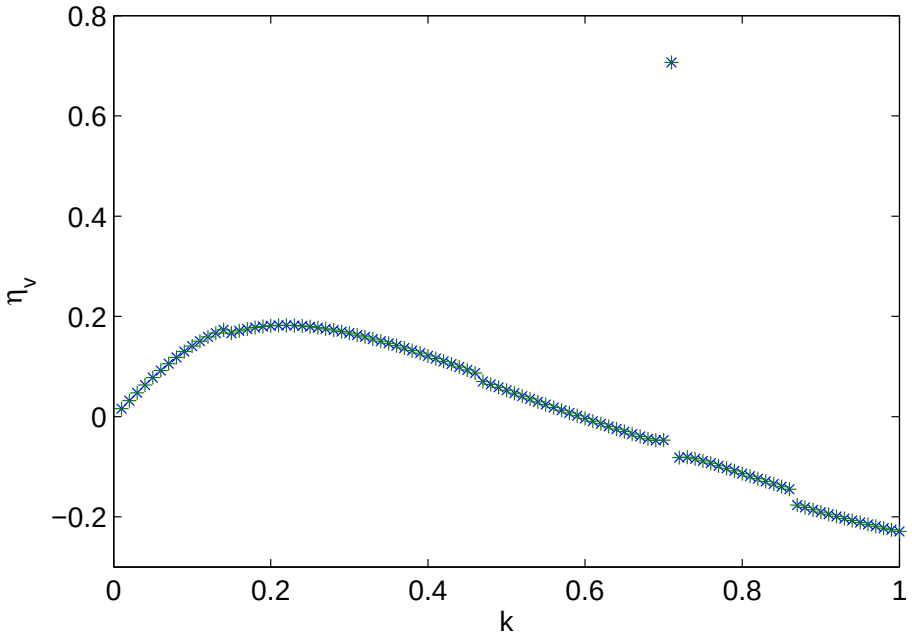

Figure 3.5: Values of $\eta_v(k)$ for $\Psi_t^{(1,B)}$ obtained from two optimisation schemes for τ, [$\times$] maximising $|\det(A)|$ and [+] minimising $|\mathcal{I}[\Psi_t]|$.

4. Here, continuing our inspection of this figure, we see that the discontinuities occur at the same values of k in both curves. Indeed, upon very close inspection, we have found that the results of the two optimisation schemes appear to be the same at all values of k. After some considerable effort, it is possible to show that

$$\det(A) \neq 0 \Rightarrow \det(A)\,\mathcal{I}[\Psi_t] = \Theta(k,\tau), \tag{3.3.3}$$

where $\Theta(k,\tau)$ is some function which depends on k but not on τ. Here, Ψ_t can be any trial function of the form (1.7.3) or (1.8.14). The result holds for any choice of the short-range correlation functions in Ψ_t, as well as for any form of the target wavefunction, ψ_G, provided that they are both taken to be independent of τ. A proof of (3.3.3) is given in appendix C.

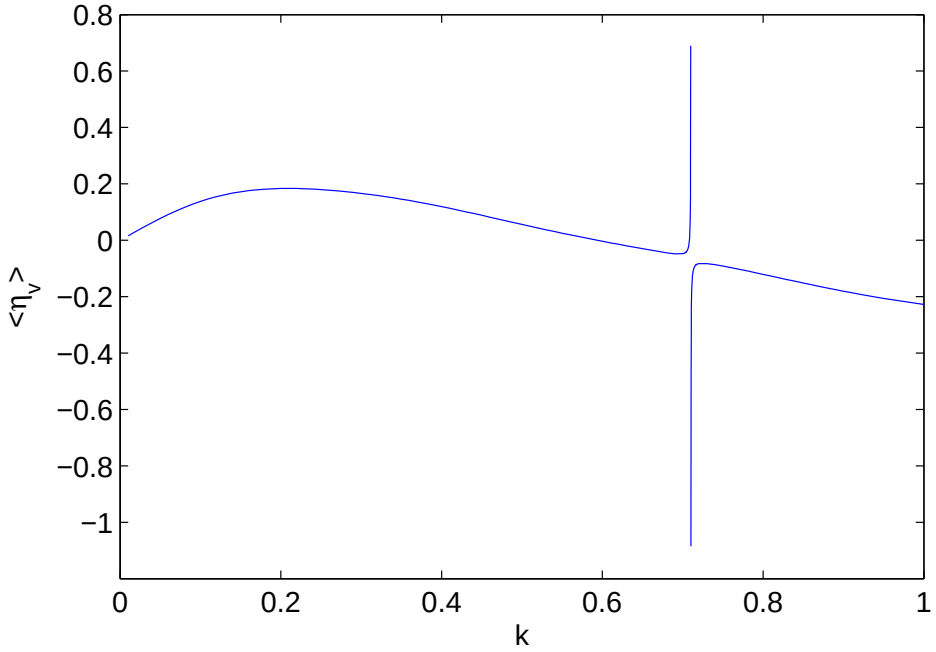

Figure 3.6: Values of $\langle \eta_v \rangle (k)$ for $\Psi_t^{(1,B)}$, in the range $0.01 \leq k \leq 1$.

For the present investigation, the most important consequence of (3.3.3) is that, since Θ is a constant at each k, it follows immediately that the methods of choosing τ either to maximise $|\det(A)|$ or to minimise $|\mathcal{I}[\Psi_t]|$ are indeed precisely equivalent. In the following chapter, we will find that (3.3.3) has a number of other interesting implications with regard to Schwartz-type behaviour.

Lastly, we consider a third optimisation method. If our Kohn calculations have been carried out with a sufficiently large value of p, choosing the median value, $\langle \eta_v \rangle$, at each k should allow anomalies due to Schwartz singularities to be avoided. The reasoning for this is simply that the values of the median are resistant to outliers in the distribution of η_v over τ at each k. We have plotted the function $\langle \eta_v \rangle (k)$ for $\Psi_t^{(1,B)}$ in figure 3.6, for $0.01 \leq k \leq 1$.

We can see from figure 3.6 that choosing τ to give $\langle \eta_v \rangle$ successfully avoids

anomalies at most values of k. Moreover, the small discontinuities appearing in figure 3.5 are not present in figure 3.6, so we can justifiably claim a preference for this method over the others we have presented here. However, the anomaly at $k = 0.71$ remains. We have illustrated this persistent anomaly in more detail by including in the figure the results of a further 100 Kohn calculations in the region $0.7 \leq k \leq 0.72$.

The resistance of the median to outliers in the distribution indicates that the value of $\langle \eta_v \rangle$ at $k = 0.71$ in figure 3.6 is not anomalously large when compared to values of η_v at other values of τ for this value of k. This is confirmed in figure 3.7, a plot of $\eta_v(\tau)$ for $\Psi_t^{(1,B)}$ at $k = 0.71$. The median value of η_v at $k = 0.71$ is indicated by a dashed line. The behaviour of $\eta_v(\tau)$ at $k = 0.71$ is qualitatively the same as that observed at other values of k, with a Schwartz singularity at $\tau \simeq 1.58$ and only small variations in η_v over τ far away from this singularity. Within this context, choosing $\langle \eta_v \rangle$ at $k = 0.71$ can thus be considered a successful optimisation of τ, in as much as it avoids the anomalous behaviour near $\tau \simeq 1.58$. The problem here is that the value of $\langle \eta_v \rangle$ at $k = 0.71$ is anomalous when compared to the corresponding results at nearby values of k, and the optimisation schemes we have considered do not explicitly take variations of k into account.

It is conceivable that the result at $k = 0.71$ in figure 3.6 is related to a resonance phenomenon, whose similarities to Schwartz-type anomalies have long been recognised [42]. However, in the following chapters, we will argue that persistent anomalies of the kind we have observed here are nonphysical, by discussing the mathematical conditions under which they might arise and establishing how they may be avoided via small changes in parameters of the Kohn trial function other than τ.

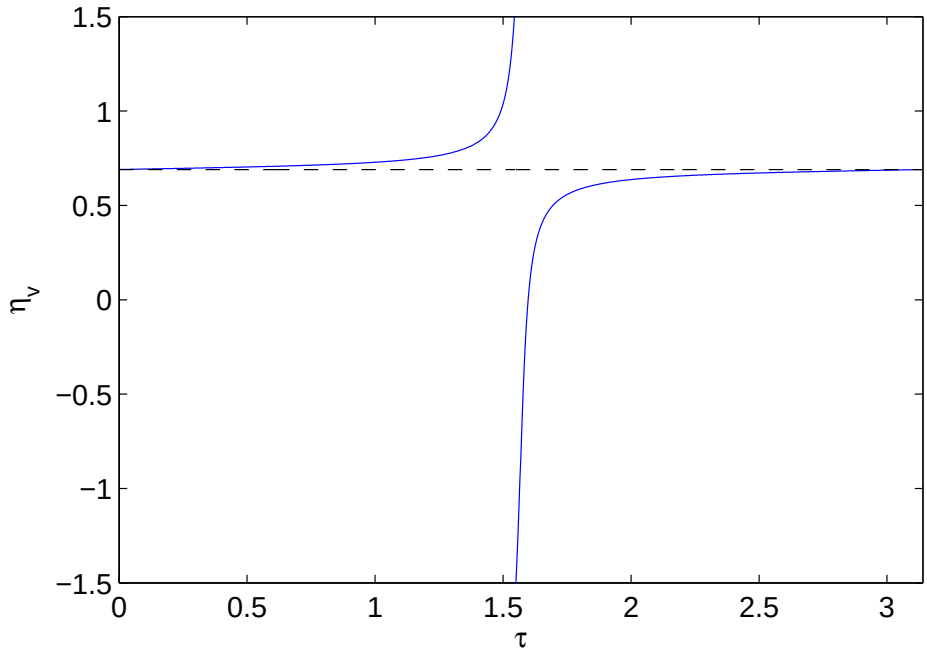

Figure 3.7: Values of $\eta_v(\tau)$ for $\Psi_t^{(1,B)}$ at $k = 0.71$.

3.4 Conclusions

Having conducted an empirical investigation of Schwartz singularities and related anomalies in our calculations of η_v, several conclusions can be drawn. Firstly, although we have found that Schwartz-type behaviour is an inherent feature of our application of the Kohn method, the smooth paths apparent in figure 3.3 suggest that anomalies appear at predictable points in the calculation. This is indicative of a structure that a more rigorous analysis might reveal in greater detail.

Secondly, the minima observed in figure 3.4 show that there are certain values of k for which anomalous values of η_v are confined to extremely narrow ranges of τ. Conversely, figures 3.5, 3.6 and 3.7 point to the existence of anomalies at certain values of k which cannot satisfactorily be avoided with any choice of τ.

It might be possible to explain both of these findings through further analysis.

We have evaluated three candidate optimisation schemes for τ and have found that choosing the median value, $\langle \eta_{\mathrm{v}} \rangle$, of η_{v} over τ gives the most consistent results. It is, however, important to determine whether or not the continued presence of the anomalous region around $k = 0.71$ in figure 3.6 is a genuine example of Schwartz-type behaviour, or has instead some physical meaning.

We have yet to explore the underlying processes giving rise to the anomalies that we have observed. For this reason, as well as for those given above, a deeper investigation of Schwartz singularities is needed; this is the purpose of the following two chapters.

Chapter 4

Formal Analysis of Singular Behaviour

4.1 Introduction

In this chapter, we will develop in greater detail the concepts introduced in chapter 3. In particular, we will find that the determinant of the Kohn matrix, A (1.7.36), can be expressed as a simple analytical function of the phase parameter, τ. An interesting feature of our analysis is that, using this function, it is possible to find zeros of $\det(A)$ that do not correspond to anomalous results in the Kohn calculations. We will argue that, from a physical point of view, these singularities occur legitimately within the framework of the calculation. Moreover, we find that choosing τ to produce such singularities can actually form the basis of an efficient optimisation scheme for automatically avoiding anomalous behaviour in the calculation of the phase shift approximation.

We will show that the origin of the anomalous behaviour in our Kohn calculations can be determined directly from analytic considerations. In particular, the key result (3.3.3) can be used to deduce a simple expression for the partial derivative, $\frac{\partial \eta_v}{\partial \tau}$, from which some of the results observed in the last chapter can be explained. This expression for the derivative also leads to the development of another optimisation scheme for τ since, at each k, it allows the point at which η_v varies most slowly with τ to be found.

Our analysis will provide insight into the processes giving rise to the persistent anomalous behaviour seen in the last chapter, as well as explaining the existence of those values of k for which values of $\eta_v(\tau)$ appear ostensibly free of anomalies at all values of τ under consideration.

As before, we will focus our investigation only on Kohn calculations in which the target potential is included explicitly. However, without any significant modifications, our analysis could equally well be applied to our method of models calculations involving $\Psi_t^{(1,A)}$. We will consider the trial wavefunction, $\Psi_t^{(1,B)}$, taking the values of α and β in (1.7.8) to be fixed at $\alpha = 0.6$ and $\beta = 1.0$. Throughout this chapter and the next, we will implicitly make use of the Hermiticity properties (1.7.24)-(1.7.29).

4.2 An analytical expression for $\det(A)$

From the Laplace expansion of $\det(A)$ along the first row of A (1.7.36), then subsequently along the first column of each resulting submatrix of A, it is easily shown using (1.7.4) that

$$\begin{aligned}\det(A) &= \mathcal{P}(k)\langle\bar{C}\psi_G,\bar{C}\psi_G\rangle + \mathcal{Q}(k)\langle\bar{C}\psi_G,\chi_0\psi_G\rangle^2 \\ &+ \sum_{i=1}^{M}\mathcal{R}_i(k)\langle\bar{C}\psi_G,\chi_0\psi_G\rangle\langle\bar{C}\psi_G,\chi_i\rangle \\ &+ \sum_{i=1}^{M}\sum_{j=1}^{M}\mathcal{S}_{ij}(k)\langle\bar{C}\psi_G,\chi_i\rangle\langle\bar{C}\psi_G,\chi_j\rangle \\ &= \mathcal{A}(k)\sin^2(\tau) + \mathcal{B}(k)\sin(\tau)\cos(\tau) + \mathcal{C}(k)\cos^2(\tau), \quad (4.2.1)\end{aligned}$$

where $\mathcal{A}(k)$, $\mathcal{B}(k)$, $\mathcal{C}(k)$, $\mathcal{P}(k)$, $\mathcal{Q}(k)$, $\mathcal{R}_i(k)$ and $\mathcal{S}_{ij}(k) = \mathcal{S}_{ji}(k)$ are constants with respect to variations in τ. For a given k, the constants, $\mathcal{A}(k)$, $\mathcal{B}(k)$ and $\mathcal{C}(k)$, can be determined by calculating $\det(A)$ directly from (1.7.36) at particular values of τ. Indeed, at each k, it is clear that

$$\mathcal{C}(k) = \det(A;\tau=0), \quad (4.2.2)$$

$$\mathcal{A}(k) = \det\left(A;\tau=\frac{\pi}{2}\right), \quad (4.2.3)$$

$$\mathcal{B}(k) = 2\det\left(A;\tau=\frac{\pi}{4}\right) - \mathcal{A}(k) - \mathcal{C}(k). \quad (4.2.4)$$

At each k, provided that $\mathcal{A}(k) \neq 0$, the values, τ_s, making A singular can then be found by solving the quadratic equation in $\tan(\tau_s)$,

$$\mathcal{A}(k)\tan^2(\tau_s) + \mathcal{B}(k)\tan(\tau_s) + \mathcal{C}(k) = 0. \quad (4.2.5)$$

If $k = k_a$ such that $\mathcal{A}(k_a) = 0$, then A is made singular at $\cos(\tau_s) = 0$ and, unless $\mathcal{B}(k_a) = 0$, at $\tan(\tau_s) = -\mathcal{C}(k_a)/\mathcal{B}(k_a)$.

If only τ is varied, and unless $k = k_z$ such that $\mathcal{A}(k_z) = \mathcal{B}(k_z) = \mathcal{C}(k_z) = 0$, at each k there will be no more than two zeros of $\det(A)$ in the range $\tau \in [0,\pi)$. If

$k = k_z$, then $\det(A; k = k_z)$ is identically zero and a unique value of η_v cannot be determined from the Kohn equations at any value of τ. In practice, we have found no value of $k = k_z$ in our calculations. Nevertheless, for completeness, we define

$$Z = \{k_z \in \mathbb{R} : \mathcal{A}(k_z) = \mathcal{B}(k_z) = \mathcal{C}(k_z) = 0\}. \tag{4.2.6}$$

To ensure that our Kohn calculations can always be implemented consistently for some choice of τ, we will henceforth consider only values of $k \in \mathbb{R} \setminus Z$ rather than $k \in \mathbb{R}$, although for brevity we will not usually mention this distinction explicitly.

If only τ is varied, the extrema of $\det(A)$ at a given k can be found from the requirement

$$\frac{\partial}{\partial \tau}[\det(A)] = 0, \tag{4.2.7}$$

so that, if we denote by τ_m the values making $\det(A)$ stationary with respect to variations only in τ, after differentiating (4.2.1) we can rewrite (4.2.7) as

$$[\mathcal{A}(k) - \mathcal{C}(k)] \sin(2\tau_m) + \mathcal{B}(k) \cos(2\tau_m) = 0. \tag{4.2.8}$$

In the special case where $k = k_c$, such that $\mathcal{B}(k_c) = 0$ and $\mathcal{A}(k_c) = \mathcal{C}(k_c)$, we have

$$\det(A; k = k_c) = \mathcal{A}(k_c), \tag{4.2.9}$$

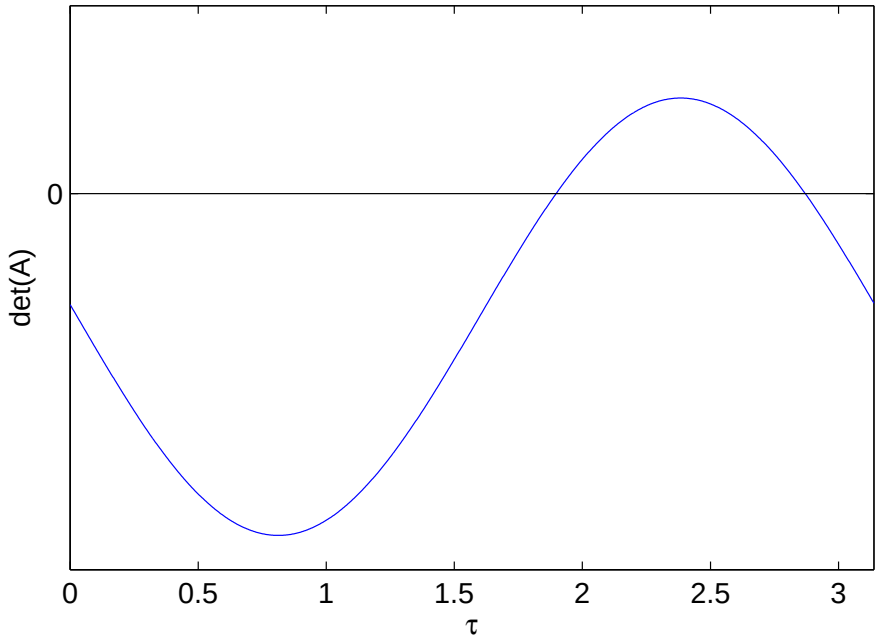

Figure 4.1: The dependence of det (A) on τ for $\Psi_t^{(1,B)}$ at $k = 0.2$.

which is everywhere constant with respect to variations in τ. In practice, we have found no value of $k = k_c$ in our calculations. If $k \neq k_c$, inspection of (4.2.8) shows that there will be exactly two values of $\tau_m \in [0, \pi)$ at each k, separated by $\pi/2$.

Figure 4.1 shows det (A) as a function of τ at $k = 0.2$ for $\Psi_t^{(1,B)}$. As in figure 3.2, the scale on the vertical axis is unimportant; the result of interest in the figure is that it indicates two values of τ at which A is singular.

The anomalous behaviour in figure 3.1 corresponds directly to the singularity observed at $\tau \simeq 2.87$ in figures 3.2 and 4.1. However, there are no anomalies in figure 3.1 corresponding to the singularity at $\tau \simeq 1.90$ in figure 4.1.

We have examined this phenomenon at other values of the positron momentum. Figure 4.2 indicates the roots of (4.2.5) for $\Psi_t^{(1,B)}$, for 100 different positron

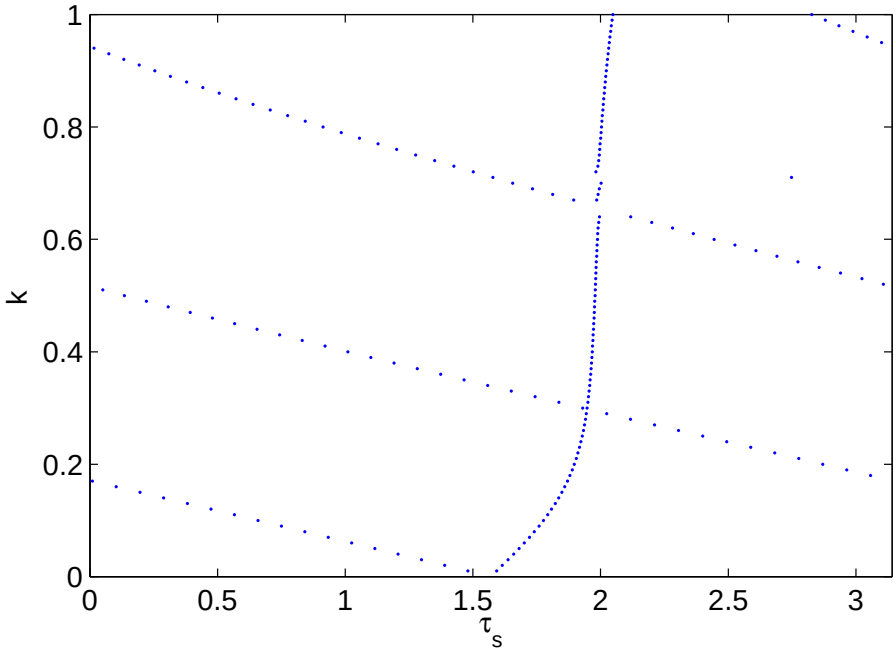

Figure 4.2: Zeros of $\det(A)$ for $\Psi_t^{(1,B)}$, in the range $0.01 \leq k \leq 1$.

momenta equidistant in the range $0.01 \leq k \leq 1$. For the majority of positron momenta considered here, $\mathcal{A}(k)$, $\mathcal{B}(k)$ and $\mathcal{C}(k)$ are such that there are two values of τ_s at each k, the exceptions being $k = 0.65$ and $k = 0.66$, for which there are no real-valued solutions of (4.2.5).

It is clear from the figure that the roots of (4.2.5) generally lie in two families of curves. The first family spans the entire range, $\tau_s \in [0, \pi)$, for $0.01 \leq k \leq 1$. It corresponds directly to the distribution of anomalous peaks in figure 3.3. The second family is confined to values of τ_s in the range $\tau_s \in [1.5, 2.1]$ and corresponds to a region of figure 3.3 in which anomalies are apparently avoided. For almost every k where real roots exist, there is precisely one root clearly belonging to each family. The exception is the result at $k = 0.71$, where there is an irregularity in the otherwise smooth variation of τ_s over k. This result corresponds directly to the persistent anomaly observed at this value of k in chapter

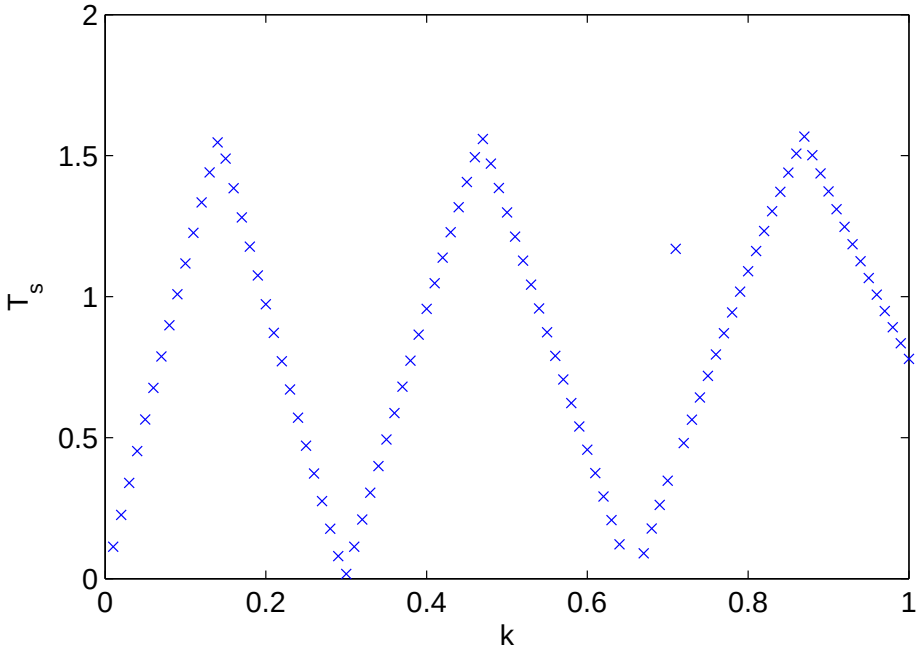

Figure 4.3: Values of $T_s(k)$ for $\Psi_t^{(1,B)}$, in the range $0.01 \leq k \leq 1$.

3 and will be discussed further in section 4.7.

The presence of singularities which do not appear to be associated with anomalous behaviour in η_v is, then, a general characteristic of our calculations. In sections 4.4 and 4.6, we will develop an understanding of how singularities of this type can occur. In the following section, we will digress briefly in order to explain the presence of the discontinuities in figure 3.5.

4.3 Separation of singularities

For those values of k where exactly two real roots of (4.2.5) exist, it is helpful to define the separation, $T_s(k)$, of the two singularities,

$$T_s(k) = \min\left[\left|\tau_s^{(1)}(k) - \tau_s^{(2)}(k)\right|, \left|\pi - \left|\tau_s^{(1)}(k) - \tau_s^{(2)}(k)\right|\right|\right], \tag{4.3.1}$$

where $\tau_s^{(1)}$ and $\tau_s^{(2)}$ are the two solutions of (4.2.5) at a given k. In figure 4.3, we have plotted values of $T_s(k)$ for $\Psi_t^{(1,B)}$, in the range $0.01 \leq k \leq 1$. The oscillations shown in the figure are similar to those found in figure 3.4 and we note that the peaks of $T_s(k)$ coincide with the discontinuities found in figure 3.5, in which values of η_v have been optimised by maximising $|\det(A)|$ over a discrete set of values of τ. Here, we will ignore the deviation in figure 4.3 at $k = 0.71$, since it is another characteristic of the persistent anomalous behaviour which will be discussed in section 4.7.

We have found that the discontinuities observed in figure 3.5 can be explained by careful consideration of $T_s(k)$. To see this, we first prove the following claim: Suppose k is such that exactly two distinct roots, $\tau_s^{(1)} \in [0, \pi)$ and $\tau_s^{(2)} \in [0, \pi)$, of (4.2.5) exist. Then, if only τ is varied, there are exactly two values of $\det(A)$ satisfying (4.2.7), which are equal and opposite if and only if $\tau_s^{(1)}$ and $\tau_s^{(2)}$ are separated by exactly $\pi/2$.

Proof. Suppose $k = k_0$, such that $T_s(k_0) = \pi/2$. Let $\tau_s^{(2)}(k_0) > \tau_s^{(1)}(k_0)$ so that, without loss of generality, we can write

$$\tau_s^{(2)}(k_0) = \tau_s^{(1)}(k_0) + \frac{\pi}{2}. \tag{4.3.2}$$

Hence,

$$\sin\left[\tau_s^{(2)}(k_0)\right] = \cos\left[\tau_s^{(1)}(k_0)\right], \tag{4.3.3}$$

$$\cos\left[\tau_s^{(2)}(k_0)\right] = -\sin\left[\tau_s^{(1)}(k_0)\right]. \tag{4.3.4}$$

Now let $\mathcal{A}_0 = \mathcal{A}(k = k_0)$, $\mathcal{B}_0 = \mathcal{B}(k = k_0)$ and $\mathcal{C}_0 = \mathcal{C}(k = k_0)$. Then, from (4.2.1), (4.3.3) and (4.3.4) we have

$$\mathcal{A}_0 \sin^2\left[\tau_s^{(1)}(k_0)\right] + \mathcal{B}_0 \sin\left[\tau_s^{(1)}(k_0)\right]\cos\left[\tau_s^{(1)}(k_0)\right] + \mathcal{C}_0 \cos^2\left[\tau_s^{(1)}(k_0)\right] = 0 \tag{4.3.5}$$

and

$$\mathcal{A}_0 \cos^2\left[\tau_s^{(1)}(k_0)\right] - \mathcal{B}_0 \sin\left[\tau_s^{(1)}(k_0)\right]\cos\left[\tau_s^{(1)}(k_0)\right] + \mathcal{C}_0 \sin^2\left[\tau_s^{(1)}(k_0)\right] = 0. \tag{4.3.6}$$

Summing (4.3.5) and (4.3.6) gives

$$\mathcal{A}_0 + \mathcal{C}_0 = 0, \tag{4.3.7}$$

so that

$$\det(A; k = k_0) = \mathcal{C}_0 \cos(2\tau) + \frac{\mathcal{B}_0}{2}\sin(2\tau). \tag{4.3.8}$$

Now, since we have assumed that $\tau_s^{(1)} \in [0, \pi)$ and $\tau_s^{(2)} \in [0, \pi)$ are the only two roots of (4.2.5) at $k = k_0$, we cannot have $\mathcal{A}_0 = \mathcal{B}_0 = \mathcal{C}_0 = 0$. Hence, using

(4.3.7), we also see that $\mathcal{B}_0$ and $(\mathcal{A}_0 - \mathcal{C}_0)$ cannot both be zero. Consequently, from (4.2.8) we find that $\det(A; k = k_0)$ is made stationary at exactly two values of τ separated by $\pi/2$. Without loss of generality, at $k = k_0$ we will take these values to be $\tau_m^{(1)}(k_0)$ and $\tau_m^{(2)}(k_0) = \tau_m^{(1)}(k_0) + \pi/2$. If $\mathcal{C}_0 \neq 0$, using (4.2.8) and (4.3.7), we can then write

$$\sin\left[2\tau_m^{(1)}(k_0)\right] = \frac{\mathcal{B}_0}{2\mathcal{C}_0}\cos\left[2\tau_m^{(1)}(k_0)\right], \tag{4.3.9}$$

so that, upon substitution of (4.3.9) into (4.3.8),

$$\begin{aligned}
\det\left(A; k = k_0, \tau = \tau_m^{(1)}\right) &= \left[\mathcal{C}_0 + \frac{\mathcal{B}_0^2}{4\mathcal{C}_0}\right]\cos\left[2\tau_m^{(1)}(k_0)\right] \\
&= -\left[\mathcal{C}_0 + \frac{\mathcal{B}_0^2}{4\mathcal{C}_0}\right]\cos\left[2\tau_m^{(1)}(k_0) + \pi\right] \\
&= -\left[\mathcal{C}_0 + \frac{\mathcal{B}_0^2}{4\mathcal{C}_0}\right]\cos\left[2\tau_m^{(2)}(k_0)\right] \\
&= -\det\left(A; k = k_0, \tau = \tau_m^{(2)}\right),
\end{aligned} \tag{4.3.10}$$

as required.

If $\mathcal{C}_0 = 0$, then $\mathcal{B}_0 \neq 0$ and

$$\begin{aligned}
\det\left(A; k = k_0, \tau = \tau_m^{(1)}\right) &= \frac{\mathcal{B}_0}{2}\sin\left[2\tau_m^{(1)}(k_0)\right] \\
&= -\frac{\mathcal{B}_0}{2}\sin\left[2\tau_m^{(1)}(k_0) + \pi\right] \\
&= -\frac{\mathcal{B}_0}{2}\sin\left[2\tau_m^{(2)}(k_0)\right] \\
&= -\det\left(A; k = k_0, \tau = \tau_m^{(2)}\right),
\end{aligned} \tag{4.3.11}$$

as required.

Conversely, we now suppose that k_0 is such that there are at least two values, $\tau_m^{(1)}(k_0) \in [0, \pi)$ and $\tau_m^{(2)}(k_0) \in [0, \pi)$, satisfying both (4.2.8) and

$$\det\left(A; k = k_0, \tau = \tau_m^{(1)}\right) = -\det\left(A; k = k_0, \tau = \tau_m^{(2)}\right). \tag{4.3.12}$$

We again let $\mathcal{A}_0 = \mathcal{A}(k = k_0)$, $\mathcal{B}_0 = \mathcal{B}(k = k_0)$ and $\mathcal{C}_0 = \mathcal{C}(k = k_0)$. Again, by assumption we cannot have $\mathcal{A}_0 = \mathcal{B}_0 = \mathcal{C}_0 = 0$, since exactly two roots of (4.2.5) exist at k_0 for $\tau \in [0, \pi)$. Moreover, inspection of (4.2.1) and (4.3.12) then shows that $\mathcal{B}_0$ and $(\mathcal{A}_0 - \mathcal{C}_0)$ cannot both be zero. Hence, $\tau_m^{(1)}(k_0)$ and $\tau_m^{(2)}(k_0)$ are the only two values of $\tau \in [0, \pi)$ making $\det(A)$ stationary at k_0 and, without loss of generality, we can again take $\tau_m^{(2)}(k_0) = \tau_m^{(1)}(k_0) + \pi/2$. It follows immediately from (4.3.12) and from equations analogous to (4.3.5) and (4.3.6), in which $\tau_s^{(1)}(k_0)$ is replaced by $\tau_m^{(1)}(k_0)$, that

$$\det\left(A; k = k_0, \tau = \tau_m^{(1)}\right) + \det\left(A; k = k_0, \tau = \tau_m^{(2)}\right) = 0 = \mathcal{A}_0 + \mathcal{C}_0, \tag{4.3.13}$$

so that (4.3.8) is satisfied, as before. It follows from (4.3.8) that

$$\tan\left[2\tau_s^{(1)}(k_0)\right] = \tan\left[2\tau_s^{(2)}(k_0)\right] = -\frac{2\mathcal{C}_0}{\mathcal{B}_0}, \tag{4.3.14}$$

if $\mathcal{B}_0 \neq 0$, or

$$\cos\left[2\tau_s^{(1)}(k_0)\right] = \cos\left[2\tau_s^{(2)}(k_0)\right] = 0, \tag{4.3.15}$$

if $\mathcal{B}_0 = 0$, recalling that $\mathcal{B}_0 = 0 \Rightarrow \mathcal{C}_0 \neq 0$.

Since, by assumption, $\tau_s^{(1)}(k_0) \in [0, \pi)$ and $\tau_s^{(2)}(k_0) \in [0, \pi)$ are distinct, it follows from (4.3.14) and (4.3.15) that $\tau_s^{(1)}(k_0)$ and $\tau_s^{(2)}(k_0)$ must always be separated by exactly $\pi/2$, as required. □

This result explains the origin of the discontinuities in figure 3.5, as well as why these discontinuities coincide with the peaks of figure 4.3. As k passes through k_0, there could be a discontinuous change in the value of τ maximising $|\det(A)|$ at each k, since at k_0 its location could shift by $\pi/2$, from one value of τ_m to the other. This would give rise to the discontinuous changes in $\eta_v(\tau)$ observed in figure 3.5.

4.4 An analytical expression for $\frac{\partial \eta_v}{\partial \tau}$

In this section, we will develop our understanding of the underlying processes giving rise to Schwartz-type anomalies by finding an analytical expression for the partial derivative, $\frac{\partial \eta_v}{\partial \tau}$.

We begin by considering the matrix, $\tilde{A}$, formed by replacing the first column of A (1.7.36) by $-b$ (1.7.37), so that

$$\tilde{A} = \begin{bmatrix} -\langle \bar{C}\psi_G, \bar{S}\psi_G \rangle & \langle \bar{C}\psi_G, \chi_0\psi_G \rangle & \cdots & \langle \bar{C}\psi_G, \chi_M \rangle \\ -\langle \chi_0\psi_G, \bar{S}\psi_G \rangle & \langle \chi_0\psi_G, \chi_0\psi_G \rangle & \cdots & \langle \chi_0\psi_G, \chi_M \rangle \\ \vdots & \vdots & \ddots & \vdots \\ -\langle \chi_M, \bar{S}\psi_G \rangle & \langle \chi_M, \chi_0\psi_G \rangle & \cdots & \langle \chi_M, \chi_M \rangle \end{bmatrix}. \quad (4.4.1)$$

By the same method used to find (4.2.1), we have

$$\begin{aligned}\det\left(\tilde{A}\right) &= -\mathcal{P}(k)\left\langle\bar{C}\psi_G,\bar{S}\psi_G\right\rangle - \mathcal{Q}(k)\left\langle\bar{C}\psi_G,\chi_0\psi_G\right\rangle\left\langle\bar{S}\psi_G,\chi_0\psi_G\right\rangle \\ &- \frac{1}{2}\sum_{i=1}^{M}\mathcal{R}_i(k)\left[\left\langle\bar{C}\psi_G,\chi_0\psi_G\right\rangle\left\langle\bar{S}\psi_G,\chi_i\right\rangle + \left\langle\bar{C}\psi_G,\chi_i\right\rangle\left\langle\bar{S}\psi_G,\chi_0\psi_G\right\rangle\right] \\ &- \sum_{i=1}^{M}\sum_{j=1}^{M}\mathcal{S}_{ij}(k)\left\langle\bar{C}\psi_G,\chi_i\right\rangle\left\langle\bar{S}\psi_G,\chi_j\right\rangle \\ &= \tilde{\mathcal{A}}(k)\sin^2(\tau) + \tilde{\mathcal{B}}(k)\sin(\tau)\cos(\tau) + \tilde{\mathcal{C}}(k)\cos^2(\tau), \qquad (4.4.2)\end{aligned}$$

where $\tilde{\mathcal{A}}(k)$, $\tilde{\mathcal{B}}(k)$ and $\tilde{\mathcal{C}}(k)$ are constants with respect to variations in τ and $\mathcal{P}(k)$, $\mathcal{Q}(k)$, $\mathcal{R}_i(k)$ and $\mathcal{S}_{ij}(k)$ are as in (4.2.1).

Now, setting $\tau = 0$ and using (4.2.1), we find

$$\begin{aligned}\det(A;\tau=0) &= \mathcal{P}(k)\left\langle C\psi_G,C\psi_G\right\rangle + \mathcal{Q}(k)\left\langle C\psi_G,\chi_0\psi_G\right\rangle^2 \\ &+ \sum_{i=1}^{M}\mathcal{R}_i(k)\left\langle C\psi_G,\chi_0\psi_G\right\rangle\left\langle C\psi_G,\chi_i\right\rangle \\ &+ \sum_{i=1}^{M}\sum_{j=1}^{M}\mathcal{S}_{ij}(k)\left\langle C\psi_G,\chi_i\right\rangle\left\langle C\psi_G,\chi_j\right\rangle \\ &= \mathcal{C}(k) \qquad (4.4.3)\end{aligned}$$

and, similarly, using (4.4.2),

$$\begin{aligned}\det\left(\tilde{A};\tau=0\right) &= -\mathcal{P}\left(k\right)\langle C\psi_{\mathrm{G}},S\psi_{\mathrm{G}}\rangle-\mathcal{Q}\left(k\right)\langle C\psi_{\mathrm{G}},\chi_0\psi_{\mathrm{G}}\rangle\langle S\psi_{\mathrm{G}},\chi_0\psi_{\mathrm{G}}\rangle\\ &- \frac{1}{2}\sum_{i=1}^{M}\mathcal{R}_i\left(k\right)\left[\langle C\psi_{\mathrm{G}},\chi_0\psi_{\mathrm{G}}\rangle\langle S\psi_{\mathrm{G}},\chi_i\rangle+\langle C\psi_{\mathrm{G}},\chi_i\rangle\langle S\psi_{\mathrm{G}},\chi_0\psi_{\mathrm{G}}\rangle\right]\\ &- \sum_{i=1}^{M}\sum_{j=1}^{M}\mathcal{S}_{ij}\left(k\right)\langle C\psi_{\mathrm{G}},\chi_i\rangle\langle S\psi_{\mathrm{G}},\chi_j\rangle\\ &= \tilde{\mathcal{C}}\left(k\right). \end{aligned}\tag{4.4.4}$$

Setting $\tau=\pi/2$ and using (4.2.1), we find

$$\begin{aligned}\det\left(A;\tau=\frac{\pi}{2}\right) &= \mathcal{P}\left(k\right)\langle S\psi_{\mathrm{G}},S\psi_{\mathrm{G}}\rangle+\mathcal{Q}\left(k\right)\langle S\psi_{\mathrm{G}},\chi_0\psi_{\mathrm{G}}\rangle^2\\ &+ \sum_{i=1}^{M}\mathcal{R}_i\left(k\right)\langle S\psi_{\mathrm{G}},\chi_0\psi_{\mathrm{G}}\rangle\langle S\psi_{\mathrm{G}},\chi_i\rangle\\ &+ \sum_{i=1}^{M}\sum_{j=1}^{M}\mathcal{S}_{ij}\left(k\right)\langle S\psi_{\mathrm{G}},\chi_i\rangle\langle S\psi_{\mathrm{G}},\chi_j\rangle\\ &= \mathcal{A}\left(k\right)\end{aligned}\tag{4.4.5}$$

and, similarly, using (4.4.2),

$$\begin{aligned}\det\left(\tilde{A};\tau=\frac{\pi}{2}\right) &= \mathcal{P}\left(k\right)\langle S\psi_{\mathrm{G}},C\psi_{\mathrm{G}}\rangle+\mathcal{Q}\left(k\right)\langle S\psi_{\mathrm{G}},\chi_0\psi_{\mathrm{G}}\rangle\langle C\psi_{\mathrm{G}},\chi_0\psi_{\mathrm{G}}\rangle\\ &+ \frac{1}{2}\sum_{i=1}^{M}\mathcal{R}_i\left(k\right)\left[\langle S\psi_{\mathrm{G}},\chi_0\psi_{\mathrm{G}}\rangle\langle C\psi_{\mathrm{G}},\chi_i\rangle+\langle S\psi_{\mathrm{G}},\chi_i\rangle\langle C\psi_{\mathrm{G}},\chi_0\psi_{\mathrm{G}}\rangle\right]\\ &+ \sum_{i=1}^{M}\sum_{j=1}^{M}\mathcal{S}_{ij}\left(k\right)\langle S\psi_{\mathrm{G}},\chi_i\rangle\langle C\psi_{\mathrm{G}},\chi_j\rangle\\ &= \tilde{\mathcal{A}}\left(k\right).\end{aligned}\tag{4.4.6}$$

Finally, setting $\tau=\pi/4$ and using (4.2.1), after a little work we find

$$
\begin{aligned}
& 2\det\left(A;\tau=\frac{\pi}{4}\right)-\mathcal{A}(k)-\mathcal{C}(k)= \\
-\ & \mathcal{P}(k)\left[\langle S\psi_G,C\psi_G\rangle+\langle C\psi_G,S\psi_G\rangle\right] \\
-\ & \mathcal{Q}(k)\left[\langle C\psi_G,\chi_0\psi_G\rangle\langle S\psi_G,\chi_0\psi_G\rangle+\langle S\psi_G,\chi_0\psi_G\rangle\langle C\psi_G,\chi_0\psi_G\rangle\right] \\
-\ & \sum_{i=1}^{M}\mathcal{R}_i(k)\left[\langle C\psi_G,\chi_0\psi_G\rangle\langle S\psi_G,\chi_i\rangle+\langle S\psi_G,\chi_0\psi_G\rangle\langle C\psi_G,\chi_i\rangle\right] \\
-\ & \sum_{i=1}^{M}\sum_{j=1}^{M}\mathcal{S}_{ij}(k)\left[\langle C\psi_G,\chi_i\rangle\langle S\psi_G,\chi_j\rangle+\langle S\psi_G,\chi_i\rangle\langle C\psi_G,\chi_j\rangle\right] \\
=\ & \mathcal{B}(k)
\end{aligned}
\tag{4.4.7}
$$

and, similarly, using (4.4.2),

$$
\begin{aligned}
& 2\det\left(\tilde{A};\tau=\frac{\pi}{4}\right)-\tilde{\mathcal{A}}(k)-\tilde{\mathcal{C}}(k)= \\
& \mathcal{P}(k)\left[\langle S\psi_G,S\psi_G\rangle-\langle C\psi_G,C\psi_G\rangle\right] \\
+\ & \mathcal{Q}(k)\left[\langle S\psi_G,\chi_0\psi_G\rangle^2-\langle C\psi_G,\chi_0\psi_G\rangle^2\right] \\
+\ & \sum_{i=1}^{M}\mathcal{R}_i(k)\left[\langle S\psi_G,\chi_0\psi_G\rangle\langle S\psi_G,\chi_i\rangle-\langle C\psi_G,\chi_0\psi_G\rangle\langle C\psi_G,\chi_i\rangle\right] \\
+\ & \sum_{i=1}^{M}\sum_{j=1}^{M}\mathcal{S}_{ij}(k)\left[\langle S\psi_G,\chi_i\rangle\langle S\psi_G,\chi_j\rangle-\langle C\psi_G,\chi_i\rangle\langle C\psi_G,\chi_j\rangle\right] \\
=\ & \tilde{\mathcal{B}}(k).
\end{aligned}
\tag{4.4.8}
$$

Inspection of (4.4.3)-(4.4.8) then gives

$$
\mathcal{A}(k)-\mathcal{C}(k) = \tilde{\mathcal{B}}(k), \tag{4.4.9}
$$

$$
\tilde{\mathcal{A}}(k)-\tilde{\mathcal{C}}(k) = -\mathcal{B}(k), \tag{4.4.10}
$$

so that we can rewrite (4.4.2) as

$$\begin{aligned}\det\left(\tilde{A}\right) &= \tilde{\mathcal{A}}\left(k\right)\sin^2\left(\tau\right) + \left[\mathcal{A}\left(k\right) - \mathcal{C}\left(k\right)\right]\sin\left(\tau\right)\cos\left(\tau\right) \\ &+ \left[\tilde{\mathcal{A}}\left(k\right) + \mathcal{B}\left(k\right)\right]\cos^2\left(\tau\right). \end{aligned} \tag{4.4.11}$$

Now, we recall from (1.7.40) that

$$\tan\left(\eta_{\mathrm{v}} - \tau + c\right) = a_{\mathrm{t}} - \frac{1}{\tilde{k}}\mathcal{I}\left[\Psi_{\mathrm{t}}\right] \tag{4.4.12}$$

and note that, by Cramer's rule, we can write

$$a_{\mathrm{t}} = \frac{\det\left(\tilde{A}\right)}{\det\left(A\right)}, \tag{4.4.13}$$

for any nonsingular A. Using (3.3.3), for nonsingular A we can then rewrite (4.4.12) as

$$\tan\left(\eta_{\mathrm{v}} - \tau + c\right) = \frac{\det\left(\tilde{A}\right) - \Gamma\left(k\right)}{\det\left(A\right)}, \tag{4.4.14}$$

where we have defined the function, $\Gamma\left(k\right)$, which is independent of τ, as

$$\Gamma\left(k\right) = \frac{\Theta\left(k\right)}{\tilde{k}}, \tag{4.4.15}$$

where $\Theta\left(k\right)$ is as in (3.3.3).

Since, for $k \in \mathbb{R} \setminus Z$, it is always possible to find a nonsingular A for some choice of τ, the expressions (C.1.13), (C.1.22) and (C.1.23) together define $\Theta\left(k\right)$ completely in this domain. The integrals comprising these expressions vary continuously with k such that both $\Theta\left(k\right)$ and $\Gamma\left(k\right)$ are continuous in $k \in \mathbb{R} \setminus Z$.

Now, we will find it convenient to define the functions,

$$\begin{aligned} f(\tau;k) &= \det\left(\tilde{A}\right) - \Gamma(k) \\ &= \tilde{\mathcal{A}}(k)\sin^2(\tau) + [\mathcal{A}(k) - \mathcal{C}(k)]\sin(\tau)\cos(\tau) \\ &+ \left[\tilde{\mathcal{A}}(k) + \mathcal{B}(k)\right]\cos^2(\tau) - \Gamma(k) \end{aligned} \tag{4.4.16}$$

and

$$\begin{aligned} g(\tau;k) = \det(A) &= \mathcal{A}(k)\sin^2(\tau) + \mathcal{B}(k)\sin(\tau)\cos(\tau) \\ &+ \mathcal{C}(k)\cos^2(\tau), \end{aligned} \tag{4.4.17}$$

where we have explicitly denoted the parametric dependence of $f(\tau;k)$ and $g(\tau;k)$ on k. For nonsingular A, we then have

$$\tan(\eta_{\mathrm{v}} - \tau + c) = \frac{f(\tau;k)}{g(\tau;k)}. \tag{4.4.18}$$

Next, we see that

$$f'(\tau;k) = [\mathcal{A}(k) - \mathcal{C}(k)]\cos(2\tau) - \mathcal{B}(k)\sin(2\tau) \tag{4.4.19}$$

and

$$g'(\tau;k) = [\mathcal{A}(k) - \mathcal{C}(k)]\sin(2\tau) + \mathcal{B}(k)\cos(2\tau), \tag{4.4.20}$$

where, in both cases, the prime indicates partial differentiation with respect to τ. Moreover, differentiating (4.4.18) with respect to τ, we find

$$\begin{aligned}\sec^2(\eta_v - \tau + c)\left[\frac{\partial \eta_v}{\partial \tau} - 1\right] &= \left(1 + \frac{f^2(\tau;k)}{g^2(\tau;k)}\right)\left[\frac{\partial \eta_v}{\partial \tau} - 1\right] \\ &= \frac{g(\tau;k) f'(\tau;k) - f(\tau;k) g'(\tau;k)}{g^2(\tau;k)},\end{aligned} \tag{4.4.21}$$

so that

$$\frac{\partial \eta_v}{\partial \tau} = \frac{f^2(\tau;k) + g^2(\tau;k) + g(\tau;k) f'(\tau;k) - f(\tau;k) g'(\tau;k)}{f^2(\tau;k) + g^2(\tau;k)}. \tag{4.4.22}$$

It is easily shown using (4.4.16), (4.4.17), (4.4.19) and (4.4.20) that

$$\begin{aligned}f^2(\tau;k) + g^2(\tau;k) + g(\tau;k) f'(\tau;k) - f(\tau;k) g'(\tau;k) = \\ \left[\tilde{\mathcal{A}}(k) - \Gamma(k)\right]\left[\tilde{\mathcal{A}}(k) - \Gamma(k) + \mathcal{B}(k)\right] + \mathcal{A}(k)\mathcal{C}(k),\end{aligned} \tag{4.4.23}$$

which is independent of τ. Defining

$$\mathcal{G}(k) = \left[\tilde{\mathcal{A}}(k) - \Gamma(k)\right]\left[\tilde{\mathcal{A}}(k) - \Gamma(k) + \mathcal{B}(k)\right] + \mathcal{A}(k)\mathcal{C}(k), \tag{4.4.24}$$

we obtain

$$\frac{\partial \eta_v}{\partial \tau} = \frac{\mathcal{G}(k)}{f^2(\tau;k) + g^2(\tau;k)}, \tag{4.4.25}$$

which is valid for any nonsingular A. In particular, it is valid in the limit as $\det(A) \to 0$.

Anomalous behaviour in η_v will arise whenever the ratio given by (4.4.25) is large, as this will correspond to rapidly changing values of η_v with τ. Singu-

larities in the Kohn calculation appear whenever $g(\tau;k) = 0$, though it is clear from (4.4.25) that the presence of singularities is neither a sufficient nor a necessary condition for anomalies to occur. For a fixed value of k, values of $\frac{\partial \eta_v}{\partial \tau}$ can be large even if $g(\tau;k)$ is never zero. Conversely, for fixed k, large values of $\frac{\partial \eta_v}{\partial \tau}$ are not guaranteed in the limit as τ varies so that $g(\tau;k) \to 0$, owing to the fact that both $f(\tau;k)$ and $g(\tau;k)$ appear in the denominator of the expression for $\frac{\partial \eta_v}{\partial \tau}$ and their zeros will not coincide in general.

Consequently, the presence of anomalous behaviour in figure 3.4 at $k = 0.65$ and $k = 0.66$ is not inconsistent with the observation made in section 4.2 that we have found no zeros of $\det(A)$ at these values of k. More importantly, (4.4.25) also explains how the anomaly-free singularities found in section 4.2 can arise. In the limit as τ varies so that $g(\tau;k) \to 0$, if k is such that $f(\tau;k)$ is not small in comparison to $\mathcal{G}(k)$, then $\frac{\partial \eta_v}{\partial \tau}$ will not be large in this limit and values of η_v in the region of the singularity will not be anomalous. This is confirmed by figure 4.4, a plot of (4.4.25) for $\Upsilon_t^{(1,B)}$, for values of k in the range $0.01 \leq k \leq 1$. When k is such that two singularities exist for $\tau \in [0, \pi)$, the figure indicates that $\frac{\partial \eta_v}{\partial \tau}$ will be large near only one of the two singularities. The results shown in figure 4.4 thus explain the origin of the results shown in figure 3.3. In section 4.6, we will attach a physical meaning to the anomaly-free singularities we have found.

We see from (4.4.25) that, for a given k, the sign of $\frac{\partial \eta_v}{\partial \tau}$ is the same for any τ. In fact, in appendix D we show that

$$\mathcal{G}(k) = \Gamma^2(k), \tag{4.4.26}$$

so that the value of $\frac{\partial \eta_v}{\partial \tau}$ can never be negative. The non-negativity of $\frac{\partial \eta_v}{\partial \tau}$ was demonstrated by Plummer [79] before we explicitly proved the result (4.4.26);

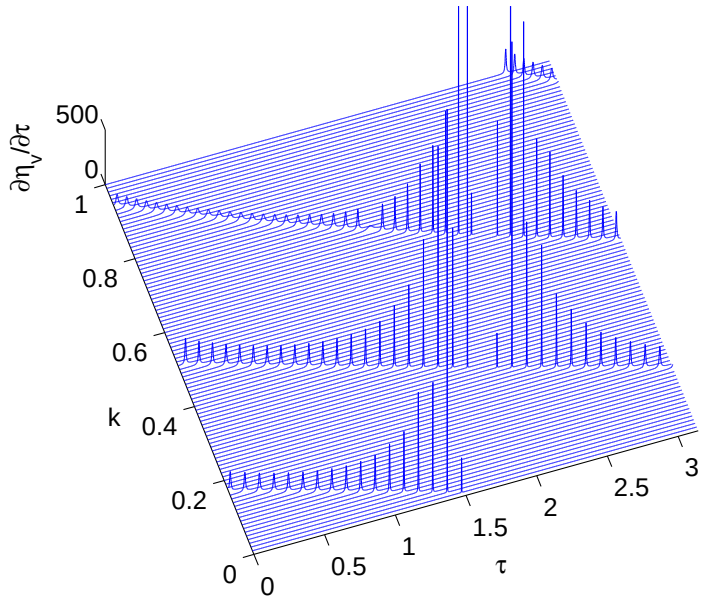

Figure 4.4: Values of $\frac{\partial \eta_v}{\partial \tau}$ for $\Psi_t^{(1,B)}$, in the range $0.01 \leq k \leq 1$.

it explains why, as noted in section 3.2, we have found that all of the anomalies in our calculations are characterised initially by a rapid increase in η_v towards $+\pi/2$ from below as τ is increased, rather than a rapid decrease in η_v towards $-\pi/2$ from above. At this point, we should also qualify the result (3.2.1), since it will not be satisfied if, by accident, $k = k_g$ such that $\mathcal{G}(k_g) = 0$. Under these circumstances, η_v will be constant over τ for any nonsingular A and anomalies will not be observed anywhere.

In figures 4.5 and 4.6 we have plotted $\mathcal{G}(k)$ for $\Psi_t^{(1,B)}$, in the ranges $0.29 \leq k \leq 0.31$ and $0.61 \leq k \leq 0.63$. As in figure 4.1, the scale on the vertical axes in these figures is not important as the value of $\mathcal{G}$ over k can be made arbitrarily large or small by an appropriate choice of the normalisation constant, N, in $\Psi_t^{(1,B)}$. As might intuitively be expected, we see that $\mathcal{G}(k)$ passes relatively very close to zero in the regions of k corresponding to the two minima observed

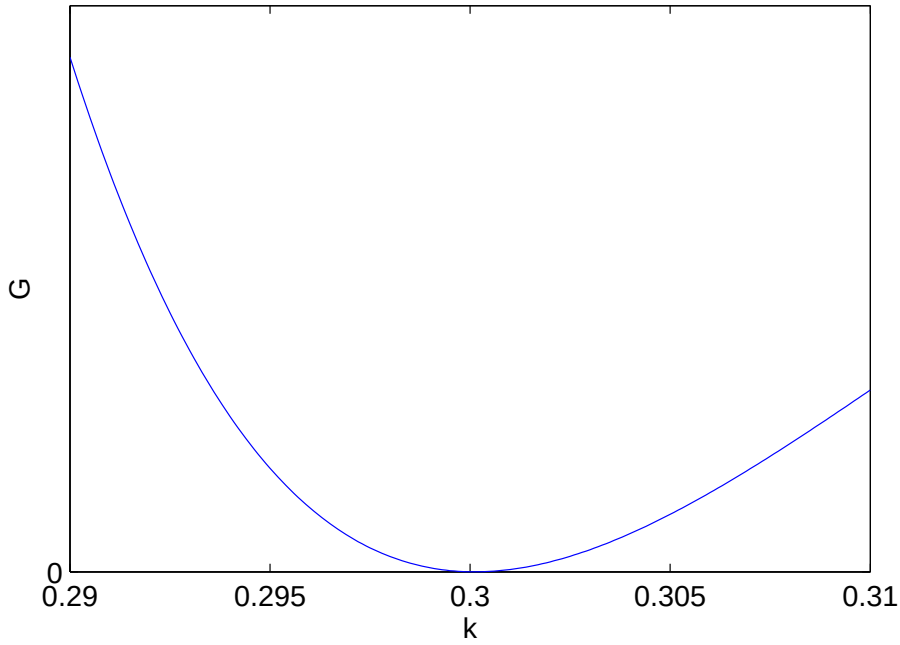

Figure 4.5: Values of $\mathcal{G}(k)$ for $\Psi_{\mathrm{t}}^{(1,\mathrm{B})}$, in the range $0.29 \leq k \leq 0.31$.

in figure 3.4, where anomalies are confined to very small regions of τ. Figure 3.4 suggests that a third minimum of $\Pi_1^{99}(k)$ exists in the limit as $k \to 0$, although we have not investigated this in any detail due to difficulties obtaining accurate values of the integrals involved in the Kohn equations for $k \ll 0.01$. In practice, we have found no value of k_{g} in our calculations.

An immediate consequence of (4.4.26) is that, using (4.4.24) and provided k is such that $2\tilde{\mathcal{A}}(k) + \mathcal{B}(k) \neq 0$, we can write

$$\Gamma(k) = \frac{\left[\tilde{\mathcal{A}}(k) + \mathcal{B}(k)\right]\tilde{\mathcal{A}}(k) + \mathcal{A}(k)\,\mathcal{C}(k)}{2\tilde{\mathcal{A}}(k) + \mathcal{B}(k)}, \tag{4.4.27}$$

so that the τ-independent functions in (4.4.16) can be expressed purely in terms of $\mathcal{A}(k)$, $\mathcal{B}(k)$, $\mathcal{C}(k)$ and $\tilde{\mathcal{A}}(k)$. Hence, in calculating the value of η_{v} from (4.4.18), in general there is actually no need to solve the Kohn equations (1.7.35).

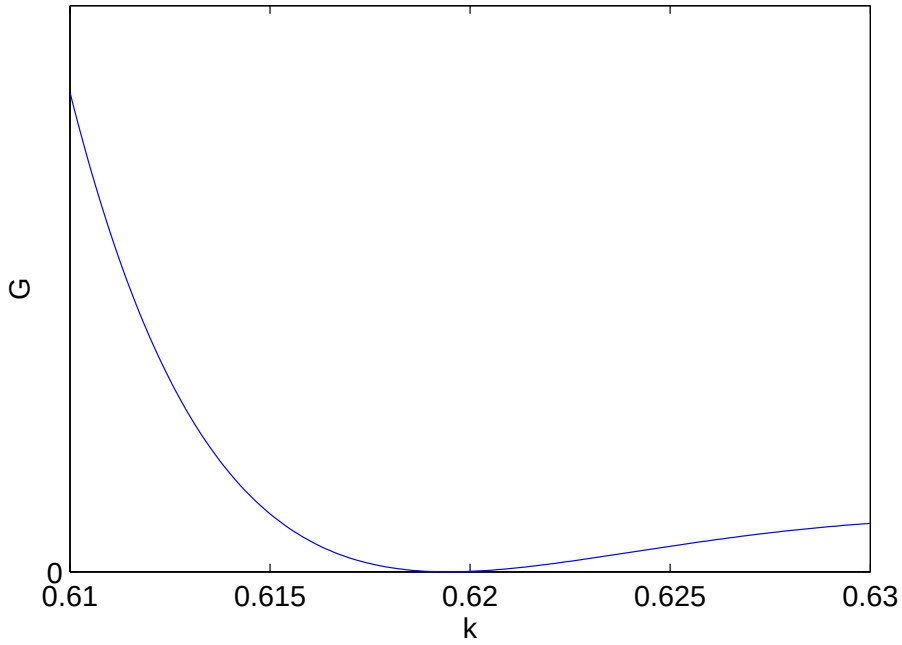

Figure 4.6: Values of $\mathcal{G}(k)$ for $\Psi_{\mathrm{t}}^{(1,\mathrm{B})}$, in the range $0.61 \leq k \leq 0.63$.

All that is required to determine $\eta_{\mathrm{v}}(\tau)$ completely at each k is to find the values of the four determinants, $\mathcal{A}(k)$, $\mathcal{B}(k)$, $\mathcal{C}(k)$ and $\tilde{\mathcal{A}}(k)$; substituting (4.4.27) into (4.4.16), we find that (4.4.18) can be rewritten

$$\tan(\eta_{\mathrm{v}} - \tau + c) = \frac{[\mathcal{A}(k) - \mathcal{C}(k)]\sin(\tau)\cos(\tau) + \mathcal{B}(k)\cos^2(\tau) + \mathcal{D}(k)}{\mathcal{A}(k)\sin^2(\tau) + \mathcal{B}(k)\sin(\tau)\cos(\tau) + \mathcal{C}(k)\cos^2(\tau)}, \tag{4.4.28}$$

for nonsingular A, where we have defined

$$\mathcal{D}(k) = \frac{\tilde{\mathcal{A}}^2(k) - \mathcal{A}(k)\mathcal{C}(k)}{2\tilde{\mathcal{A}}(k) + \mathcal{B}(k)}. \tag{4.4.29}$$

If $k = k_{\mathrm{f}} \in \mathbb{R} \setminus Z$ such that $2\tilde{\mathcal{A}}(k_{\mathrm{f}}) + \mathcal{B}(k_{\mathrm{f}}) = 0$, then from (D.1.1) and (D.1.2) we also have $\left[\tilde{\mathcal{A}}(k_{\mathrm{f}}) + \mathcal{B}(k_{\mathrm{f}})\right]\tilde{\mathcal{A}}(k_{\mathrm{f}}) + \mathcal{A}(k_{\mathrm{f}})\mathcal{C}(k_{\mathrm{f}}) = 0$. Here, the continuity of

$\Gamma(k)$ for $k \in \mathbb{R} \setminus Z$ ensures that the value of $\Gamma(k)$ determined from (4.4.27) in the limit as $k \to k_f$ is well-defined and equal to the value of $\Gamma(k_f)$ determined using (C.1.13), (C.1.22), (C.1.23) and (4.4.15). In practice, we have found no value of $k = k_f$ in our calculations.

4.5 Optimising the derivative

Having found an analytical form for $\frac{\partial \eta_v}{\partial \tau}$, an obvious extension to our investigation is to optimise this expression with respect to τ. Since $\frac{\partial \eta_v}{\partial \tau} \geq 0$, finding a global minimum of $\frac{\partial \eta_v}{\partial \tau}$ with respect to $\tau \in [0, \pi)$ at each k would locate the point at which $\eta_v(\tau)$ varies most slowly with τ. This forms a natural optimisation scheme for choosing τ to avoid anomalous behaviour.

For nonsingular A, partial differentiation of (4.4.25) with respect to τ gives

$$\frac{\partial^2 \eta_v}{\partial \tau^2} = -2 \frac{\mathcal{G}(k)}{\left[f^2(\tau;k) + g^2(\tau;k)\right]^2} \left[f(\tau;k) f'(\tau;k) + g(\tau;k) g'(\tau;k)\right] \tag{4.5.1}$$

and, after some manipulation, it is easily shown that

$$f(\tau;k) f'(\tau;k) + g(\tau;k) g'(\tau;k) = \mathcal{X}(k) \sin(2\tau) + \mathcal{Y}(k) \cos(2\tau), \tag{4.5.2}$$

where we have defined

$$\mathcal{X}(k) = \frac{\mathcal{A}^2(k) - \mathcal{B}^2(k) - \mathcal{C}^2(k)}{2} + \mathcal{B}(k) \left[\Gamma(k) - \tilde{\mathcal{A}}(k)\right] \tag{4.5.3}$$

and

$$\mathcal{Y}(k) = \left[\Gamma(k) - \tilde{\mathcal{A}}(k)\right]\left[\mathcal{C}(k) - \mathcal{A}(k)\right] + \mathcal{A}(k)\,\mathcal{B}(k), \tag{4.5.4}$$

both of which are independent of τ. Denoting by τ_i any value of τ for which $\frac{\partial^2 \eta_v}{\partial \tau^2} = 0$, if $k \neq k_g$ so that $\mathcal{G}(k) \neq 0$, for nonsingular A we then have

$$\mathcal{X}(k)\sin(2\tau_i) + \mathcal{Y}(k)\cos(2\tau_i) = 0. \tag{4.5.5}$$

In the special case where $k = k_g$, then $\frac{\partial \eta_v}{\partial \tau}$ is everywhere zero and optimisation is not required since η_v is constant over τ. In the special case where $k = k_h$, such that $\mathcal{X}(k_h) = \mathcal{Y}(k_h) = 0$, then for nonsingular A the value of $\frac{\partial^2 \eta_v}{\partial \tau^2}$ is everywhere zero. Hence, $\frac{\partial \eta_v}{\partial \tau}$ is constant with respect to variations in τ. If this constant is equal to zero, optimisation of $\frac{\partial \eta_v}{\partial \tau}$ is not required since η_v is constant over τ. If this constant is nonzero, η_v varies linearly with τ and no preferred optimisation can reasonably be defined. In practice, we have found no value of $k = k_h$ in our calculations.

Discounting these two special cases, at each k there will be exactly two values of $\tau_i \in [0, \pi)$ satisfying (4.5.5), separated by $\pi/2$. In this case, using (4.5.2) and (4.5.5) and differentiating (4.5.1) with respect to τ, at $\tau = \tau_i$ and for nonsingular A we see that

$$\frac{\partial^3 \eta_v}{\partial \tau^3}(\tau = \tau_i) = -4\mathcal{G}(k)\,\frac{\left[\mathcal{X}(k)\cos(2\tau_i) - \mathcal{Y}(k)\sin(2\tau_i)\right]}{\left[f^2(\tau_i;k) + g^2(\tau_i;k)\right]^2}. \tag{4.5.6}$$

In general, when k is such that both $\mathcal{G}(k)$ and at least one of $\mathcal{X}(k)$ or $\mathcal{Y}(k)$ is nonzero, then (4.5.5) ensures that $\frac{\partial^3 \eta_v}{\partial \tau^3}$ is nonzero at $\tau = \tau_i$. Moreover, since the two values of τ_i are separated by $\pi/2$, we see from (4.5.6) that the signs of $\frac{\partial^3 \eta_v}{\partial \tau^3}$

at the two values of τ_i are opposite. Hence, in general, $\frac{\partial \eta_v}{\partial \tau}$ has one minimum and one maximum for $\tau \in [0, \pi)$. At each k, we will denote by τ_0 and τ_1 the values of τ_i minimising and maximising $\frac{\partial \eta_v}{\partial \tau}$ respectively. We will denote by $\eta_v^{(0)}$ and $\eta_v^{(1)}$ the respective corresponding values of η_v.

Next, assuming that A is nonsingular and k is such that τ_0 and τ_1 exist, we note the following. Firstly, we see from (4.5.3) and (4.5.4) that this choice of k precludes having $k = k_c$ such that both $\mathcal{A}(k_c) = \mathcal{C}(k_c)$ and $\mathcal{B}(k_c) = 0$, since $\mathcal{X}(k_c) = \mathcal{Y}(k_c) = 0$ by inspection. Consequently, we note from (4.4.19) and (4.4.20) that $f'(\tau_i; k)$ and $g'(\tau_i; k)$ cannot both be zero. In fact, $f'(\tau_i; k)$ cannot be zero, since this would require $g'(\tau_i; k) \neq 0$ and, using (4.5.5), we see that (4.5.2) could not then be satisfied, since we have assumed that $g(\tau_i; k) \neq 0$. Hence, using (4.4.18), (4.5.2) and (4.5.5), we write

$$f'(\tau_i; k) \tan\left(\eta_v^{(i)} - \tau_i + c\right) + g'(\tau_i; k) = 0, \tag{4.5.7}$$

where $f'(\tau_i; k) \neq 0$.

Both τ_0 and τ_1 must satisfy (4.5.7). Recalling that τ_0 and τ_1 are separated by $\pi/2$, we can then immediately conclude

$$\tan\left(\eta_v^{(0)} - \tau_0 + c\right) = \tan\left(\eta_v^{(1)} - \tau_1 + c\right), \tag{4.5.8}$$

so that, for $\eta_v \in (-\pi/2, \pi/2]$, the values of $\eta_v^{(0)}$ and $\eta_v^{(1)}$ must also be separated by $\pi/2$. In fact, using (4.4.19), (4.4.20), (4.5.3), (4.5.4), (4.5.5) and (4.5.7), it is straightforward to show that

$$\begin{aligned}\tan\left(\eta_{\mathrm{v}}^{(i)}-\tau_i+c\right) &= \frac{\left[\mathcal{A}(k)-\mathcal{C}(k)\right]\mathcal{Y}(k)-\mathcal{B}(k)\,\mathcal{X}(k)}{\left[\mathcal{A}(k)-\mathcal{C}(k)\right]\mathcal{X}(k)+\mathcal{B}(k)\,\mathcal{Y}(k)} \\ &= \frac{2\tilde{\mathcal{A}}(k)+\mathcal{B}(k)-2\Gamma(k)}{\mathcal{A}(k)+\mathcal{C}(k)}. \end{aligned} \tag{4.5.9}$$

At each k, the magnitude of $\frac{\partial \eta_{\mathrm{v}}}{\partial \tau}$ at τ_1 indicates the spread of the anomalies in η_{v} over τ. A relatively large value of $\frac{\partial \eta_{\mathrm{v}}}{\partial \tau}$ at τ_1 results in anomalies being confined to a small range of values of τ, whereas a smaller value of $\frac{\partial \eta_{\mathrm{v}}}{\partial \tau}$ at τ_1 will give rise to anomalies appearing over a broader range of τ. We can use this fact to explain the behaviour seen in figure 3.4. The peaks and troughs in this plot indicate regions where, respectively, anomalies are broadly spread and tightly confined in τ. The overall behaviour found in figure 3.4 can now be seen to be governed by the values over k of $\frac{\partial \eta_{\mathrm{v}}}{\partial \tau}$ at τ_1. By defining

$$\mathcal{Z}(k)=\left[\frac{\partial \eta_{\mathrm{v}}}{\partial \tau}(\tau=\tau_1;k)\right]^{-1}, \tag{4.5.10}$$

we should expect the behaviour of $\mathcal{Z}(k)$ and $\Pi_1^{99}(k)$ to be qualitatively the same. This is confirmed by figure 4.7, a plot of $\mathcal{Z}(k)$ for $\Psi_{\mathrm{t}}^{(1,\mathrm{B})}$, in the range $0.01 \leq k \leq 1$. Thus, $\mathcal{Z}(k)$ can be regarded as a formal measure of the width of a given anomalous region.

At each k, the choice $\tau = \tau_0$ describes a scheme for optimising τ to avoid anomalous behaviour, since it identifies the point at which η_{v} is varying most slowly with τ. A plot of $\eta_{\mathrm{v}}^{(0)}(k)$ is given in figure 4.8 for $\Psi_{\mathrm{t}}^{(1,\mathrm{B})}$, in the range $0.01 \leq k \leq 1$. It illustrates that anomalies are indeed avoided, except in the region around $k = 0.71$. This will be discussed further in section 4.7. Excellent agreement is obtained with the results shown in figure 3.6, the values of $\langle \eta_{\mathrm{v}} \rangle$ and $\eta_{\mathrm{v}}^{(0)}$ concurring, on average, to $\sim 10^{-3}$ % of each other.

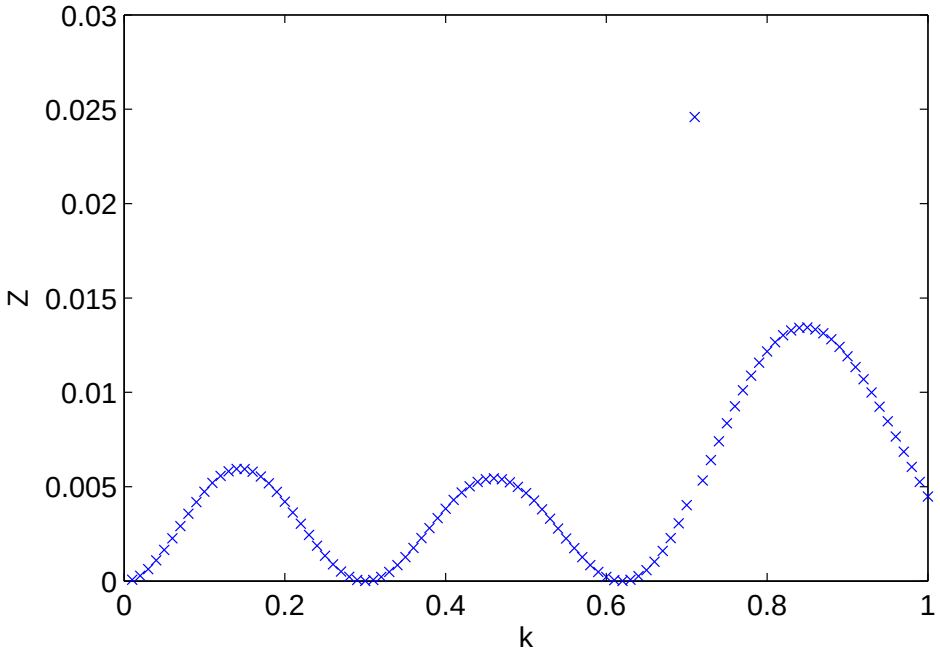

Figure 4.7: Values of $\mathcal{Z}(k)$ for $\Psi_t^{(1,B)}$, in the range $0.01 \leq k \leq 1$.

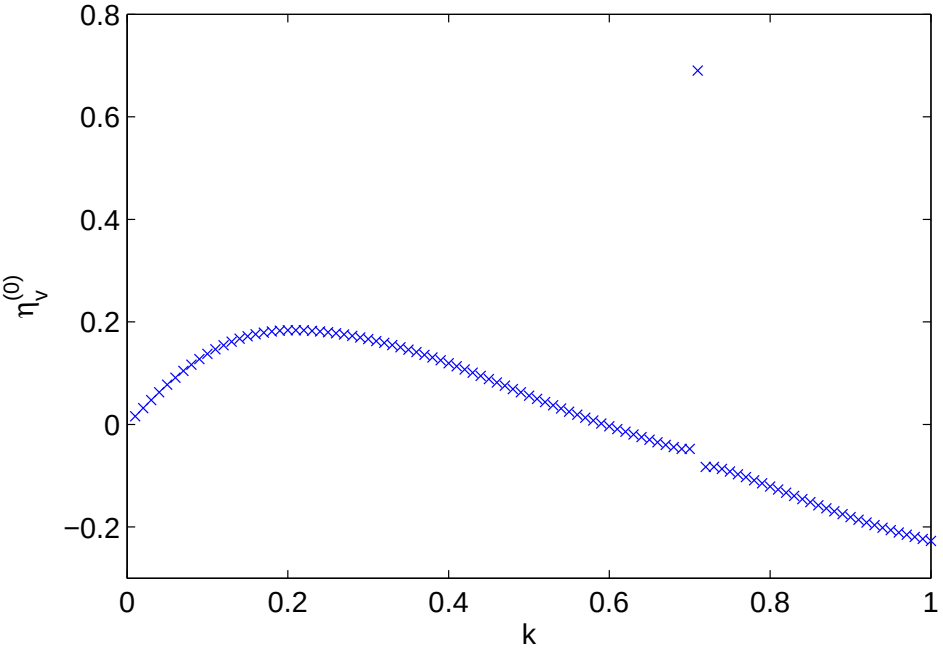

Figure 4.8: Values of $\eta_v^{(0)}(k)$ for $\Psi_t^{(1,B)}$, in the range $0.01 \leq k \leq 1$.

4.6 Anomaly-free singularities

In this section, we will provide a physical argument for the existence of the singularities found in section 4.2, which do not correspond to anomalous behaviour in η_v. We will find it convenient in the following discussion to use a terminology allowing us to distinguish those singularities which are associated with anomalous behaviour from those which are not. Those zeros of $\det(A)$ occurring at any $\tau_s \in [0, \pi)$ and giving rise to anomalous behaviour in the calculations of $\eta_v(\tau)$ when τ is near τ_s, will be called Schwartz singularities, or spurious singularities. Those zeros of $\det(A)$ which do not correspond to anomalous results will be called anomaly-free singularities, or legitimate singularities.

We have developed our understanding of the existence of anomaly-free singularities in collaboration with Dr. Martin Plummer of STFC Daresbury Laboratory [80]. To see how anomaly-free singularities might arise, it is helpful to consider first the exact phase shift, $\eta \in (-\pi/2, \pi/2]$. At each k, there will always be some value, $\tau_e \in [0, \pi)$, such that

$$\eta - \tau_e + c = \left(n + \frac{1}{2}\right)\pi, \tag{4.6.1}$$

for some integer value of n, chosen to keep $\eta \in (-\pi/2, \pi/2]$. The value of $\cot(\eta - \tau + c)$ then passes continuously through zero as τ passes through τ_e.

Now, inverting (4.4.18), for $f(\tau; k) \neq 0$ we have

$$\cot(\eta_v - \tau + c) = \frac{g(\tau; k)}{f(\tau; k)} \tag{4.6.2}$$

and, since the zeros of $f(\tau;k)$ and $g(\tau;k)$ will coincide only by accident, there is a general correspondence between singularities, for which $g(\tau;k) = 0$, and zeros of $\cot(\eta_v - \tau + c)$. At most values of k that we have considered, we have found two distinct values of τ_s such that $g(\tau_s;k) = 0$. Both of these singularities correspond to a zero of $\cot(\eta_v - \tau + c)$.

Brownstein and McKinley [41] note that the widths of anomalous regions should generally decrease as the accuracy of the Kohn trial function is increased. Away from anomalous regions of τ, we can regard $\eta_v(\tau)$ as a slowly varying function of τ. Hence, for a sufficiently accurate trial function where anomalies are confined to small regions of τ, it is reasonable to claim that there will usually be some value, $\hat{\tau}_s$, away from the anomalous region of τ and such that

$$\hat{\eta}_v - \hat{\tau}_s + c = \left(n + \frac{1}{2}\right)\pi, \tag{4.6.3}$$

where we have defined $\hat{\eta}_v = \eta_v(\hat{\tau}_s)$ and where n is such that $\hat{\eta}_v \in (-\pi/2, \pi/2]$.

Unlike the existence of τ_e in (4.6.1), the existence of a value of $\hat{\tau}_s$ away from anomalous regions is not automatically guaranteed. Even in anomaly-free regions where $\eta_v(\tau)$ varies slowly, it is conceivable that it will vary in such a way so as to avoid a zero of $\cot(\eta_v - \tau + c)$ that would otherwise be encountered if η_v were independent of τ. As the trial function is made increasingly accurate, we would expect this particular phenomenon to become less likely.

The results we have so far observed, both in this chapter and the last, suggest that values of $\hat{\tau}_s$ exist in the way we have described, at most values of k. If this is indeed the case, we can obtain phase shift approximations directly from (4.6.3) that should be free of anomalies. The existence of anomaly-free singularities indicates that, at each value of k where such a value of τ exists, choosing $\tau = \hat{\tau}_s$

forms another optimisation scheme for τ that avoids Schwartz-type behaviour.

Strictly speaking, this optimisation method is not formally defined at each value of k. Firstly, we have already noted that the existence of $\hat{\tau}_s$ at each k is not guaranteed; indeed, we recall that we have found no real-valued singularities at all for $\Psi_t^{(1,B)}$ at $k = 0.65$ and $k = 0.66$. Secondly, for values of k where two solutions of (4.2.5) are found to exist, from a purely mathematical perspective it is not immediately obvious which of the two available roots should be labelled as $\hat{\tau}_s$. A method is needed for identifying at each k the root of (4.2.5) corresponding to a legitimate singularity. This could easily be achieved by inspecting values of $\eta_v(\tau)$ at values of τ either side of each singularity. In practice, though, at each k it should be possible to determine immediately which of the two singularities is anomaly-free, by examining other singularities at nearby values of k. For example, figure 4.2 clearly shows that only one curve in the (τ, k) plane corresponds to a physically acceptable variation of phase shift over k.

With these considerations in mind, we claim that choosing $\tau = \hat{\tau}_s$ at applicable values of k defines a consistent optimisation that can be used to avoid anomalies due to Schwartz singularities. A plot of the values of $\hat{\eta}_v(k)$ determined for $\Psi_t^{(1,B)}$ via (4.6.3) is given in figure 4.9 for $0.01 \leq k \leq 1$. No results are included at $k = 0.65$ and $k = 0.66$. At each other value of k under consideration, from the two candidates for $\hat{\eta}_v$ corresponding to the two singularities, we have chosen the one whose value is closest to $\langle \eta_v \rangle$, as calculated in chapter 3.

Inspection of the figure shows that choosing values of τ to coincide with the anomaly-free singularities forms a successful optimisation scheme, with anomalies being avoided except at $k = 0.71$. The results shown in the figure are in fair agreement with those shown in figure 3.6, the values of $\langle \eta_v \rangle$ and $\hat{\eta}_v$ agreeing,

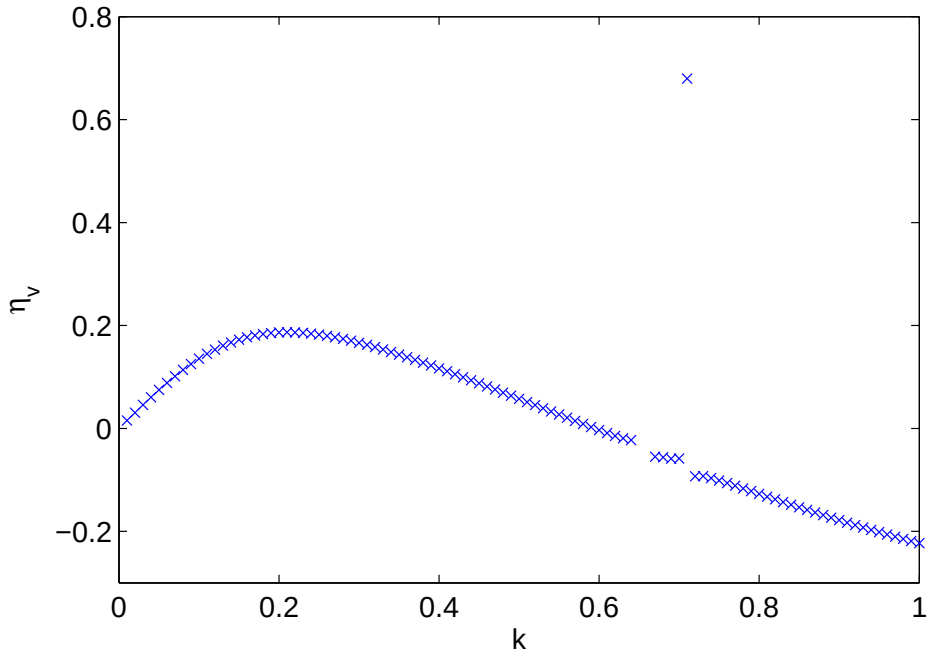

Figure 4.9: Values of $\hat{\eta}_v$ for $\Psi_t^{(1,B)}$, in the range $0.01 \leq k \leq 1$.

on average, to $\sim$ 2 % of each other. This level of concurrence is weaker than that found earlier between the values of $\langle \eta_v \rangle$ and $\eta_v^{(0)}$. Nevertheless, we have demonstrated a novel and efficient way of calculating phase shift approximations directly from (4.2.5). Broadly speaking, this method avoids the problem of Schwartz-type behaviour as effectively as any other method we have considered up to this point.

4.7 Persistent anomalies

So far, we have investigated variations only in τ in our attempts to avoid Schwartz-type behaviour. This consideration has allowed us to handle anomalies which are characterised by a large value of $\frac{\partial \eta_v}{\partial \tau}$. However, it is clear that anomalies of

a different type could arise, where the value of η_v is found to change unusually rapidly with respect to changes in some other parameter of the trial function.

Anomalies arising from the choice of τ are particularly conspicuous because, from a physical point of view, we would expect the value of $\frac{\partial \eta_v}{\partial \tau}$ to be typically very small for a sufficiently accurate trial function. In contrast, the value of $\frac{\partial \eta_v}{\partial k}$, for example, generally takes appreciable values, regardless of whether or not a given calculation is anomalous. However, it is still possible to identify unusually large values of $\frac{\partial \eta_v}{\partial k}$ by inspection. Figure 4.8 provides numerical evidence that, for the choice of $\alpha = 0.6$, $\beta = 1.0$ and $\tau = \tau_0$, the derivative, $\frac{\partial \eta_v}{\partial k}$, is anomalously large near $k = 0.71$ for $\Psi_t^{(1,B)}$. Moreover, it is to be expected that $\frac{\partial \eta_v}{\partial k}$ near $k = 0.71$ will remain large for most other choices of τ in addition to $\tau = \tau_0$, since $\frac{\partial \eta_v}{\partial \tau}$ will generally be small. This shows how persistent anomalies of the kind we have observed can arise. It might be possible significantly to reduce $\frac{\partial \eta_v}{\partial k}$ near $k = 0.71$ by choosing τ so that $\frac{\partial \eta_v}{\partial \tau}$ is large, but this is obviously unsatisfactory.

Our analysis of this problem is restricted by the lack of an analytical expression for $\frac{\partial \eta_v}{\partial k}$. However, we note the following with interest. In section 4.2, we found that (4.2.5) has, in general, no more than two roots if variations only in τ are considered. As we have already mentioned, though, if $k = k_z \in \mathbb{R}$ such that $\mathcal{A}(k_z) = \mathcal{B}(k_z) = \mathcal{C}(k_z) = 0$, then $\det(A)$ is identically zero and no unique value of η_v can be calculated from the Kohn equations at any value of τ. There is no obvious physical reason why this circumstance should arise at any $k \in \mathbb{R}$. However, it is conceivable that $\mathcal{A}(k)$, $\mathcal{B}(k)$ and $\mathcal{C}(k)$ could coincidentally be *close* to zero, in some sense, over a narrow range of k. In figure 4.10, for $\Psi_t^{(1,B)}$ we have plotted the values of $\mathcal{A}(k)$, $\mathcal{B}(k)$ and $\mathcal{C}(k)$ in the range $0.7 \leq k \leq 0.75$. As in figures 4.5 and 4.6, the scale on the vertical axis in this fig-

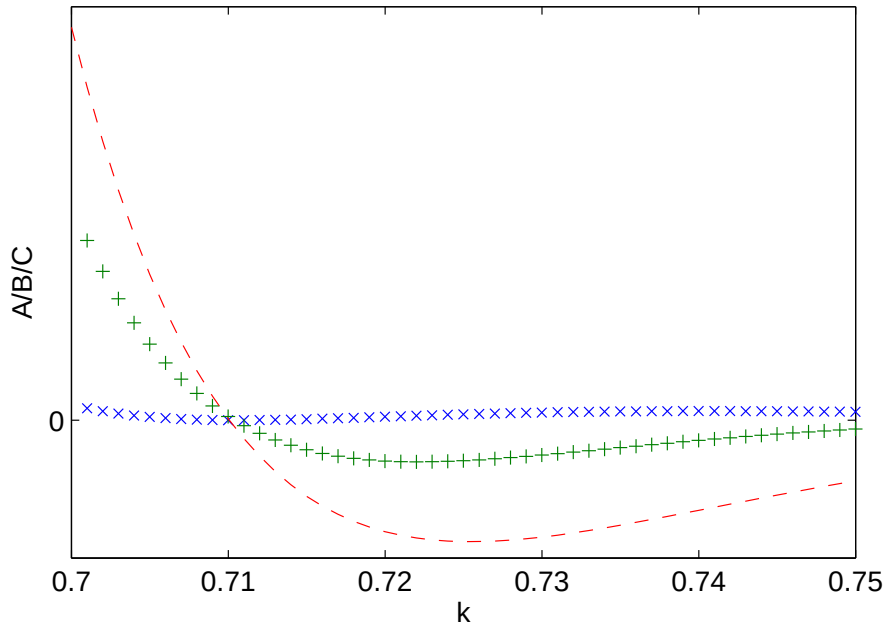

Figure 4.10: Values of [×] $\mathcal{A}(k)$, [+] $\mathcal{B}(k)$ and [- - - -] $\mathcal{C}(k)$ for $\Psi_t^{(1,B)}$, in the neighbourhood of $k = 0.71$.

ure is not important as values of $\mathcal{A}$, $\mathcal{B}$ and $\mathcal{C}$ over k can be made arbitrarily large or small by an appropriate choice of the normalisation constant, N, in $\Psi_t^{(1,B)}$. It is clear from the figure that all three functions become relatively small close to $k = 0.71$. Upon closer inspection, we have found that $\mathcal{A}(k)$, $\mathcal{B}(k)$ and $\mathcal{C}(k)$ all pass through zero at least once between $k = 0.71$ and $k = 0.7104$, although not at precisely the same value of k.

Despite not knowing the analytical form of $\frac{\partial \eta_v}{\partial k}$, we can infer from figure 4.10 that, when $\frac{\partial \eta_v}{\partial \tau}$ has been made small, $\frac{\partial \eta_v}{\partial k}$ is made unusually large whenever values of $\mathcal{A}(k)$, $\mathcal{B}(k)$ and $\mathcal{C}(k)$ are coincidentally small. It is reasonable to conclude that this is the underlying cause of the persistent anomalous behaviour we have observed in our calculations. It remains unclear whether the convergence of $\mathcal{A}(k)$, $\mathcal{B}(k)$ and $\mathcal{C}(k)$ around $k = 0.71$ is accidental or, as seems more

likely, indicative of an underlying relationship between these three functions. We will not examine this problem in any detail here.

4.8 Conclusions

We have developed an analytical framework for the investigation of singularities in the generalised Kohn method, enabling us to explain the results of calculations carried out in the previous chapter. We have found that, although there is a general correlation between the appearance of singularities in the Kohn matrix and anomalies in the calculations of η_{v}, it is possible for each to occur without the other.

The evaluation of an analytical expression for $\frac{\partial \eta_{\mathrm{v}}}{\partial \tau}$, together with our formulation of a theory of anomaly-free singularities, has led to the development of two more optimisation schemes for choosing τ to avoid anomalous behaviour. Both of these schemes are largely successful, but neither avoids the persistent anomalies observed for $\Psi_{\mathrm{t}}^{(1,\mathrm{B})}$ in the region of $k = 0.71$. We have argued that the persistent anomalies occur when the partial derivatives of η_{v}, with respect to parameters of the trial function other than τ, are unusually large.

We have shown that solutions of the Kohn equations (1.7.35) are not required to determine approximations to the scattering phase shift at each value of k. In the general case, $\eta_{\mathrm{v}}(\tau)$ can be obtained immediately from the four determinants, $\mathcal{A}(k)$, $\mathcal{B}(k)$, $\mathcal{C}(k)$ and $\tilde{\mathcal{A}}(k)$, via (4.4.28). In the case where values of $\hat{\eta}_{\mathrm{v}}$ are calculated from (4.6.3) using the theory of anomaly-free singularities, the values of only $\mathcal{A}(k)$, $\mathcal{B}(k)$ and $\mathcal{C}(k)$ are needed, in order to solve (4.2.5).

In the following chapter, we will investigate methods of avoiding persistent Schwartz-type behaviour. The first of these involves a reformulation of the Kohn method itself, in which the trial function is taken to be complex-valued. Although we will find that it is unsuccessful in avoiding the persistent anomalies, this modification of the Kohn method is of great interest as it will be seen automatically to avoid those anomalies arising in the generalised Kohn method due to the choice of τ. In fact, this was the motivation behind the introduction of this method [44, 45].

Chapter 5

The Complex Kohn Method

5.1 Introduction

The complex Kohn method is an extension of the original variational approach in which the trial wavefunction is taken to be complex-valued. It was originally believed [44, 45] that this method was inherently free of the effects of Schwartz singularities, although anomalies were subsequently reported by Lucchese [46].

In this chapter, we will implement the complex Kohn method for our calculations on $(e^+ - H_2)$ scattering. Our original motivation for this work was to attempt to address the persistent anomalous behaviour observed in chapters 3 and 4. However, although we will find that application of the complex Kohn method automatically avoids the Schwartz-type behaviour arising in the generalised Kohn method from the choice of τ, we will show that the persistent anomalies are still present. The reason for this continued persistence is easily understood in the context of the framework we have developed for the analysis

of Schwartz singularities.

We will prove that the variational approximation to the scattering phase shift is independent of the choice of τ in our complex-valued trial function. Moreover, we will show that the value of the phase shift approximation obtained in the complex Kohn method for any τ is precisely equal to that which is obtained in the generalised Kohn method for the choice of τ which minimises the derivative, $\frac{\partial \eta_\nu}{\partial \tau}$. This demonstrates that the two methods are effectively equivalent, at least within the boundaries of our own calculations.

As in the two preceding chapters, we will focus our investigation on Kohn calculations in which the target potential is included explicitly. Our analysis could be applied equally well to our method of models calculations without any significant modifications. The values of α and β in (1.7.8) will initially be fixed at $\alpha = 0.6$ and $\beta = 1.0$, although in section 5.6 we will vary these parameters as part of our investigation into persistent Schwartz-type behaviour.

5.2 The complex Kohn method

For our calculations on $(e^+ - H_2)$ scattering, a requirement of any complex-valued trial wavefunction is that it has the general asymptotic form (1.7.13). As such, we will here consider trial wavefunctions, $\breve{\Psi}_t$, having the form

$$\breve{\Psi}_t = \left(\bar{S} + a'_t \bar{T} + p'_0 \chi_0\right) \psi_G + \sum_{i=1}^{M} p'_i \chi_i, \tag{5.2.1}$$

where

$$\bar{T} = \bar{S} + \mathrm{i}\bar{C}, \tag{5.2.2}$$

the functions, $\bar{S}$, $\bar{C}$, ψ_{G} and $\{\chi_0, \ldots, \chi_M\}$ being as in (1.7.3). The unknowns, $\{a_{\mathrm{t}}', p_0', \ldots, p_M'\}$, will not, in general, be real. The primes on $\{a_{\mathrm{t}}', p_0', \ldots, p_M'\}$ distinguish them from the corresponding values found in (1.7.3). Throughout this chapter, unless otherwise noted we will use primes in this way to distinguish various quantities used in applications of the complex Kohn method from the corresponding quantities used in applications of the generalised Kohn method involving real-valued trial functions.

In what follows, we will find it helpful to refer to calculations involving trial functions of the form (5.2.1) simply as complex Kohn calculations, rather than generalised complex Kohn calculations. We will restrict use of the term 'generalised' to describe only those Kohn calculations carried out in earlier chapters with real-valued trial functions, in which τ was included as an adjustable parameter. In the case of the complex Kohn method, we will see in section 5.4 that the role of τ in (5.2.1) is not important.

Henceforth, we will consider only the case $a_{\mathrm{t}}' \neq -1$; this is necessary in order for $\bar{S}$ to appear in (5.2.1). When $a_{\mathrm{t}}' \neq -1$, if we define a value, η_{t}', such that

$$\tan\left(\eta_{\mathrm{t}}' - \tau + c\right) = \frac{\mathrm{i}a_{\mathrm{t}}'}{1 + a_{\mathrm{t}}'} \tag{5.2.3}$$

and let

$$\xi_{\mathrm{t}}' = \eta_{\mathrm{t}}' - \tau + c, \tag{5.2.4}$$

then it is straightforward to show that the asymptotic form of (5.2.1) is

$$\breve{\Psi}_t \underset{\lambda_3 \to \infty}{\sim} D \frac{\sin\left(kr_3 + \eta_t'\right)}{r_3} \psi_G, \tag{5.2.5}$$

which has the general form (1.7.2) as required, where

$$D = \frac{NR\left(1 + a_t'\right)}{2\cos\left(\xi_t'\right)}. \tag{5.2.6}$$

Kohn variational calculations involving $\breve{\Psi}_t$ then proceed in a manner analogous to that discussed in chapter 1. Following this method, we derive complex Kohn equations analogous to (1.7.33) and (1.7.34),

$$\frac{\partial \mathcal{I}'\left[\breve{\Psi}_t\right]}{\partial a_t'} = i\tilde{k} \tag{5.2.7}$$

and

$$\frac{\partial \mathcal{I}'\left[\breve{\Psi}_t\right]}{\partial p_i'} = 0 \quad (i = 0, \ldots, M), \tag{5.2.8}$$

where

$$\mathcal{I}'\left[\breve{\Psi}_t\right] = \langle \breve{\Psi}_t^* | \left(\hat{H} - E\right) | \breve{\Psi}_t \rangle = \langle \breve{\Psi}_t^*, \breve{\Psi}_t \rangle \tag{5.2.9}$$

is analogous to (1.7.19). Here, $\breve{\Psi}_t^*$ is the complex conjugate of $\breve{\Psi}_t$. In the usual Dirac notation, $\langle \breve{\Psi}_t |$ implicitly denotes complex conjugation of $\breve{\Psi}_t$. As pointed out by Chamberlain [81], however, in a consistent implementation of the complex Kohn method this conjugation should not, in fact, be performed. Hence, we replace $\langle \breve{\Psi}_t |$ by $\langle \breve{\Psi}_t^* |$ to indicate that the conjugation is not carried out.

The solutions of (5.2.7) and (5.2.8) make the functional,

$$\begin{aligned}\mathcal{J}'\left[\breve{\Psi}_{\mathrm{t}}\right] &= -\mathrm{i}\sin\left(\eta'_{\mathrm{v}}-\tau+c\right)\exp\left[-\mathrm{i}\left(\eta'_{\mathrm{v}}-\tau+c\right)\right] \\ &= a'_{\mathrm{t}}+\frac{\mathrm{i}}{\tilde{k}}\mathcal{I}'\left[\breve{\Psi}_{\mathrm{t}}\right], \end{aligned} \tag{5.2.10}$$

stationary with respect to variations in a'_{t} and $\{p'_0,\ldots,p'_M\}$. This expression is analogous to (1.7.40) and implicitly defines an approximation, η'_{v}, to the scattering phase shift.

The Kohn equations (5.2.7) and (5.2.8) can be expressed as a matrix equation,

$$A'x' = -b', \tag{5.2.11}$$

having the same form as (1.7.35). For nonsingular A', determining A' and b' allows

$$x' = \begin{bmatrix} a'_t \\ p'_0 \\ \vdots \\ p'_M \end{bmatrix} \tag{5.2.12}$$

to be found. A' and b' here take the form

$$A' = \begin{bmatrix} \langle \bar{T}^* \psi_G, \bar{T} \psi_G \rangle & \langle \bar{T}^* \psi_G, \chi_0 \psi_G \rangle & \cdots & \langle \bar{T}^* \psi_G, \chi_M \rangle \\ \langle \chi_0 \psi_G, \bar{T} \psi_G \rangle & \langle \chi_0 \psi_G, \chi_0 \psi_G \rangle & \cdots & \langle \chi_0 \psi_G, \chi_M \rangle \\ \vdots & \vdots & \ddots & \vdots \\ \langle \chi_M, \bar{T} \psi_G \rangle & \langle \chi_M, \chi_0 \psi_G \rangle & \cdots & \langle \chi_M, \chi_M \rangle \end{bmatrix}, \quad (5.2.13)$$

$$b' = \begin{bmatrix} \langle \bar{T}^* \psi_G, \bar{S} \psi_G \rangle \\ \langle \chi_0 \psi_G, \bar{S} \psi_G \rangle \\ \vdots \\ \langle \chi_M, \bar{S} \psi_G \rangle \end{bmatrix}, \quad (5.2.14)$$

the matrix elements of which are immediately available from simple combinations of the elements of B (1.7.42). Thus, our implementation of the complex Kohn method involves no effort in evaluating integrals beyond that already expended in our application of the generalised Kohn method.

When the Kohn equations (5.2.11) are satisfied, we can write an expression analogous to (1.7.39), namely

$$\mathcal{I}' \left[\breve{\Psi}_t \right] = \langle \bar{S} \psi_G, \bar{S} \psi_G \rangle + a'_t \langle \bar{S} \psi_G, \bar{T} \psi_G \rangle + p'_0 \langle \bar{S} \psi_G, \chi_0 \psi_G \rangle + \sum_{i=1}^{M} p'_i \langle \bar{S} \psi_G, \chi_i \rangle. \quad (5.2.15)$$

Determining a'_t and $\{p'_0, \ldots, p'_M\}$ allows η'_v to be found, by rearranging (5.2.10) to give, for nonsingular A',

$$\tan \left(\eta'_v - \tau + c \right) = \frac{i a'_t - \tilde{k}^{-1} \mathcal{I}' \left[\breve{\Psi}_t \right]}{1 + a'_t + i \tilde{k}^{-1} \mathcal{I}' \left[\breve{\Psi}_t \right]}. \quad (5.2.16)$$

As with the calculations of η_t and η_v in the generalised Kohn method, the error

in $\tan\left(\eta_{\mathrm{t}}' - \tau + c\right)$ from $\tan\left(\eta - \tau + c\right)$ is first order in the error of $\breve{\Psi}_{\mathrm{t}}$ from Ψ, while the error in $\tan\left(\eta_{\mathrm{v}}' - \tau + c\right)$ from $\tan\left(\eta - \tau + c\right)$ is second order in the error of $\breve{\Psi}_{\mathrm{t}}$ from Ψ. We will refer to η_{t}' and η_{v}' respectively as the first and second order approximations to the phase shift.

For an inexact trial wavefunction, η_{v}' will generally not be real. We write

$$\eta_{\mathrm{v}}'\left(\tau\right) = \eta_{\mathrm{v}}\left(\tau\right) + \mathrm{i}\varsigma_{\mathrm{v}}\left(\tau\right), \tag{5.2.17}$$

for some real-valued functions, $\eta_{\mathrm{v}}\left(\tau\right)$ and $\varsigma_{\mathrm{v}}\left(\tau\right)$. Here, it is understood that $\eta_{\mathrm{v}}\left(\tau\right)$ is not the same function obtained in the preceding chapters from the generalised Kohn calculations and that we have reused the notation only for convenience. For an accurate trial wavefunction, $\varsigma_{\mathrm{v}}\left(\tau\right)$ will be small. It should be ignored as an error term since the exact phase shift, η, must be real.

5.3 An analytical expression for $\det\left(A'\right)$

It has been noted by several authors [44–46] that the principal advantage of the complex Kohn method over its real-valued counterpart is that it automatically avoids many of the difficulties associated with Schwartz singularities. In this section and the next, we will see how this is achieved for our calculations on $\left(e^{+} - \mathrm{H}_2\right)$ scattering.

By analogy with (4.2.1), we find that the determinant, $\det\left(A'\right)$, of (5.2.13) can be written

$$\begin{aligned}\det\left(A'\right) &= \mathcal{P}\left(k\right)\left\langle \bar{T}^{*}\psi_{\mathrm{G}},\bar{T}\psi_{\mathrm{G}}\right\rangle + \mathcal{Q}\left(k\right)\left\langle \bar{T}^{*}\psi_{\mathrm{G}},\chi_{0}\psi_{\mathrm{G}}\right\rangle^{2}\\ &+ \sum_{i=1}^{M}\mathcal{R}_{i}\left(k\right)\left\langle \bar{T}^{*}\psi_{\mathrm{G}},\chi_{0}\psi_{\mathrm{G}}\right\rangle\left\langle \bar{T}^{*}\psi_{\mathrm{G}},\chi_{i}\right\rangle\\ &+ \sum_{i=1}^{M}\sum_{j=1}^{M}\mathcal{S}_{ij}\left(k\right)\left\langle \bar{T}^{*}\psi_{\mathrm{G}},\chi_{i}\right\rangle\left\langle \bar{T}^{*}\psi_{\mathrm{G}},\chi_{j}\right\rangle\\ &= \mathcal{A}'\left(k\right)\sin^{2}\left(\tau\right)+\mathcal{B}'\left(k\right)\sin\left(\tau\right)\cos\left(\tau\right)+\mathcal{C}'\left(k\right)\cos^{2}\left(\tau\right),\end{aligned} \tag{5.3.1}$$

where we have used (1.7.4). Note that $\mathcal{P}\left(k\right)$, $\mathcal{Q}\left(k\right)$, $\mathcal{R}_{i}\left(k\right)$ and $\mathcal{S}_{ij}\left(k\right)$ are the same functions as those appearing in (4.2.1). Note further that, if there exists some τ_1, τ_2 such that

$$\bar{T}\left(\tau=\tau_{2}\right)=\vartheta\bar{T}\left(\tau=\tau_{1}\right), \tag{5.3.2}$$

for some constant, ϑ, then inspection of (5.3.1) gives

$$\det\left(A';\tau=\tau_{2}\right)=\vartheta^{2}\det\left(A';\tau=\tau_{1}\right). \tag{5.3.3}$$

Now, from (1.7.4) and (5.2.2) it is clear that

$$\bar{T}\left(\tau=\frac{\pi}{2}\right) = C-\mathrm{i}S=-\mathrm{i}\left(S+\mathrm{i}C\right)=-\mathrm{i}\bar{T}\left(\tau=0\right), \tag{5.3.4}$$

$$\bar{T}\left(\tau=\frac{\pi}{4}\right) = \frac{\left(1-\mathrm{i}\right)}{\sqrt{2}}\left(S+\mathrm{i}C\right)=\frac{\left(1-\mathrm{i}\right)}{\sqrt{2}}\bar{T}\left(\tau=0\right), \tag{5.3.5}$$

so that it follows immediately from (5.3.2) and (5.3.3) that

$$\det\left(A';\tau=\frac{\pi}{2}\right) = -\det\left(A';\tau=0\right), \tag{5.3.6}$$

$$\det\left(A';\tau=\frac{\pi}{4}\right) = -\mathrm{i}\det\left(A';\tau=0\right). \tag{5.3.7}$$

Substitution of (5.3.6) and (5.3.7) into (5.3.1) yields

$$\mathcal{A}'(k)+\mathcal{C}'(k) = 0, \tag{5.3.8}$$

$$\begin{aligned}\mathcal{B}'(k) &= 2\det\left(A';\tau=\frac{\pi}{4}\right)-\mathcal{A}'(k)-\mathcal{C}'(k)\\ &= -2\mathrm{i}\mathcal{C}'(k),\end{aligned} \tag{5.3.9}$$

so that

$$\begin{aligned}\det\left(A'\right) &= \mathcal{A}'(k)\sin^2(\tau)+\mathcal{B}'(k)\sin(\tau)\cos(\tau)+\mathcal{C}'(k)\cos^2(\tau)\\ &= \mathcal{C}'(k)\left[\cos^2(\tau)-\sin^2(\tau)\right]-2\mathrm{i}\mathcal{C}'(k)\sin(\tau)\cos(\tau)\\ &= \mathcal{C}'(k)\exp(-2\mathrm{i}\tau).\end{aligned} \tag{5.3.10}$$

At each k, for variations of $\tau\in[0,\pi)$ the values of $\det\left(A'\right)$ thus describe a circle of radius $|\mathcal{C}'(k)|$ in the complex plane. Hence, singularities are obtained if and only if both the real and imaginary parts of $\mathcal{C}'(k)$ are zero; they can neither be located nor avoided by varying only τ. This suggests that, with particular regard to anomalous behaviour, results of complex Kohn calculations will be less sensitive to changes in τ than the results of those calculations we have carried out with real-valued trial functions. In section 5.4, we will find that this is the case.

Now, setting $\tau = 0$, (5.3.1) gives

$$\begin{aligned}
& \det\left(A';\tau=0\right) = \\
& \mathcal{P}\left(k\right)\left[\langle S\psi_{\mathrm{G}}, S\psi_{\mathrm{G}}\rangle - \langle C\psi_{\mathrm{G}}, C\psi_{\mathrm{G}}\rangle + \mathrm{i}\langle S\psi_{\mathrm{G}}, C\psi_{\mathrm{G}}\rangle + \mathrm{i}\langle C\psi_{\mathrm{G}}, S\psi_{\mathrm{G}}\rangle\right] \\
+ \;& \mathcal{Q}\left(k\right)\Big[\langle S\psi_{\mathrm{G}}, \chi_0\psi_{\mathrm{G}}\rangle^2 - \langle C\psi_{\mathrm{G}}, \chi_0\psi_{\mathrm{G}}\rangle^2 \\
+ \;& \mathrm{i}\langle S\psi_{\mathrm{G}}, \chi_0\psi_{\mathrm{G}}\rangle\langle C\psi_{\mathrm{G}}, \chi_0\psi_{\mathrm{G}}\rangle + \mathrm{i}\langle C\psi_{\mathrm{G}}, \chi_0\psi_{\mathrm{G}}\rangle\langle S\psi_{\mathrm{G}}, \chi_0\psi_{\mathrm{G}}\rangle\Big] \\
+ \;& \sum_{i=1}^{M}\mathcal{R}_i\left(k\right)\left[\langle S\psi_{\mathrm{G}}, \chi_0\psi_{\mathrm{G}}\rangle\langle S\psi_{\mathrm{G}}, \chi_i\rangle - \langle C\psi_{\mathrm{G}}, \chi_0\psi_{\mathrm{G}}\rangle\langle C\psi_{\mathrm{G}}, \chi_i\rangle\right. \\
+ \;& \left.\mathrm{i}\langle S\psi_{\mathrm{G}}, \chi_0\psi_{\mathrm{G}}\rangle\langle C\psi_{\mathrm{G}}, \chi_i\rangle + \mathrm{i}\langle C\psi_{\mathrm{G}}, \chi_0\psi_{\mathrm{G}}\rangle\langle S\psi_{\mathrm{G}}, \chi_i\rangle\right] \\
+ \;& \sum_{i=1}^{M}\sum_{j=1}^{M}\mathcal{S}_{ij}\left(k\right)\left[\langle S\psi_{\mathrm{G}}, \chi_i\rangle\langle S\psi_{\mathrm{G}}, \chi_j\rangle - \langle C\psi_{\mathrm{G}}, \chi_i\rangle\langle C\psi_{\mathrm{G}}, \chi_j\rangle\right. \\
+ \;& \left.\mathrm{i}\langle S\psi_{\mathrm{G}}, \chi_i\rangle\langle C\psi_{\mathrm{G}}, \chi_j\rangle + \mathrm{i}\langle C\psi_{\mathrm{G}}, \chi_i\rangle\langle S\psi_{\mathrm{G}}, \chi_j\rangle\right] \\
= \;& \mathcal{C}'\left(k\right). \qquad (5.3.11)
\end{aligned}$$

Then, upon inspection of (4.4.3), (4.4.5), (4.4.7) and (5.3.11), we have

$$\mathcal{C}'\left(k\right) = -\mathcal{A}'\left(k\right) = \mathcal{A}\left(k\right) - \mathcal{C}\left(k\right) - \mathrm{i}\mathcal{B}\left(k\right), \qquad (5.3.12)$$

so that we may rewrite (5.3.10) as

$$\det\left(A'\right) = \left[\mathcal{A}\left(k\right) - \mathcal{C}\left(k\right) - \mathrm{i}\mathcal{B}\left(k\right)\right]\exp\left(-2\mathrm{i}\tau\right). \qquad (5.3.13)$$

We might reasonably expect anomalous results due to the choice of τ to be absent in the complex Kohn method. However, the form of (5.3.13) suggests that, even in the complex case, Schwartz-type behaviour will not be eliminated entirely. At $k = 0.71$, for example, the value of $\mathcal{C}'\left(k\right) = \mathcal{A}\left(k\right) - \mathcal{C}\left(k\right) - \mathrm{i}\mathcal{B}\left(k\right)$

will be close to zero in the same sense that $\mathcal{A}(k)$, $\mathcal{B}(k)$ and $\mathcal{C}(k)$, as calculated for $\Psi_t^{(1,B)}$, have already been seen to be close to zero at this value of k in chapter 4. It is therefore conceivable that persistent anomalies of the kind we have observed in earlier chapters will also be present in the results of our complex Kohn calculations. In section 5.5, we will demonstrate this explicitly to be true.

5.4 An analytical expression for $\frac{\partial \eta'_V}{\partial \tau}$

In this section, we will formally establish that our implementation of the complex Kohn method avoids the Schwartz-type anomalies that arise in the generalised Kohn method due to the choice of τ. We will do this by considering the derivative, $\frac{\partial \eta'_V}{\partial \tau}$.

Proceeding by a method analogous to that followed in section 4.4, we begin by considering the matrix, $\tilde{A}'$, formed by replacing the first column of A' (5.2.13) by $-b'$ (5.2.14), so that

$$\tilde{A}' = \begin{bmatrix} -\langle \bar{T}^* \psi_G, \bar{S} \psi_G \rangle & \langle \bar{T}^* \psi_G, \chi_0 \psi_G \rangle & \cdots & \langle \bar{T}^* \psi_G, \chi_M \rangle \\ -\langle \chi_0 \psi_G, \bar{S} \psi_G \rangle & \langle \chi_0 \psi_G, \chi_0 \psi_G \rangle & \cdots & \langle \chi_0 \psi_G, \chi_M \rangle \\ \vdots & \vdots & \ddots & \vdots \\ -\langle \chi_M, \bar{S} \psi_G \rangle & \langle \chi_M, \chi_0 \psi_G \rangle & \cdots & \langle \chi_M, \chi_M \rangle \end{bmatrix} \tag{5.4.1}$$

and

$$\begin{aligned}
\det\left(\tilde{A}'\right) &= -\mathcal{P}(k)\langle\bar{T}^*\psi_G,\bar{S}\psi_G\rangle - \mathcal{Q}(k)\langle\bar{T}^*\psi_G,\chi_0\psi_G\rangle\langle\bar{S}\psi_G,\chi_0\psi_G\rangle \\
&- \frac{1}{2}\sum_{i=1}^{M}\mathcal{R}_i(k)\left[\langle\bar{T}^*\psi_G,\chi_0\psi_G\rangle\langle\bar{S}\psi_G,\chi_i\rangle + \langle\bar{T}^*\psi_G,\chi_i\rangle\langle\bar{S}\psi_G,\chi_0\psi_G\rangle\right] \\
&- \sum_{i=1}^{M}\sum_{j=1}^{M}\mathcal{S}_{ij}(k)\langle\bar{T}^*\psi_G,\chi_i\rangle\langle\bar{S}\psi_G,\chi_j\rangle \\
&= \tilde{\mathcal{A}}'(k)\sin^2(\tau) + \tilde{\mathcal{B}}'(k)\sin(\tau)\cos(\tau) + \tilde{\mathcal{C}}'(k)\cos^2(\tau), \qquad (5.4.2)
\end{aligned}$$

where $\tilde{\mathcal{A}}'(k)$, $\tilde{\mathcal{B}}'(k)$, $\tilde{\mathcal{C}}'(k)$ are constants with respect to variations in τ and $\mathcal{P}(k)$, $\mathcal{Q}(k)$, $\mathcal{R}_i(k)$ and $\mathcal{S}_{ij}(k)$ are as in (4.2.1).

Setting $\tau = 0$ in (5.4.2) gives

$$\begin{aligned}
\det\left(\tilde{A}';\tau=0\right) &= -\mathcal{P}(k)\left[\langle S\psi_G,S\psi_G\rangle + \mathrm{i}\langle C\psi_G,S\psi_G\rangle\right] \\
&- \mathcal{Q}(k)\left[\langle S\psi_G,\chi_0\psi_G\rangle^2 + \mathrm{i}\langle C\psi_G,\chi_0\psi_G\rangle\langle S\psi_G,\chi_0\psi_G\rangle\right] \\
&- \frac{1}{2}\sum_{i=1}^{M}\mathcal{R}_i(k)\left[\langle S\psi_G,\chi_0\psi_G\rangle\langle S\psi_G,\chi_i\rangle + \mathrm{i}\langle C\psi_G,\chi_0\psi_G\rangle\langle S\psi_G,\chi_i\rangle\right. \\
&+ \left.\langle S\psi_G,\chi_i\rangle\langle S\psi_G,\chi_0\psi_G\rangle + \mathrm{i}\langle C\psi_G,\chi_i\rangle\langle S\psi_G,\chi_0\psi_G\rangle\right] \\
&- \sum_{i=1}^{M}\sum_{j=1}^{M}\mathcal{S}_{ij}(k)\left[\langle S\psi_G,\chi_i\rangle\langle S\psi_G,\chi_j\rangle + \mathrm{i}\langle C\psi_G,\chi_i\rangle\langle S\psi_G,\chi_j\rangle\right] \\
&= \tilde{\mathcal{C}}'(k), \qquad (5.4.3)
\end{aligned}$$

while setting $\tau = \pi/2$ gives

$$\begin{aligned}
\det\left(\tilde{A}';\tau=\frac{\pi}{2}\right) &= -\mathcal{P}(k)\left[\langle C\psi_G, C\psi_G\rangle - \mathrm{i}\langle S\psi_G, C\psi_G\rangle\right] \\
&- \mathcal{Q}(k)\left[\langle C\psi_G, \chi_0\psi_G\rangle^2 - \mathrm{i}\langle S\psi_G, \chi_0\psi_G\rangle\langle C\psi_G, \chi_0\psi_G\rangle\right] \\
&- \frac{1}{2}\sum_{i=1}^{M}\mathcal{R}_i(k)\left[\langle C\psi_G, \chi_0\psi_G\rangle\langle C\psi_G, \chi_i\rangle - \mathrm{i}\langle S\psi_G, \chi_0\psi_G\rangle\langle C\psi_G, \chi_i\rangle\right. \\
&+ \left.\langle C\psi_G, \chi_i\rangle\langle C\psi_G, \chi_0\psi_G\rangle - \mathrm{i}\langle S\psi_G, \chi_i\rangle\langle C\psi_G, \chi_0\psi_G\rangle\right] \\
&- \sum_{i=1}^{M}\sum_{j=1}^{M}\mathcal{S}_{ij}(k)\left[\langle C\psi_G, \chi_i\rangle\langle C\psi_G, \chi_j\rangle - \mathrm{i}\langle S\psi_G, \chi_i\rangle\langle C\psi_G, \chi_j\rangle\right] \\
&= \tilde{\mathcal{A}}'(k). \qquad (5.4.4)
\end{aligned}$$

Meanwhile, setting $\tau = \pi/2$ in (5.3.1), we have

$$\begin{aligned}
&\det\left(A';\tau=\frac{\pi}{2}\right) = \\
&\mathcal{P}(k)\left[\langle C\psi_G, C\psi_G\rangle - \langle S\psi_G, S\psi_G\rangle - \mathrm{i}\langle S\psi_G, C\psi_G\rangle - \mathrm{i}\langle C\psi_G, S\psi_G\rangle\right] \\
+ &\mathcal{Q}(k)\left[\langle C\psi_G, \chi_0\psi_G\rangle^2 - \langle S\psi_G, \chi_0\psi_G\rangle^2\right. \\
- &\left.\mathrm{i}\langle S\psi_G, \chi_0\psi_G\rangle\langle C\psi_G, \chi_0\psi_G\rangle - \mathrm{i}\langle C\psi_G, \chi_0\psi_G\rangle\langle S\psi_G, \chi_0\psi_G\rangle\right] \\
+ &\sum_{i=1}^{M}\mathcal{R}_i(k)\left[\langle C\psi_G, \chi_0\psi_G\rangle\langle C\psi_G, \chi_i\rangle - \langle S\psi_G, \chi_0\psi_G\rangle\langle S\psi_G, \chi_i\rangle\right. \\
- &\left.\mathrm{i}\langle S\psi_G, \chi_0\psi_G\rangle\langle C\psi_G, \chi_i\rangle - \mathrm{i}\langle C\psi_G, \chi_0\psi_G\rangle\langle S\psi_G, \chi_i\rangle\right] \\
+ &\sum_{i=1}^{M}\sum_{j=1}^{M}\mathcal{S}_{ij}(k)\left[\langle C\psi_G, \chi_i\rangle\langle C\psi_G, \chi_j\rangle - \langle S\psi_G, \chi_i\rangle\langle S\psi_G, \chi_j\rangle\right. \\
- &\left.\mathrm{i}\langle S\psi_G, \chi_i\rangle\langle C\psi_G, \chi_j\rangle - \mathrm{i}\langle C\psi_G, \chi_i\rangle\langle S\psi_G, \chi_j\rangle\right] \\
= &\mathcal{A}'(k). \qquad (5.4.5)
\end{aligned}$$

Comparing (5.4.3), (5.4.4) and (5.4.5), it is then clear that

$$\tilde{\mathcal{C}}'(k) = \tilde{\mathcal{A}}'(k) + \mathcal{A}'(k). \tag{5.4.6}$$

Next, setting $\tau = \pi/4$ and using (5.4.2), after a little work we find

$$\begin{aligned}
& 2\det\left(\tilde{A}'; \tau = \frac{\pi}{4}\right) - \tilde{\mathcal{A}}'(k) - \tilde{\mathcal{C}}'(k) = \\
& \mathcal{P}(k)\left[\mathrm{i}\langle S\psi_G, S\psi_G\rangle - \mathrm{i}\langle C\psi_G, C\psi_G\rangle - \langle S\psi_G, C\psi_G\rangle - \langle C\psi_G, S\psi_G\rangle\right] \\
+ \quad & \mathcal{Q}(k)\Big[\mathrm{i}\langle S\psi_G, \chi_0\psi_G\rangle^2 - \mathrm{i}\langle C\psi_G, \chi_0\psi_G\rangle^2 \\
- \quad & \langle S\psi_G, \chi_0\psi_G\rangle\langle C\psi_G, \chi_0\psi_G\rangle - \langle C\psi_G, \chi_0\psi_G\rangle\langle S\psi_G, \chi_0\psi_G\rangle\Big] \\
+ \quad & \sum_{i=1}^{M} \mathcal{R}_i(k)\left[\mathrm{i}\langle S\psi_G, \chi_0\psi_G\rangle\langle S\psi_G, \chi_i\rangle - \mathrm{i}\langle C\psi_G, \chi_0\psi_G\rangle\langle C\psi_G, \chi_i\rangle\right. \\
- \quad & \left.\langle S\psi_G, \chi_0\psi_G\rangle\langle C\psi_G, \chi_i\rangle - \langle C\psi_G, \chi_0\psi_G\rangle\langle S\psi_G, \chi_i\rangle\right] \\
+ \quad & \sum_{i=1}^{M}\sum_{j=1}^{M} \mathcal{S}_{ij}(k)\left[\mathrm{i}\langle S\psi_G, \chi_i\rangle\langle S\psi_G, \chi_j\rangle - \mathrm{i}\langle C\psi_G, \chi_i\rangle\langle C\psi_G, \chi_j\rangle\right. \\
- \quad & \left.\langle S\psi_G, \chi_i\rangle\langle C\psi_G, \chi_j\rangle - \langle C\psi_G, \chi_i\rangle\langle S\psi_G, \chi_j\rangle\right] \\
= \quad & \tilde{\mathcal{B}}'(k),
\end{aligned} \tag{5.4.7}$$

giving, upon comparison of (5.3.11) and (5.4.7),

$$\tilde{\mathcal{B}}'(k) = \mathrm{i}\mathcal{C}'(k). \tag{5.4.8}$$

Using (5.3.8), (5.4.6) and (5.4.8), after some rearrangement we can then rewrite (5.4.2) as

$$\det\left(\tilde{A}'\right) = \tilde{\mathcal{A}}'(k) + \mathcal{A}'(k)\cos(\tau)\exp(-\mathrm{i}\tau). \tag{5.4.9}$$

In appendix C we show that, in the complex Kohn method and for trial functions of the form (5.2.1),

$$\det\left(A'\right) \neq 0 \Rightarrow \det\left(A'\right)\mathcal{I}'\left[\breve{\Psi}_{\mathrm{t}}\right] = -\Theta\left(k,\mathscr{x}\right), \tag{5.4.10}$$

where $\Theta\left(k,\mathscr{x}\right)$ is as in (3.3.3).

We next define

$$u\left(\tau;k\right) = \mathrm{i}\tilde{\mathcal{A}}'\left(k\right) + \mathrm{i}\mathcal{A}'\left(k\right)\cos\left(\tau\right)\exp\left(-\mathrm{i}\tau\right) + \Gamma\left(k\right) \tag{5.4.11}$$

and

$$\begin{aligned} v\left(\tau;k\right) &= -\mathcal{A}'\left(k\right)\exp\left(-2\mathrm{i}\tau\right) + \tilde{\mathcal{A}}'\left(k\right) + \mathcal{A}'\left(k\right)\cos\left(\tau\right)\exp\left(-\mathrm{i}\tau\right) - \mathrm{i}\Gamma\left(k\right) \\ &= \det\left(A'\right) - \mathrm{i}u\left(\tau;k\right), \end{aligned} \tag{5.4.12}$$

noting that, after some work, we find

$$u^2\left(\tau;k\right) + v^2\left(\tau;k\right) + v\left(\tau;k\right)u'\left(\tau;k\right) - u\left(\tau;k\right)v'\left(\tau;k\right) = 0, \tag{5.4.13}$$

where the primes on $u'\left(\tau;k\right)$ and $v'\left(\tau;k\right)$ indicate partial differentiation with respect to τ.

Using Cramer's rule, together with (4.4.15) and (5.4.10), for nonsingular A' we can rewrite (5.2.16) as

$$\tan\left(\eta'_{\mathrm{v}} - \tau + c\right) = \frac{\mathrm{i}\det\left(\tilde{A}'\right) + \Gamma\left(k\right)}{\det\left(A'\right) + \det\left(\tilde{A}'\right) - \mathrm{i}\Gamma\left(k\right)}, \tag{5.4.14}$$

so that, using (5.3.8), (5.3.10), (5.4.9), (5.4.11) and (5.4.12), we find

$$\tan\left(\eta_{\mathrm{v}}' - \tau + c\right) = \frac{u\left(\tau;k\right)}{v\left(\tau;k\right)}, \tag{5.4.15}$$

provided that $v\left(\tau;k\right)$ is nonzero.

By analogy with (4.4.22), we then see that

$$\frac{\partial \eta_{\mathrm{v}}'}{\partial \tau} = \frac{u^2\left(\tau;k\right) + v^2\left(\tau;k\right) + v\left(\tau;k\right)u'\left(\tau;k\right) - u\left(\tau;k\right)v'\left(\tau;k\right)}{u^2\left(\tau;k\right) + v^2\left(\tau;k\right)}, \tag{5.4.16}$$

where the primes on $u'\left(\tau;k\right)$ and $v'\left(\tau;k\right)$ indicate partial differentiation with respect to τ.

Inspection of (5.4.12) shows that the zeros of $u\left(\tau;k\right)$ and $v\left(\tau;k\right)$ coincide if and only if A' is singular. Hence, for nonsingular A', the denominator of (5.4.16) is nonzero so that, using (5.4.13), (5.4.16) becomes

$$\frac{\partial \eta_{\mathrm{v}}'}{\partial \tau} = 0, \tag{5.4.17}$$

giving

$$\frac{\partial \eta_{\mathrm{v}}}{\partial \tau} = \frac{\partial \varsigma_{\mathrm{v}}}{\partial \tau} = 0, \tag{5.4.18}$$

where we have used (5.2.17).

Thus, whenever $\det\left(A'\right)$ and $v\left(\tau;k\right)$ are both nonzero, the second order approximation to the scattering phase shift obtained from (5.2.16) is independent of the choice of τ in (5.2.1). Therefore, complex Kohn calculations of $\eta_{\mathrm{v}} = \Re\left[\eta_{\mathrm{v}}'\right]$ will, in general, automatically be free of the Schwartz-type anomalies arising in

our generalised Kohn calculations from the choice of τ. Without loss of generality, we can set $\tau = 0$ in (5.2.1) for convenience.

We note from inspection of (4.4.3), (4.4.6) and (5.4.4) that

$$\tilde{\mathcal{A}}'(k) = -\mathcal{C}(k) + \mathrm{i}\tilde{\mathcal{A}}(k). \tag{5.4.19}$$

If $v(\tau;k) = 0$, then from (5.4.13) we either have $u(\tau;k) = v(\tau;k) = 0$, in which case $\det(A') = 0$, or we have $u(\tau;k) = v'(\tau;k)$. Using (5.4.19), together with (4.2.1), (5.3.12), (5.4.11) and (5.4.12), we find that

$$\Im\left[u(\tau;k) - v'(\tau;k)\right] = -\det(A), \tag{5.4.20}$$

where A is as in (1.7.36). Hence, $v(\tau;k)$ is zero only if at least one of A or A' is singular. In the following section, we will carry out a formal comparison of the results of the generalised and complex Kohn methods. In so doing, we will assume that the parameters of our trial functions are such that both A and A' are nonsingular, so that the Kohn equations in each case can uniquely be solved. As a result, we henceforth restrict ourselves to calculations in which $v(\tau;k) \neq 0$.

For completeness, we consider the first order approximation, η_{t}', to the phase shift, obtained from (5.2.3). Equations analogous to (5.4.17) and (5.4.18) for η_{t}' can be obtained simply by omitting any terms containing $\Gamma(k)$ from each expression in the above argument. For nonsingular A' and provided that $v(\tau;k) + \mathrm{i}\Gamma(k) \neq 0$, we can then immediately write

$$\frac{\partial \eta'_t}{\partial \tau} = \frac{\partial \eta_t}{\partial \tau} = \frac{\partial \varsigma_t}{\partial \tau} = 0, \tag{5.4.21}$$

where we have defined

$$\eta'_t(\tau) = \eta_t(\tau) + i\varsigma_t(\tau), \tag{5.4.22}$$

which is analogous to (5.2.17). Thus, in general, the value of $\eta_t = \Re[\eta'_t]$ is also independent of τ.

Although we have shown that the choice of τ in (5.2.1) has no effect on the value of η'_v, we have yet to describe the connection, if any, between the value of $\eta_v = \Re[\eta'_v]$ defined by (5.2.17) and the function, $\eta_v(\tau)$, investigated in our application of the generalised Kohn method in the last two chapters. It is the purpose of the following section to establish such a connection.

5.5 Comparison of the generalised and complex Kohn methods

In our complex Kohn calculations, we consider a trial wavefunction, $\breve{\Psi}_t^{(1,B)}$, of the form (5.2.1). As implied by our notation for $\breve{\Psi}_t^{(1,B)}$, it contains the same set of correlation functions and target basis functions as used for $\Psi_t^{(1,B)}$. We have set $\tau = 0$ in $\breve{\Psi}_t^{(1,B)}$ and have fixed the nonlinear parameters in (1.7.8) at $\alpha = 0.6$ and $\beta = 1.0$. The resulting values of $\eta_v = \Re[\eta'_v]$, obtained from (5.2.16), are shown in figure 5.1 for positron momenta in the range $0.01 \leq k \leq 1$.

As expected from the arguments given in the last two sections, the introduc-

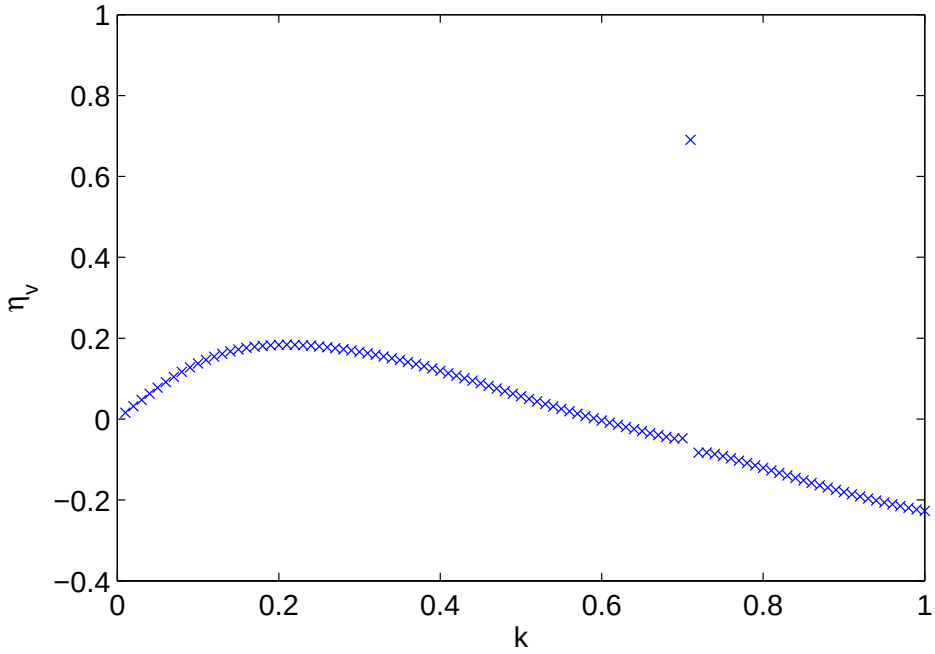

Figure 5.1: Values of $\eta_{\mathrm{v}}(k) = \Re[\eta'_{\mathrm{v}}](k)$ for $\breve{\Psi}_{\mathrm{t}}^{(1,\mathrm{B})}$, in the range $0.01 \leq k \leq 1$.

tion of the complex-valued trial function automatically avoids Schwartz-type anomalies except in the region around $k = 0.71$. In table 5.1, for $\breve{\Psi}_{\mathrm{t}}^{(1,\mathrm{B})}$ and for $0.01 \leq k \leq 0.2$, we compare the values of $\eta_{\mathrm{v}} = \Re[\eta'_{\mathrm{v}}]$ with the optimised results of the earlier generalised Kohn calculations, carried out using $\Psi_{\mathrm{t}}^{(1,\mathrm{B})}$. We have presented in the table the results corresponding to the three most successful optimisation schemes considered in chapters 3 and 4, viz.

(i) finding the value, $\eta_{\mathrm{v}}^{(0)}$, where $\frac{\partial \eta_{\mathrm{v}}}{\partial \tau}$ is minimised,

(ii) finding the median value, $\langle \eta_{\mathrm{v}} \rangle$, over the $p = 1001$ values of τ,

(iii) finding the value, $\hat{\eta}_{\mathrm{v}}$, corresponding to the anomaly-free singularity.

There is generally good agreement in table 5.1 between the values of $\Re[\eta'_{\mathrm{v}}]$ and $\hat{\eta}_{\mathrm{v}}$ and excellent agreement between the values of $\Re[\eta'_{\mathrm{v}}]$ and $\langle \eta_{\mathrm{v}} \rangle$. The level

k	$\Re\left[\eta_{\mathrm{v}}'\right]$	(i) $\eta_{\mathrm{v}}^{(0)}$	(ii) $\langle\eta_{\mathrm{v}}\rangle$	(iii) $\hat{\eta}_{\mathrm{v}}$
0.01	0.01588	0.01588	0.01588	0.01527
0.02	0.03179	0.03179	0.03178	0.03057
0.03	0.04752	0.04752	0.04751	0.04574
0.04	0.06281	0.06281	0.06280	0.06057
0.05	0.07745	0.07745	0.07744	0.07486
0.06	0.09134	0.09134	0.09131	0.08853
0.07	0.10440	0.10440	0.10436	0.10151
0.08	0.11654	0.11654	0.11648	0.11372
0.09	0.12765	0.12765	0.12771	0.12503
0.1	0.13768	0.13768	0.13774	0.13539
0.11	0.14664	0.14664	0.14670	0.14478
0.12	0.15454	0.15454	0.15459	0.15320
0.13	0.16138	0.16138	0.16143	0.16063
0.14	0.16719	0.16719	0.16723	0.16704
0.15	0.17200	0.17200	0.17204	0.17248
0.16	0.17591	0.17591	0.17594	0.17699
0.17	0.17896	0.17896	0.17898	0.18060
0.18	0.18120	0.18120	0.18122	0.18333
0.19	0.18270	0.18270	0.18272	0.18524
0.2	0.18354	0.18354	0.18355	0.18638

Table 5.1: A comparison of the results of the complex Kohn calculations using $\breve{\Psi}_{\mathrm{t}}^{(1,\mathrm{B})}$ with optimised results of the generalised Kohn calculations using $\Psi_{\mathrm{t}}^{(1,\mathrm{B})}$.

of concurrence between the values of $\Re\left[\eta_{\mathrm{v}}'\right]$ and $\eta_{\mathrm{v}}^{(0)}$, though, is particularly high. For each k considered in table 5.1, these two sets of results agree to the five decimal places shown. In fact, for $0.01 \leq k \leq 1$, we have found that these results agree, on average, to $\sim 10^{-4}$ % of each other. This suggests that the values of $\Re\left[\eta_{\mathrm{v}}'\right]$ and $\eta_{\mathrm{v}}^{(0)}$ are, in fact, algebraically identical, with the very small discrepancies we have observed here being due to the limits of computational precision inherent to our calculations. For the rest of this section, we will focus on proving this claim.

Consider two trial wavefunctions, Ψ_{t} and $\breve{\Psi}_{\mathrm{t}}$, respectively of the form (1.7.3) and (5.2.1), containing the same approximate target wavefunction and identical sets of short-range correlation functions. Suppose that the corresponding Kohn matrices, A (1.7.36) and A' (5.2.13), are nonsingular so that solutions of the Kohn equations, (1.7.35) and (5.2.11), uniquely exist. Suppose further that $k \neq k_{\mathrm{g}}$ and $k \neq k_{\mathrm{h}}$ in order that (4.4.25) can uniquely be minimised, as discussed in chapter 4. Under these circumstances, we claim that

$$\eta_{\mathrm{v}}^{(0)} = \Re\left[\eta_{\mathrm{v}}'\right], \tag{5.5.1}$$

where, as discussed in chapter 4, $\eta_{\mathrm{v}}^{(0)}$ is the phase shift approximation obtained in the generalised Kohn method at the unique value, $\tau = \tau_0$, which minimises (4.4.25).

Proof. Firstly, combining (5.3.12) and (5.3.13) with (5.4.19), we can rewrite (5.4.11) and (5.4.12) as

$$u(\tau;k) = -\mathrm{i}\mathcal{C}(k) - \tilde{\mathcal{A}}(k) + \mathrm{i}\left[\mathcal{C}(k) - \mathcal{A}(k) + \mathrm{i}\mathcal{B}(k)\right]\cos(\tau)\exp(-\mathrm{i}\tau) + \Gamma(k) \tag{5.5.2}$$

and

$$v(\tau;k) = \left[\mathcal{A}(k) - \mathcal{C}(k) - \mathrm{i}\mathcal{B}(k)\right]\exp(-2\mathrm{i}\tau) - \mathrm{i}u(\tau;k) \tag{5.5.3}$$

respectively.

Using (4.4.16), (4.4.17), (4.5.9), (5.4.15), (5.5.2) and (5.5.3), together with the standard result

$$\tan(P-Q) = \frac{\tan(P) - \tan(Q)}{1 + \tan(P)\tan(Q)}, \tag{5.5.4}$$

after some considerable manipulation, it can be shown that

$$\Re\left[\tan\left(\eta_{\mathrm{v}}^{(i)} - \eta_{\mathrm{v}}' - \tau_i + \tau\right)\right] = \frac{a(\tau;k)}{b(\tau;k)} \tag{5.5.5}$$

and

$$\Im\left[\tan\left(\eta_{\mathrm{v}}^{(i)} - \eta_{\mathrm{v}}' - \tau_i + \tau\right)\right] = \frac{\Gamma^2(k)}{b(\tau;k)}, \tag{5.5.6}$$

where we have defined

$$a(\tau;k) = \mathcal{X}(k)\sin(2\tau) + \mathcal{Y}(k)\cos(2\tau) \tag{5.5.7}$$

and

$$b(\tau;k) = -f^2(\tau;k) - g^2(\tau;k), \tag{5.5.8}$$

noting that $b(\tau;k) < 0$, since we have assumed $g(\tau;k) \neq 0$ so that A is nonsingular. Here, we recall that τ_i is either of the two values of $\tau \in [0,\pi)$ such that $\frac{\partial^2 \eta_v}{\partial \tau^2}$ is zero in the generalised Kohn method and that $\eta_v^{(i)}$ is the corresponding value of the phase shift approximation. As in chapter 4, we label $i = 0$ for the value of τ_i minimising $\frac{\partial \eta_v}{\partial \tau}$ and $i = 1$ for the value of τ_i maximising $\frac{\partial \eta_v}{\partial \tau}$.

Now, setting $\tau = \tau_i$, $a(\tau_i;k)$ is zero by (4.5.5). Hence,

$$\Re\left[\tan\left(\eta_v^{(i)} - \eta_v'\right)\right] = \frac{\sin\left(\eta_v^{(i)} - \Re[\eta_v']\right)\cos\left(\eta_v^{(i)} - \Re[\eta_v']\right)}{\cos^2\left(\eta_v^{(i)} - \Re[\eta_v']\right) + \sinh^2(\Im[\eta_v'])} = 0 \tag{5.5.9}$$

and

$$\Im\left[\tan\left(\eta_v^{(i)} - \eta_v'\right)\right] = -\frac{\sinh(\Im[\eta_v'])\cosh(\Im[\eta_v'])}{\cos^2\left(\eta_v^{(i)} - \Re[\eta_v']\right) + \sinh^2(\Im[\eta_v'])} = \frac{\Gamma^2(k)}{b(\tau_i;k)} < 0. \tag{5.5.10}$$

Taking $\eta_v^{(i)} \in (-\pi/2, \pi/2]$ and $\Re[\eta_v'] \in (-\pi/2, \pi/2]$, since $\eta_v^{(0)}$ and $\eta_v^{(1)}$ are separated by $\pi/2$ we can immediately conclude from (5.5.9) that we have either $\Re[\eta_v'] = \eta_v^{(0)}$ or $\Re[\eta_v'] = \eta_v^{(1)}$. Moreover, using (4.4.25), (4.4.26) and (5.5.8), by the definitions of τ_0 and τ_1 it is plain that

$$\frac{\Gamma^2(k)}{b(\tau_1;k)} < \frac{\Gamma^2(k)}{b(\tau_0;k)} < 0, \tag{5.5.11}$$

noting from (5.5.9) and (5.5.10) that $b(\tau_0;k)$ and $b(\tau_1;k)$ cannot be equal, since $\eta_{\mathrm{v}}^{(0)}$ and $\eta_{\mathrm{v}}^{(1)}$ are separated by $\pi/2$ and exactly one of $\eta_{\mathrm{v}}^{(0)}$ or $\eta_{\mathrm{v}}^{(1)}$ must give $\cos\left(\eta_{\mathrm{v}}^{(i)} - \Re\left[\eta_{\mathrm{v}}'\right]\right) = 0$.

It follows directly from (5.5.10) and (5.5.11) that $\cos^2\left(\eta_{\mathrm{v}}^{(0)} - \Re\left[\eta_{\mathrm{v}}'\right]\right) > 0$. Consequently, inspection of (5.5.9) reveals

$$\eta_{\mathrm{v}}^{(0)} = \Re\left[\eta_{\mathrm{v}}'\right], \tag{5.5.12}$$

which is the desired result. □

For completeness, we note that expressions for first order calculations of η_{t}' analogous to (5.5.12) can be obtained in the following way. An analysis similar to that given in section 4.4 yields

$$\frac{\partial \eta_{\mathrm{t}}}{\partial \tau} = \frac{\bar{\mathcal{G}}(k)}{\bar{f}^2(\tau;k) + \bar{g}^2(\tau;k)}, \tag{5.5.13}$$

where $\bar{f}(\tau;k)$, $\bar{g}(\tau;k)$ and $\bar{\mathcal{G}}(k)$ are respectively as in (4.4.16), (4.4.17) and (4.4.24), but for the omission in each case of any term in $\Gamma(k)$. By further defining a function analogous to (5.5.8), namely

$$\bar{b}(\tau;k) = -\bar{f}^2(\tau;k) - \bar{g}^2(\tau;k), \tag{5.5.14}$$

we can also derive equations analogous to (5.5.9) and (5.5.10), viz.

$$\Re\left[\tan\left(\eta_{\mathrm{t}}^{(i)} - \eta_{\mathrm{t}}'\right)\right] = \frac{\sin\left(\eta_{\mathrm{t}}^{(i)} - \Re\left[\eta_{\mathrm{t}}'\right]\right)\cos\left(\eta_{\mathrm{t}}^{(i)} - \Re\left[\eta_{\mathrm{t}}'\right]\right)}{\cos^2\left(\eta_{\mathrm{t}}^{(i)} - \Re\left[\eta_{\mathrm{t}}'\right]\right) + \sinh^2\left(\Im\left[\eta_{\mathrm{t}}'\right]\right)} = 0 \tag{5.5.15}$$

and

$$\Im\left[\tan\left(\eta_t^{(i)}-\eta_t'\right)\right]=-\frac{\sinh\left(\Im\left[\eta_t'\right]\right)\cosh\left(\Im\left[\eta_t'\right]\right)}{\cos^2\left(\eta_t^{(i)}-\Re\left[\eta_t'\right]\right)+\sinh^2\left(\Im\left[\eta_t'\right]\right)}=\frac{\bar{\mathcal{G}}\left(k\right)}{\bar{b}\left(\tau_i;k\right)}, \tag{5.5.16}$$

where $i\in\{1,2\}$, with $\eta_t^{(0)}$ and $\eta_t^{(1)}$ being the first order approximations to the phase shift obtained in the generalised Kohn method at the values of τ respectively minimising and maximising $\frac{\partial\eta_t}{\partial\tau}$.

Proceeding in the same manner as in the previous proof, when $\bar{\mathcal{G}}\left(k\right)>0$ we obtain

$$\eta_t^{(0)}=\Re\left[\eta_t'\right]. \tag{5.5.17}$$

In the case where $\bar{\mathcal{G}}\left(k\right)<0$, using the same method we obtain

$$\eta_t^{(1)}=\Re\left[\eta_t'\right], \tag{5.5.18}$$

which is in fact the desired result since, if $\frac{\partial\eta_t}{\partial\tau}<0$ for all $\tau\in[0,\pi)$, η_t varies most slowly with τ when $\frac{\partial\eta_t}{\partial\tau}$ is maximised.

Thus, we have formally demonstrated the effective equivalence of the generalised and complex Kohn methods for trial functions of the form (1.7.3) and (5.2.1). Although we will not do so here, it should be possible to extend our analysis to a more abstract implementation of the two methods which avoids specific consideration of the (e^+-H_2) system.

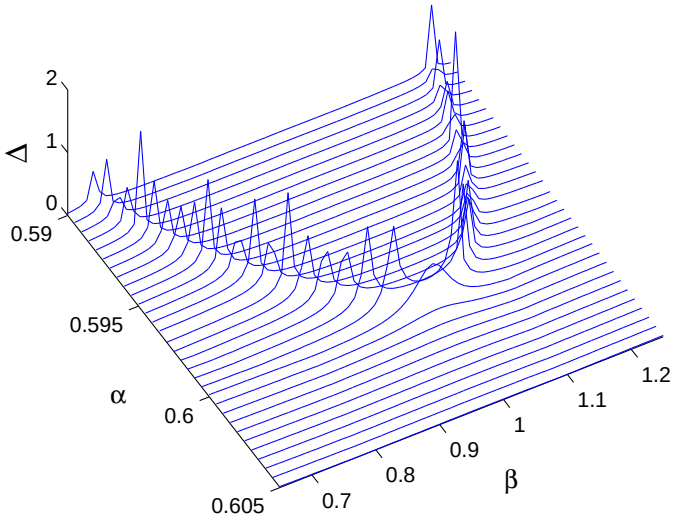

Figure 5.2: Values of $\Delta(\alpha, \beta)$ for $\breve{\Psi}_t^{(1,B)}$ at $k = 0.71$.

5.6 Avoiding persistent anomalies

As our application of the complex Kohn method has failed to resolve the problem of persistent Schwartz-type behaviour, we will conclude this chapter by briefly considering a more *ad hoc* approach. If the persistent anomalies we have observed are genuinely nonphysical, it should be possible to avoid them by variation of some free parameter in the Kohn trial function. We have found that variations in τ are not always successful and now consider other candidates. In our complex Kohn calculations involving $\breve{\Psi}_t^{(1,B)}$, we have varied the values of α and β in (1.7.8), recalling that they have, so far, remained fixed at $\alpha = 0.6$ and $\beta = 1.0$. 31 different values of α in the range $0.59 \leq \alpha \leq 0.605$ and 61 different values of β in the range $0.65 \leq \beta \leq 1.25$ have been investigated.

To illustrate persistent anomalous behaviour, it is helpful to define a function

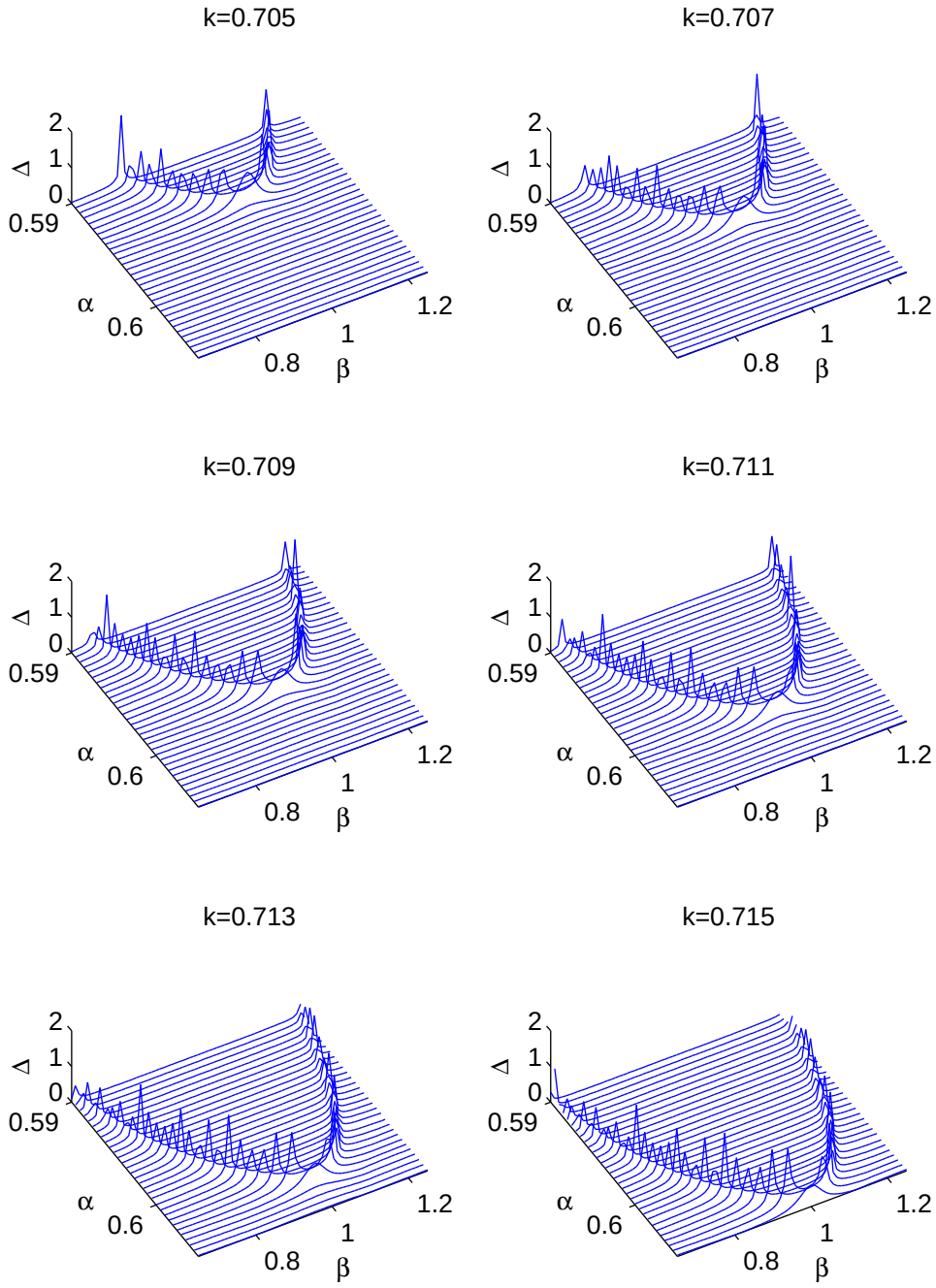

Figure 5.3: Values of $\Delta(\alpha, \beta)$ for $\breve{\Psi}_t^{(1,B)}$ near $k = 0.71$.

analogous to (3.2.3),

$$\Delta(\alpha,\beta) = |\eta_{\mathrm{v}}(\alpha,\beta) - \langle\eta_{\mathrm{v}}\rangle(\alpha)|, \tag{5.6.1}$$

where, for each of the values of α considered, $\langle\eta_{\mathrm{v}}\rangle$ is the median value of $\eta_{\mathrm{v}} = \Re[\eta'_{\mathrm{v}}]$ evaluated across the range of values of β. Values of $\Delta(\alpha,\beta)$ for $\breve{\Psi}_{\mathrm{t}}^{(1,\mathrm{B})}$ at $k = 0.71$ are shown in figure 5.2, from which it is clear that persistent anomalies appear distributed about a curve in the (α,β) plane. For values of α and β away from this curve, the calculations are free of anomalies. Hence, a small change in the value of α or β can indeed be shown successfully to avoid persistent anomalous behaviour.

Investigating further, we have found persistent anomalies in the (α,β) plane for values of k near to $k = 0.71$. Plots of $\Delta(\alpha,\beta)$ for $\breve{\Psi}_{\mathrm{t}}^{(1,\mathrm{B})}$ and for k in the range $0.705 \leq k \leq 0.715$ are shown in figure 5.3. The plots clearly indicate that the curve of persistent anomalies is a general feature of the calculation, moving through the (α,β) plane as k varies.

5.7 Conclusions

We have completed our investigation of Schwartz-type anomalies by implementing the complex Kohn method for our calculations on $(e^+ - \mathrm{H}_2)$ scattering. We have shown that the results of our complex Kohn calculations are independent of the choice of the phase parameter, τ, so that the use of an appropriate complex-valued trial function automatically avoids most of the Schwartz-type anomalies encountered in our earlier applications of the Kohn method.

We have found that, in the complex Kohn method, the second order approximation to the scattering phase shift is a complex number whose imaginary part can be ignored as an error term from the exact phase shift, η. We have shown that the real part of this complex number is equal to the value, $\eta_v^{(0)}$, obtained in the generalised Kohn method by minimising the derivative, $\frac{\partial \eta_v}{\partial \tau}$. This result formally describes an equivalence between the results of the generalised and complex Kohn methods.

The equivalence of the two methods explains why the persistent anomalies observed in chapters 3 and 4 remain present in our complex Kohn calculations involving $\breve{\Psi}_t^{(1,B)}$. We have successfully avoided these anomalies here by making small variations in the nonlinear parameters, α and β, found in the short-range correlation functions. In practice, at values of k where persistent anomalies are found, it should be necessary to consider only a small number of alternative values of α or β in order to avoid them.

This chapter concludes our analysis of Schwartz singularities and related anomalies. Our understanding of the underlying causes of the anomalous behaviour is now sufficiently advanced completely to avoid the effects of Schwartz singularities with ease. Our investigation has also identified a number of very interesting results concerning the mechanics of the Kohn method. In the following chapter, however, we will move away from abstract considerations of this kind and concentrate instead on calculations for the $(e^+ - H_2)$ system whose results can be compared with experimental data.

Chapter 6

Positron Annihilation and Z_{eff}

6.1 Introduction

For the very low positron energies with which our study of $(e^+ - H_2)$ interactions is most concerned, the only energetically accessible processes are elastic scattering and positron annihilation. We have presented calculations of elastic scattering parameters in the preceding chapters. It is the purpose of this chapter to introduce calculations involving positron annihilation with the electrons bound to the molecular target.

In theoretical models of positron annihilation processes, it is of great interest to calculate rates of annihilation as these can easily be compared with experimental results. For positron annihilation in molecules, it is convenient to express this rate in terms of a parameter, Z_{eff}. The value of Z_{eff} is proportional to the annihilation rate and can be regarded as the effective number of electrons per molecule available for annihilation. Generally, Z_{eff} is larger than the actual

number, Z, of electrons in each molecule, since the correlation of the positron with the target electrons tends to increase the electronic charge density in the region of the positron when it is close to the molecule.

We will show how estimates of Z_{eff} can be calculated from approximate scattering wavefunctions determined via the Kohn method. We will present Kohn calculations of Z_{eff}, both within the framework of the method of models and for an explicit consideration of the target potential. We find that, as with our calculations of η_{v} in chapter 2, there are marked differences in the results for these two cases, most notably at very low positron energies. We will discuss the possible causes of these differences. We will compare our results against experimental data and find that, in the case of calculations carried out with the method of models, good agreement is observed. However, for the more accurate calculations in which the target potential is treated explicitly, there remain notable differences between the experimental result and our theoretical estimates of Z_{eff}.

Our calculations of Z_{eff} differ from those of η_{v} in two important respects. Firstly, the error in the value of Z_{eff} obtained from an inexact trial function is first order in the error of that trial function. Thus, calculations of Z_{eff} provide a much more sensitive test of the accuracy of the trial function than do the variational phase shift calculations. Secondly, unlike our calculations of η_{v}, the choice of the normalisation constant in the trial function is important for determining a value of Z_{eff} which can legitimately be compared with experimental data.

6.2 Annihilation rates and Z_{eff}

Annihilation of a positron with an electron typically results in the emission of two or three photons, γ. Ore and Powell [82] have shown that 2γ emission is approximately 370 times more likely than 3γ emission. Emission of more than three photons is possible but, relatively, very unlikely [6]. For the calculations presented here, we will consider only 2γ emission. Dirac [3] has shown that, in the absence of any correlation, if the electron density in the region of the positron is n_e, then the nonrelativistic free annihilation rate, $\varrho_{2\gamma}$, into two photons is given by

$$\varrho_{2\gamma} = 4\pi r_0^2 c n_e, \tag{6.2.1}$$

c being the speed of light and where

$$r_0 = \frac{1}{4\pi\epsilon_0}\frac{e^2}{m_e c^2} \tag{6.2.2}$$

is the classical electron radius [83].

However, as noted by Charlton and Humberston [6], annihilation into two photons requires the positron-electron pair to be in a singlet spin state. Only one quarter of the electrons in an unpolarised ensemble would form such a state with the positron; the remainder would form a triplet spin state giving rise to annihilation into three photons at the much lower rate we have noted. Again in the absence of any correlation, the free annihilation rate, ϱ_f, in an unpolarised electron gas is hence given approximately by

$$\varrho_{\text{f}} \simeq \pi r_0^2 c n_e, \tag{6.2.3}$$

or, for electrons bound to molecules each having Z electrons,

$$\varrho_{\text{f}} \simeq \pi r_0^2 c n Z, \tag{6.2.4}$$

where n is the number density of molecules.

Calculating ϱ_{f} in this way does not generally give good agreement with experimentally measured annihilation rates of positrons in molecular gases, owing to the failure of (6.2.4) to take short-range correlations between the positron and the target electrons into account. These effects can be accounted for by implicitly defining a parameter, Z_{eff}, such that the experimentally observed annihilation rate, ϱ, satisfies

$$\varrho = \pi r_0^2 c n Z_{\text{eff}} \tag{6.2.5}$$

and in which Z_{eff} can be regarded as the effective number of electrons in each molecule available for annihilation. For H_2, the established experimental value of Z_{eff} for thermal positrons at 297 K is 14.61 ± 0.14 [25]. In our calculations, theoretical values of Z_{eff} can, in principle, be determined [11] from

$$Z_{\text{eff}}(k) = \sum_{i=1}^{2} \langle \Phi(\mathbf{r}_1, \mathbf{r}_2, \mathbf{r}_3, \mathbf{R}) \, | \delta(\mathbf{r}_i - \mathbf{r}_3) \, | \Phi(\mathbf{r}_1, \mathbf{r}_2, \mathbf{r}_3, \mathbf{R}) \rangle, \tag{6.2.6}$$

with $\Phi(\mathbf{r}_1, \mathbf{r}_2, \mathbf{r}_3, \mathbf{R})$ being an eigenfunction of $\mathbb{H}$ as in (1.2.9). This is the sum over both electrons of the expectation values of the Dirac delta functions, $\delta(\mathbf{r}_i - \mathbf{r}_3)$. As such, it is proportional to the probability that the coordinates of the positron effectively coincide with those of one of the target electrons.

In the fixed-nuclei approximation [53–55], Armour and Humberston [11] remark that (6.2.6) reduces to

$$\begin{aligned} Z_{\text{eff}}(k) &= \sum_{i=1}^{2} \overline{\langle \Psi(\mathbf{r}_1, \mathbf{r}_2, \mathbf{r}_3; \mathbf{R}) \, | \delta(\mathbf{r}_i - \mathbf{r}_3) \, | \Psi(\mathbf{r}_1, \mathbf{r}_2, \mathbf{r}_3; \mathbf{R}) \rangle} \\ &= 2\overline{\langle \Psi(\mathbf{r}_1, \mathbf{r}_2, \mathbf{r}_3; \mathbf{R}) \, | \delta(\mathbf{r}_1 - \mathbf{r}_3) \, | \Psi(\mathbf{r}_1, \mathbf{r}_2, \mathbf{r}_3; \mathbf{R}) \rangle}, \end{aligned} \tag{6.2.7}$$

with $\Psi(\mathbf{r}_1, \mathbf{r}_2, \mathbf{r}_3; \mathbf{R})$ as in (1.2.10) and where the bar above the integral indicates that it is averaged over all molecular orientations. However, at very low energies, since the incident positron wave effectively has no explicit orientation asymptotically far from the target molecule, for the same reasons as given in section 1.5 we can regard the value of Z_{eff} as being essentially independent of the orientation of the nuclear axis. For Kohn trial functions, $\Psi_t(\mathbf{r}_1, \mathbf{r}_2, \mathbf{r}_3; R)$, we can then obtain approximate values of Z_{eff} at low positron energies from

$$Z_{\text{eff}}(k) \simeq 2 \int |\Psi_t(\mathbf{r}_1, \mathbf{r}_2, \mathbf{r}_3; R)|^2 \delta(\mathbf{r}_1 - \mathbf{r}_3) \, d\mathbf{r}_1 d\mathbf{r}_2 d\mathbf{r}_3, \tag{6.2.8}$$

where we have dropped the Dirac integral notation to indicate explicitly the coordinates over which the integral is evaluated.

The error in the value of Z_{eff} obtained from (6.2.8) is first order in the error of Ψ_t from Ψ. Further, the choice of normalisation of Ψ_t in (6.2.8) is important for determining values of Z_{eff} which can be compared with experimental data. In the following section, we will show how the correct normalisation constant can be found. Comparisons with experimental data at 297 K can reasonably be made by considering trial wavefunctions which take into account only the lowest partial wave of Σ_g^+ symmetry. As noted by Armour and coworkers [29] for thermal positrons around this temperature, the contribution to Z_{eff} from this

partial wave is far greater than from any other. It is, therefore, reasonable in our calculations of Z_{eff} to continue with trial wavefunctions of the form already used in our calculations of scattering parameters.

6.3 Normalisation of the trial function

As noted, for example, by Armour and Baker [26], in order for theoretical calculations of Z_{eff} to be compared with experimental data, the Kohn trial function should be normalised to unit positron density when the positron is asymptotically far from the target. In the case of a real-valued trial function, Ψ_t, this corresponds to the choice $B = 1$ in (1.7.16). Hence, we require

$$\frac{\Psi_t}{\psi_G} - \exp\left(i\mathbf{k}.\mathbf{r}_3\right) \underset{r_3\to\infty}{\sim} \frac{\exp\left(ikr_3\right)}{r_3} f\left(k, R\right). \tag{6.3.1}$$

The normalisation constant, N, found in trial wavefunctions of the form (1.7.3) and (1.8.14) should therefore be chosen so that (6.3.1) is satisfied. Recalling (1.5.5), at sufficiently small values of k we can write

$$\exp\left(i\mathbf{k}.\mathbf{r}_3\right) \underset{r_3\to\infty}{\sim} \frac{1}{2ikr_3}\left[\exp\left(ikr_3\right) - \exp\left(-ikr_3\right)\right]. \tag{6.3.2}$$

Moreover, for trial wavefunctions of the form (1.7.3) and (1.8.14), using (1.7.13) and (1.7.14) we have

$$\frac{\Psi_t}{\psi_G} \underset{r_3\to\infty}{\sim} \frac{NR}{2\cos\left(\xi_t\right)} \frac{\sin\left(kr_3 + \eta_t\right)}{r_3}, \tag{6.3.3}$$

which we can rewrite as

$$\frac{\Psi_t}{\psi_G} \underset{r_3\to\infty}{\sim} \frac{NR}{4i\cos(\xi_t)\, r_3} \left[\exp\left(i\left[kr_3+\eta_t\right]\right) - \exp\left(-i\left[kr_3+\eta_t\right]\right)\right]. \tag{6.3.4}$$

Substituting (6.3.4) into (6.3.1) and using (6.3.2), for sufficiently small values of k we can then write

$$\begin{aligned} & \frac{1}{2i}\left[\frac{NR}{2\cos(\xi_t)}\exp(i\eta_t) - \frac{1}{k}\right]\frac{\exp(ikr_3)}{r_3} \\ - \quad & \frac{1}{2i}\left[\frac{NR}{2\cos(\xi_t)}\exp(-i\eta_t) - \frac{1}{k}\right]\frac{\exp(-ikr_3)}{r_3} \\ \underset{r_3\to\infty}{\sim} \quad & \frac{\exp(ikr_3)}{r_3} f(k,R). \end{aligned} \tag{6.3.5}$$

The two terms on the left hand side of (6.3.5) describe outgoing and incoming spherical waves. The term on the right hand side is a purely outgoing spherical wave. The coefficient of $\exp(-ikr_3)/r_3$ in (6.3.5) must, therefore, be zero. Hence, we choose N in (1.7.3) and (1.8.14) so that

$$N = \frac{2\cos(\xi_t)}{kR}\exp(i\eta_t) = \frac{\cos(\xi_t)}{c}\exp(i\eta_t). \tag{6.3.6}$$

In fact, since only $|N|^2$ appears in (6.2.8), it is sufficient to take N to be

$$N = \frac{\cos(\xi_t)}{c}. \tag{6.3.7}$$

The results presented in the remainder of this thesis will be from calculations carried out only with real-valued trial wavefunctions of the form (1.7.3) and

(1.8.14). Using the methods developed in chapter 4, in each trial function we will consider, we will implicitly take the value of τ to be equal to τ_0, so that the effects of Schwartz singularities are minimised. The corresponding calculations of $\eta_v^{(0)}$ require no more computational effort than the calculations of η_v' in the complex Kohn method and, as was shown in the last chapter, give equivalent results. In practice, we have found that anomalies in calculations of $Z_{\text{eff}}(\tau)$ appear over the same regions of τ as anomalies in the corresponding calculations of $\eta_v(\tau)$. Hence, in calculations of both η_v and Z_{eff}, choosing $\tau = \tau_0$ avoids Schwartz-type anomalies due to the choice of τ.

For brevity, we will not use an explicit notation to denote that each trial function has been optimised in τ. For example, henceforth when we write $\Psi_t^{(1,A)}$ we will implicitly take it to be evaluated at $\tau = \tau_0$. Moreover, we will implicitly use η_t and η_v respectively to denote the values of $\eta_t(\tau)$ and $\eta_v(\tau)$ obtained when each varies most slowly with τ. Finally, we will generally refer to our calculations simply as 'Kohn calculations' rather than 'optimised Kohn calculations'.

6.4 Calculations of Z_{eff}

We have calculated values of Z_{eff} for $\Psi_t^{(1,A)}$ and $\Psi_t^{(1,B)}$ by direct substitution into (6.2.8). It is straightforward to evaluate the integrals required by (6.2.8) without making any modifications to the existing computational framework. They are of a similar form to the Y integrals defined by (1.8.26), with the simplification that the integration over the coordinates of one of the electrons is omitted, owing to the presence of the Dirac delta function in (6.2.8). The values of α and β in the short-range correlation functions have been taken to be the same as those used prior to chapter 3, namely $(\alpha, \beta) = (0.5, -0.1)$ for $\Psi_t^{(1,A)}$

and $(\alpha, \beta) = (0.5, 1.0)$ for $\Psi_t^{(1,B)}$. The dependence of our calculations of Z_{eff} on α and β will be investigated in chapter 7.

We have also calculated values of Z_{eff} for two trial wavefunctions, $\Psi_t^{(1',A)}$ and $\Psi_t^{(1',B)}$. The basis functions used in these trial functions are respectively identical to those used in $\Psi_t^{(1,A)}$ and $\Psi_t^{(1,B)}$, but for the omission in each case of the 18 Hylleraas-type short-range correlation functions in the electron-positron coordinates. Comparing results for $\Psi_t^{(1,A)}$ with those for $\Psi_t^{(1',A)}$, as well as for $\Psi_t^{(1,B)}$ with those for $\Psi_t^{(1',B)}$, will illustrate the significance of the Hylleraas-type correlation functions in determining accurate values of Z_{eff}.

The dependence of Z_{eff} on k for $\Psi_t^{(1,A)}$ and $\Psi_t^{(1',A)}$ is shown in figure 6.1. The corresponding results for $\Psi_t^{(1,B)}$ and $\Psi_t^{(1',B)}$ are illustrated in figure 6.2. In both figures, we have compared our results with those reported in tables 1(6) and 4(ii) of the account given by Armour and Baker [65]. They carried out Kohn calculations using the method of models, with a trial wavefunction which included 8 Hylleraas-type correlation functions in the electron-positron coordinates. Until now, these were the highest values of Z_{eff} reported for Kohn calculations on $(e^+ - H_2)$ scattering using open-channel functions of the form (1.7.5) and (1.7.6) and involving only separable or Hylleraas-type correlation functions.

The figures illustrate a number of important points. Firstly, the inclusion of the Hylleraas-type correlation functions in the electron-positron coordinates leads, in both cases, to a dramatic increase in the value of Z_{eff}, bringing the results at the lower end of the energy scale into much closer agreement with the experimental value of $Z_{\text{eff}} = 14.6$ [25] for thermal positrons at 297 K. In fact, the importance of including these Hylleraas-type functions in calculations of Z_{eff} is even greater than in calculations of η_v. The reason for this is that accurate

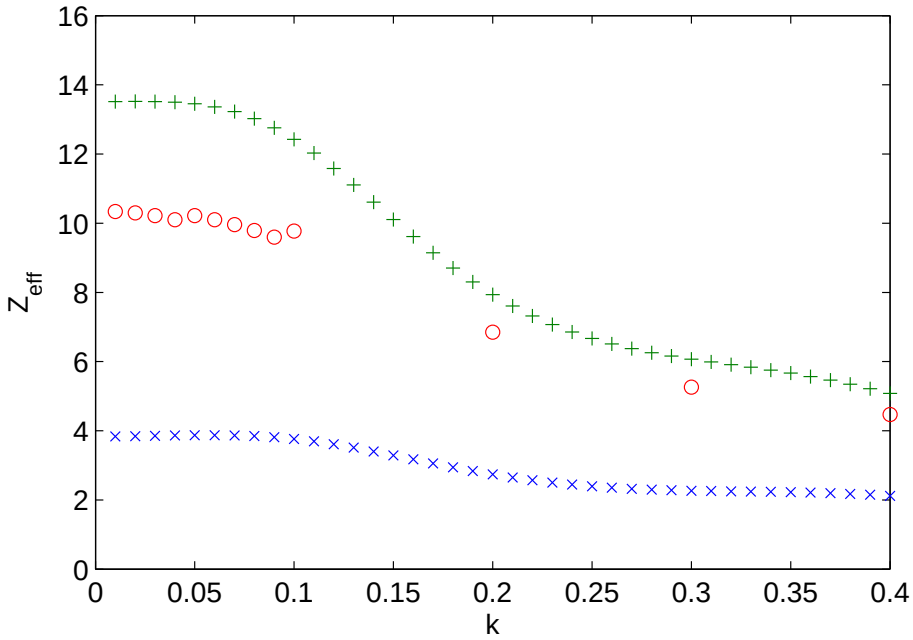

Figure 6.1: Values of $Z_{\text{eff}}(k)$ for [×] $\Psi_{\text{t}}^{(1',\text{A})}$, [+] $\Psi_{\text{t}}^{(1,\text{A})}$ and [○] as reported by Armour and Baker [65].

values of Z_{eff} will be obtained only if the trial wavefunction used in the calculation is accurate at a point where the coordinates of the positron coincide with those of one of the electrons. At a point of coincidence the exact wavefunction, Ψ, satisfies the Kato cusp condition [84],

$$\left(\frac{\partial\hat{\Psi}}{\partial r_{i3}}\right)_{r_{i3}=0} = -\frac{1}{2}\left(\Psi\right)_{r_{i3}=0}, \tag{6.4.1}$$

where $i \in \{1,2\}$ and $\hat{\Psi}$ is the average value of Ψ taken over a small sphere with r_{i3} constant, all other variables being fixed. Armour [85] explains that the inclusion of Hylleraas-type terms in the electron-positron coordinates makes it possible for the trial wavefunction to satisfy this condition approximately.

A second result evident from figures 6.1 and 6.2 is that values of Z_{eff} for $\Psi_{\text{t}}^{(1,\text{A})}$

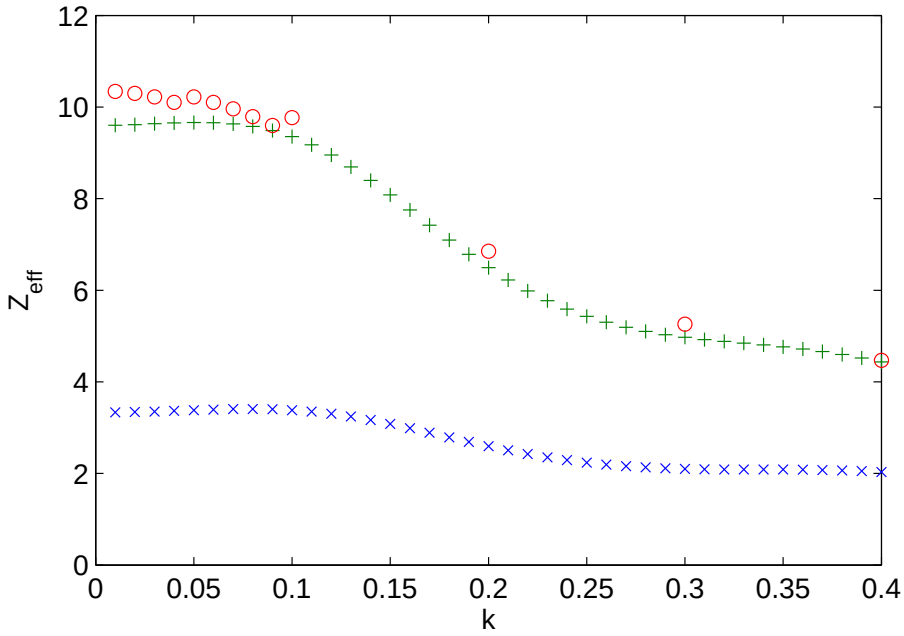

Figure 6.2: Values of $Z_{\text{eff}}\,(k)$ for [×] $\Psi_t^{(1',B)}$, [+] $\Psi_t^{(1,B)}$ and [○] as reported by Armour and Baker [65].

are noticeably higher at small values of k than those for $\Psi_t^{(1,B)}$. Indeed, in figure 6.1, at low energies the calculated values are as high as $Z_{\text{eff}} = 13.5$, giving much closer agreement with the experimental result than any previous calculation for this system. The corresponding results in figure 6.2, however, do not exceed $Z_{\text{eff}} = 9.66$. The most significant difference in the construction of $\Psi_t^{(1,A)}$ and $\Psi_t^{(1,B)}$ is the accuracy of the approximate target wavefunction, ψ_G, used in each case. It is possible that the values of Z_{eff} we have reported here for calculations involving $\Psi_t^{(1,A)}$ are spuriously high due to inaccuracies in the relatively simplistic target wavefunction, $\psi_G^{(A)}$. In chapter 8, we will investigate in more detail the importance of an accurate target wavefunction in our Kohn calculations.

We remark that the results for $\Psi_t^{(1,B)}$ are in broad agreement with those reported

by Armour and Baker [65], if slightly lower at small values of k. However, it is more instructive to compare those earlier results with the results obtained here for $\Psi_t^{(1,A)}$, since both sets of calculations used the method of models and employed target wavefunctions of similar accuracy. From figure 6.1, we see that the values of Z_{eff} obtained with $\Psi_t^{(1,A)}$ are significantly higher at low energies than those reported in the earlier calculations. A likely cause of this improvement in the method of models calculations is that the set, $\Omega^{(1)}$, of 279 correlation functions used in $\Psi_t^{(1,A)}$ provides a more accurate description of leptonic interactions than that given by the 72 correlation functions used by Armour and Baker [65]. A second factor could be that the calculations of Z_{eff} are sensitive to variations in the values of α and β; the values of $(\alpha, \beta) = (0.575, 0.2)$ used by Armour and Baker differ from the choice of $(\alpha, \beta) = (0.5, -0.1)$ made here. We will investigate the dependence of our results on the values of α and β in chapter 7.

6.5 Comparison with experimental data

Experimentally measured values of Z_{eff} reflect the average properties of a positron ensemble and correspond to a distribution of positron speeds. This distribution, $g(T, k)$, is dependent on the temperature, T, of the ensemble. By determining a thermal average, $\overline{Z_{\text{eff}}}$, of our calculations of $Z_{\text{eff}}(k)$ over such a distribution at a fixed temperature, we can obtain values suitable for comparison with experimental data. In principle, such averages are found directly from

$$\overline{Z_{\text{eff}}}(T) = \int_0^\infty g(T, k)\, Z_{\text{eff}}(k)\, \mathrm{d}k. \tag{6.5.1}$$

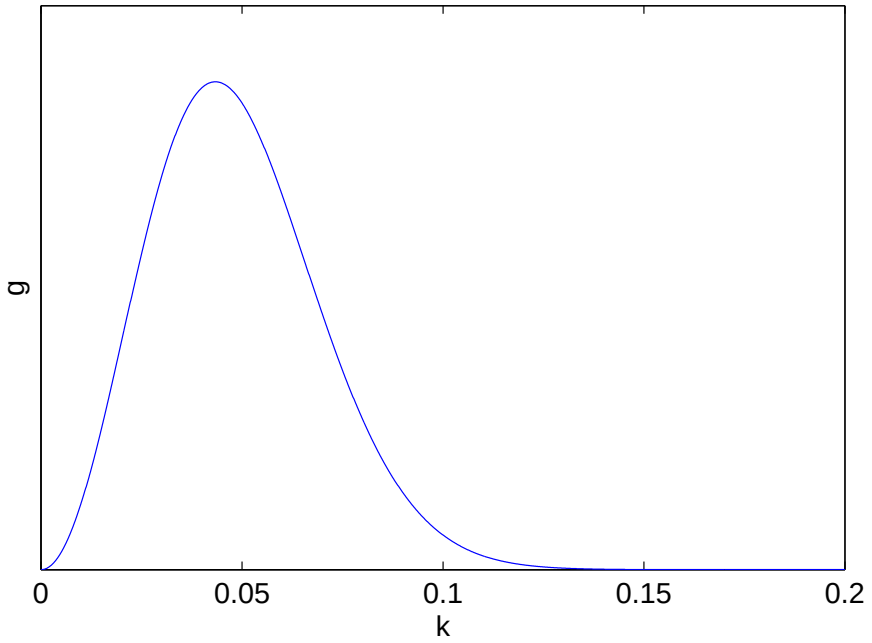

Figure 6.3: The Maxwell-Boltzmann speed distribution for positrons at 297 K.

In atomic units, the magnitude, k, of the positron momentum is equal to its speed. Taking $g(T,k)$ to be the Maxwell-Boltzmann distribution of speeds for positrons at a fixed temperature, T_0, we write

$$g(k) \propto k^2 \exp\left[-\frac{k^2}{2k_{\text{B}}T_0}\right], \tag{6.5.2}$$

where $k_{\text{B}} \simeq 3.17 \times 10^{-6}$ K^{-1} is the Boltzmann constant in atomic units. This distribution is illustrated in figure 6.3 for $T_0 = 297$ K, the temperature of the positron gas used by Laricchia *et al.* [25]. Inspection of the figure shows that the fraction of the distribution above $k \simeq 0.12$ is negligible.

In practice, since an analytic expression for $Z_{\text{eff}}(k)$ is not available, the integral (6.5.1) cannot be evaluated directly. Values of $\overline{Z_{\text{eff}}}$ can instead be estimated by averaging values of $Z_{\text{eff}}(k)$ at discrete values of k over the distribution (6.5.2).

When these calculations are carried out for the results illustrated in figures 6.1 and 6.2 for $\Psi_t^{(1,A)}$ and $\Psi_t^{(1,B)}$, respective values of $\overline{Z_{\text{eff}}} = 13.4$ and $\overline{Z_{\text{eff}}} = 9.63$ are obtained. These are very similar to the respective maximum values of $Z_{\text{eff}} = 13.5$ and $Z_{\text{eff}} = 9.66$ quoted in the preceding section. This is to be expected, since figures 6.1 and 6.2 show that the values of Z_{eff} for $\Psi_t^{(1,A)}$ and $\Psi_t^{(1,B)}$ do not vary considerably in the region of k where the distribution of positron speeds is most appreciable. In fact, for $k < 0.1$, because Z_{eff} is found to vary slowly with k for both $\Psi_t^{(1,A)}$ and $\Psi_t^{(1,B)}$, and $g(k)$ as shown in figure 6.3 is not heavily skewed, it should be sufficient to consider only values of Z_{eff} near the maximum of $g(k)$ in order to obtain results suitable for comparison with experiment. The modal value of the distribution (6.5.2) is $\bar{k} = \sqrt{2k_B T_0} \simeq 0.04$. The values of Z_{eff} obtained at $k = 0.04$ for $\Psi_t^{(1,A)}$ and $\Psi_t^{(1,B)}$ are, respectively, $Z_{\text{eff}} = 13.5$ and $Z_{\text{eff}} = 9.65$.

Particularly in the case of $\Psi_t^{(1,B)}$, the lack of agreement between our calculations of Z_{eff} and the experimental result indicates that the description of leptonic correlations given by the short-range correlation functions is deficient in some respect, to the extent that the lack of a second order correction term for Z_{eff} is important. Some measure of this importance can be obtained by comparing values over k of the second order approximation, η_v, to the scattering phase shift with the corresponding first order approximation, η_t. In figures 6.4 and 6.5 we provide such a comparison, respectively for $\Psi_t^{(1,A)}$ and $\Psi_t^{(1,B)}$. Further, in figures 6.6 and 6.7 we have plotted the ratio, η_v/η_t, as a function of k, respectively for $\Psi_t^{(1,A)}$ and $\Psi_t^{(1,B)}$.

The figures indicate that, especially at low energies, the second order approximation, η_v, to the scattering phase shift can be considerably larger than the first order approximation, η_t. Although we cannot necessarily draw direct quanti-

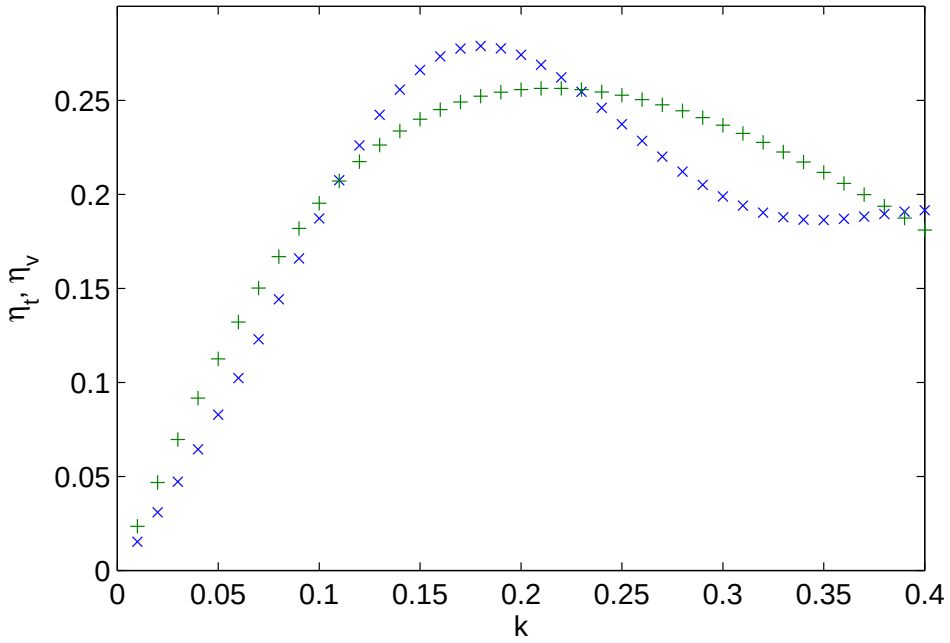

Figure 6.4: A comparison of [×] $\eta_t(k)$ with [+] $\eta_v(k)$ for $\Psi_t^{(1,A)}$.

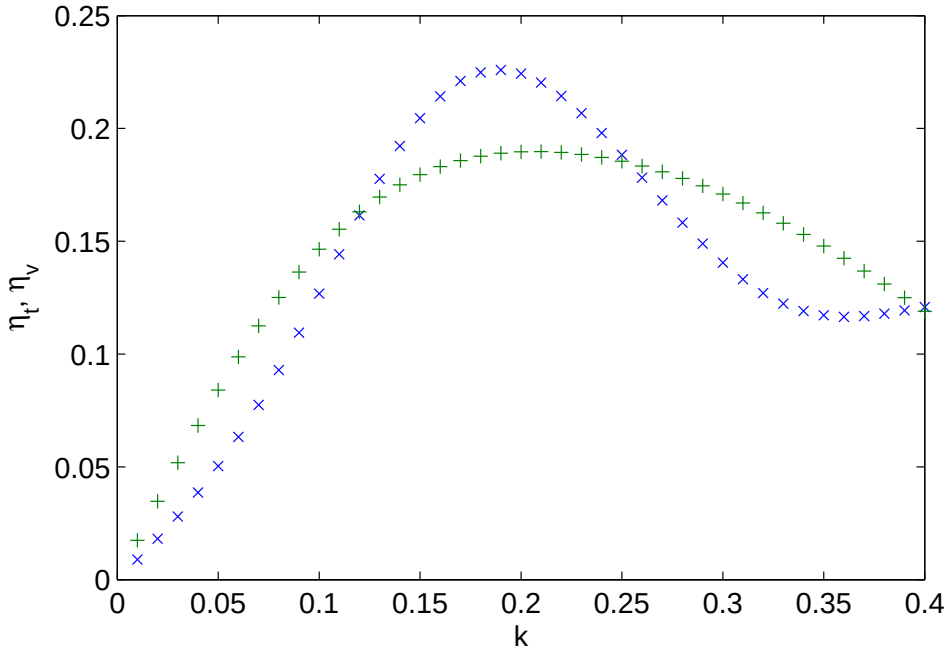

Figure 6.5: A comparison of [×] $\eta_t(k)$ with [+] $\eta_v(k)$ for $\Psi_t^{(1,B)}$.

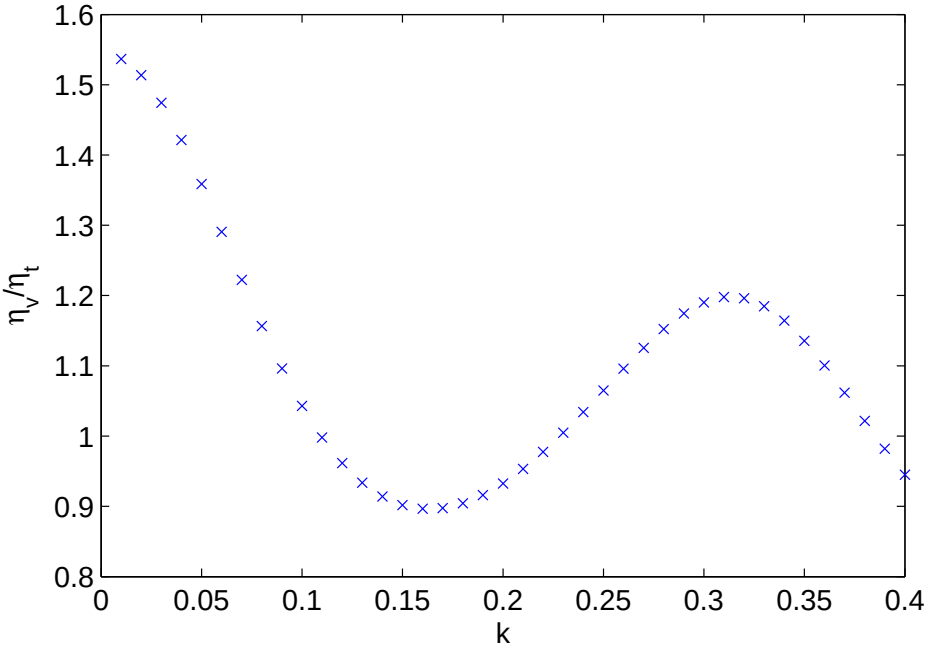

Figure 6.6: Values of η_v / η_t over k for $\Psi_t^{(1,A)}$.

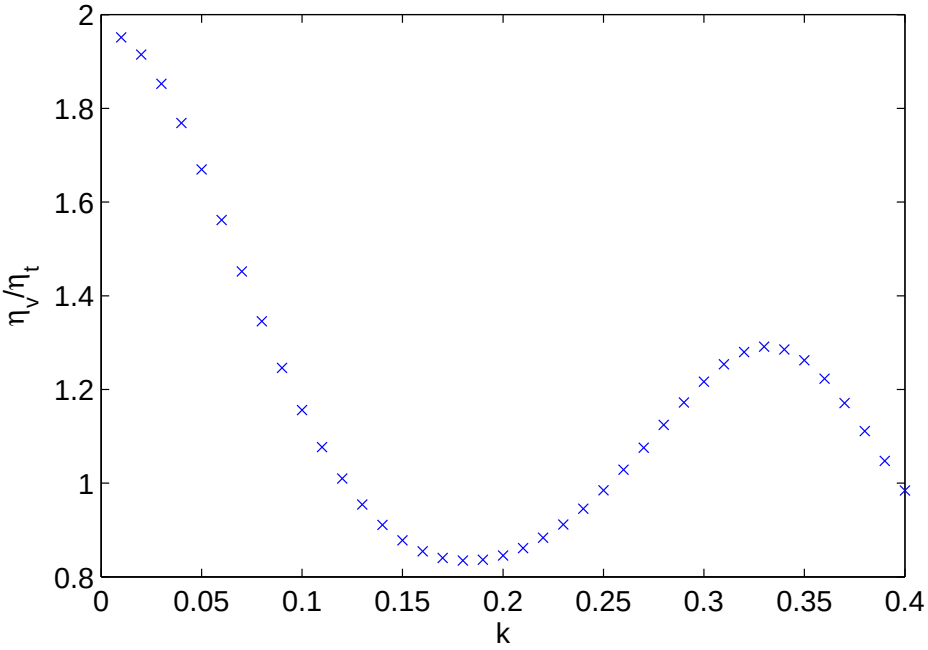

Figure 6.7: Values of η_v / η_t over k for $\Psi_t^{(1,B)}$.

tative comparisons here with our calculations of Z_{eff}, the figures suggest that, under the influence of a second order correction, we might conceivably expect our values of $\overline{Z_{\text{eff}}}$ to increase beyond the values determined in the previous section. It is frustrating that such a correction is not available.

6.6 Conclusions

We have determined estimates of the annihilation parameter, Z_{eff}, both within the framework of the method of models and for calculations in which the target potential is considered explicitly. There are significant differences between the results obtained in each case. The thermal average, $\overline{Z_{\text{eff}}} = 13.4$, obtained with the method of models and using $\Psi_t^{(1,A)}$, compares favourably with established experimental data and is higher than the values obtained in any previous Kohn calculation for the $(e^+ - H_2)$ system. In fact, as far as we are aware, our value of $\overline{Z_{\text{eff}}}$ for $\Psi_t^{(1,A)}$ gives the closest agreement with experiment of any consistent model to date, exceeding even the value of $Z_{\text{eff}} = 11.6$ obtained by Franz and Gianturco [39]. Their calculations were augmented by the inclusion of a semi-empirical enhancement factor, modelling the increased charge density near the positron when it is close to the target electrons.

The values of Z_{eff} calculated here using $\Psi_t^{(1,B)}$ are, by contrast, much lower and notable discrepancies remain between theory and experiment. The greatly improved accuracy of the approximate target wavefunction used in $\Psi_t^{(1,B)}$ over that used in $\Psi_t^{(1,A)}$ leads us to regard calculations involving $\Psi_t^{(1,B)}$ as being fundamentally more reliable. By returning to the elastic scattering phase shift calculations and comparing η_t with η_v, we have provided evidence to suggest that the errors in both $\Psi_t^{(1,A)}$ and $\Psi_t^{(1,B)}$ are sufficiently large to have had a significant

effect on the calculations of Z_{eff}.

There are several possible lines of further investigation. An obvious option is to improve the Kohn trial functions by including more flexible correlation functions than those defined by (1.7.8); terms linear in both ρ_{12} and ρ_{j3}, for example. However, modifications of this type require nontrivial extensions to be made to the computational framework we use to set up and solve the Kohn equations. In chapter 8, we will implement a more modest improvement to the set of short-range correlation functions.

Alternatively, we could examine how our calculations of both η_{v} and Z_{eff} depend on variations of the nonlinear parameters, α and β. The sensitivity of the Kohn calculations to changes in these parameters should decrease as the accuracy of the trial function increases. Here, the deficiencies in our description of the leptonic correlations are apparently considerable at low energies, so we might expect the choice of these nonlinear parameters to be of some importance. Our study of variations of α and β is presented in the next chapter.

Chapter 7

Optimisation of α and β

7.1 Introduction

In this chapter, we will discuss the effects on our Kohn calculations of varying the nonlinear parameters, α and β, that characterise the rate of exponential decline of the short-range correlation functions (1.7.8) far from the nuclei. In chapter 5, we saw how the choice of α and β could dramatically affect the results of Kohn calculations in the region of persistent Schwartz-type anomalies. Here, we will consider more general variations in the results of the calculations due to changes in these nonlinear parameters. Although not the first account of this kind for Kohn calculations on $(e^+ - H_2)$ scattering, ours is more extensive than those which have been given by other authors [26, 28, 29].

In the case where a given set of correlation functions is complete and the corresponding trial wavefunction is exact, the results of Kohn calculations will be independent of the choice of α and β. For an inexact trial function, as the de-

scription of leptonic interactions given by the short-range correlation functions converges, it is reasonable to expect that, away from Schwartz singularities, the results of Kohn calculations will depend less strongly on the chosen values of α and β. Hence, for an accurate trial wavefunction, we would expect values of η_v and Z_{eff} to vary slowly with α and β. In the last chapter, however, we presented evidence that a significant part of the leptonic correlations remained unaccounted for in the description given by the set of 279 correlation functions used in our Kohn calculations. Consequently, it is important to investigate how calculations involving these correlation functions are affected by the choice of α and β.

We will consider Kohn calculations carried out with the method of models using $\Psi_t^{(1,A)}$, as well as those carried out with an explicit consideration of the target potential using $\Psi_t^{(1,B)}$. We will find that, for both trial wavefunctions, the choice of α and β can significantly affect the calculated values of η_v and Z_{eff}. We will argue that a simple optimisation scheme for the nonlinear parameters can be developed by choosing α and β approximately to maximise η_v at low positron energies. In the neighbourhood of the optimum values of α and β, at low positron energies the calculated values of Z_{eff} will be seen to be much more sensitive to changes in α and β than the calculated values of η_v.

7.2 Optimisation

In contrast to variational calculations of bound states, there is no energy minimisation principle associated with scattering wavefunctions. As a result, it is not immediately clear how an optimisation of nonlinear parameters such as α and β might be achieved. However, for atomic scattering it has been shown

[86] that, for a system where no bound state exists, the Kohn method gives an upper bound on the scattering length, a, where

$$a = \lim_{k \to 0} \left(-\frac{\tan \eta}{k} \right), \tag{7.2.1}$$

and hence a lower bound on the exact phase shift, η, in the limit of zero positron energy. Obtaining bounds on scattering phase shifts at all nonzero energies is not generally possible in the Kohn method, owing to the occurrence of Schwartz-type anomalies. However, an analysis of potential scattering by Brownstein and McKinley [41] showed that, away from energies giving rise to Schwartz-type behaviour, the variational approximation to the phase shift is bounded, provided the Kohn trial function is, in some sense, sufficiently accurate.

Kohn calculations using exact target wavefunctions have been carried out by Humberston and are described, for example, in [11]. He found that, at low energies, the variational approximation to the phase shift tended to increase monotonically as the flexibility of the trial wavefunction was improved by the inclusion of a greater number of short-range correlation functions. He concluded that it was reasonable to expect the variational approximation to converge upwards to the exact phase shift with the use of an increasingly flexible trial wavefunction.

For inexact treatments of target states, however, accounts of Kohn calculations on low energy elastic positron scattering [19, 87] report that the monotonic increase in phase shift may continue well above the exact value if the description of scattering electronic correlation is made noticeably more sophisticated than the description of target electronic correlation. This highlights the need for determining, in a given calculation, whether or not the target wavefunction is suf-

ficiently accurate to give reliable values for scattering parameters. A detailed discussion on the importance of an accurate target wavefunction in our Kohn calculations will be given in chapter 8.

Returning to our own implementation of the Kohn method we see that, assuming our calculations are reliable in the sense that they are free of Schwartz-type anomalies and involve a sufficiently accurate description of the target state, we may regard η_v as an effective lower bound for η. Under these circumstances, values of α and β can justifiably be chosen approximately to maximise η_v at low energies.

7.3 Calculations of $\eta_v(\alpha,\beta)$ and $Z_{eff}(\alpha,\beta)$

We have carried out Kohn calculations using $\Psi_t^{(1,A)}$ and $\Psi_t^{(1,B)}$ for a range of values of α and β. Repeating our Kohn calculations for different values of α and β is computationally very expensive; each iteration necessitates the evaluation of a large number of integrals that can be obtained only numerically via a triple Neumann expansion. The current analysis has, therefore, been restricted to a set of candidate values for the nonlinear parameters which is relatively small in comparison with the extensive variation of τ explored in chapters 3 and 4.

For the method of models calculations carried out using $\Psi_t^{(1,A)}$, we have taken $\alpha \in \{0.2, 0.3, \ldots, 0.9, 1.0\}$ and $\beta \in \{-0.5, 0.4, \ldots, 0.4, 0.5\}$. For the calculations carried out using $\Psi_t^{(1,B)}$ involving explicit consideration of the target potential, we have taken $\alpha \in \{0.2, 0.3, \ldots, 0.9, 1.0\}$ and $\beta \in \{0.2, 0.3, \ldots, 1.4, 1.5\}$. As usual, the values of δ in $\Psi_t^{(1,A)}$ and $\Psi_t^{(1,B)}$ have been taken to be $\delta = 1.1$ and $\delta = 1.14$ respectively. For both trial wavefunctions, calculations involving val-

ues of $\alpha < 0.2$ have been avoided. In the case of $\Psi_t^{(1,B)}$, calculations involving values of $\beta < 0.2$ have also been avoided. The reason for this is that the correlation functions are more diffuse for smaller values of α and β; if either of these values is very small, problems can arise in obtaining converged values for the numerical integrals comprising the coefficients of the Kohn equations.

Calculated values of $\eta_v(\alpha, \beta)$ and $Z_{eff}(\alpha, \beta)$ at $k = 0.1$ are given in figures 7.1 and 7.2, respectively for $\Psi_t^{(1,A)}$ and $\Psi_t^{(1,B)}$. For both trial wavefunctions, the behaviour of η_v and Z_{eff} over α and β is smooth and broad maxima in all four plots are apparent. These figures also show that values of η_v and Z_{eff} are much smaller for values of β appearing at the lower end of the set of candidate values, an effect which is particularly striking for the calculations carried out with $\Psi_t^{(1,B)}$. Clearly, then, the choice of α and β in both sets of calculations is significant.

We will denote by α_m and β_m the values of α and β found, from the set of candidate values under consideration, to maximise η_v at a given value of k. On the understanding that it does not necessarily represent an optimisation, it is also of interest to consider the values, α'_m and β'_m, found approximately to maximise Z_{eff} at each k. For $\Psi_t^{(1,A)}$, values of α_m, β_m, α'_m and β'_m for a range of positron momenta are given in table 7.1, together with the values of $\eta_v(\alpha_m, \beta_m)$ and $Z_{eff}(\alpha'_m, \beta'_m)$. The corresponding values for $\Psi_t^{(1,B)}$ are given in table 7.2.

The maxima of $\eta_v(\alpha, \beta)$ and $Z_{eff}(\alpha, \beta)$ shown in the tables do not coincide. Further, for both $\Psi_t^{(1,A)}$ and $\Psi_t^{(1,B)}$, it appears from the tables that the optimal values of α tend to increase with k. This preference towards smaller values of α at very low energies is consistent with the findings of Armour and coworkers [29]. Those authors argue that smaller values of α allow for better representation of long-range polarisation effects brought about by the positron, which are most

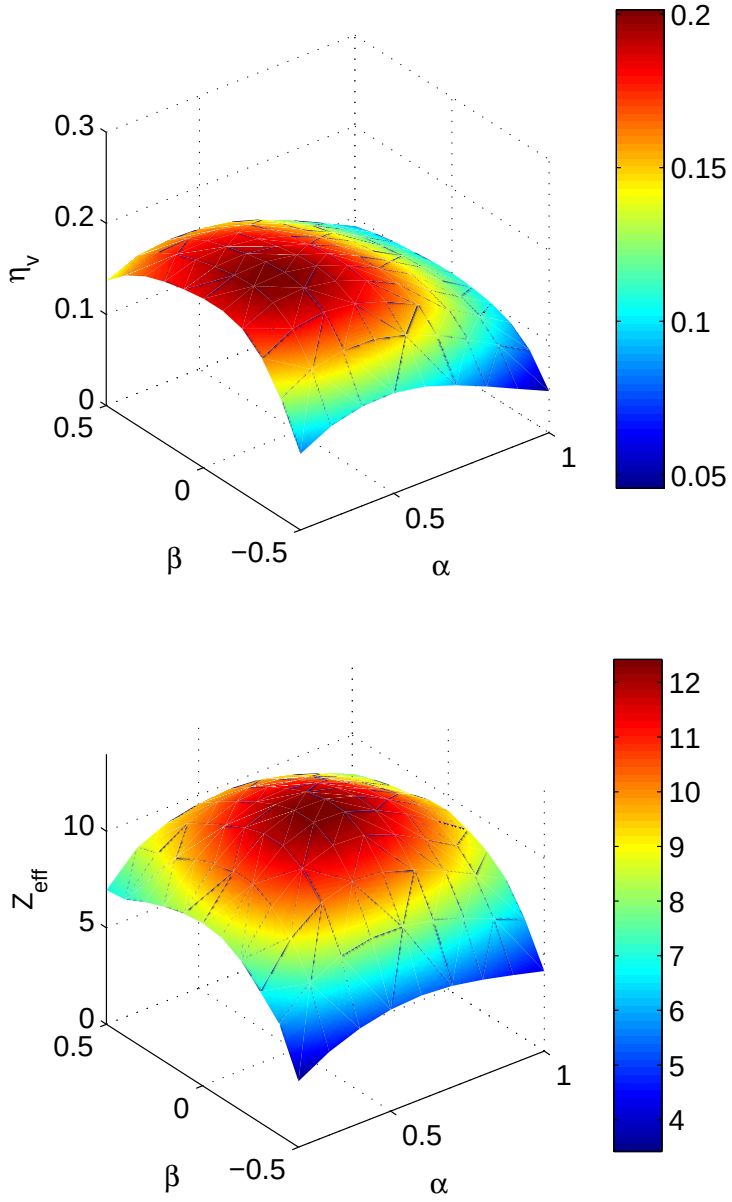

Figure 7.1: Values of $\eta_v(\alpha, \beta)$ and $Z_{eff}(\alpha, \beta)$ for $\Psi_t^{(1,A)}$ at $k = 0.1$.

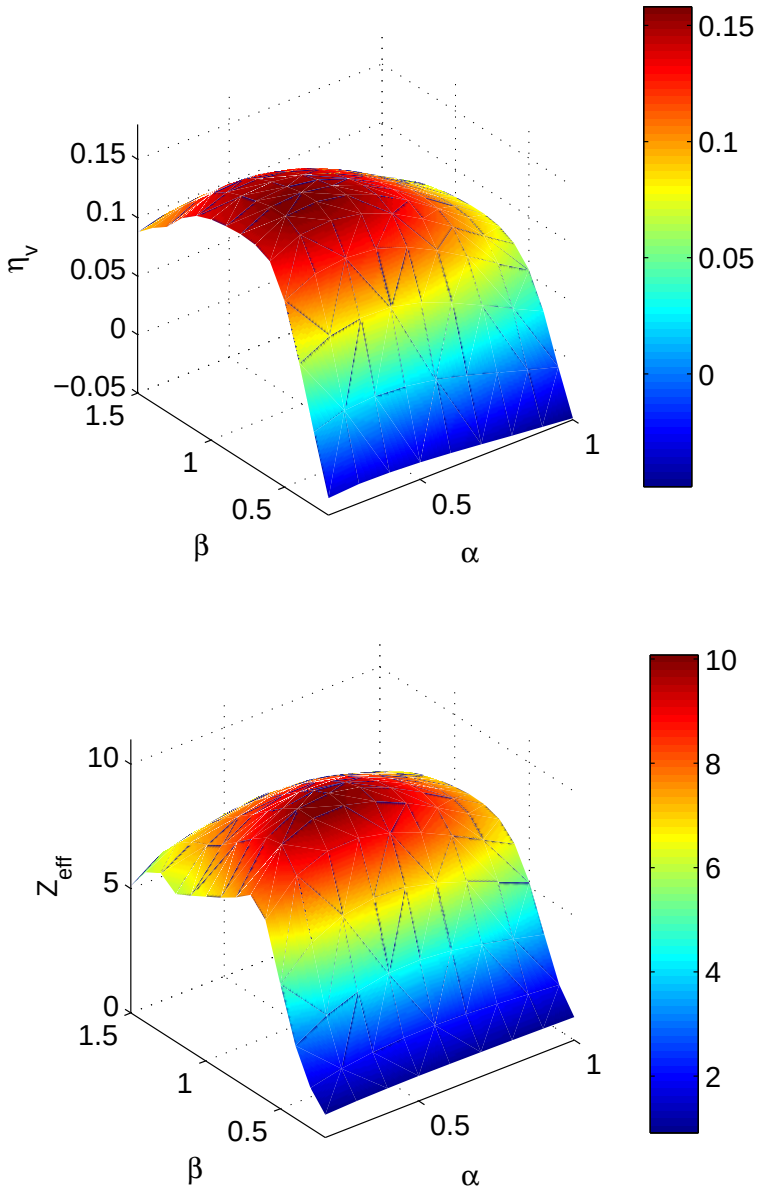

Figure 7.2: Values of $\eta_v(\alpha, \beta)$ and $Z_{eff}(\alpha, \beta)$ for $\Psi_t^{(1,B)}$ at $k = 0.1$.

k	α_{m}	β_{m}	$\eta_{\mathrm{v}}\left(\alpha_{\mathrm{m}}, \beta_{\mathrm{m}}\right)$	α'_{m}	β'_{m}	$Z_{\mathrm{eff}}\left(\alpha'_{\mathrm{m}}, \beta'_{\mathrm{m}}\right)$
0.01	0.3	-0.1	0.0256	0.5	-0.1	13.5
0.02	0.3	-0.1	0.0509	0.5	-0.1	13.5
0.03	0.3	-0.1	0.0754	0.5	-0.1	13.5
0.04	0.3	-0.1	0.0985	0.5	-0.1	13.5
0.05	0.3	-0.1	0.120	0.5	-0.1	13.5
0.06	0.3	-0.1	0.140	0.5	-0.1	13.4
0.07	0.3	-0.1	0.157	0.5	-0.1	13.2
0.08	0.4	-0.1	0.173	0.5	-0.1	13.0
0.09	0.4	-0.1	0.188	0.5	-0.1	12.8
0.1	0.4	-0.1	0.201	0.5	-0.1	12.4
0.2	0.4	-0.1	0.259	0.8	0.0	8.79
0.3	0.5	-0.1	0.237	0.4	0.0	6.28
0.4	0.5	-0.1	0.181	0.6	0.0	5.18

Table 7.1: Values of α and β approximately maximising η_{v} and Z_{eff} for $\Psi_{\mathrm{t}}^{(1,\mathrm{A})}$.

k	α_m	β_m	$\eta_v(\alpha_m, \beta_m)$	α'_m	β'_m	$Z_{eff}(\alpha'_m, \beta'_m)$
0.01	0.2	0.7	0.0211	0.5	0.8	10.2
0.02	0.2	0.7	0.0417	0.5	0.8	10.2
0.03	0.2	0.7	0.0612	0.5	0.8	10.3
0.04	0.3	0.7	0.0790	0.5	0.8	10.3
0.05	0.3	0.7	0.0961	0.4	0.8	10.3
0.06	0.3	0.7	0.112	0.4	0.8	10.3
0.07	0.3	0.7	0.125	0.5	0.8	10.3
0.08	0.3	0.7	0.137	0.5	0.8	10.3
0.09	0.4	0.7	0.148	0.5	0.8	10.2
0.1	0.4	0.7	0.158	0.5	0.8	10.1
0.2	0.4	0.8	0.197	0.7	0.8	7.58
0.3	0.4	0.8	0.177	1.0	0.8	5.45
0.4	0.5	0.8	0.126	0.3	1.1	5.75

Table 7.2: Values of α and β approximately maximising η_v and Z_{eff} for $\Psi_t^{(1,B)}$.

important at low energies. At higher energies, where the long-range polarisation interaction becomes less important, higher values of α are preferred as they give a better description of short-range correlation effects.

There is no variational principle to support choosing α and β to maximise Z_{eff}, so few conclusions can be drawn from the results tabulated for α'_{m} and β'_{m}. However, for $\Psi_{\text{t}}^{(1,\text{A})}$ we observe that the values of α and β approximately maximising Z_{eff} at low energies are, by accident, equal to the test parameters, $\alpha = 0.5$ and $\beta = -0.1$, used in chapter 6. This suggests that the values of Z_{eff} reported in that chapter for $\Psi_{\text{t}}^{(1,\text{A})}$ may be artificially large when compared with genuinely optimal results.

Plots of $\eta_{\text{v}}(\alpha, \beta)$ and $Z_{\text{eff}}(\alpha, \beta)$ for a range of values of k are given in figures 7.3 and 7.4 for $\Psi_{\text{t}}^{(1,\text{A})}$ and in figures 7.5 and 7.6 for $\Psi_{\text{t}}^{(1,\text{B})}$. Particularly in the case of $\Psi_{\text{t}}^{(1,\text{A})}$, the figures show that the values of η_{v} near a maximum are less sensitive to changes in α and β at higher values of k. The peaks in $\eta_{\text{v}}(\alpha, \beta)$ at $k = 0.3$ and $k = 0.4$ in figure 7.4, for example, are noticeably broader and flatter than those observed at $k = 0.01$, $k = 0.02$ and $k = 0.04$ in figure 7.3. In the case of $\Psi_{\text{t}}^{(1,\text{B})}$, figure 7.5 suggests that the genuinely optimal value of α at very low energies is probably less than $\alpha = 0.2$. That is, at $k = 0.01$, for example, it is not obvious that the plot of $\eta_{\text{v}}(\alpha, \beta)$ in figure 7.5 has reached a stationary point within the range of α considered. Unfortunately, for the reasons already given, we have found it impractical to consider calculations having $\alpha < 0.2$.

For both $\Psi_{\text{t}}^{(1,\text{A})}$ and $\Psi_{\text{t}}^{(1,\text{B})}$, it is interesting to see from figures 7.4 and 7.6 that, at higher values of k, the values of Z_{eff} do not vary as smoothly over α and β as they do at lower values of k. There is evidence of persistent Schwartz-type behaviour in Z_{eff} at $k = 0.4$ in figure 7.6. However, there are wider fluctuations

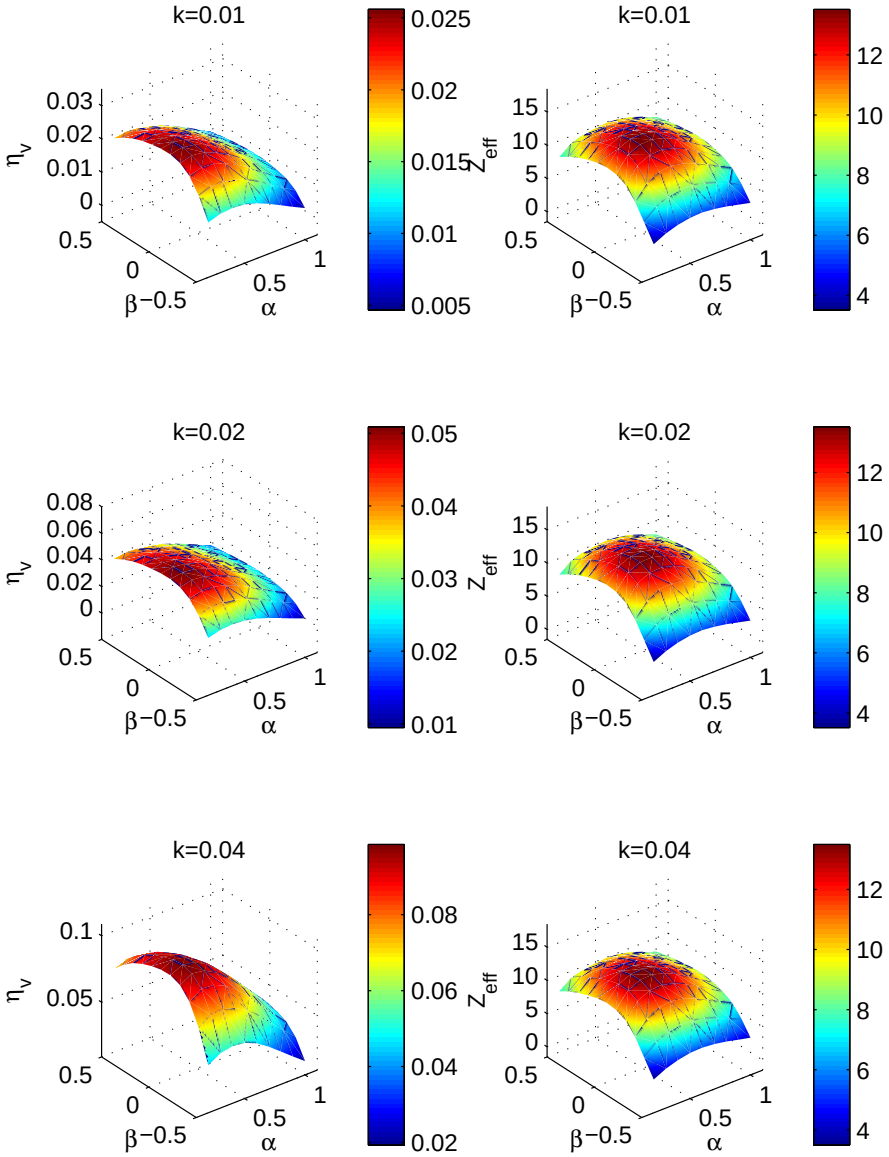

Figure 7.3: Values of $\eta_v(\alpha, \beta)$ and $Z_{eff}(\alpha, \beta)$ for $\Psi_t^{(1,A)}$ at various k.

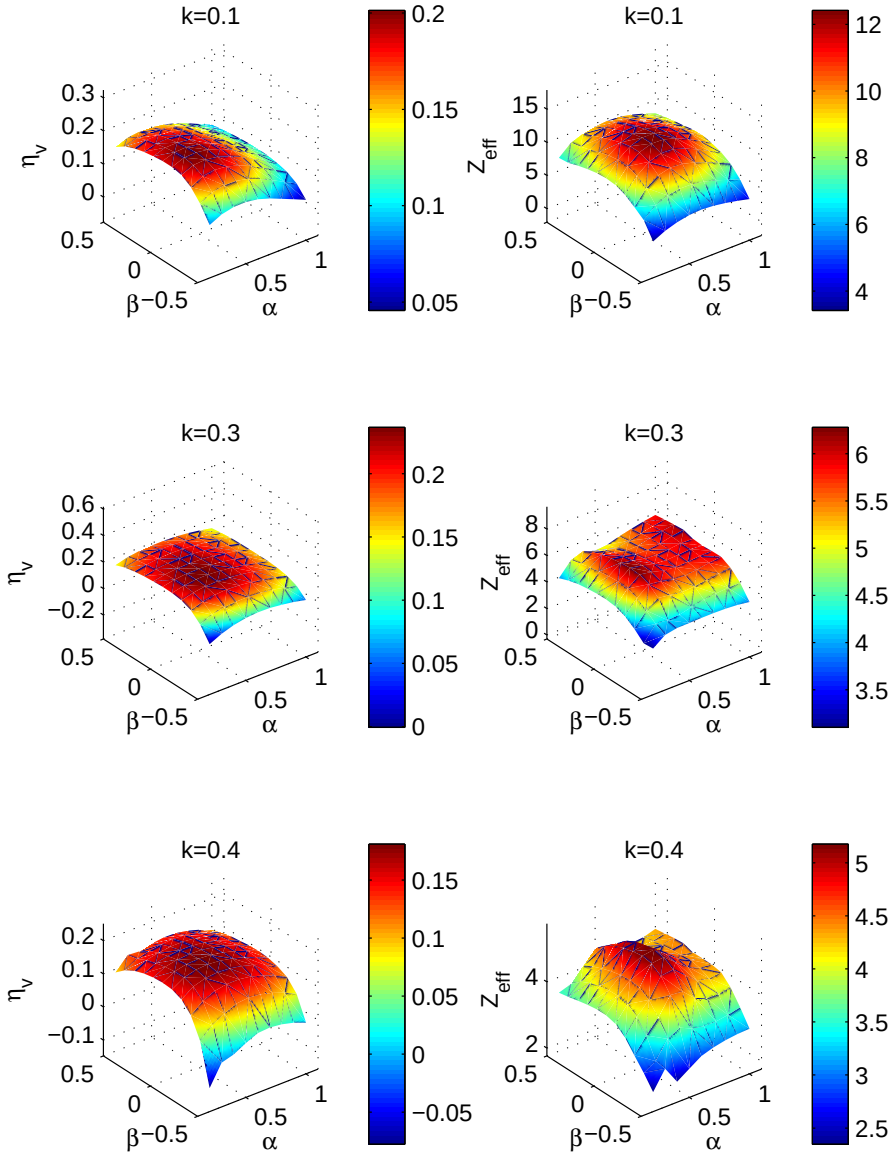

Figure 7.4: Values of $\eta_v(\alpha, \beta)$ and $Z_{eff}(\alpha, \beta)$ for $\Psi_t^{(1,A)}$ at various k.

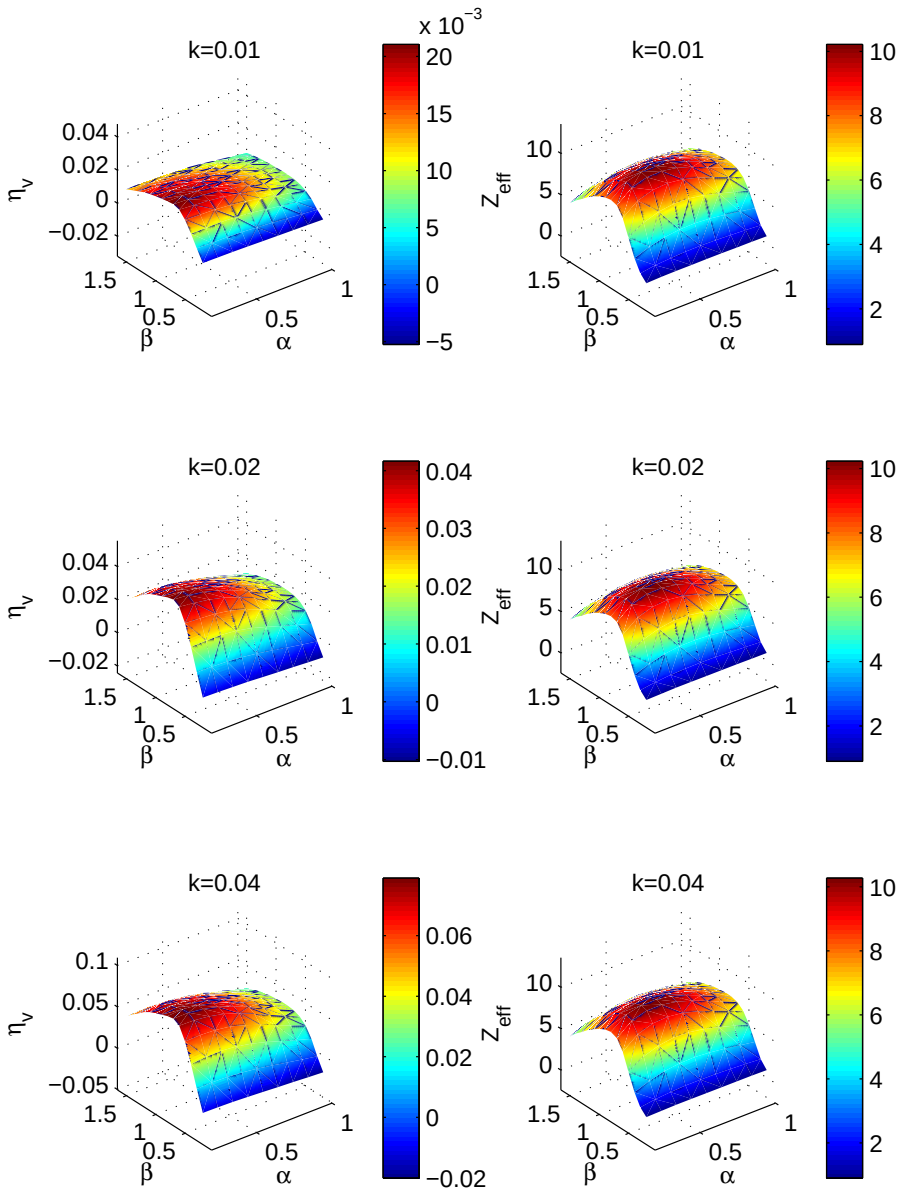

Figure 7.5: Values of $\eta_v(\alpha, \beta)$ and $Z_{eff}(\alpha, \beta)$ for $\Psi_t^{(1,B)}$ at various k.

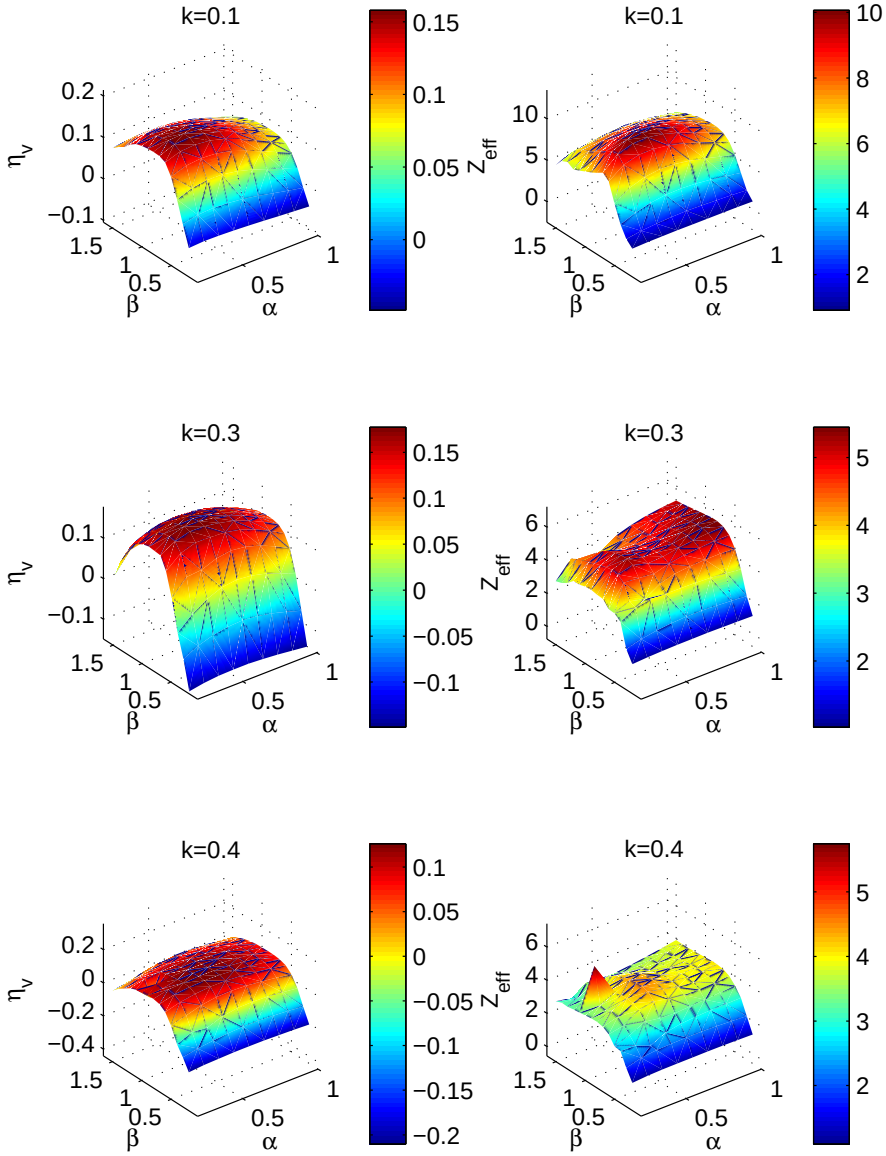

Figure 7.6: Values of $\eta_v(\alpha, \beta)$ and $Z_{eff}(\alpha, \beta)$ for $\Psi_t^{(1,B)}$ at various k.

in $Z_{\text{eff}}(\alpha, \beta)$ at $k = 0.3$ and $k = 0.4$ in both figures 7.4 and 7.6, that are of a different kind to the persistent Schwartz-type behaviour. It is conceivable that these effects could arise from the fact that, as discussed in chapter 6, the error in the calculated value of Z_{eff} from the exact value is large compared with the error of η_{v} from η. It is not clear, though, why such behaviour should be apparent only at higher energies. We remark upon these effects in passing and it is not our intention to investigate them in any more detail here. Provided that they remain confined to higher values of k, they will not affect those calculations of Z_{eff} which contribute significantly to the thermal average at 297 K.

7.4 Sensitivity of η_{v} and Z_{eff} to changes in α and β near a maximum

Figures 7.3–7.6 provide a useful qualitative overview of the behaviour of $\eta_{\text{v}}(\alpha, \beta)$ and $Z_{\text{eff}}(\alpha, \beta)$. It is also helpful to examine a smaller number of results in greater, quantitative detail. Plots of $\eta_{\text{v}}(k)$ and $Z_{\text{eff}}(k)$ for $\Psi_{\text{t}}^{(1,\text{A})}$ are given respectively in figures 7.7 and 7.8. Four choices of (α, β) are considered in each figure, these choices being made broadly in the region of $\alpha = 0.3$ and $\beta = -0.1$, which we have found approximately to maximise η_{v} for $k \leq 0.07$. Corresponding plots for $\Psi_{\text{t}}^{(1,\text{B})}$ are given in figures 7.9 and 7.10, for four choices of (α, β) near to $\alpha = 0.2$ and $\beta = 0.7$, which we have found approximately to maximise η_{v} for $k \leq 0.03$.

In the limit of low k, the differences in η_{v} between the different choices of (α, β) are negligible, for both $\Psi_{\text{t}}^{(1,\text{A})}$ and $\Psi_{\text{t}}^{(1,\text{B})}$. In this sense, we can regard the maxima of $\eta_{\text{v}}(\alpha, \beta)$ as being stable at low values of k. At higher values of k, differ-

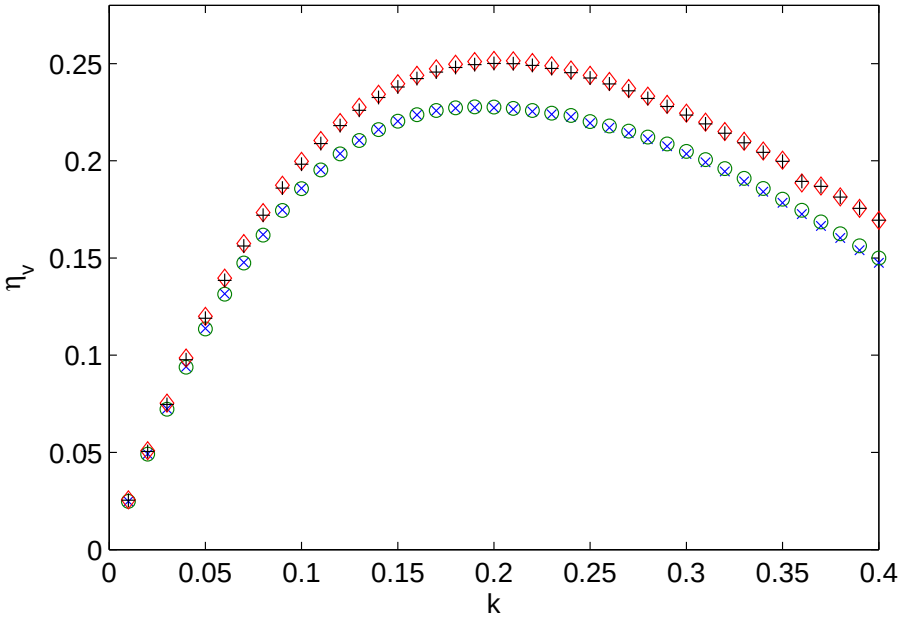

Figure 7.7: Values of $\eta_v(k)$ for $\Psi_t^{(1,A)}$ with [×] $(\alpha, \beta) = (0.2, -0.1)$, [○] $(\alpha, \beta) = (0.2, 0)$, [◇] $(\alpha, \beta) = (0.3, -0.1)$ and [+] $(\alpha, \beta) = (0.3, 0)$.

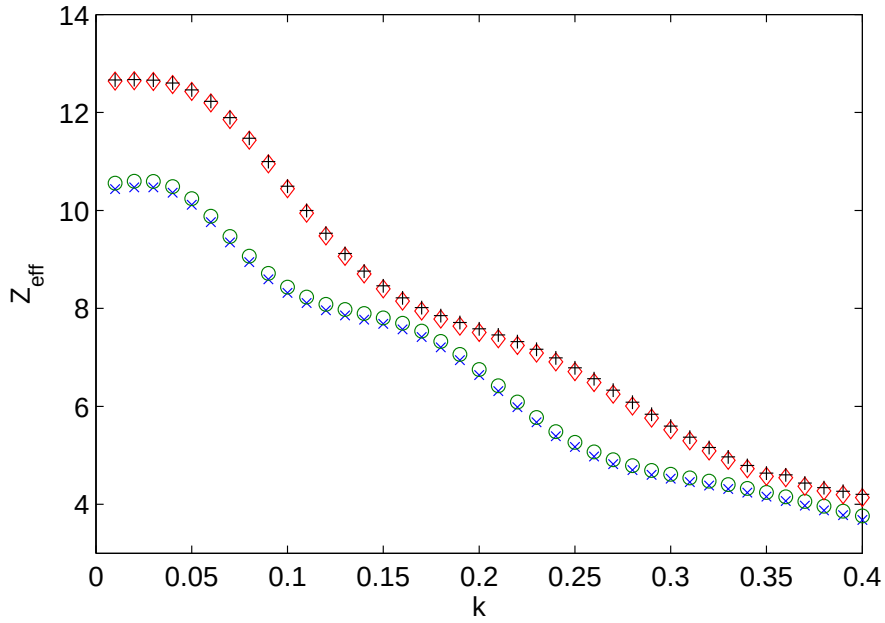

Figure 7.8: Values of $Z_{eff}(k)$ for $\Psi_t^{(1,A)}$ with [×] $(\alpha, \beta) = (0.2, -0.1)$, [○] $(\alpha, \beta) = (0.2, 0)$, [◇] $(\alpha, \beta) = (0.3, -0.1)$ and [+] $(\alpha, \beta) = (0.3, 0)$.

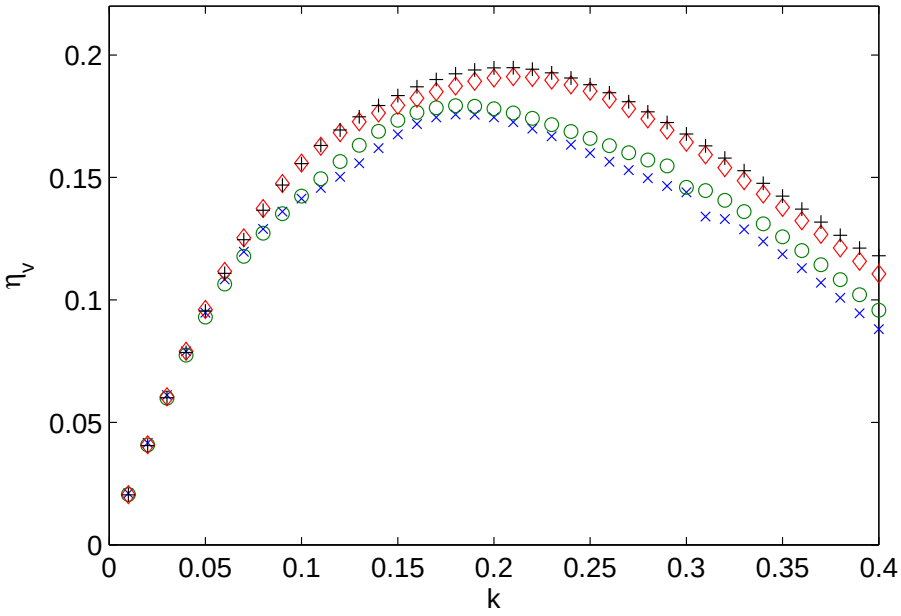

Figure 7.9: Values of $\eta_v(k)$ for $\Psi_t^{(1,B)}$ with [×] $(\alpha,\beta) = (0.2, 0.7)$, [○] $(\alpha,\beta) = (0.2, 0.8)$, [◇] $(\alpha,\beta) = (0.3, 0.7)$ and [+] $(\alpha,\beta) = (0.3, 0.8)$.

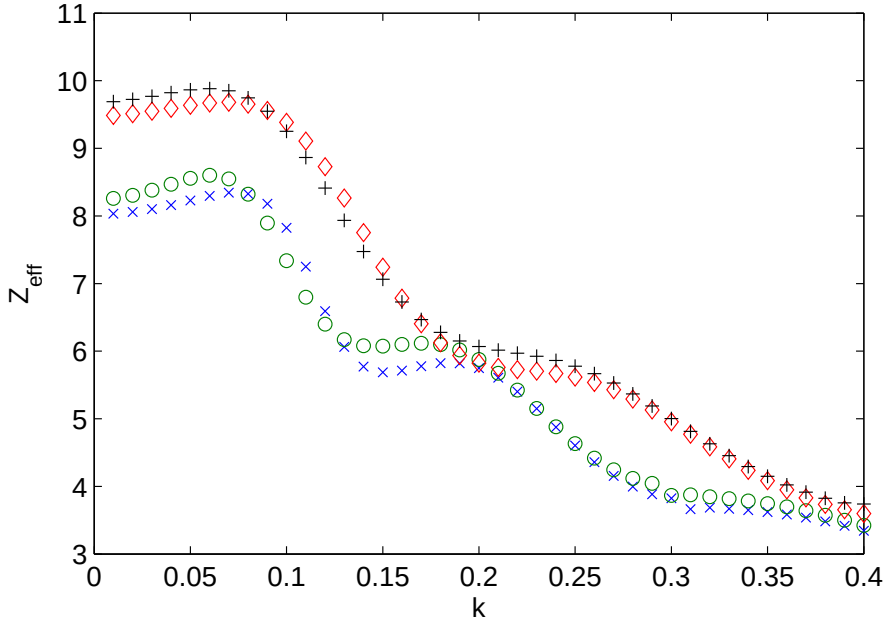

Figure 7.10: Values of $Z_{eff}(k)$ for $\Psi_t^{(1,B)}$ with [×] $(\alpha,\beta) = (0.2, 0.7)$, [○] $(\alpha,\beta) = (0.2, 0.8)$, [◇] $(\alpha,\beta) = (0.3, 0.7)$ and [+] $(\alpha,\beta) = (0.3, 0.8)$.

ences between the plots become more significant. We note that, for both trial wavefunctions, the changes in η_v due to small changes from the optimal value of α are larger than those due to small changes from the optimal value of β.

In contrast, for both $\Psi_t^{(1,A)}$ and $\Psi_t^{(1,B)}$, at low energies the calculated values of Z_{eff} are strongly dependent on the choice of (α, β), with the choice of α being of far greater importance. This increased sensitivity is a direct consequence of the fact that the maxima we have observed for $\eta_v(\alpha, \beta)$ and $Z_{eff}(\alpha, \beta)$ do not generally coincide. Hence, choices of (α, β) made close to the values approximately maximising $\eta_v(\alpha, \beta)$ do not typically correspond to the most stable regions of $Z_{eff}(\alpha, \beta)$.

The results shown in figures 7.8 and 7.10 highlight the importance of a careful consideration of α and β if accurate calculations of Z_{eff} are to be obtained. For example, the value of $Z_{eff} = 13.5$ found at $k = 0.04$ for $\Psi_t^{(1,A)}$ in chapter 6 was determined with the test parameters, $\alpha = 0.5$ and $\beta = -0.1$, and found to be in reasonable agreement with the experimental value of $Z_{eff} = 14.6$ [25]. Here, however, the more informed choice of $\alpha = 0.3$ and $\beta = -0.1$ for $\Psi_t^{(1,A)}$ gives a smaller value of $Z_{eff} = 12.6$ at $k = 0.04$.

7.5 Conclusions

We have demonstrated that the choice of the nonlinear parameters in our Kohn calculations can be significant, particularly for calculations of Z_{eff} at very low energies. This is a consequence of the fact that our Kohn trial functions are not exact. As a given trial function is made increasingly flexible and convergence is approached, the dependence of η_v on α and β should become very weak.

Eventually, the dependence of Z_{eff} on α and β should also become weak.

Despite the lack of an explicit variational bound principle, we have argued that the Kohn calculations can be optimised at low energies by selecting α and β approximately to maximise η_{v}. We have seen that these maxima are generally stable, so that different values of α and β in the region of each maximum tend to give rise to similar values of η_{v}. However, because the maxima of $\eta_{\text{v}}(\alpha, \beta)$ and $Z_{\text{eff}}(\alpha, \beta)$ do not generally coincide, our calculations of Z_{eff} have been found to be much more sensitive to small changes in the region of $(\alpha_{\text{m}}, \beta_{\text{m}})$.

In chapter 6, we found that the modal momentum of a Maxwellian distribution of positrons at 297 K is $k \simeq 0.04$. For convenience, in the following chapters we will usually carry out Kohn calculations for $\Psi_{\text{t}}^{(1,\text{A})}$ and $\Psi_{\text{t}}^{(1,\text{B})}$ at the values of α and β determined in section 7.3 approximately to maximise η_{v} at $k = 0.04$. This will allow us to explore other phenomena independently of the effects of varying the choices of α and β over k.

Chapter 8

The Importance of an Accurate Target Wavefunction

8.1 Introduction

In this chapter, we will examine the sensitivity of our Kohn calculations to changes in the accuracy of the part of the trial function representing the hydrogen molecule. In particular, we will discuss a number of unexpected results that arise when attempts are made to improve the quality of the Kohn calculations by extending the description of leptonic correlations to include Hylleraas-type terms in the interelectronic coordinate, ρ_{12}, in the closed-channel part of the trial function. Under these circumstances, we will see that Kohn calculations involving $\psi_G^{(B)}$ can be unreliable at very low positron energies, despite its taking into account of 96.8% of the correlation energy of H_2.

In the course of investigating this problem, we will find it necessary to extend

the computational framework used to evaluate the integrals required to construct the Kohn equations. The extensions we will describe allow for Kohn calculations to be carried out with trial wavefunctions in which the target wavefunction itself contains Hylleraas-type terms in ρ_{12}. As we have already discussed, descriptions of electronic correlations are known to converge much more quickly when basis functions of this type are used in the target wavefunction and their inclusion typically leads to a noticeable improvement in accuracy.

Here, we will carry out Kohn calculations using the target wavefunction, $\psi_G^{(C)}$, identical to $\psi_G^{(B)}$ but for the inclusion of a single Hylleraas-type basis function in ρ_{12}. $\psi_G^{(C)}$ is found to be extremely accurate, accounting for 99.7% of the correlation energy of H_2. We will see that reliable results are obtained for those Kohn calculations involving $\psi_G^{(C)}$ in which Hylleraas-type terms in ρ_{12} are included in the description of the target as well as in the short-range correlation functions. This is in contrast to results obtained for those Kohn calculations involving $\psi_G^{(B)}$ in which Hylleraas-type terms in ρ_{12} are included only in the short-range correlation functions.

The majority of this chapter is concerned with Kohn calculations in which the target potential is included explicitly and where the target wavefunctions are of a very high accuracy. For calculations using the method of models, we have already seen that the presence of the target wavefunction as a factor in the trial function restricts calculations to target wavefunctions accounting for a much smaller percentage of the correlation energy. We will conclude this chapter with a rudimentary study of the effects of varying the accuracy of the target wavefunction in the method of models framework, although it will be difficult to draw any definite conclusions from this investigation for the reason we have just given.

8.2 Correlation functions containing Hylleraas-type terms in ρ_{12}

We will examine first the results of Kohn calculations for trial wavefunctions having the general form (1.7.3) and containing the target wavefunction, $\psi_G^{(B)}$. In addition to the trial function, $\Psi_t^{(1,B)}$, used in the preceding chapters, we will consider a second wavefunction, $\Psi_t^{(2,B)}$. The forms of the two wavefunctions are identical, but for the fact that the set, $\Omega^{(2)}$, of $M = 297$ correlation functions used in $\Psi_t^{(2,B)}$ contains 18 Hylleraas-type terms in ρ_{12} having $\theta_i = 1$ in (1.7.9), in addition to the 279 terms comprising $\Omega^{(1)}$. Details of these functions are given in appendix A. Unless otherwise noted, for both $\Psi_t^{(1,B)}$ and $\Psi_t^{(2,B)}$ we will take the values of the nonlinear parameters in (1.7.8) to be $\alpha = 0.3$ and $\beta = 0.7$.

Values of $\eta_v(k)$ and $Z_{eff}(k)$ are shown respectively in figures 8.1 and 8.2 for both $\Psi_t^{(1,B)}$ and $\Psi_t^{(2,B)}$, for positron momenta in the range $0.01 \leq k \leq 0.4$. The effect of including in $\Psi_t^{(2,B)}$ the Hylleraas-type correlation functions in ρ_{12} is clear. The calculated values of both η_v and Z_{eff} for $\Psi_t^{(2,B)}$ are significantly greater at low positron momenta than the corresponding values obtained with $\Psi_t^{(1,B)}$. The differences between the results become smaller at higher positron momenta, with the two sets of results for Z_{eff} being essentially equivalent above $k \simeq 0.15$. We note that the calculated value of Z_{eff} for $\Psi_t^{(2,B)}$ at $k = 0.04$ is 13.5, in reasonable agreement with the accepted experimental value of $Z_{eff} = 14.6$ for thermal positrons at 297 K [25].

The influence of the Hylleraas-type functions in ρ_{12} on the calculated values of η_v and Z_{eff} becomes even more pronounced if the values of the nonlinear parameters, α and β, are varied. Figures 8.3 and 8.4 illustrate the respective

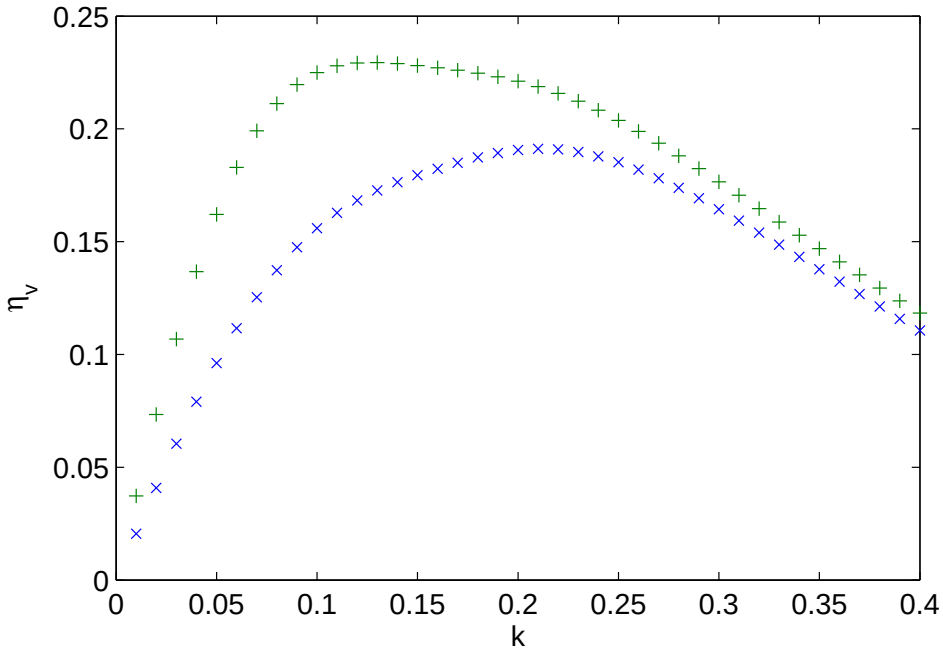

Figure 8.1: Values of $\eta_v\,(k)$ for [×] $\Psi_t^{(1,B)}$ and [+] $\Psi_t^{(2,B)}$.

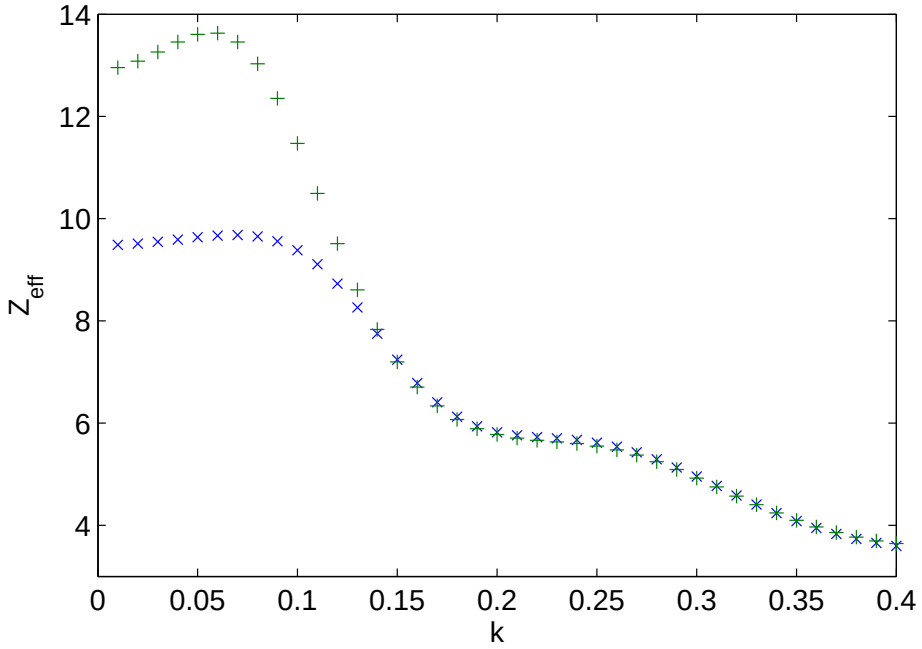

Figure 8.2: Values of $Z_{\text{eff}}\,(k)$ for [×] $\Psi_t^{(1,B)}$ and [+] $\Psi_t^{(2,B)}$.

dependence of η_v and Z_{eff} on α and β at $k = 0.04$, for $\Psi_t^{(1,B)}$ and $\Psi_t^{(2,B)}$. The effects of the Hylleraas-type functions in ρ_{12} included in $\Psi_t^{(2,B)}$ are most obvious for $\alpha < 0.5$ and become more dramatic as the value of α decreases.

In view of this, it is important to examine the possibility that the effects we have observed are not genuine and, instead, arise from inaccuracies in the numerical evaluation of the integrals required to formulate the Kohn equations. These could occur because the short-range correlation functions become more diffuse as the value of α decreases, increasing the range of the configuration space of the positron over which the effects of the correlation functions are significant. To investigate this, we have carried out a more detailed study of the Kohn calculations at $(\alpha, \beta) = (0.2, 1.1)$ and $(\alpha, \beta) = (0.2, 0.8)$, corresponding respectively to the maximum values of η_v and Z_{eff} observed for $\Psi_t^{(2,B)}$ in figures 8.3 and 8.4. If the effects observed for $\Psi_t^{(2,B)}$ are due to problems with convergence of integrals, increasing the range of integration in the λ_3 coordinate should have a significant effect on the results for η_v and Z_{eff}. However, when the range of integration in λ_3 is increased by 50%, we find that the values of η_v at $(\alpha, \beta) = (0.2, 1.1)$ and Z_{eff} at $(\alpha, \beta) = (0.2, 0.8)$ change respectively by only 0.1% and 0.2% from the values obtained prior to extending the range of integration. It is very unlikely, therefore, that the effects we have described have been caused by errors in the numerical integration.

Figures 8.1–8.4 indicate that the apparent importance of the Hylleraas-type correlation functions in ρ_{12} is a general feature of the calculation at low positron momenta. This is somewhat unexpected, since functions of this type do not address explicitly the key difficulty of describing correlations in terms of the electron-positron separation. It is conceivable that the observed behaviour is a result of inaccuracies in the calculation due to the use of the inexact target wave-

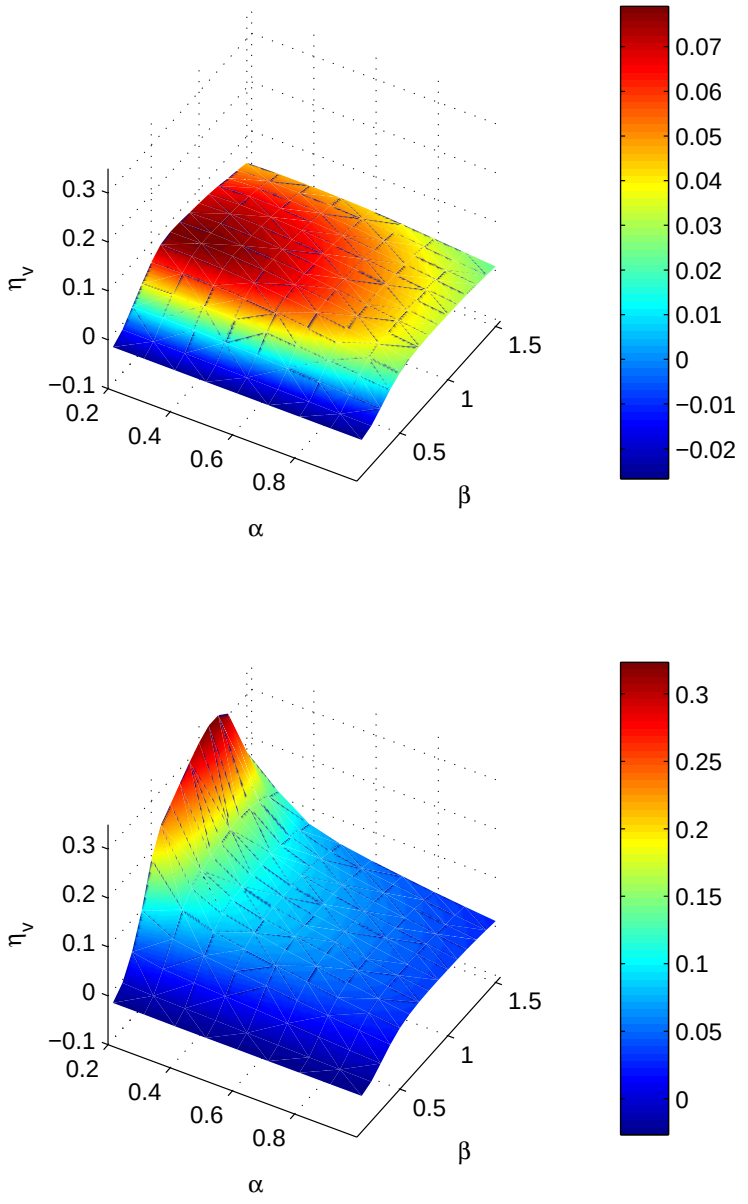

Figure 8.3: Values of $\eta_v(\alpha, \beta)$ for $\Psi_t^{(1,B)}$ (top) and $\Psi_t^{(2,B)}$ (bottom) at $k = 0.04$.

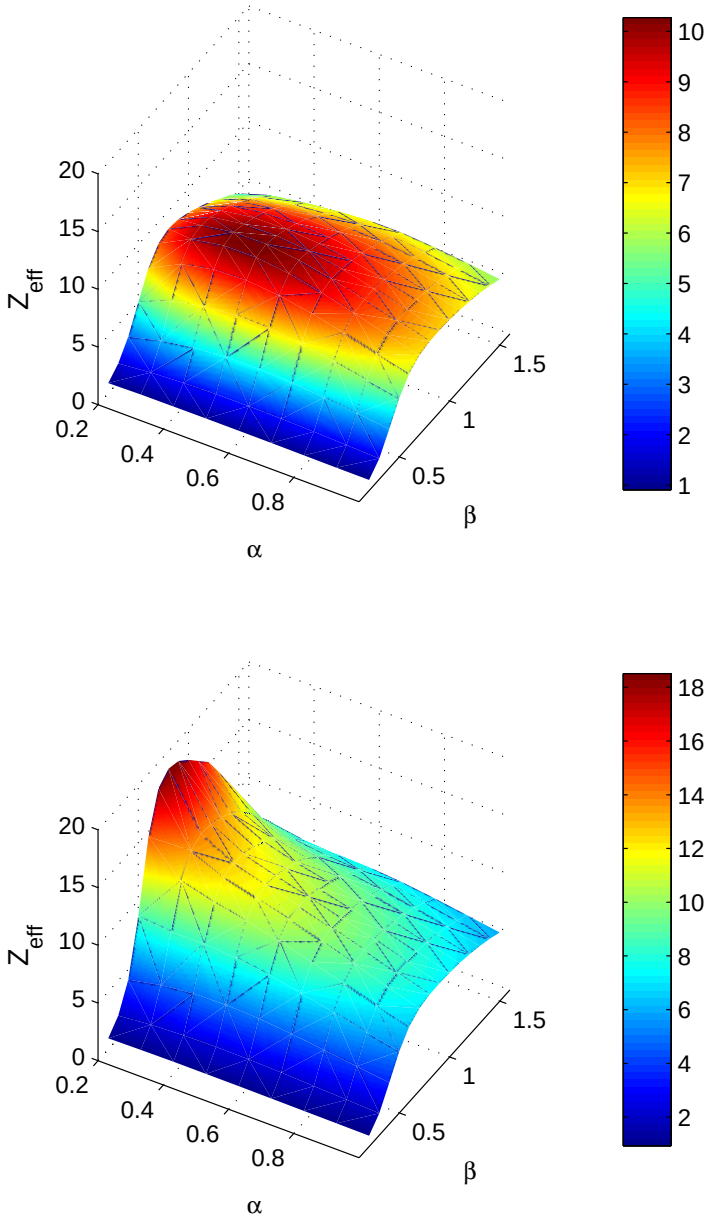

Figure 8.4: Values of $Z_{\text{eff}}(\alpha, \beta)$ for $\Psi_t^{(1,B)}$ (top) and $\Psi_t^{(2,B)}$ (bottom) at $k = 0.04$.

function, $\psi_G^{(B)}$, despite its taking into account of 96.8% of the correlation energy. This claim is consistent with the findings of Van Reeth and Humberston [88], who carried out Kohn calculations of s-wave phase shifts for positron scattering by atomic helium. They noted that if the flexibility of their trial wavefunction was increased by inclusion of additional short-range correlation terms, the results of Kohn calculations could be unreliable if a corresponding improvement was not also made to their target wavefunction.

Here, for Kohn calculations carried out with $\Psi_t^{(2,B)}$, there are no Hylleraas-type terms in ρ_{12} in $\psi_G^{(B)}$ to match those already contained in $\Omega^{(2)}$. Such terms have been omitted from all target wavefunctions considered in earlier chapters, as their inclusion generates integrals whose evaluation would require a significant extension to be made to the computational framework used in the calculations. However, in light of the conclusions drawn by Van Reeth and Humberston, as well as the results shown in figures 8.1–8.4, we have determined to make this extension. The nature of the improvements will be discussed in section 8.4. As a preliminary, we will first investigate the sensitivity of our Kohn calculations to changes in the accuracy of the target wavefunction without explicit consideration of Hylleraas-type terms in ρ_{12}.

8.3 Varying the correlation energy

We again consider trial functions having the general form (1.7.3) and begin with the target wavefunction, $\psi_G^{(B)}$. Removing basis functions incrementally at random from $\psi_G^{(B)}$ then generates a series of target wavefunctions accounting for successively smaller fractions of the correlation energy of H_2. After

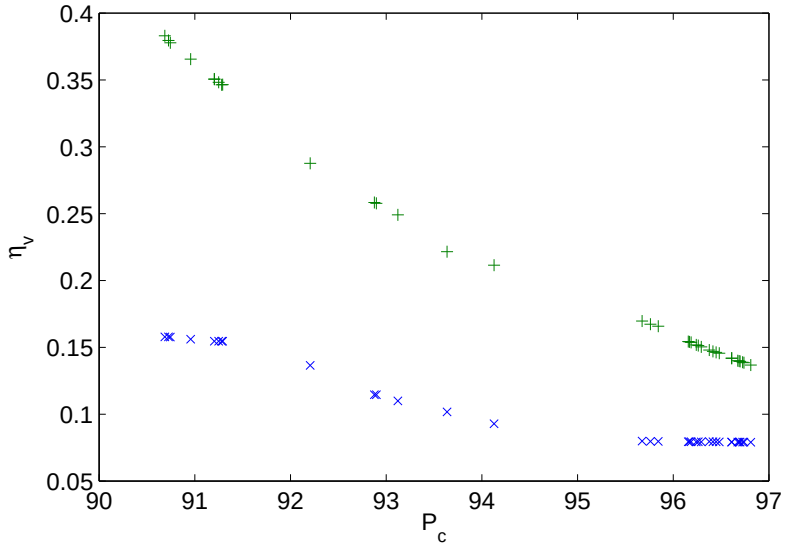

Figure 8.5: The dependence of η_v on P_c at $k = 0.04$, for trial functions containing [×] $\Omega^{(1)}$ and [+] $\Omega^{(2)}$. Basis functions have been removed successively from $\psi_G^{(B)}$.

each removal, carrying out Kohn calculations using the target wavefunction of reduced accuracy allows the dependence of η_v and Z_{eff} on P_c (1.6.14) to be investigated.

We have performed Kohn calculations in this way, each time for two trial wavefunctions containing the sets of correlation functions, $\Omega^{(1)}$ or $\Omega^{(2)}$. A maximum of 70 basis functions have been removed from the original set of 144 functions comprising $\psi_G^{(B)}$, at which point the target wavefunction accounts for 90.7% of the correlation energy of H_2. The dependence of η_v and Z_{eff} on the accuracy, P_c, of each target wavefunction is shown in figures 8.5 and 8.6 respectively, for $k = 0.04$.

The values of η_v and Z_{eff} tend to decrease monotonically with increasing P_c, for both $\Omega^{(1)}$ and $\Omega^{(2)}$. However, there is a distinct convergence in η_v and

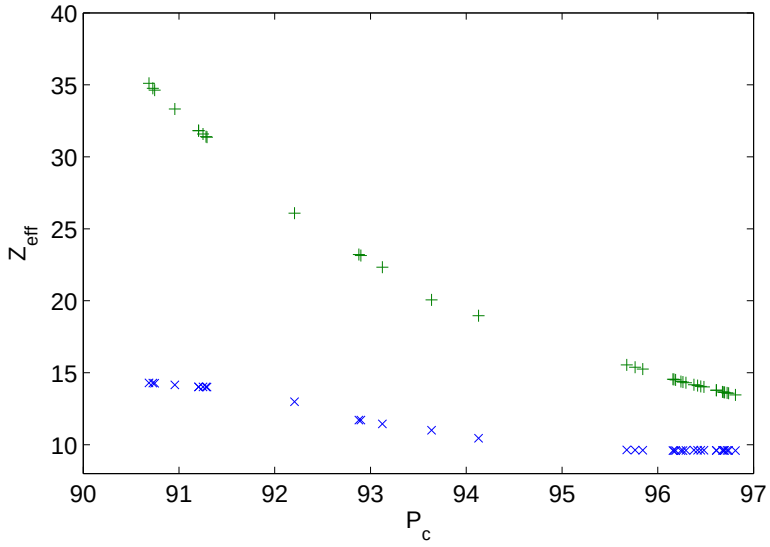

Figure 8.6: The dependence of Z_{eff} on P_{c} at $k = 0.04$, for trial functions containing [$\times$] $\Omega^{(1)}$ and [+] $\Omega^{(2)}$. Basis functions have been removed successively from $\psi_{\text{G}}^{(\text{B})}$.

Z_{eff} for the results corresponding to $\Omega^{(1)}$ above $P_{\text{c}} \simeq 96$, which is not evident for the results corresponding to $\Omega^{(2)}$. More generally, we have observed similar behaviour for analogous calculations performed at different values of k. We conclude that Kohn calculations carried out using $\psi_{\text{G}}^{(\text{B})}$ are reliable when Hylleraas-type terms in ρ_{12} are omitted from the correlation functions, but are unreliable when functions of this type are included. From inspection of figures 8.5 and 8.6, for trial wavefunctions containing the set, $\Omega^{(2)}$, we would expect any increase in the accuracy of a target wavefunction beyond that of $\psi_{\text{G}}^{(\text{B})}$ to be accompanied by a noticeable drop in the values of η_{v} and Z_{eff}.

8.4 Improving the accuracy of the target wavefunction

Target wavefunctions of an appreciably higher accuracy than $\psi_{\mathrm{G}}^{(\mathrm{B})}$ can be obtained via the inclusion of basis functions containing Hylleraas-type terms in ρ_{12}. It is easily shown that consideration of such basis functions in our Kohn calculations requires the evaluation of integrals, $\mathcal{V}'$, that can be written in a general form analogous to that used for the $\mathcal{V}$ integrals (1.8.29), viz.

$$\begin{aligned}
\mathcal{V}' \quad & [\sigma_1, \sigma_2, \sigma_3, \zeta_1, \zeta_2, \zeta_3, \alpha_1, \alpha_2, \alpha_3] \\
= \quad & \frac{1}{8\pi^3} \int_0^{2\pi} \int_0^{2\pi} \int_0^{2\pi} \int_{-1}^{1} \int_{-1}^{1} \int_{-1}^{1} \int_{1}^{\infty} \int_{1}^{\infty} \int_{1}^{\infty} \lambda_1^{\sigma_1} \lambda_2^{\sigma_2} \lambda_3^{\sigma_3} \mu_1^{\zeta_1} \mu_2^{\zeta_2} \mu_3^{\zeta_3} \\
\times \quad & \frac{\rho_{ij}\rho_{ik}}{\rho_{jk}} \exp\left(-\alpha_1\lambda_1 - \alpha_2\lambda_2 - \alpha_3\lambda_3\right) f_3\left(\lambda_3\right) \\
\times \quad & \left(\lambda_1^2 - \mu_1^2\right)\left(\lambda_2^2 - \mu_2^2\right)\left(\lambda_3^2 - \mu_3^2\right) \\
\times \quad & \mathrm{d}\lambda_1 \mathrm{d}\lambda_2 \mathrm{d}\lambda_3 \mathrm{d}\mu_1 \mathrm{d}\mu_2 \mathrm{d}\mu_3 \mathrm{d}\phi_1 \mathrm{d}\phi_2 \mathrm{d}\phi_3, \qquad (8.4.1)
\end{aligned}$$

where $f_3\left(\lambda_3\right)$ is one of S (1.7.5), C (1.7.6) or χ_0 (1.7.7) and $\{i, j, k\}$ is some permutation of $\{1, 2, 3\}$. By inspection, the general form of (8.4.1) is the same for $f_3\left(\lambda_3\right) = C$ and $f_3\left(\lambda_3\right) = \chi_0$, so we will here discuss only the cases $f_3\left(\lambda_3\right) = S$ and $f_3\left(\lambda_3\right) = C$. It is necessary to evaluate integrals of this form as they appear in Kohn matrix elements in the leptonic potential (1.3.10) between open and closed-channel parts of the trial function, whenever the target basis function and short-range correlation function under consideration contain a Hylleraas-type term respectively in the electron-electron and electron-positron distances.

Integrals of the form (8.4.1) differ from the original $\mathcal{V}$ integrals by the inclusion of the open-channel factor, $f_3\left(\lambda_3\right)$. In collaboration with Dr. Martin Plum-

mer of STFC Daresbury Laboratory [89], we have extended the computational framework used in our calculations to allow the necessary $\mathcal{V}'$ integrals to be determined numerically. As a principal component of this extension, it was necessary to evaluate one-dimensional integrals, $I[m,\alpha]$ and $J[m,\alpha]$, of the form

$$I[m,\alpha] = \int_1^w \lambda_3^m \exp(-\alpha\lambda_3) \frac{\sin[c(\lambda_3-1)]}{\lambda_3-1} \mathrm{d}\lambda_3 \tag{8.4.2}$$

and

$$J[m,\alpha] = \int_1^w \lambda_3^m \exp(-\alpha\lambda_3) \frac{\cos[c(\lambda_3-1)]}{\lambda_3-1} (1-\exp[-\gamma(\lambda_3-1)])\,\mathrm{d}\lambda_3, \tag{8.4.3}$$

for $m \in \mathbb{N}$, $\alpha > 0$ and $w > 1$. Although $I[m,\alpha]$ and $J[m,\alpha]$ can easily be evaluated using numerical integration, an analytic determination is preferable to minimise computational expense. Efficiency considerations of this kind are important in this context as the integrals (8.4.2) and (8.4.3) need to be calculated a great many times for different values of m and w as part of an iterative procedure used to calculate each $\mathcal{V}'$ integral. We will not discuss the design aspects of the computational algorithms here, although in appendix B we will show that $I[m,\alpha]$ and $J[m,\alpha]$ can, in fact, be found analytically.

Having provided Dr. Plummer with the method for the analytic evaluation of $I[m,\alpha]$ and $J[m,\alpha]$, the necessary modifications to the computational framework were made by him at Daresbury Laboratory. To verify the correctness of these changes, independent tests were devised at Nottingham in the following way: Using Taylor series expansions for S and C, it is straightforward to see that integrals of the form (8.4.1) can be expressed as a sum of $\mathcal{V}$ integrals (1.8.29). Terminating the expansion at an appropriate point allows approximate values,

$\tilde{\mathcal{V}}'$, of the $\mathcal{V}'$ integrals to be determined directly from the truncated summation of $\mathcal{V}$ integrals. Obtaining values of $\tilde{\mathcal{V}}'$ in this way generally is not practical, since the Taylor series expansions may converge slowly, depending on the values of the parameters contained in S and C. Each term in the expansion corresponds to a different $\mathcal{V}$ integral, whose calculation adds significantly to the computational expense. However, under circumstances where the expansions converge reasonably quickly, this method of obtaining approximations to $\mathcal{V}'$ integrals is clearly useful as part of a test framework.

The Taylor series expansions for S and C about $\lambda_3 = 1$ are, respectively,

$$\begin{aligned}\frac{N}{\lambda_3 - 1}\sin\left[c\left(\lambda_3 - 1\right)\right] = N\Bigg[c &- \frac{1}{6}c^3\left(\lambda_3 - 1\right)^2 \\ &+ \frac{1}{120}c^5\left(\lambda_3 - 1\right)^4 \\ &- \frac{1}{5040}c^7\left(\lambda_3 - 1\right)^6 \\ &+ \mathcal{O}\left[\left(\lambda_3 - 1\right)^8\right]\Bigg] \end{aligned} \tag{8.4.4}$$

and

$$\begin{aligned}&\frac{N}{\lambda_3 - 1}\cos\left[c\left(\lambda_3 - 1\right)\right]\left(1 - \exp\left[-\gamma\left(\lambda_3 - 1\right)\right]\right) \\ = \; & N\Bigg[\gamma - \frac{1}{2}\gamma^2\left(\lambda_3 - 1\right) + \left(\frac{1}{6}\gamma^3 - \frac{1}{2}\gamma c^2\right)\left(\lambda_3 - 1\right)^2 \\ + \; & \left(\frac{1}{4}\gamma^2 c^2 - \frac{1}{24}\gamma^4\right)\left(\lambda_3 - 1\right)^3 + \mathcal{O}\left[\left(\lambda_3 - 1\right)^4\right]\Bigg]. \end{aligned} \tag{8.4.5}$$

When $c = kR/2 \ll 1$, the Taylor series for S converges quickly. For example,

at $k = 0.01$, we have found that considering only the first five terms of the expansion (8.4.4) and neglecting terms in λ_3^3 and above allows values of $\tilde{\mathcal{V}}'$ to be found in very close agreement with the corresponding $\mathcal{V}'$ integrals provided by Dr. Plummer [90]. In table 8.1, we compare values of $\tilde{\mathcal{V}}'$ and $\mathcal{V}'$ for $f_3(\lambda_3) = S$ at $k = 0.01$, where the integrals are taken to contain a factor of $\rho_{12}\rho_{13}/\rho_{23}$. The integrals are evaluated for 18 sets of $\{\sigma_1, \sigma_2, \sigma_3, \zeta_1, \zeta_2, \zeta_3\}$ corresponding directly to the values of $\{a_i, b_i, r_i, c_i, d_i, s_i\}$ defining the 18 Hylleraas-type correlation functions detailed in appendix A. For the purposes of the test, the values of the nonlinear parameters are taken to be $\alpha_1 = 2.0$, $\alpha_2 = 2.0$ and $\alpha_3 = 0.3$. The normalisation constant, N, in S is chosen to be $N = 2 \times (R/2)^8$. We have also included in table 8.1 the percentage error, ε, of $\tilde{\mathcal{V}}'$ from $\mathcal{V}'$. Excellent agreement between the values of $\tilde{\mathcal{V}}'$ and $\mathcal{V}'$ is observed in each case.

Next, we consider $f_3(\lambda_3) = C$. In this case, the evaluation of $\tilde{\mathcal{V}}'$ becomes more complicated. The shielding exponent, $\gamma = 0.75$, is not small and the Taylor series (8.4.5) does not converge quickly, even for $c \ll 1$. However, we note that

$$\begin{aligned}
& (1 - \exp[-\gamma(\lambda_3 - 1)]) \\
= \; & \left(1 + \exp\left[-\frac{\gamma}{2}(\lambda_3 - 1)\right]\right)\left(1 - \exp\left[-\frac{\gamma}{2}(\lambda_3 - 1)\right]\right) \\
= \; & \left(1 + \exp\left[-\frac{\gamma}{2}(\lambda_3 - 1)\right]\right)\left(1 + \exp\left[-\frac{\gamma}{4}(\lambda_3 - 1)\right]\right)\left(1 - \exp\left[-\frac{\gamma}{4}(\lambda_3 - 1)\right]\right) \\
= \; & \left[\prod_{p=1}^{q}\left(1 + \exp\left[-\frac{\gamma}{2^p}(\lambda_3 - 1)\right]\right)\right]\left(1 - \exp\left[-\frac{\gamma}{2^q}(\lambda_3 - 1)\right]\right) \\
= \; & \left[\sum_{p=1}^{2^q} \exp\left[-\frac{(2^q - p)}{2^q}\gamma(\lambda_3 - 1)\right]\right]\left(1 - \exp\left[-\frac{\gamma}{2^q}(\lambda_3 - 1)\right]\right), \qquad (8.4.6)
\end{aligned}$$

where we have used the standard result

No.	$\tilde{\mathcal{V}}'$	$\mathcal{V}'$	ε (%)
1	5.792602×10^{-2}	5.792589×10^{-2}	2.20×10^{-4}
2	2.620995×10^{-2}	2.620997×10^{-2}	8.33×10^{-5}
3	2.587822×10^{-1}	2.587828×10^{-1}	2.04×10^{-4}
4	-1.447476×10^{-3}	-1.447477×10^{-3}	8.40×10^{-5}
5	5.659880×10^{-1}	5.659697×10^{-1}	3.24×10^{-3}
6	-1.395753×10^{-2}	-1.395755×10^{-2}	1.65×10^{-4}
7	1.224288×10^{-1}	1.224285×10^{-1}	1.95×10^{-4}
8	-3.162583×10^{-3}	-3.162586×10^{-3}	1.06×10^{-4}
9	-6.852718×10^{-3}	-6.852725×10^{-3}	1.08×10^{-4}
10	9.321040×10^{-4}	9.321044×10^{-4}	5.04×10^{-5}
11	2.073656×10^{-3}	2.073656×10^{-3}	1.35×10^{-5}
12	-2.126935×10^{-3}	-2.126943×10^{-3}	3.70×10^{-4}
13	-4.499447×10^{-3}	-4.499463×10^{-3}	3.52×10^{-4}
14	6.678507×10^{-3}	6.678514×10^{-3}	1.01×10^{-4}
15	1.466134×10^{-2}	1.466120×10^{-2}	9.17×10^{-4}
16	-1.593187×10^{-2}	-1.593264×10^{-2}	4.85×10^{-3}
17	-3.397477×10^{-2}	-3.397629×10^{-2}	4.48×10^{-3}
18	1.203351×10^{0}	1.203315×10^{0}	2.97×10^{-3}

Table 8.1: A comparison of $\tilde{\mathcal{V}}'$ and $\mathcal{V}'$ [90] at $k = 0.01$ for $f_3(\lambda_3) = S$.

No.	$\tilde{\mathcal{V}}'$	$\mathcal{V}'$	ε (%)
1	1.409175×10^{0}	1.409172×10^{0}	1.76×10^{-4}
2	6.248133×10^{-1}	6.248135×10^{-1}	2.34×10^{-5}
3	4.180550×10^{0}	4.180553×10^{0}	7.61×10^{-5}
4	-3.580328×10^{-2}	-3.580329×10^{-2}	2.44×10^{-5}
5	9.238980×10^{0}	9.239173×10^{0}	2.09×10^{-3}
6	-2.311165×10^{-1}	-2.311168×10^{-1}	9.82×10^{-5}
7	2.933759×10^{0}	2.933755×10^{0}	1.62×10^{-4}
8	-7.953456×10^{-2}	-7.953459×10^{-2}	4.24×10^{-5}
9	-1.705392×10^{-1}	-1.705393×10^{-1}	4.47×10^{-5}
10	3.085022×10^{-2}	3.085024×10^{-2}	4.05×10^{-5}
11	6.995714×10^{-2}	6.995714×10^{-2}	1.09×10^{-5}
12	-6.652764×10^{-2}	-6.652778×10^{-2}	2.03×10^{-4}
13	-1.385496×10^{-1}	-1.385498×10^{-1}	1.95×10^{-4}
14	1.507340×10^{-1}	1.507340×10^{-1}	2.75×10^{-5}
15	3.351020×10^{-1}	3.351035×10^{-1}	4.56×10^{-4}
16	-3.440744×10^{-1}	-3.440672×10^{-1}	2.10×10^{-3}
17	-7.284975×10^{-1}	-7.284833×10^{-1}	1.95×10^{-3}
18	1.953535×10^{1}	1.953573×10^{1}	1.95×10^{-3}

Table 8.2: A comparison of $\tilde{\mathcal{V}}'$ and $\mathcal{V}'$ [90] at $k = 0.01$ for $f_3(\lambda_3) = C$.

$$\prod_{i=1}^{n}\left(1+\exp\left[-\frac{x}{2^i}\right]\right)=\sum_{i=1}^{2^n}\exp\left[-\frac{(2^n-i)}{2^n}x\right]. \tag{8.4.7}$$

Hence, q can be chosen to make $\gamma/2^q$ arbitrarily small, so that values of $\tilde{\mathcal{V}}'$ can be calculated in a similar way as for $f_3(\lambda_3)=S$, by considering the first few terms in the Taylor series expansion of

$$C_q(\lambda_3)=\frac{N}{\lambda_3-1}\cos\left[c(\lambda_3-1)\right]\left(1-\exp\left[-\frac{\gamma}{2^q}(\lambda_3-1)\right]\right), \tag{8.4.8}$$

albeit with the drawback of having to calculate a significantly greater number of $\mathcal{V}$ integrals than in the case $f_3(\lambda_3)=S$, owing to the summation appearing in the final line of (8.4.6).

In table 8.2, we compare values of $\tilde{\mathcal{V}}'$ and $\mathcal{V}'$ for $f_3(\lambda_3)=C$ at $k=0.01$, where the integrals are again taken to contain a factor of $\rho_{12}\rho_{13}/\rho_{23}$. The integrals are evaluated for the same 18 sets of $\{\sigma_1,\sigma_2,\sigma_3,\zeta_1,\zeta_2,\zeta_3\}$ as in the case $f_3(\lambda_3)=S$. For the choice $q=4$ in (8.4.6), we have found it necessary to consider only the first 8 terms in the Taylor expansion of (8.4.8), neglecting terms in λ_3^7 and above. The values of the nonlinear parameters are again chosen to be $\alpha_1=2.0$, $\alpha_2=2.0$ and $\alpha_3=0.3$, with $N=(R/2)^8$. We have also included in table 8.2 the percentage error, ε, of $\tilde{\mathcal{V}}'$ from $\mathcal{V}'$. Excellent agreement between the values of $\tilde{\mathcal{V}}'$ and $\mathcal{V}'$ is observed in each case.

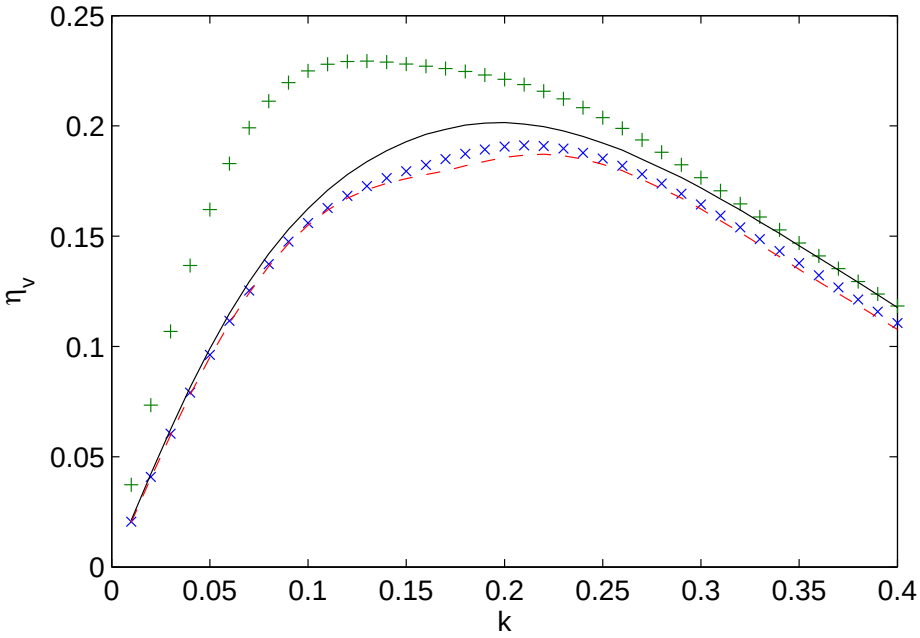

Figure 8.7: Values of $\eta_v\,(k)$ for [×] $\Psi_t^{(1,B)}$, [+] $\Psi_t^{(2,B)}$, [- - - -] $\Psi_t^{(1,C)}$ and [——] $\Psi_t^{(2,C)}$.

8.5 Calculations involving $\psi_G^{(C)}$

The improvements made to the computational framework allow Kohn calculations to be carried out for trial wavefunctions containing $\psi_G^{(C)}$, the 145-term target wavefunction accounting for 99.7% of the correlation energy of H_2. In the usual notation, we consider two trial functions, $\Psi_t^{(1,C)}$ and $\Psi_t^{(2,C)}$, both of the form (1.7.3). The dependence of η_v and Z_{eff} on k for $\Psi_t^{(1,C)}$ and $\Psi_t^{(2,C)}$ is shown in figures 8.7 and 8.8. We have also reproduced in these figures the values of η_v and Z_{eff} determined earlier for $\Psi_t^{(1,B)}$ and $\Psi_t^{(2,B)}$.

In the case of both η_v and Z_{eff}, there is excellent agreement between calculations using $\Psi_t^{(1,B)}$ and those using $\Psi_t^{(1,C)}$, corroborating our earlier claim that $\psi_G^{(B)}$ is a sufficiently accurate target wavefunction for Kohn calculations using

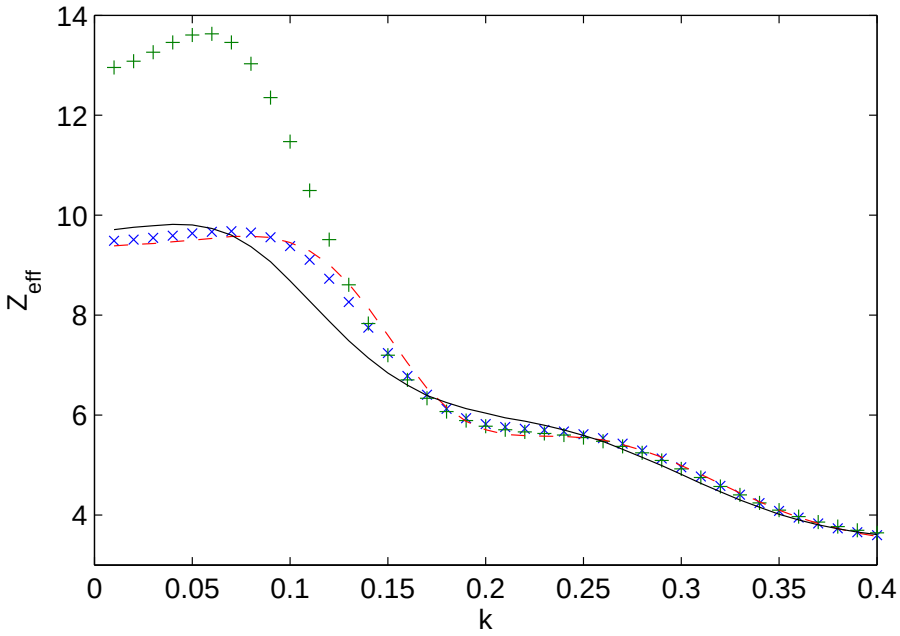

Figure 8.8: Values of $Z_{\text{eff}}\,(k)$ for [×] $\Psi_{\text{t}}^{(1,\text{B})}$, [+] $\Psi_{\text{t}}^{(2,\text{B})}$, [- - - -] $\Psi_{\text{t}}^{(1,\text{C})}$ and [——] $\Psi_{\text{t}}^{(2,\text{C})}$.

$\Psi_{\text{t}}^{(1,\text{B})}$ to have converged and hence to be considered reliable. In sharp contrast, there are significant differences in the results for $\Psi_{\text{t}}^{(2,\text{B})}$ and $\Psi_{\text{t}}^{(2,\text{C})}$. The improvement in the accuracy of the target wavefunction has brought the results for $\Psi_{\text{t}}^{(2,\text{C})}$ broadly into line with those for $\Psi_{\text{t}}^{(1,\text{B})}$ and $\Psi_{\text{t}}^{(1,\text{C})}$. When the more accurate Kohn calculations using $\psi_{\text{G}}^{(\text{C})}$ are carried out, therefore, the effect of including Hylleraas-type short-range correlation functions in ρ_{12} is small.

It remains to be shown that $\psi_{\text{G}}^{(\text{C})}$ is a sufficiently accurate target wavefunction for calculations involving $\Psi_{\text{t}}^{(2,\text{C})}$ to be considered reliable. To do this, we again remove basis functions successively at random from the target wavefunction to reduce its accuracy, then calculate values of η_{v} and Z_{eff} after each removal for trial functions containing $\Omega^{(1)}$ or $\Omega^{(2)}$. Here, a maximum of 104 basis functions have been removed from the original set of 145 functions comprising $\psi_{\text{G}}^{(\text{C})}$, at

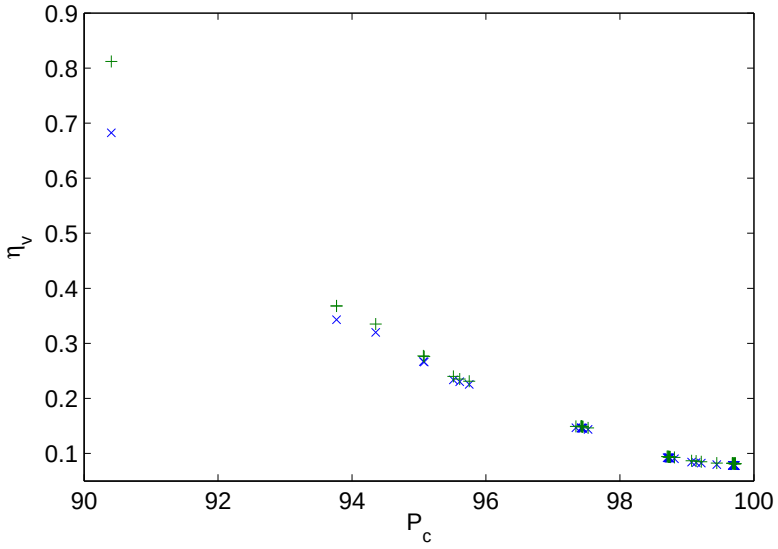

Figure 8.9: The dependence of η_v on P_c at $k = 0.04$, for trial functions containing [×] $\Omega^{(1)}$ and [+] $\Omega^{(2)}$. Basis functions have been removed successively from $\psi_G^{(C)}$.

which point the target wavefunction accounts for 90.4% of the correlation energy of H_2. The first 70 basis functions removed correspond directly to the 70 functions removed earlier from $\psi_G^{(B)}$. Thereafter, the remaining 34 basis functions have been removed successively at random, with the condition that the Hylleraas-type basis function in ρ_{12} is not removed. The dependence of η_v and Z_{eff} on the accuracy, P_c, of each target wavefunction is shown in figures 8.9 and 8.10 respectively, for $k = 0.04$.

The convergence of η_v and Z_{eff} with increasing P_c is not as clear as it was in the previous calculations illustrated in figures 8.5 and 8.6; however, the slopes of the curves in figures 8.9 and 8.10 are becoming noticeably flatter in the upper limit of P_c. We have already concluded that the Kohn calculations involving $\Psi_t^{(1,B)}$, and hence those involving $\Psi_t^{(1,C)}$, are reliable. Further, the behaviour of the curves corresponding to $\Omega^{(1)}$ and $\Omega^{(2)}$ is very similar in the limit of high

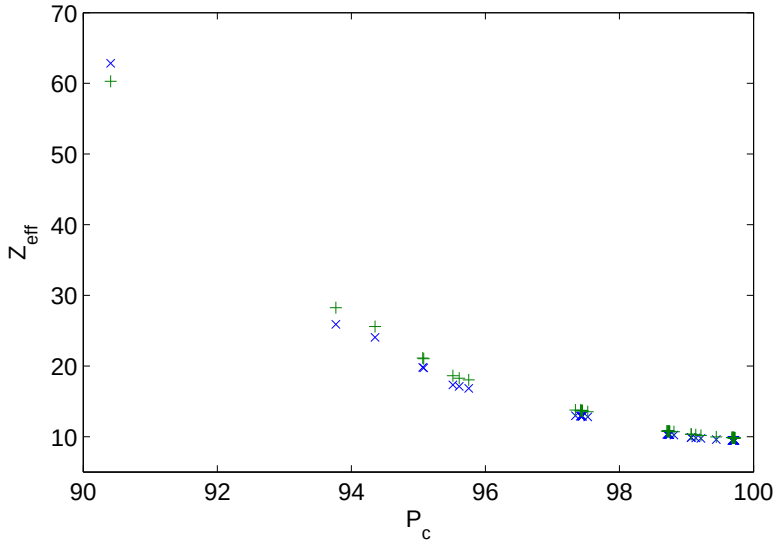

Figure 8.10: The dependence of Z_{eff} on P_{c} at $k = 0.04$, for trial functions containing [×] $\Omega^{(1)}$ and [+] $\Omega^{(2)}$. Basis functions have been removed successively from $\psi_{\text{G}}^{(\text{C})}$.

P_{c} in both figures 8.9 and 8.10. Inspection of these figures suggests that neither set of results would change significantly if the target wavefunction was again extended to account for most of the remaining 0.3% of the correlation energy. Hence, we may reasonably take the calculations involving $\Psi_{\text{t}}^{(2,\text{C})}$ to be reliable.

An interesting feature apparent from figures 8.9 and 8.10 is that the inclusion of the Hylleraas-type target basis function in ρ_{12} raises the threshold of P_{c} beyond which the calculations involving $\Omega^{(1)}$ converge. The figures clearly show that values of η_{v} and Z_{eff} calculated for $\Psi_{\text{t}}^{(1,\text{C})}$ are still declining at $P_{\text{c}} \simeq 96$, though the corresponding results for $\Psi_{\text{t}}^{(1,\text{B})}$ in figures 8.5 and 8.6 have converged at this point. This suggests that the overall *accuracy* of the target wavefunction is not the only factor determining the reliability of the Kohn calculation; it appears that the improvement in *flexibility* brought about by the inclusion of the Hylleraas-type target basis function in ρ_{12}, relative to the flexibility of the short-

range correlation functions, itself plays an important role.

8.6 Target accuracy in the method of models

A natural extension of the present analysis is to examine how our calculations carried out within the framework of the method of models are affected by improvements in the accuracy of the target wavefunction. There are, however, two elements limiting investigations of this type, both due to the presence of ψ_G as a factor in (1.8.14). Firstly, by an argument analogous to that given in chapter 1, the inclusion of ψ_G as a factor in (1.8.14) means that the integrals comprising the Kohn equations can be evaluated in the existing framework only if $s_{12}(\omega_v) = 1$ in (1.6.11). This severely restricts the accuracy of the target wavefunction as it does not allow for the consideration of explicitly correlated basis functions. Secondly, the use of L basis functions in ψ_G, in a trial wavefunction of the form (1.8.14) containing M short-range correlation functions, requires the evaluation of L^2M^2 integrals to form the matrix elements between the closed-channel parts of the trial function. Thus, the inclusion of any additional basis functions in ψ_G brings about a considerable increase in the computational expense required to perform the calculations.

As a result, in extending our method of models calculations, the most accurate target function we will consider here will be $\psi_G^{(D)}$, which again has the form (1.6.9) with $s_{12}(\omega_v) = 1$, containing $L = 27$ basis functions detailed in appendix A and accounting for 66.5% of the correlation energy of H_2. The set of basis functions comprising $\psi_G^{(D)}$ contains within it the set of 6 functions defining $\psi_G^{(A)}$, which itself accounts for 57.1% of the correlation energy.

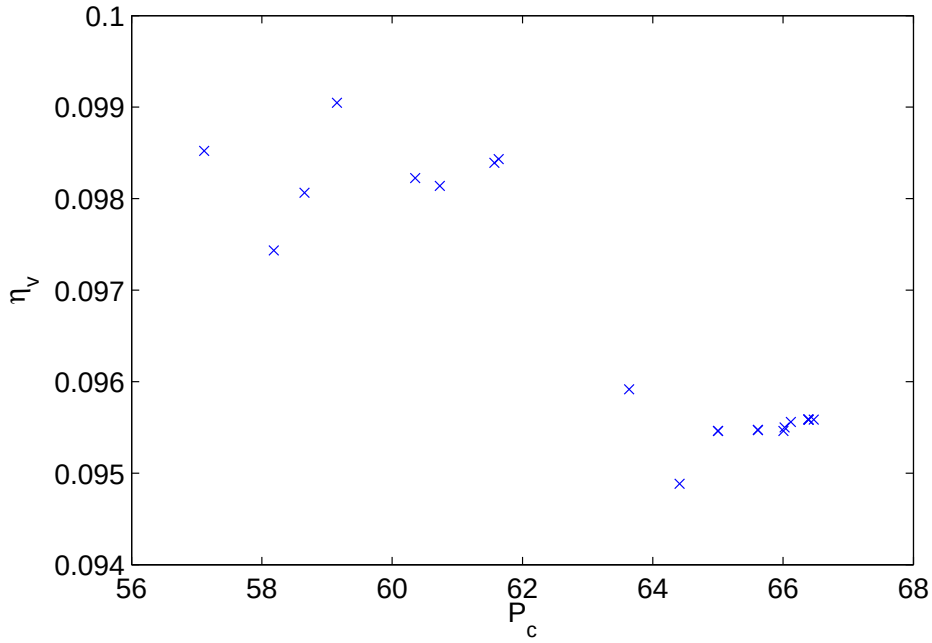

Figure 8.11: The dependence of η_v on P_c at $k = 0.04$, for trial functions containing $\Omega^{(1)}$. Basis functions have been removed successively from $\psi_G^{(D)}$.

Individual basis functions have been removed successively at random from $\psi_G^{(D)}$, on the condition that those functions also found in $\psi_G^{(A)}$ are not removed, creating a series of target wavefunctions of decreasing accuracy. A maximum of 21 functions have been removed, at which point the target wavefunction is equal to $\psi_G^{(A)}$. After each removal, Kohn calculations of η_v and Z_{eff} have been carried out for trial functions of the form (1.8.14) with the set of correlation functions, $\Omega^{(1)}$, in which we have taken $\alpha = 0.3$ and $\beta = -0.1$. For practical reasons, calculations involving $\Omega^{(2)}$ are not investigated here, owing to the very large number of $\mathcal{V}$ integrals (1.8.29) it would be necessary to evaluate in such a calculation. The value of δ in (1.6.10) is fixed at $\delta = 1.1$. The calculated values of η_v and Z_{eff} as a function of P_c at $k = 0.04$ are shown respectively in figures 8.11 and 8.12.

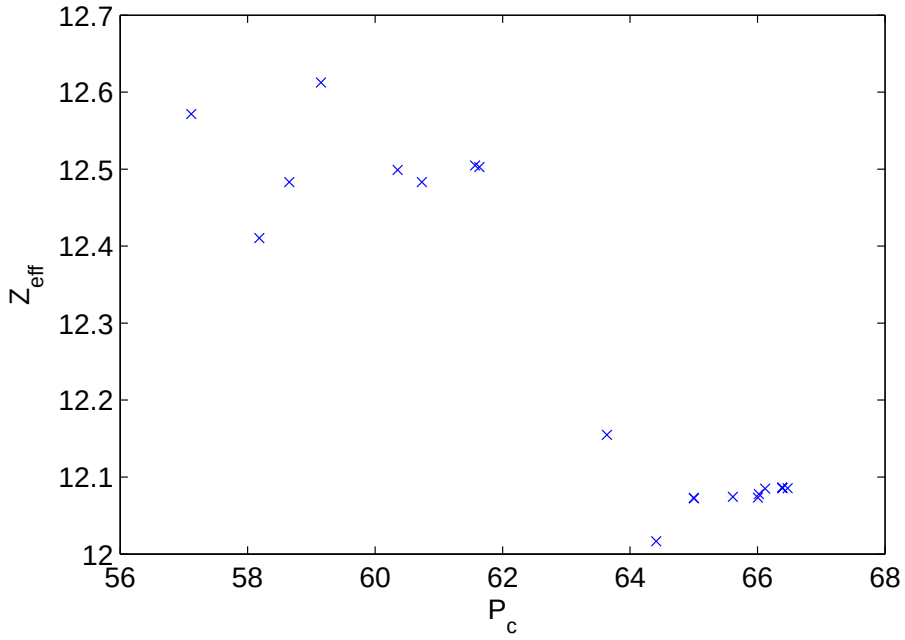

Figure 8.12: The dependence of Z_{eff} on P_{c} at $k = 0.04$, for trial functions containing $\Omega^{(1)}$. Basis functions have been removed successively from $\psi_{\text{G}}^{(\text{D})}$.

Unlike the Kohn calculations carried out with an explicit consideration of the target potential, there is little discernible structure in the behaviour of either η_{v} or Z_{eff} over P_{c}, although there is some evidence of convergence above $P_{\text{c}} \simeq 65$. We also note that, for both η_{v} and Z_{eff}, the size of the variations over P_{c} is much smaller than the variations observed in figures 8.5 and 8.6 over the range of P_{c} considered there. We can speculate that calculations carried out with the method of models might be more robust to changes in the accuracy of the target wavefunction, although nothing definitive can be said here due to the overall accuracy of the target wavefunctions being very much lower than those considered in the previous sections.

8.7 Conclusions

We have demonstrated that the reliability of our Kohn calculations can depend upon the flexibility of the set of short-range correlation functions, relative to the flexibility and accuracy of the approximate target wavefunction. This dependence is most obvious at very low positron momenta. Our findings are similar to those reported by Van Reeth and Humberston [88] for positron-helium scattering and highlight the need for rigorous testing of the reliability of Kohn calculations whenever inexact target wavefunctions are used. This is particularly relevant here for the calculations carried out with $\Psi_t^{(2,B)}$, for which the values of Z_{eff} at low energies are, erroneously, in good agreement with experimental data.

We have implemented a numerical method to test the stability of any given calculation to variations in the accuracy of the approximate target wavefunction. This has allowed us to distinguish between reliable and unreliable results. Having carried out the most accurate of our Kohn calculations, we have observed that the effect of including Hylleraas-type correlation functions in ρ_{12} is to increase the calculated values of η_v only slightly. The corresponding changes in the values of Z_{eff} are also small, so that there is still disagreement between our reported values and the experimental result of $Z_{\text{eff}} = 14.6$ at 297 K [25]. The low importance of Hylleraas-type correlation functions in ρ_{12} makes it very likely that they can safely be omitted from future calculations. This is helpful as, under these circumstances, reliable Kohn calculations can be carried out with $\psi_G^{(B)}$ and these are much more convenient to handle than calculations involving $\psi_G^{(C)}$.

We have found some evidence that values of η_v and Z_{eff} obtained with the method of models are less sensitive to changes in the accuracy of the target

wavefunction. However, due to the limitations of the integral framework used in our calculations, we have been unable to investigate this behaviour to any great extent.

Chapter 9

The Adiabatic Nuclei Approximation

9.1 Introduction

In this chapter, we will discuss the inclusion of nuclear motion in our treatment of $(e^+ - H_2)$ scattering, using a method analogous to the Born-Oppenheimer approximation [52] found to be so successful in molecular bound state calculations. As far as we are aware, this is the first time that nuclear dynamics of any level of complexity have been investigated in Kohn calculations for this system. We will consider two models of ground state nuclear vibrations in the hydrogen molecule; the quantum harmonic oscillator and oscillations due to a Morse potential [91]. Rotational motion of the nuclei will be ignored.

We will find that consideration of adiabatic nuclear vibrations has very little overall effect on the Kohn calculations carried out with $\Psi_t^{(1,B)}$, with the vibra-

tionally averaged values of η_v and Z_{eff} differing only slightly from those values obtained in previous chapters at the equilibrium internuclear separation, $R_0 = 1.4$. For calculations carried out with the method of models using $\Psi_t^{(1,A)}$, the effects of including nuclear motion are more noticeable. In particular, at very low energies, the vibrationally averaged values of Z_{eff} are found to be appreciably higher in the Morse potential calculations than the values already obtained at $R_0 = 1.4$.

9.2 Scattering functions in the adiabatic nuclei approximation

Complete treatments of molecular geometry are more complicated than the atomic case as they must account for coupled motion between nuclei and electrons. However, accurate approximations of molecular dynamics can be obtained much more easily by exploiting the fact that the masses of the nuclei in molecules are three or more orders of magnitude greater than those of the electrons, while the electromagnetic forces experienced by both electrons and nuclei are similar. Consequently, the motion of the nuclei is typically very much slower than that of the electrons and, in an approximate treatment, coupling between the two can ordinarily be neglected. This is the physical basis of the Born-Oppenheimer approximation [52].

Here, we briefly recount the derivation of the Born-Oppenheimer approximation for the case of the hydrogen molecule, largely following Bransden and Joachain [57].

Initially regarding the internuclear position vector, $\mathbf{R}$, as fixed, we consider the electronic Hamiltonian, $\hat{H}_{\mathrm{T}}$ (1.2.6), for the hydrogen molecule. It is convenient here to adopt a slightly different notation to that used in chapter 1, such that we denote the eigenvalue and eigenfunction of $\hat{H}_{\mathrm{T}}$ for the electronic state, q, respectively by $\epsilon^{(q)}$ and $\psi^{(q)}$. Hence,

$$\hat{H}_{\mathrm{T}}\psi^{(q)}\left(\mathbf{r}_1, \mathbf{r}_2; \mathbf{R}\right) = \epsilon^{(q)}\left(R\right)\psi^{(q)}\left(\mathbf{r}_1, \mathbf{r}_2; \mathbf{R}\right), \tag{9.2.1}$$

where the energies, $\epsilon^{(q)}$, depend only on the magnitude of $\mathbf{R}$ and not its orientation. For each fixed $\mathbf{R}$, the electronic eigenfunctions form a complete set. Without loss of generality, we can choose this set to be orthonormal, so that

$$\langle\psi^{(p)}|\psi^{(q)}\rangle = \delta_{pq}, \tag{9.2.2}$$

δ_{pq} being the Kronecker delta.

Next, we consider the full Hamiltonian, $\mathbb{H}_{\mathrm{T}}$ (1.2.3), for the molecule, which accounts for nuclear motion and satisfies

$$\mathbb{H}_{\mathrm{T}}\phi\left(\mathbf{r}_1, \mathbf{r}_2, \mathbf{R}\right) = \left(\hat{H}_{\mathrm{T}} - \frac{1}{2\mu_{\mathrm{N}}}\nabla^2_{\mathbf{R}}\right)\phi\left(\mathbf{r}_1, \mathbf{r}_2, \mathbf{R}\right) = \mathbb{E}_{\mathrm{T}}\phi\left(\mathbf{r}_1, \mathbf{r}_2, \mathbf{R}\right), \tag{9.2.3}$$

where ϕ is the exact wavefunction for the molecule having a total energy given by $\mathbb{E}_{\mathrm{T}}$. The reduced proton mass is denoted by μ_{N}. By completeness of the set, $\{\psi^{(q)}\}$, we can immediately expand ϕ as

$$\phi\left(\mathbf{r}_1, \mathbf{r}_2, \mathbf{R}\right) = \sum_q \Pi^{(q)}\left(\mathbf{R}\right)\psi^{(q)}\left(\mathbf{r}_1, \mathbf{r}_2; \mathbf{R}\right), \tag{9.2.4}$$

where the expansion coefficients, $\Pi^{(q)}(\mathbf{R})$, will be seen to be wavefunctions representing nuclear motion. Substitution of (9.2.4) into (9.2.3) gives

$$\left(\hat{H}_{\mathrm{T}} - \frac{1}{2\mu_{\mathrm{N}}}\nabla^2_{\mathbf{R}}\right)\sum_q \Pi^{(q)}(\mathbf{R})\,\psi^{(q)}(\mathbf{r}_1,\mathbf{r}_2;\mathbf{R}) = \mathbb{E}_{\mathrm{T}}\sum_q \Pi^{(q)}(\mathbf{R})\,\psi^{(q)}(\mathbf{r}_1,\mathbf{r}_2;\mathbf{R})\,. \tag{9.2.5}$$

Projecting (9.2.5) with the electronic wavefunction, $\psi^{(p)}$, using (9.2.1) and the orthonormality of the set, $\{\psi^{(q)}\}$, we then have

$$-\sum_q \langle\psi^{(p)}|\frac{1}{2\mu_{\mathrm{N}}}\nabla^2_{\mathbf{R}}|\left(\psi^{(q)}\Pi^{(q)}\right)\rangle + \left(\epsilon^{(p)}(R) - \mathbb{E}_{\mathrm{T}}\right)\Pi^{(p)} = 0, \tag{9.2.6}$$

where the Dirac notation indicates integration over the coordinates of the electrons only.

This set of coupled equations is simplified in the Born-Oppenheimer approximation by recognising that, because the nuclear motion is much slower than that of the electrons, the electronic wavefunctions vary very slowly with respect to the nuclear coordinates. In the expansion,

$$\nabla^2_{\mathbf{R}}\left[\psi^{(q)}\Pi^{(q)}\right] = \psi^{(q)}\nabla^2_{\mathbf{R}}\Pi^{(q)} + 2\nabla_{\mathbf{R}}\psi^{(q)}.\nabla_{\mathbf{R}}\Pi^{(q)} + \Pi^{(q)}\nabla^2_{\mathbf{R}}\psi^{(q)}, \tag{9.2.7}$$

terms in $\nabla_{\mathbf{R}}\psi^{(q)}$ can thus be neglected with respect to terms in $\nabla_{\mathbf{R}}\Pi^{(q)}$. Under these circumstances, (9.2.6) uncouples and reduces to

$$\left[-\frac{1}{2\mu_{\mathrm{N}}}\nabla^2_{\mathbf{R}} + \epsilon^{(p)}(R) - \mathbb{E}_{\mathrm{T}}\right]\Pi^{(p)}(\mathbf{R}) \sim 0. \tag{9.2.8}$$

For a given electronic state, p, (9.2.8) has the form of a Schrödinger equation for

two nuclei moving in an effective potential whose general form is described by $\epsilon^{(p)}(R)$. The function, $\Pi^{(p)}(\mathbf{R})$, can thus be regarded as describing vibrational and rotational nuclear motion uncoupled from the electrons. From (9.2.4), the total wavefunction for a given electronic state, p, then reduces to

$$\phi^{(p)}(\mathbf{r}_1, \mathbf{r}_2, \mathbf{R}) \sim \Pi^{(p)}(\mathbf{R})\, \psi^{(p)}(\mathbf{r}_1, \mathbf{r}_2; \mathbf{R}), \tag{9.2.9}$$

the product of the two wavefunctions describing the uncoupled electronic and nuclear motion.

In principle, by first determining accurate approximations of $\epsilon^{(p)}(R)$ at different values of R using the Rayleigh-Ritz variational method, numerical solutions of (9.2.8) can be found. In practice, there exist analytic functions, $\tilde{V}(R)$, which can be used to approximate $\epsilon^{(p)}(R)$ up to an arbitrary constant. The resulting wave equation, which has the same general form as (9.2.8), with $\tilde{V}(R)$ replacing $\epsilon^{(p)}(R)$, can then be solved analytically for certain choices of $\tilde{V}(R)$. We will discuss appropriate forms of $\tilde{V}(R)$ in section 9.3.

Owing to its similarity with the adiabatic theorem [92], the Born-Oppenheimer approximation is often referred to as the adiabatic nuclei approximation. However, the Born-Oppenheimer approximation denotes calculations involving only bound states, while the adiabatic nuclei approximation can also be used when referring to calculations involving scattering states. Adiabatic treatments of scattering processes were first discussed by Chase [48] and later by Temkin and coworkers [53, 54]. In studies of electron-molecule scattering, Shugard and Hazi [51] showed that, provided the collision time is short compared to the vibrational and rotational periods of nuclear motion, total scattering wavefunctions can be well approximated by products of leptonic and nuclear wave-

functions, in a manner analogous to the Born-Oppenheimer approximation for bound states. They also demonstrated that, in such an approximation, the effective potential governing the nuclear motion should be taken to be that due only to the target electrons and not the projectile. This is consistent with the assumption that, on the timescale of nuclear motion, the projectile spends only a short time in the region of the molecule and does not noticeably affect the nuclear dynamics.

In this chapter, we will consider only ground state descriptions of the electronic and nuclear motion in the target H_2 molecule. We write the corresponding total $(e^+ - H_2)$ scattering wavefunction, Φ, as

$$\Phi\left(\mathbf{r}_1, \mathbf{r}_2, \mathbf{r}_3, \mathbf{R}\right) \sim \Pi\left(\mathbf{R}\right) \Psi\left(\mathbf{r}_1, \mathbf{r}_2, \mathbf{r}_3; \mathbf{R}\right), \tag{9.2.10}$$

where $\Psi\left(\mathbf{r}_1, \mathbf{r}_2, \mathbf{r}_3; \mathbf{R}\right)$ is the leptonic scattering wavefunction evaluated at a fixed $\mathbf{R}$ and $\Pi\left(\mathbf{R}\right)$ is the ground state nuclear wavefunction for the unperturbed hydrogen molecule.

As we have discussed in earlier chapters, at the very low energies of most interest to us in the scattering problem, the incident positron wave has no preferred orientation with respect to the target molecule when they are asymptotically far apart. Consequently, the results of our Kohn calculations are effectively independent of the orientation of the nuclear axis. In our calculations of adiabatic nuclear motion, we will therefore ignore rotational dynamics and consider only one-dimensional vibrational motion. We can thus approximate (9.2.10) further by introducing a trial wavefunction, Φ_t, of the form

$$\Phi_t\left(\mathbf{r}_1, \mathbf{r}_2, \mathbf{r}_3, R\right) = \Pi_t\left(R\right) \Psi_t\left(\mathbf{r}_1, \mathbf{r}_2, \mathbf{r}_3; R\right), \tag{9.2.11}$$

where Ψ_t has the usual form of a Kohn trial function, explicitly parameterised in terms of R, and $\Pi_t(R)$ is the ground state solution of

$$\left[-\frac{1}{2\mu_N}\frac{d^2}{dR^2}+\tilde{V}(R)\right]\Pi_t(R)=\mathbb{E}_T\Pi_t(R), \tag{9.2.12}$$

where, up to an arbitrary constant, $\tilde{V}(R)$ is an analytic approximation to the exact electronic ground state energy in the Born-Oppenheimer approximation. For convenience, following the notation of chapter 1, hereafter we will denote this exact energy by $\epsilon(R)$. In the following section, we will discuss two forms of $\tilde{V}(R)$ for which (9.2.12) can be solved analytically.

9.3 Modelling the effective potential

There are two widely used choices of $\tilde{V}(R)$ for which analytic solutions of (9.2.12) exist. Firstly, the nuclear vibrations can be regarded as oscillations due to a harmonic potential described by

$$\tilde{V}_H(R)=\kappa(R-R_0)^2, \tag{9.3.1}$$

for some force constant, κ. The ground state solution, $\Pi_H(R)$, of (9.2.12) with $\tilde{V}=\tilde{V}_H$ is then

$$\Pi_H(R)=A\exp\left[-\frac{\sqrt{\kappa\mu_N}}{2}(R-R_0)^2\right], \tag{9.3.2}$$

A being a normalisation constant.

The harmonic potential has the advantage that the solution (9.3.2) is easily

found. However, $\tilde{V}_{\mathrm{H}}(R)$ provides an accurate description of the effective potential experienced by the nuclei only when R is close to R_0. A better description is given by the potential due to Morse [91],

$$\tilde{V}_{\mathrm{M}}(R) = D_{\mathrm{e}}\left(1 - \exp\left[-\xi(R - R_0)\right]\right)^2, \tag{9.3.3}$$

where D_{e} is the electronic dissociation energy of H_2 and

$$\xi = \sqrt{\frac{\kappa}{2D_{\mathrm{e}}}}. \tag{9.3.4}$$

The Morse potential is a more suitable candidate for $\tilde{V}(R)$ than (9.3.1) as it reflects the tendency of H_2 to dissociate at large values of R, which the harmonic potential does not. Exact solutions of (9.2.12) with $\tilde{V} = \tilde{V}_{\mathrm{M}}$ have been obtained by Chen [93] using Laplace transforms. The ground state solution, $\Pi_{\mathrm{M}}(R)$, is

$$\Pi_{\mathrm{M}}(R) = B y^{\frac{1}{2}(g-1)} \exp\left(-\frac{y}{2}\right), \tag{9.3.5}$$

where

$$y = g \exp\left[-\xi\left(R - R_0\right)\right], \tag{9.3.6}$$

with

$$g = \frac{2\sqrt{2\mu_{\mathrm{N}} D_{\mathrm{e}}}}{\xi} \tag{9.3.7}$$

and where B is a normalisation constant.

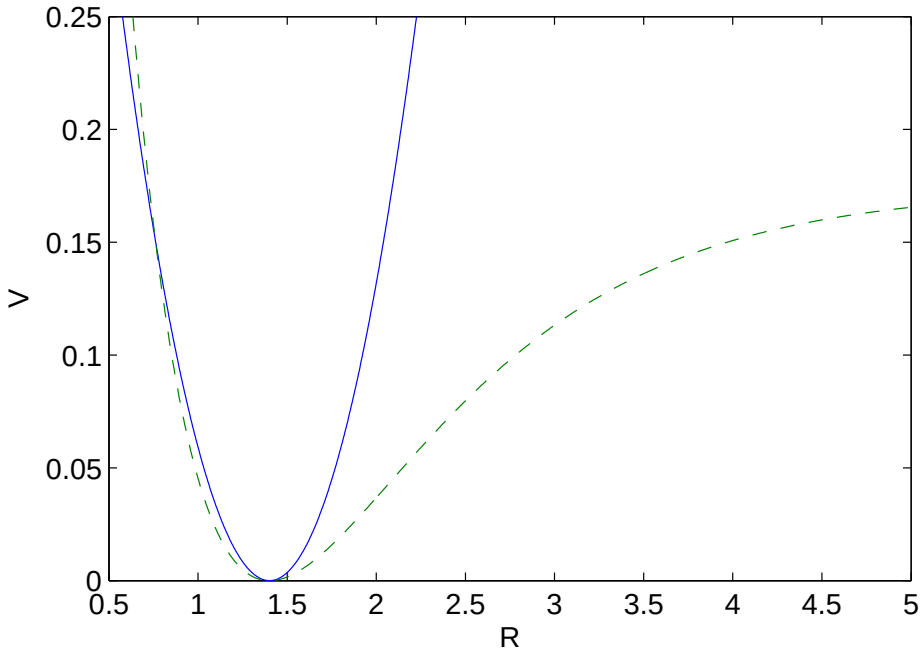

Figure 9.1: A comparison of [——] $\tilde{V}_{\mathrm{H}}(R)$ and [- - - -] $\tilde{V}_{\mathrm{M}}(R)$.

A comparison of the harmonic and Morse potentials is given in figure 9.1, where the difference between the two functions at larger values of R is clear. Here, a value of $\mu_{\mathrm{N}} = 918.076$ in atomic units has been taken from CODATA [83] and values of $\xi = 1.028$ and $D_{\mathrm{e}} = 0.174$ in atomic units have been taken from Bransden and Joachain [57]. A value of $\kappa = 0.369$ in atomic units can then be calculated from (9.3.4). A comparison of the unit-normalised ground state probability density functions generated by $\Pi_{\mathrm{H}}(R)$ and $\Pi_{\mathrm{M}}(R)$ is given in figure 9.2. For both potentials, it is clear from figure 9.2 that there is a negligible probability that the internuclear separation exceeds $R = 2.1$ or is smaller than $R = 0.8$.

It is interesting to note that, in the case of the Morse potential, the modal value, $\overline{R}$, of the internuclear separation is not equal to R_0, but is instead given by

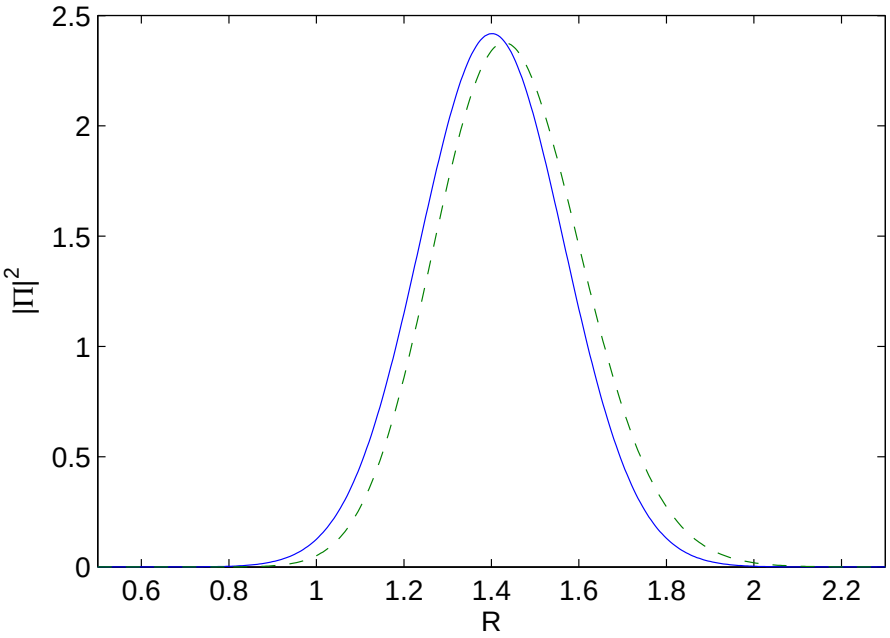

Figure 9.2: A comparison of the unit-normalised ground state probability density functions, [——] $|\Pi_{\mathrm{H}}(R)|^2$ and [- - - -] $|\Pi_{\mathrm{M}}(R)|^2$.

$$\overline{R} = R_0 + \frac{1}{\xi}\log\left(\frac{g}{g-1}\right), \tag{9.3.8}$$

so that the peak of the distribution corresponding to the Morse potential in figure 9.2 occurs at a slightly higher value of R than the peak, at $R = R_0$, of the harmonic distribution. This tendency of the internuclear separation to be greater than the equilibrium value is a consequence of the asymmetry in the Morse potential (9.3.3). For the values of g and ξ used in our calculations, we have found that the modal internuclear separation for the Morse potential is $\overline{R} \simeq 1.43$.

In the following section, we will present the results of Kohn calculations carried out with trial wavefunctions parameterised at different values of R, before using (9.2.11) and the solutions, (9.3.2) and (9.3.5), to estimate average values of

η_v and Z_{eff} over ground state nuclear vibrations.

9.4 Calculations of $\eta_v(R)$ and $Z_{eff}(R)$

We have carried out fixed-nuclei Kohn calculations of η_v and Z_{eff} using $\Psi_t^{(1,A)}$ and $\Psi_t^{(1,B)}$ for 66 values of R equidistant in the range $0.8 \leq R \leq 2.1$. To obtain accurate parameterisations of $\Psi_t^{(1,A)}$ and $\Psi_t^{(1,B)}$ in terms of R, at each value of R the approximate target wavefunctions, $\psi_G^{(A)}$ and $\psi_G^{(B)}$, have been reformulated using the Rayleigh-Ritz variational method. The optimal value, δ_{opt}, of the nonlinear parameter, δ, found in both target wavefunctions, has also been recalculated at each R to minimise the approximation to the exact ground state energy. We will denote by $\epsilon_G^{(A)}(R)$ and $\epsilon_G^{(B)}(R)$ the minimised ground state energy approximations determined respectively from $\psi_G^{(A)}$ and $\psi_G^{(B)}$.

In figure 9.3, we have plotted $\left[\epsilon_G^{(A)}(R) - \epsilon(R_0)\right]$ and $\left[\epsilon_G^{(B)}(R) - \epsilon(R_0)\right]$ for $0.8 \leq R \leq 2.1$. Shifting $\epsilon_G^{(A)}(R)$ and $\epsilon_G^{(B)}(R)$ in this way allows a comparison to be made in the figure with the Morse potential determined in the previous section. There is generally good agreement in the figure between $\tilde{V}_M(R)$ and $\left[\epsilon_G^{(B)}(R) - \epsilon(R_0)\right]$, which corresponds to the more accurate target wavefunction, $\psi_G^{(B)}$. The figure highlights both the suitability of $\tilde{V}_M(R)$ for modelling the effective potential experienced by the nuclei and the difference in accuracy between the two approximate target wavefunctions.

It is important to evaluate the relative accuracies of $\psi_G^{(A)}$ and $\psi_G^{(B)}$ at different values of R, with respect to the accuracies already determined at $R = R_0$. In tables 9.1 and 9.2, we compare a selection of values of $\epsilon_G^{(A)}(R)$ and $\epsilon_G^{(B)}(R)$ with $\epsilon(R)$. As in chapter 1, we have taken values of $\epsilon(R)$ from Wolniewicz [62]. As

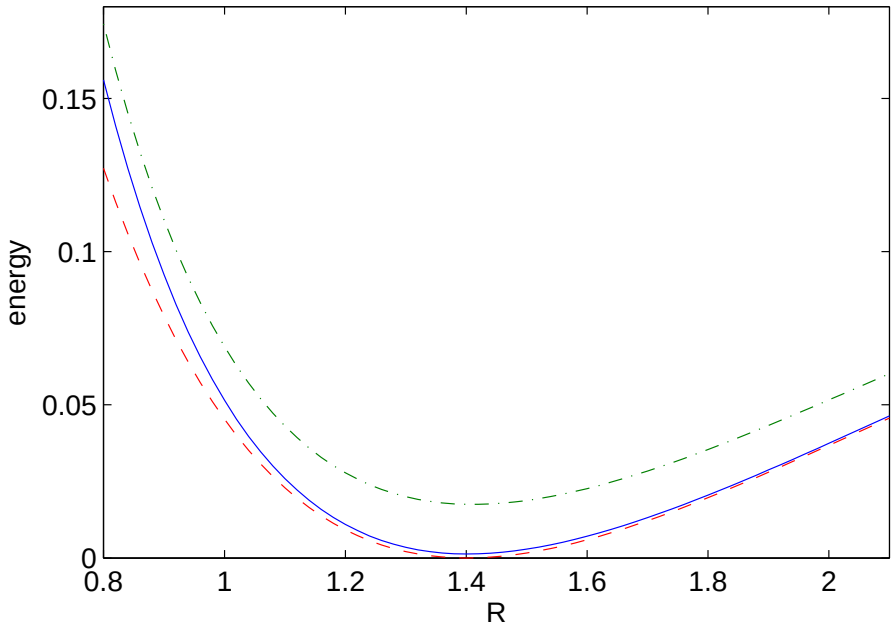

Figure 9.3: A comparison of [— · —] $\left[\epsilon_{\mathrm{G}}^{(\mathrm{A})}(R)-\epsilon(R_0)\right]$, [——] $\left[\epsilon_{\mathrm{G}}^{(\mathrm{B})}(R)-\epsilon(R_0)\right]$ and [- - - -] $\tilde{V}_{\mathrm{M}}(R)$.

usual, the accuracy of each target wavefunction is measured by the percentage, P_{c}, of the correlation energy of H_2 that it takes into account. In calculating P_{c} from (1.6.14), at $R = R_0$ we have again taken the value of E_{HF} from Jensen [61]. At other values of R, we have used the values of E_{HF} determined by Ivanov [94]. In the case of $\psi_{\mathrm{G}}^{(\mathrm{B})}$, the values of P_{c} are found to be similar at each value of R, with the accuracy of $\psi_{\mathrm{G}}^{(\mathrm{B})}$ tending to increase slightly as R is increased. In the case of $\psi_{\mathrm{G}}^{(\mathrm{A})}$, the variations in P_{c} over R are seen to be much larger. However, the least accurate wavefunction at $R = 0.8$, having $P_{\mathrm{c}} = 49.4$, is still broadly comparable with the wavefunction at $R = R_0$, having $P_{\mathrm{c}} = 57.1$. Consequently, for both $\psi_{\mathrm{G}}^{(\mathrm{A})}$ and $\psi_{\mathrm{G}}^{(\mathrm{B})}$, we would not expect Kohn calculations carried out over $0.8 \leq R \leq 2.1$ to be significantly less reliable than the corresponding calculations already carried out at $R = R_0$.

R	$\epsilon_{\mathrm{G}}^{(\mathrm{A})}(R)$	$\epsilon(R)$	$P_{\mathrm{c}}(R)$ (%)
0.8	-1.00015001	-1.02005666	49.4
1.0	-1.10548508	-1.12453972	51.6
1.2	-1.14666622	-1.16493524	54.2
1.4	-1.15695925	-1.17447571	57.1
1.6	-1.15181258	-1.16858337	60.3
1.8	-1.13905288	-1.15506874	63.7
2.0	-1.12287987	-1.13813296	67.2

Table 9.1: Values of $\epsilon_{\mathrm{G}}^{(\mathrm{A})}(R)$ and $P_{\mathrm{c}}(R)$ for $\psi_{\mathrm{G}}^{(\mathrm{A})}$.

R	$\epsilon_{\mathrm{G}}^{(\mathrm{B})}(R)$	$\epsilon(R)$	$P_{\mathrm{c}}(R)$ (%)
0.8	-1.01838244	-1.02005666	95.7
1.0	-1.12300537	-1.12453972	96.1
1.2	-1.16352439	-1.16493524	96.5
1.4	-1.17317293	-1.17447571	96.8
1.6	-1.16737199	-1.16858337	97.1
1.8	-1.15392908	-1.15506874	97.4
2.0	-1.13704077	-1.13813296	97.7

Table 9.2: Values of $\epsilon_{\mathrm{G}}^{(\mathrm{B})}(R)$ and $P_{\mathrm{c}}(R)$ for $\psi_{\mathrm{G}}^{(\mathrm{B})}$.

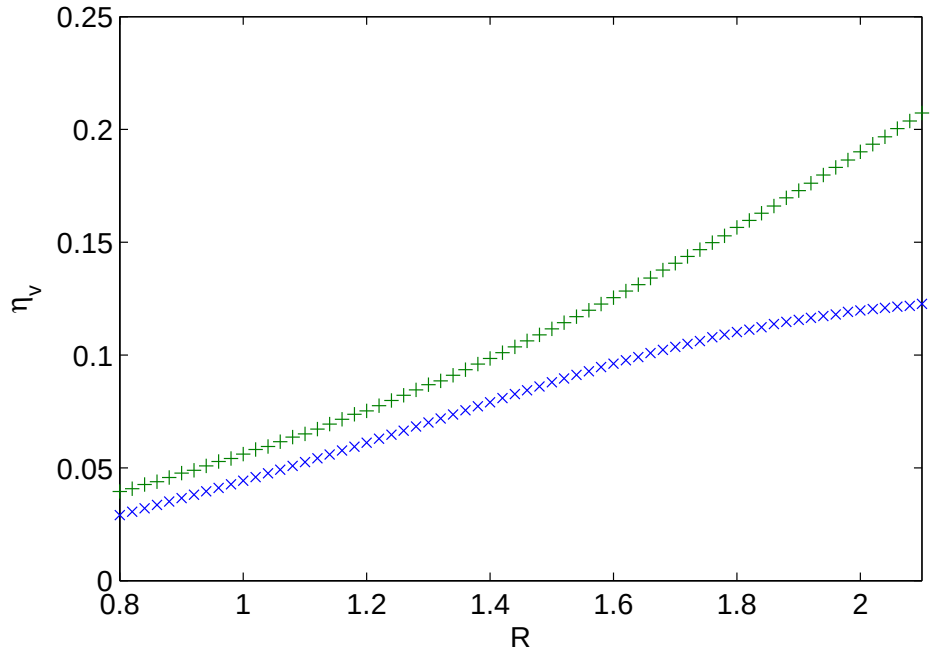

Figure 9.4: Values of $\eta_v\,(R)$ for [+] $\Psi_t^{(1,A)}$ and [×] $\Psi_t^{(1,B)}$ at $k = 0.04$.

The values of $\eta_v\,(R)$ and $Z_{eff}\,(R)$ determined from our Kohn calculations at $k = 0.04$ are shown in figures 9.4 and 9.5 respectively. From a computational point of view, we have found it impractical to recalculate optimal choices for the nonlinear parameters, α and β, at each value of R. As in chapter 8, we have therefore taken values of $(\alpha, \beta) = (0.3, -0.1)$ and $(\alpha, \beta) = (0.3, 0.7)$, respectively for $\Psi_t^{(1,A)}$ and $\Psi_t^{(1,B)}$. These are the values determined for $\Psi_t^{(1,A)}$ and $\Psi_t^{(1,B)}$ in chapter 7 to maximise η_v at $k = 0.04$ and $R = R_0$. It is possible that this simplification has an appreciable effect on our calculations, although we have been unable to carry out a detailed investigation of any such effect here due to the computational expense it would involve.

Both $\Psi_t^{(1,A)}$ and $\Psi_t^{(1,B)}$ exhibit monotonic increases in η_v with increasing R. For both η_v and Z_{eff}, the results of the method of models calculations carried out with $\Psi_t^{(1,A)}$ begin to diverge from the results of the more accurate calculations

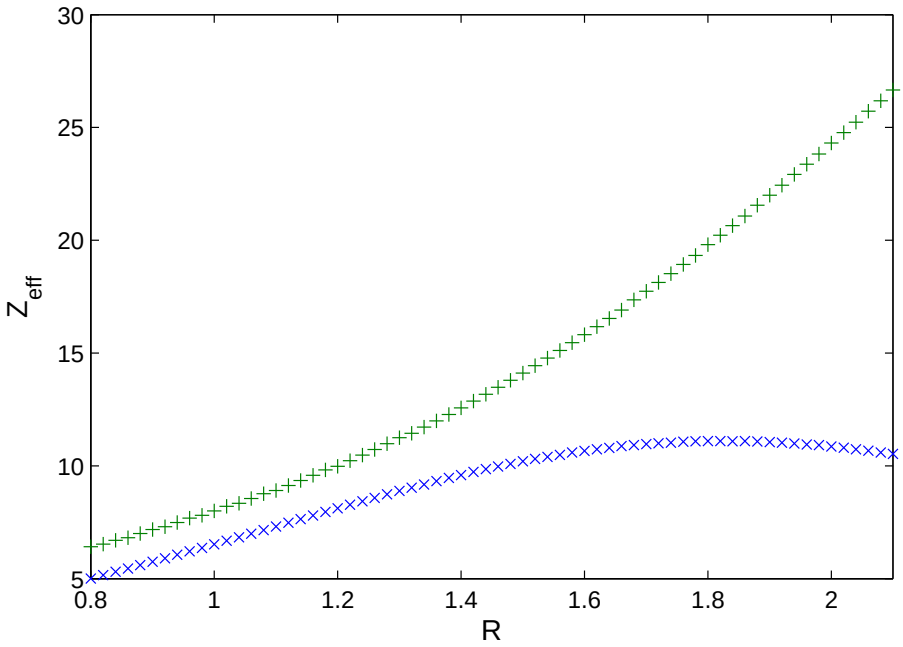

Figure 9.5: Values of $Z_{\text{eff}}(R)$ for [+] $\Psi_{\text{t}}^{(1,\text{A})}$ and [×] $\Psi_{\text{t}}^{(1,\text{B})}$ at $k = 0.04$.

carried out with $\Psi_{\text{t}}^{(1,\text{B})}$ as R increases beyond the equilibrium separation. The differences in the values of both η_{v} and Z_{eff} around $R \simeq 2.0$ is surprisingly large. Furthermore, the qualitative behaviour of $Z_{\text{eff}}(R)$ at larger values of R is different for $\Psi_{\text{t}}^{(1,\text{A})}$ and $\Psi_{\text{t}}^{(1,\text{B})}$. In the case of $\Psi_{\text{t}}^{(1,\text{A})}$, Z_{eff} increases with R, with the rate of increase becoming larger as R is increased. In contrast, for $\Psi_{\text{t}}^{(1,\text{B})}$, Z_{eff} is found to be a decreasing function of R beyond the maximum observed at $R \simeq 1.8$.

There is also evidence in figure 9.4 that, at larger values of R, the qualitative behaviour of $\eta_{\text{v}}(R)$ is different for $\Psi_{\text{t}}^{(1,\text{A})}$ and $\Psi_{\text{t}}^{(1,\text{B})}$. For $\Psi_{\text{t}}^{(1,\text{A})}$, the values of η_{v} are found to increase more quickly with increasing R, while for $\Psi_{\text{t}}^{(1,\text{B})}$ the values of η_{v} are apparently beginning to reach a plateau at higher values of R. These differences demonstrate once again how the results of our Kohn calculations can depend very strongly on the accuracy of the approximate target

wavefunction.

We can determine the overall effects of including nuclear vibrations in our calculations by evaluating vibrational averages of $\eta_{\mathrm{v}}(R)$ and $Z_{\mathrm{eff}}(R)$. In principle, these averages are obtained respectively from the expectations,

$$\mathfrak{E}[\eta_{\mathrm{v}}] = \int_0^\infty \eta_{\mathrm{v}}(R)\, p(R)\, \mathrm{d}R \tag{9.4.1}$$

and

$$\mathfrak{E}[Z_{\mathrm{eff}}] = \int_0^\infty Z_{\mathrm{eff}}(R)\, p(R)\, \mathrm{d}R, \tag{9.4.2}$$

where $p(R)$ is some unit-normalised probability density function for the internuclear separation. However, since analytic expressions for $\eta_{\mathrm{v}}(R)$ and $Z_{\mathrm{eff}}(R)$ are unavailable, these integrals cannot immediately be calculated. It is convenient instead to calculate averages across a discrete set of values of R, over which the integrands in (9.4.1) and (9.4.2) are appreciably large.

For both $\Psi_{\mathrm{t}}^{(1,\mathrm{A})}$ and $\Psi_{\mathrm{t}}^{(1,\mathrm{B})}$, we have determined vibrational averages of $\eta_{\mathrm{v}}(R)$ and $Z_{\mathrm{eff}}(R)$ over 66 values of R in the range $0.8 \leq R \leq 2.1$, using weightings determined from the probability density functions shown in figure 9.2 and corresponding to the harmonic and Morse potentials. We have denoted by $\eta_{\mathrm{v}}^{(\mathrm{H})}$ and $\eta_{\mathrm{v}}^{(\mathrm{M})}$ the vibrational averages of $\eta_{\mathrm{v}}(R)$ corresponding respectively to the harmonic and Morse potentials. An analogous notation is used for the vibrational averages of $Z_{\mathrm{eff}}(R)$. In figure 9.6, we have plotted values of $\eta_{\mathrm{v}}^{(\mathrm{H})}(k)$ and $\eta_{\mathrm{v}}^{(\mathrm{M})}(k)$ as determined for $\Psi_{\mathrm{t}}^{(1,\mathrm{A})}$, in the range $0.01 \leq k \leq 0.4$, together with the results already obtained at $R = R_0$. Analogous plots for $\Psi_{\mathrm{t}}^{(1,\mathrm{B})}$ are given in figure 9.7. In figure 9.8, we have plotted values of $Z_{\mathrm{eff}}^{(\mathrm{H})}(k)$ and $Z_{\mathrm{eff}}^{(\mathrm{M})}(k)$ as

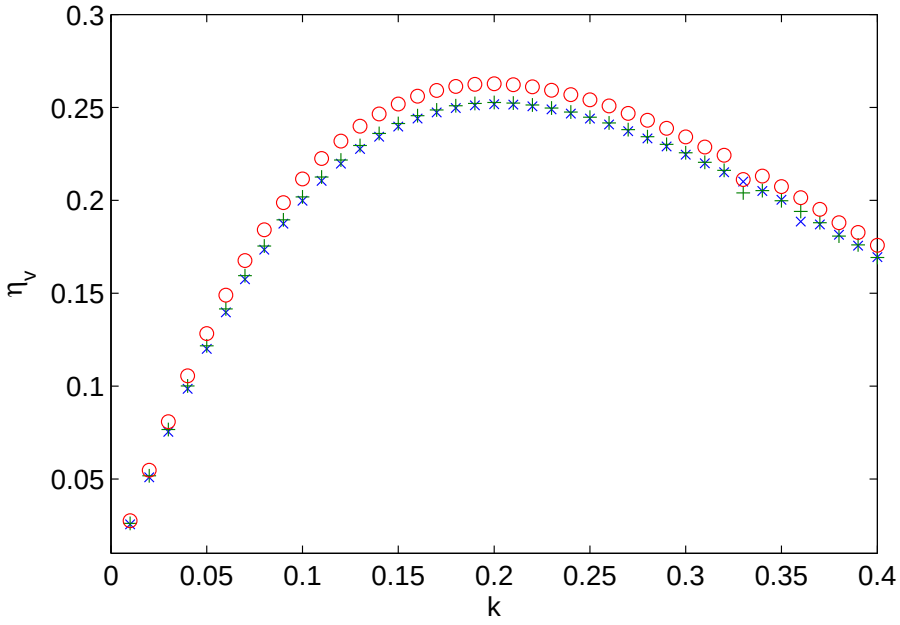

Figure 9.6: Values of [+] $\eta_v^{(H)}(k)$, [○] $\eta_v^{(M)}(k)$ and [×] $\eta_v(k; R = R_0)$ for $\Psi_t^{(1,A)}$.

determined for $\Psi_t^{(1,A)}$, in the range $0.01 \leq k \leq 0.4$, together with the results already obtained at $R = R_0$. Analogous plots for $\Psi_t^{(1,B)}$ are given in figure 9.9.

For both $\Psi_t^{(1,A)}$ and $\Psi_t^{(1,B)}$, the average effect of including nuclear vibrations in the way we have described is found to be small for calculations of the scattering phase shift. For $\Psi_t^{(1,A)}$, the values of $\eta_v^{(M)}$ are slightly higher than the values of $\eta_v^{(H)}$, which are themselves marginally higher than the values of η_v calculated at the equilibrium separation. At $k = 0.04$, for example, we have calculated values of $\eta_v^{(H)} = 0.100$ and $\eta_v^{(M)} = 0.106$; the corresponding value of η_v at $R = R_0$ is $\eta_v = 0.0985$.

For $\Psi_t^{(1,B)}$, values of $\eta_v^{(M)}$ are again seen generally to be slightly higher than the values of η_v determined at $R = R_0$. Values of $\eta_v^{(H)}$ in this case are actually marginally lower than the values obtained at the equilibrium separation. At

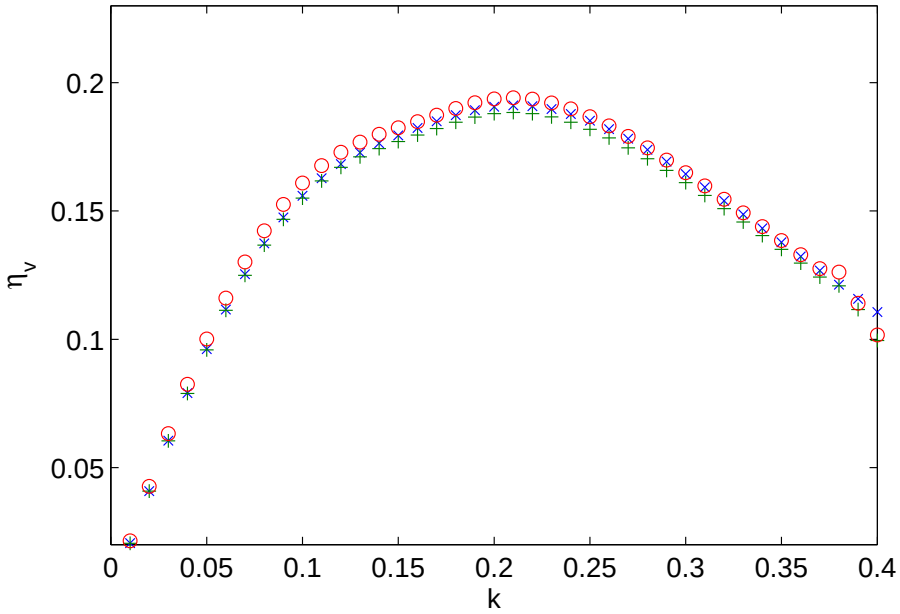

Figure 9.7: Values of [+] $\eta_{\mathrm{v}}^{(\mathrm{H})}(k)$, [○] $\eta_{\mathrm{v}}^{(\mathrm{M})}(k)$ and [×] $\eta_{\mathrm{v}}(k; R = R_0)$ for $\Psi_{\mathrm{t}}^{(1,\mathrm{B})}$.

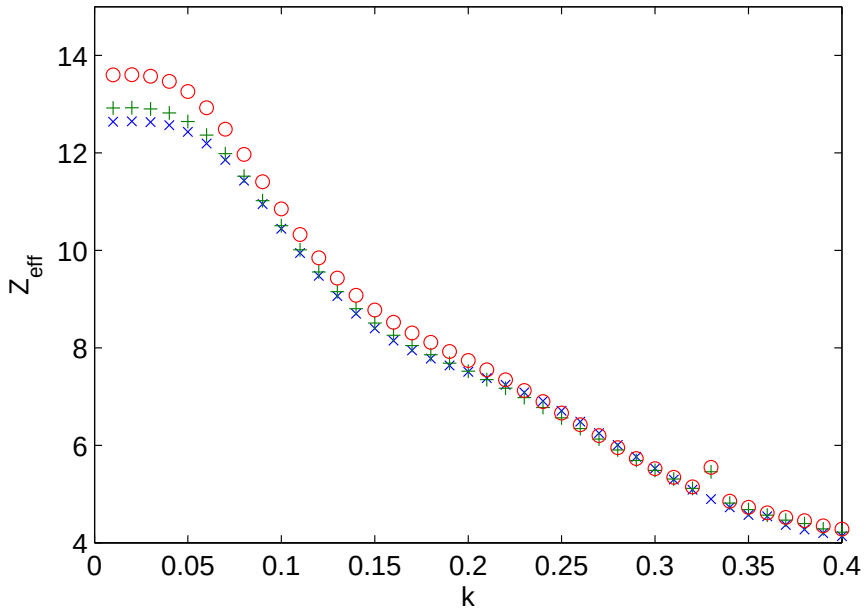

Figure 9.8: Values of [+] $Z_{\mathrm{eff}}^{(\mathrm{H})}(k)$, [○] $Z_{\mathrm{eff}}^{(\mathrm{M})}(k)$ and [×] $Z_{\mathrm{eff}}(k; R = R_0)$ for $\Psi_{\mathrm{t}}^{(1,\mathrm{A})}$.

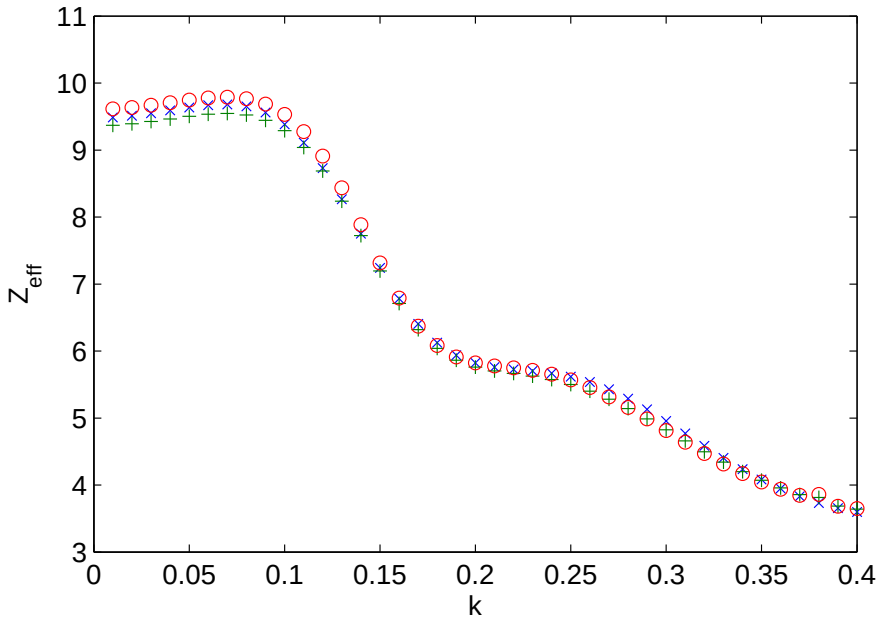

Figure 9.9: Values of [+] $Z_{\mathrm{eff}}^{(\mathrm{H})}(k)$, [○] $Z_{\mathrm{eff}}^{(\mathrm{M})}(k)$ and [×] $Z_{\mathrm{eff}}(k; R = R_0)$ for $\Psi_{\mathrm{t}}^{(1,\mathrm{B})}$.

$k = 0.04$, we have calculated values of $\eta_{\mathrm{v}}^{(\mathrm{H})} = 0.0789$ and $\eta_{\mathrm{v}}^{(\mathrm{M})} = 0.0825$; the corresponding value of η_{v} at $R = R_0$ is $\eta_{\mathrm{v}} = 0.0790$.

In the case of $\Psi_{\mathrm{t}}^{(1,\mathrm{A})}$ and at small values of k, the values of $Z_{\mathrm{eff}}^{(\mathrm{M})}$ are appreciably higher than the values calculated at the equilibrium separation. We have calculated a value of $Z_{\mathrm{eff}}^{(\mathrm{M})} = 13.5$ at $k = 0.04$, where the corresponding calculation at $R = R_0$ gives $Z_{\mathrm{eff}} = 12.6$. The values of $Z_{\mathrm{eff}}^{(\mathrm{H})}$ are less striking, being generally only slightly higher than the results of calculations carried out at the equilibrium separation. At $k = 0.04$, we have calculated a value of $Z_{\mathrm{eff}}^{(\mathrm{H})} = 12.8$.

The value of $Z_{\mathrm{eff}}^{(\mathrm{M})} = 13.5$ at $k = 0.04$ is in broad agreement with the experimental value of $Z_{\mathrm{eff}} = 14.6$ [25]. However, we should take care in drawing conclusions from this result, owing to the potential weaknesses we have identified in calculations involving $\Psi_{\mathrm{t}}^{(1,\mathrm{A})}$ that arise from the inaccuracy of the target

wavefunction, $\psi_{\mathrm{G}}^{(\mathrm{A})}$.

For the more accurate calculations carried out with $\Psi_{\mathrm{t}}^{(1,\mathrm{B})}$, the differences between the three sets of results shown in figure 9.9 are small. At small values of k, the values of $Z_{\mathrm{eff}}^{(\mathrm{H})}$ are generally a little lower than the values of Z_{eff} obtained at the equilibrium separation, which are themselves slightly smaller than the values of $Z_{\mathrm{eff}}^{(\mathrm{M})}$. At $k = 0.04$, we have calculated values of $Z_{\mathrm{eff}}^{(\mathrm{H})} = 9.46$ and $Z_{\mathrm{eff}}^{(\mathrm{M})} = 9.71$. The corresponding value determined at $R = R_0$ is $Z_{\mathrm{eff}} = 9.59$.

9.5 Persistent anomalies

There is some evidence of persistent Schwartz-type behaviour appearing in the calculations at $k = 0.33$ in figures 9.6 and 9.8 and at $k = 0.38$ in figures 9.7 and 9.9. Anomalies in $\eta_{\mathrm{v}}(R)$ and $Z_{\mathrm{eff}}(R)$ occur at particular choices of R; their effects are suppressed to a large extent in figures 9.6-9.9, since the majority of the values of R, over which the averages are calculated, give results which are free of anomalies.

To investigate in greater detail the persistent anomalies arising from the choice of R, we have examined Kohn calculations of $\eta_{\mathrm{v}}(k, R)$ for $\Psi_{\mathrm{t}}^{(1,\mathrm{A})}$ and $\Psi_{\mathrm{t}}^{(1,\mathrm{B})}$, for 66 values of R in the range $0.8 \leq R \leq 2.1$ and for 80 values of k in the range $0.01 \leq k \leq 0.8$. To illustrate persistent anomalous behaviour, it is helpful to define a function analogous to (5.6.1),

$$\Delta(k, R) = |\eta_{\mathrm{v}}(k, R) - \langle \eta_{\mathrm{v}} \rangle (k)|, \tag{9.5.1}$$

where, for each of the values of k considered, $\langle \eta_{\mathrm{v}} \rangle$ is the median value of η_{v}

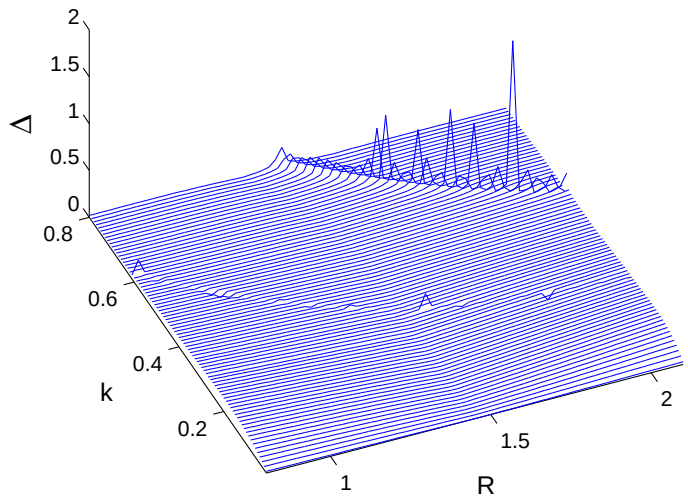

Figure 9.10: Values of $\Delta(k, R)$ for $\Psi_t^{(1,A)}$.

evaluated across the range of the values of R.

Values of $\Delta(k, R)$ for $\Psi_t^{(1,A)}$ and $\Psi_t^{(1,B)}$ are shown in figures 9.10 and 9.11 respectively. Both figures clearly indicate persistent anomalies distributed about curves in the (k, R) plane. The curves are reminiscent of those observed earlier in figures 5.2 and 5.3, illustrating persistent anomalies in the (α, β) plane. Here, the curves appearing at the lower end of the range of k values correspond to the small anomalies found in figures 9.6-9.9. It is clear from figures 9.10 and 9.11 that a small change in k or R can usually be made to avoid the persistent anomalies.

Finally, we remark that the anomalies appearing in figures 9.10 and 9.11 occur in similar regions of the (k, R) plane. This supports the claim made in chapter 2 that the major difference between the trial functions, namely the approximate target wavefunction used in each case, does not typically have a significant

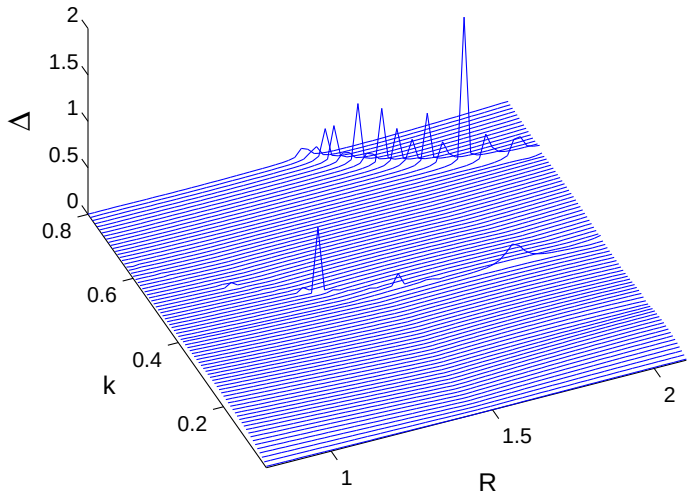

Figure 9.11: Values of $\Delta\left(k, R\right)$ for $\Psi_{\mathrm{t}}^{(1,\mathrm{B})}$.

effect on the location of anomalies.

9.6 Conclusions

We have introduced a basic description of adiabatic nuclear motion to our Kohn calculations. With the exception of the calculations of $Z_{\mathrm{eff}}^{(\mathrm{M})}$ for $\Psi_{\mathrm{t}}^{(1,\mathrm{A})}$, we have found that there are only small differences between our vibrationally averaged results and those results obtained at the equilibrium internuclear separation.

By modelling the effective potential experienced by the nuclei with a Morse potential, vibrational averages of Z_{eff} obtained with $\Psi_{\mathrm{t}}^{(1,\mathrm{A})}$ have been found to be in reasonable agreement with experiment. However, the relative inaccuracy of the target wavefunction used in this case, together with the divergent

behaviour of $Z_{\text{eff}}(R)$ observed in figure 9.5, cast doubt on the legitimacy of comparing these results with experimental data.

Despite the fact that the inclusion of nuclear dynamics has had relatively little effect on our results, this work is important as we believe it represents the first attempt to include nuclear motion of any kind in Kohn calculations for the $(e^+ - H_2)$ system. An obvious extension to our analysis would be to examine the nonadiabatic coupling of leptonic and nuclear motion, although these effects are unlikely to be significant and would require considerable mathematical effort to investigate rigorously. There are, however, possibilities for further research which avoid this complication. For example, a more thorough adiabatic analysis might optimise the values of the nonlinear parameters, α and β, at each value of R under consideration. We have already found in chapter 7 that variations of these parameters can have a significant effect on the results of the Kohn calculations carried out at $R = R_0$.

The existence of persistent Schwartz-type behaviour arising from the choice of R highlights, once again, the importance of making the effort to detect and avoid anomalies, even after the trial wavefunction has been optimised in τ. In a manner similar to that seen in chapter 5, we have found that the persistent anomalies are distributed about well-defined curves in the (k, R) plane; this makes it possible broadly to predict their appearance and take appropriate measures to avoid them.

Chapter 10

Concluding Remarks

In this thesis, we have presented details of the most accurate Kohn variational calculations on low energy $(e^+ - H_2)$ scattering presently available. Our work is distinguished from all previous implementations of the Kohn method for this system by the explicit consideration of the interelectronic potential in the target molecule. By adapting code designed originally for helium-antihydrogen scattering calculations [69], we have been able numerically to evaluate integrals that had previously been regarded as intractable. This has allowed us to carry out Kohn calculations free of the simplifying constraints of the method of models and, as such, has permitted a much more accurate consideration of the unperturbed target.

In chapter 2, we have presented the first calculations of scattering parameters using a trial wavefunction involving the very accurate target wavefunction, $\psi_G^{(B)}$. We have compared the results of these calculations with results obtained using the method of models and a trial function involving the less accurate target wavefunction, $\psi_G^{(A)}$. Values of η_v obtained with the method of models have

been found generally to be larger than the results of corresponding calculations involving explicit consideration of the target potential. Both sets of results have been found to be susceptible to the effects of Schwartz singularities.

In chapters 3 and 4, we have given a comprehensive account of singularities and related anomalies found in our generalised Kohn calculations. This analysis represents a significant development in understanding beyond that established in previous works. We have demonstrated that the anomalies are characteristic of an underlying structure and that their appearance can be predicted from purely analytic considerations. Moreover, we have found that singularities are neither sufficient nor necessary for anomalies to occur. A variety of optimisation schemes have been developed to choose the phase parameter, τ, so as automatically to avoid anomalous behaviour. Though each is largely successful, we have observed persistent anomalies in our calculations that are not satisfactorily avoided by any choice of τ.

In chapter 5, we have carried out the first complex Kohn calculations for the $(e^+ - H_2)$ system. We have proved that values of η'_v obtained in these calculations are independent of the choice of τ. We have shown also that the real part of the phase shift approximation obtained in our implementation of the complex Kohn method is precisely equal to the value of η_v found in the generalised Kohn method when the derivative, $\frac{\partial \eta_v}{\partial \tau}$, is minimised. It follows immediately that the persistent anomalous behaviour observed in our generalised Kohn calculations must also be present in the corresponding complex Kohn calculations. We have found that these persistent anomalies can be avoided by a small change in the nonlinear parameters, α and β.

In chapter 6, we have presented calculations of the annihilation parameter, Z_{eff},

both within the framework of the method of models and for calculations involving explicit consideration of the target potential. Of these two sets of calculations, we have found that the values of Z_{eff} determined with the method of models and involving $\psi_{\text{G}}^{(\text{A})}$ are appreciably larger, being very broadly in agreement with experimental data [25]. However, we have argued that these results are likely to be artificially high, owing to the relative inaccuracy of the target wavefunction used in the calculations.

In chapter 7, we have conducted a systematic investigation of the sensitivity of our calculations to changes in the nonlinear parameters, α and β. We have found that, particularly at low energies, the values of η_{v} and Z_{eff} are strongly dependent on the choice of α and β. We have argued that, in the absence of persistent Schwartz-type behaviour, values of these parameters can be optimised by choosing them to maximise the phase shift approximation at low energies. We have found that the maxima of $\eta_{\text{v}}(\alpha, \beta)$ and $Z_{\text{eff}}(\alpha, \beta)$ do not generally occur at the same point. Consequently, in the region of the optimised values, calculations of Z_{eff} have been found to be more sensitive to small changes in α and β than the calculations of η_{v}.

In chapter 8, we have reported the unexpected results observed in our Kohn calculations when attempting to include short-range correlation functions containing Hylleraas-type terms in the interelectronic distance. For calculations involving the target wavefunction, $\psi_{\text{G}}^{(\text{B})}$, we have found that inclusion of these terms gives rise to a very significant increase in the calculated values of η_{v} and Z_{eff} at low energies; indeed, the values of Z_{eff} are brought broadly into line with experimental data [25]. However, we have presented strong evidence that the results of these calculations are unreliable and have sought to verify this claim by improving the accuracy of the target wavefunction still further. By extending

the computational framework to admit trial functions containing interelectronic Hylleraas-type terms in the target wavefunction as well as the short-range correlation functions, we have been able to carry out Kohn calculations involving extremely accurate target wavefunctions, accounting for over 99% of the correlation energy of H_2. This is in contrast to the 96.8% of the correlation energy accounted for by $\psi_G^{(B)}$, the most accurate target wavefunction we have considered that does not involve Hylleraas-type terms. For the calculations involving $\Psi_t^{(2,C)}$, we have found that including the Hylleraas-type correlation functions in the interelectronic distance has only a small effect on the calculated values of η_v and Z_{eff}.

In chapter 9, we have introduced an adiabatic consideration of nuclear motion to our Kohn calculations. In the case of Kohn calculations of η_v and Z_{eff} involving explicit consideration of the target potential, we have found that the overall effect of including ground state nuclear vibrations is small. In the case of the method of models calculations, we have found that the values of Z_{eff} are noticeably increased upon taking into account the nuclear motion, bringing them closer into agreement with experimental data [25]. However, the reliability of these results is again debatable, owing to the relative inaccuracy of the target wavefunction used in the calculations.

A key feature of this thesis has been the thorough discussion of nonphysical problems associated with the Kohn method. Previous implementations of the method for the $(e^+ - H_2)$ system [10, 23, 29] have tended to concentrate on improving the physical understanding of scattering processes by the use of increasingly sophisticated trial wavefunctions. By its very nature, research of this kind has often been encumbered by limitations in the computer processing power available at the time. Here, by investigating abstract topics more

amenable to analytic treatment, we have made relatively quick progress in our understanding of certain aspects of the scattering problem.

Nevertheless, the overriding difficulty in reducing the size of the discrepancies between theoretical and experimental results still lies in the limitations of the computational framework. Despite the improvements we have made to this framework, we are still able to consider only relatively simple short-range correlation functions. We can reasonably expect that the inclusion of more flexible correlation functions would significantly improve the level of agreement between theory and experiment. In their calculations on positron-helium scattering, Van Reeth and Humberston [19, 88] had the advantage of a spherically symmetric target. This made is possible for these authors to include more elaborate short-range correlation functions, such as those containing factors of $r_{13}r_{23}$. Our results seem to indicate that an extension of this kind may be necessary in the case of $(e^+ - H_2)$ scattering, if very accurate results are to be obtained.

In addition to improvements to the framework used to calculate the matrix elements, several opportunities for further research exist. In particular, an analysis of Feshbach resonances [95], believed to be responsible [96] for the very high values of Z_{eff} observed in polyatomic molecules [5], could be conducted. Ground state molecular hydrogen does not exhibit these resonances as the positron is too light to form a bound state with it. However, it might eventually be possible to perform a qualitative investigation of Feshbach resonances computationally, by artificially increasing the mass of the positron so that an $(e^+ - H_2)$ bound state is permitted. Moreover, the resonant capture model developed by Gribakin and Lee [96] is based upon infrared-active vibrational modes. In our calculations, the vibrational states of H_2 could be made artificially infrared-active by adjusting the charge on the two nuclei to $(1 + a)$ and $(1 - a)$, for

some $0 < a < 1$. Work on this is in progress [97] and indicates that, in the Kohn method, quasi-bound vibrational states of $(e^+ - H_2)$ are coupled to the continuum by the terms in the Hamiltonian that are neglected in the Born-Oppenheimer approximation. The relative simplicity of the H_2 molecule would allow for more accurate calculations than could be carried out for larger molecules and may provide a greater understanding of the underlying mechanics responsible for the experimentally observed resonances.

Having removed the dependence of our Kohn calculations on the method of models, we can in principle investigate inelastic processes. These processes dominate at positron energies higher than those considered in this thesis. It is of particular interest to carry out calculations in the region of the positronium formation threshold at 8.63 eV, corresponding to $k \simeq 0.8$. This is the first inelastic channel with a significant cross section. An important consideration at these energies is the contribution of higher partial waves to scattering processes. Several partial waves were accounted for in the $(e^+ - H_2)$ scattering calculations made by Armour and coworkers [29]. They considered mixing of the two lowest partial waves in the Σ_g^+, Σ_u^+ and Π_u symmetries as well as the lowest partial wave of Π_g symmetry. They found that the mixing of partial waves became more important as the energy of the incident positron was increased.

It is hoped that the calculations presented in this thesis will provide a strong foundation for the future work we have outlined above, as well as for related research problems. There remain fundamental, unresolved issues in the study of interactions between positrons and molecular gases. However, the progress made in this field in recent years suggests that these challenges are not insurmountable.

Appendix A

Basis Functions Used in the Trial Wavefunctions

A.1 Basis functions of ψ_G

The majority of our Kohn calculations carried out with the method of models use the 6-term target wavefunction, $\psi_G^{(A)}$, introduced by Armour [23]. The choice of the nonlinear parameter, δ, in this wavefunction depends on the value of R at which the calculation is carried out. At the equilibrium separation, $R_0 = 1.4$, we have chosen a value of $\delta = 1.1$ to minimise the ground state energy expectation, so that $\psi_G^{(A)}$ accounts for 57.1% of the correlation energy of H_2. In chapter 8, a more accurate 27-term wavefunction, $\psi_G^{(D)}$, is introduced, accounting for 66.5% of the correlation energy and again having $\delta = 1.1$. Details of the basis functions used in $\psi_G^{(A)}$ and $\psi_G^{(D)}$ appear overleaf, following the notation introduced in (1.6.10).

APPENDIX A: BASIS FUNCTIONS USED IN THE TRIAL WAVEFUNCTIONS

Basis functions comprising $\psi_{\mathrm{G}}^{(\mathrm{A})}$ ($s_{12}(\omega_v) = 1$ in each case):

No.	m_v	n_v	j_v	k_v
1	0	0	0	0
2	0	0	2	0
3	1	0	0	0
4	0	0	1	1
5	1	0	1	1
6	2	0	0	0

Basis functions comprising $\psi_{\mathrm{G}}^{(\mathrm{D})}$ ($s_{12}(\omega_v) = 1$ in each case):

No.	m_v	n_v	j_v	k_v
1	0	0	0	0
2	0	0	2	0
3	1	0	0	0
4	0	0	1	1
5	1	0	1	1
6	2	0	0	0
7	2	0	2	0
8	2	0	1	1
9	1	1	0	2

No.	m_v	n_v	j_v	k_v
10	1	2	0	2
11	1	0	2	0
12	1	0	0	2
13	2	2	2	2
14	1	2	1	1
15	1	2	0	0
16	1	2	2	0
17	2	2	0	0
18	1	1	0	0

No.	m_v	n_v	j_v	k_v
19	0	2	2	2
20	1	1	2	2
21	2	0	0	2
22	2	2	1	1
23	1	1	1	1
24	1	2	2	2
25	0	1	2	2
26	2	2	0	2
27	0	0	2	2

APPENDIX A: BASIS FUNCTIONS USED IN THE TRIAL WAVEFUNCTIONS

The majority of our Kohn calculations involving explicit consideration of the target potential use the 144-term target wavefunction, $\psi_G^{(B)}$, having the form (1.6.9). These 144 terms consist of two sets of 72 basis functions. The two sets correspond to values of $\omega_v = 0$ and $\omega_v = 2$ in (1.6.11). Each set of 72 functions comprises all physically distinct permutations of the non-negative integers, $\{m_v, n_v, j_v, k_v\}$, each integer being no larger than 3 and subject to the requirement of nuclear symmetry that $(j_v + k_v)$ must be even. Details of the $\{m_v, n_v, j_v, k_v\}$ used are given in the table overleaf. The value of the nonlinear parameter, δ, depends on the value of R at which the calculation is carried out. At the equilibrium separation, $R_0 = 1.4$, we have chosen a value of $\delta = 1.14$ to minimise the ground state energy expectation, so that $\psi_G^{(B)}$ accounts for 96.8% of the correlation energy of H_2. In chapter 8, a more accurate 145-term wavefunction, $\psi_G^{(C)}$, is introduced, accounting for 99.7% of the correlation energy and again having $\delta = 1.14$. $\psi_G^{(C)}$ is identical to $\psi_G^{(B)}$ but for the inclusion of one Hylleraas-type function in ρ_{12}.

APPENDIX A: BASIS FUNCTIONS USED IN THE TRIAL WAVEFUNCTIONS

Details of basis functions used in $\psi_{\mathrm{G}}^{(\mathrm{B})}$ ($\omega_v \in \{0,2\}$):

No.	m_v	n_v	j_v	k_v
1	0	0	0	0
2	0	0	0	2
3	0	0	1	1
4	0	0	1	3
5	0	0	2	2
6	0	0	3	3
7	0	1	0	0
8	0	1	0	2
9	0	1	1	1
10	0	1	1	3
11	0	1	2	0
12	0	1	2	2
13	0	1	3	1
14	0	1	3	3
15	0	2	0	0
16	0	2	0	2
17	0	2	1	1
18	0	2	1	3
19	0	2	2	0
20	0	2	2	2
21	0	2	3	1
22	0	2	3	3
23	0	3	0	0
24	0	3	0	2

No.	m_v	n_v	j_v	k_v
25	0	3	1	1
26	0	3	1	3
27	0	3	2	0
28	0	3	2	2
29	0	3	3	1
30	0	3	3	3
31	1	1	0	0
32	1	1	0	2
33	1	1	1	1
34	1	1	1	3
35	1	1	2	2
36	1	1	3	3
37	1	2	0	0
38	1	2	0	2
39	1	2	1	1
40	1	2	1	3
41	1	2	2	0
42	1	2	2	2
43	1	2	3	1
44	1	2	3	3
45	1	3	0	0
46	1	3	0	2
47	1	3	1	1
48	1	3	1	3

No.	m_v	n_v	j_v	k_v
49	1	3	2	0
50	1	3	2	2
51	1	3	3	1
52	1	3	3	3
53	2	2	0	0
54	2	2	0	2
55	2	2	1	1
56	2	2	1	3
57	2	2	2	2
58	2	2	3	3
59	2	3	0	0
60	2	3	0	2
61	2	3	1	1
62	2	3	1	3
63	2	3	2	0
64	2	3	2	2
65	2	3	3	1
66	2	3	3	3
67	3	3	0	0
68	3	3	0	2
69	3	3	1	1
70	3	3	1	3
71	3	3	2	2
72	3	3	3	3

Additional Hylleraas-type function in ρ_{12}, having $\omega_v = 1$, included in $\psi_G^{(C)}$:

No.	m_v	n_v	j_v	k_v
145	0	0	0	0

A.2 Short-range correlation functions

The majority of our Kohn calculations use a set, $\Omega^{(1)}$, of 279 correlation functions of the form (1.7.8). The first 261 of these comprise three sets of 87 correlation functions, corresponding to values of $\theta_i = 0$, $\theta_i = 2$ and $\theta_i = 4$ in (1.7.9) and (1.7.10). Each set of 87 functions consists of all physically distinct permutations of the non-negative integers, $\{a_i, b_i, c_i, d_i, r_i, s_i\}$, such that no integer is larger than 2 and with $(a_i + b_i + c_i + d_i + r_i + s_i) \leq 5$. A further constraint imposed by nuclear symmetry is that $(c_i + d_i + s_i)$ must be even. Details of the $\{a_i, b_i, c_i, d_i, r_i, s_i\}$ used are given in the table overleaf. The remaining 18 functions in $\Omega^{(1)}$ contain Hylleraas-type terms in the electron-positron coordinates, corresponding to $\theta_i = 3$ in (1.7.9) and (1.7.10). Details of these functions are tabulated in the following pages. Finally, in chapter 8 the set, $\Omega^{(2)}$, is introduced. This set is identical to $\Omega^{(1)}$ but for the inclusion of 18 Hylleraas-type functions in the interelectronic coordinate, ρ_{12}, corresponding to $\theta_i = 1$ in (1.7.9) and (1.7.10). With respect to the choices of $\{a_i, b_i, c_i, d_i, r_i, s_i\}$, the form of these 18 functions is the same as the 18 Hylleraas-type functions already used in $\Omega^{(1)}$, corresponding to $\theta_i = 3$.

Details of short-range correlation functions ($\theta_i \in \{0, 2, 4\}$):

No.	a_i	b_i	c_i	d_i	r_i	s_i
1	0	0	0	0	0	0
2	0	0	0	0	0	2
3	0	0	0	0	1	0
4	0	0	0	0	1	2
5	0	0	0	0	2	0
6	0	0	0	0	2	2
7	0	0	0	1	0	1
8	0	0	0	2	0	2
9	0	0	0	2	2	0
10	0	0	1	0	1	1
11	0	0	1	0	2	1
12	0	0	1	1	0	0
13	0	0	1	1	0	2
14	0	0	1	1	1	0
15	0	0	1	1	1	2
16	0	0	1	1	2	0
17	0	0	2	0	0	0
18	0	0	2	0	1	0
19	0	0	2	0	1	2
20	0	0	2	1	0	1
21	0	0	2	1	1	1
22	0	0	2	2	0	0

No.	a_i	b_i	c_i	d_i	r_i	s_i
23	0	0	2	2	1	0
24	0	1	0	0	0	0
25	0	1	0	0	0	2
26	0	1	0	0	1	0
27	0	1	0	0	1	2
28	0	1	0	1	0	1
29	0	1	0	1	1	1
30	0	1	0	2	0	0
31	0	1	0	2	1	0
32	0	1	1	0	1	1
33	0	1	1	0	2	1
34	0	1	1	1	1	0
35	0	1	2	0	0	0
36	0	1	2	0	1	0
37	0	1	2	1	0	1
38	0	2	0	0	0	0
39	0	2	0	0	1	0
40	0	2	0	0	2	0
41	0	2	0	1	0	1
42	0	2	0	1	1	1
43	0	2	0	2	0	0
44	0	2	1	0	0	1

Details of short-range correlation functions ($\theta_i \in \{0, 2, 4\}$), continued:

No.	a_i	b_i	c_i	d_i	r_i	s_i
45	0	2	1	0	1	1
46	0	2	1	1	0	0
47	0	2	1	1	1	0
48	0	2	2	0	0	0
49	1	0	0	0	2	0
50	1	0	0	0	2	2
51	1	0	0	1	0	1
52	1	0	0	2	0	2
53	1	0	0	2	2	0
54	1	0	1	0	2	1
55	1	0	1	1	0	0
56	1	0	1	1	0	2
57	1	0	1	1	2	0
58	1	0	2	0	0	2
59	1	0	2	0	2	0
60	1	0	2	1	0	1
61	1	0	2	2	0	0
62	1	1	0	0	0	0
63	1	1	0	0	0	2
64	1	1	0	0	1	0
65	1	1	0	0	1	2
66	1	1	0	0	2	0

No.	a_i	b_i	c_i	d_i	r_i	s_i
67	1	1	0	1	1	1
68	1	1	0	2	0	0
69	1	1	0	2	1	0
70	1	1	1	0	0	1
71	1	1	1	1	0	0
72	1	1	1	1	1	0
73	1	2	0	0	0	2
74	1	2	0	2	0	0
75	1	2	1	0	0	1
76	1	2	1	1	0	0
77	2	0	0	0	0	2
78	2	0	0	0	1	2
79	2	0	0	2	1	0
80	2	0	2	0	1	0
81	2	1	0	0	0	0
82	2	1	0	0	1	0
83	2	1	0	0	2	0
84	2	1	0	2	0	0
85	2	1	1	0	0	1
86	2	2	0	0	0	0
87	2	2	0	0	1	0

APPENDIX A: BASIS FUNCTIONS USED IN THE TRIAL WAVEFUNCTIONS

Details of Hylleraas-type functions in interleptonic coordinates ($\theta_i \in \{1,3\}$):

No.	a_i	b_i	c_i	d_i	r_i	s_i
262	1	0	0	0	0	0
263	0	0	0	0	0	0
264	0	0	0	0	1	0
265	0	0	1	1	0	0
266	1	0	0	0	1	0
267	0	0	1	1	1	0
268	1	1	0	0	0	0
269	1	0	1	1	0	0
270	1	1	1	1	0	0
271	0	0	0	1	0	1
272	1	0	0	1	0	1
273	1	0	1	0	0	1
274	1	1	1	0	0	1
275	0	0	0	1	1	1
276	1	0	0	1	1	1
277	1	0	1	0	1	1
278	1	1	1	0	1	1
279	1	1	0	0	1	0

Appendix B

Analytic Evaluation of the I and J Integrals

B.1 Evaluating the I and J integrals

We will show that integrals of the form (8.4.2) and (8.4.3) can be evaluated analytically for $m \in \mathbb{N}$, $\alpha > 0$ and $w > 1$. To do this, we first define

$$G[n,\beta] = \int_0^p \kappa^n \exp(-\beta\kappa)\sin(c\kappa)\,\mathrm{d}\kappa, \tag{B.1.1}$$

$$H[n,\beta] = \int_0^p \kappa^n \exp(-\beta\kappa)\cos(c\kappa)\,\mathrm{d}\kappa, \tag{B.1.2}$$

$$I_0(\alpha) = \int_0^p \exp(-\alpha\kappa)\frac{\sin(c\kappa)}{\kappa}\mathrm{d}\kappa, \tag{B.1.3}$$

$$J_0(\alpha) = \int_0^p \exp(-\alpha\kappa)\frac{\cos(c\kappa)}{\kappa}[1-\exp(-\gamma\kappa)]\,\mathrm{d}\kappa, \tag{B.1.4}$$

where n is a non-negative integer, $\beta > 0$, $\kappa = (\lambda_3 - 1) \geq 0$ and $p = (w - 1) > 0$. Further, we define

$$Q[n,\beta] = \int_0^p \kappa^n \exp(-\zeta\kappa)\,\mathrm{d}\kappa = H[n,\beta] + \mathrm{i}G[n,\beta], \tag{B.1.5}$$

where $\zeta = \beta - \mathrm{i}c$. Using these definitions, we have

$$\begin{aligned} I[m,\alpha] &= \exp(-\alpha)\int_0^p (1+\kappa)^m \exp(-\alpha\kappa)\frac{\sin(c\kappa)}{\kappa}\mathrm{d}\kappa \\ &= \exp(-\alpha)\int_0^p \left[1 + m\kappa + \frac{m(m-1)}{2!}\kappa^2 + \ldots\right]\exp(-\alpha\kappa)\frac{\sin(c\kappa)}{\kappa}\mathrm{d}\kappa \\ &= \exp(-\alpha)\left(I_0(\alpha) + mG[0,\alpha] + \frac{m(m-1)}{2!}G[1,\alpha] + \ldots\right) \end{aligned} \tag{B.1.6}$$

and, by analogy,

$$\begin{aligned} J[m,\alpha] &= \exp(-\alpha)\left(J_0(\alpha) + m\left(H[0,\alpha] - H[0,\alpha+\gamma]\right)\right. \\ &+ \left.\frac{m(m-1)}{2!}\left(H[1,\alpha] - H[1,\alpha+\gamma]\right) + \ldots\right), \end{aligned} \tag{B.1.7}$$

so that the problem of evaluating $I[m,\alpha]$ and $J[m,\alpha]$ is reduced to one of evaluating $Q[n,\beta]$, $I_0(\alpha)$ and $J_0(\alpha)$.

B.1.1 Evaluating $Q[n,\beta]$

$Q[n,\beta]$ can be evaluated in one of two ways. The first method uses the Taylor series expansion for $\exp(-\zeta\kappa)$, viz.

$$\begin{aligned} Q\left[n,\beta\right] &= \int_0^p \kappa^n \exp\left(-\zeta\kappa\right) \mathrm{d}\kappa = \int_0^p \kappa^n \sum_{j=0}^{\infty} \frac{(-\zeta\kappa)^j}{j!} \mathrm{d}\kappa \\ &= \sum_{j=0}^{\infty} \frac{(-\zeta)^j \, p^{n+j+1}}{j! \, (n+j+1)}, \end{aligned} \tag{B.1.8}$$

for which accurate approximations can be obtained by terminating the expansion at an appropriately high value of j.

The second method of evaluating $Q[n,\beta]$ is via recursion. Integrating by parts for $n > 0$, we have

$$\begin{aligned} Q\left[n,\beta\right] &= \int_0^p \kappa^n \exp\left(-\zeta\kappa\right) \mathrm{d}\kappa \\ &= \left[-\frac{1}{\zeta} \exp\left(-\zeta\kappa\right) \kappa^n\right]_0^p + \frac{n}{\zeta} \int_0^p \kappa^{n-1} \exp\left(-\zeta\kappa\right) \mathrm{d}\kappa \\ &= \frac{n}{\zeta} Q\left[n-1,\beta\right] - \frac{\exp\left(-\zeta p\right) p^n}{\zeta} \end{aligned} \tag{B.1.9}$$

and

$$Q\left[0,\beta\right] = \frac{1-\exp\left(-\zeta p\right)}{\zeta}. \tag{B.1.10}$$

The recursive method is more immediately attractive as the exact result for $Q[n,\beta]$ can, in principle, be obtained, whereas any truncation of the expansion (B.1.8) guarantees only an approximate value. However, the use of recursion in computational calculations can lead to erroneous results as errors due to finite computational precision, negligible at small values of n, can compound as the value of n increases. We have found that the recursive approach is accurate up to $n \simeq 30$ if $p > 20$, but that the method begins to break down for such large values of n if $p < 20$. In contrast, we have found that the series expansion approach (B.1.8) is very accurate for $p < 20$ up to $n \simeq 30$, if terms up to $j \simeq 150$

are considered. Both methods have been implemented in our Kohn calculations, with the preferred method being chosen automatically according to the value of p. It was not required to calculate integrals having $n > 30$.

B.1.2 Evaluating $I_0(\alpha)$ and $J_0(\alpha)$

The evaluation of $I_0(\alpha)$ and $J_0(\alpha)$ is possible with the use of the exponential integral for complex argument, z, with $\Re[z] > 0$,

$$\mathrm{E}_1(z) = \int_1^\infty \frac{\exp(-zt)}{t}\mathrm{d}t, \tag{B.1.11}$$

from which it is easily deduced by substitution that

$$\mathrm{E}_1(pz) = \int_p^\infty \frac{\exp(-zt)}{t}\mathrm{d}t, \tag{B.1.12}$$

for $p > 0$. We then find

$$\begin{aligned} I_0(\alpha) &= \int_0^p \exp(-\alpha\kappa)\frac{\sin(c\kappa)}{\kappa}\mathrm{d}\kappa \\ &= \int_0^\infty \exp(-\alpha\kappa)\frac{\sin(c\kappa)}{\kappa}\mathrm{d}\kappa - \int_p^\infty \exp(-\alpha\kappa)\frac{\sin(c\kappa)}{\kappa}\mathrm{d}\kappa \\ &= \Theta_I - \Im[\mathrm{E}_1(\alpha p - \mathrm{i}cp)], \end{aligned} \tag{B.1.13}$$

where

$$\tan(\Theta_I) = \frac{c}{\alpha}. \tag{B.1.14}$$

We find also that

$$\begin{aligned} J_0(\alpha) &= \int_0^p \exp(-\alpha\kappa)\frac{\cos(c\kappa)}{\kappa}[1-\exp(-\gamma\kappa)]\,d\kappa \\ &= \int_0^\infty \exp(-\alpha\kappa)\frac{\cos(c\kappa)}{\kappa}[1-\exp(-\gamma\kappa)]\,d\kappa \\ &- \int_p^\infty \exp(-\alpha\kappa)\frac{\cos(c\kappa)}{\kappa}[1-\exp(-\gamma\kappa)]\,d\kappa \\ &= \Theta_J - \Re[E_1(\alpha p - icp) - E_1(\alpha p + \gamma p - icp)], \end{aligned} \tag{B.1.15}$$

where

$$\Theta_J = \frac{1}{2}\log\left(\frac{(\alpha+\gamma)^2+c^2}{\alpha^2+c^2}\right). \tag{B.1.16}$$

Finally, it remains to evaluate $E_1(z)$ for $\Re[z] > 0$. It can be shown that

$$E_1(z) = -\xi - \log(z) + \sum_{j=1}^{\infty}\frac{(-1)^{j+1}z^j}{j!j}, \tag{B.1.17}$$

where

$$\xi = \lim_{n\to\infty}\left[\left(\sum_{j=1}^{n}\frac{1}{j}\right) - \log(n)\right] = 0.57721566\ldots \tag{B.1.18}$$

is the Euler-Mascheroni constant. Accurate approximations to $E_1(z)$ can then be obtained by truncating the series in (B.1.17) at a suitably high value of j. The expansion (B.1.17) converges quickly for small $|z|$. For larger values of $|z|$, it is preferable to use the continued fraction definition of $E_1(z)$,

$$E_1(z) = \cfrac{\exp(-z)}{z + \cfrac{1}{1 + \cfrac{1}{z + \cfrac{2}{1 + \cfrac{2}{z + \cfrac{3}{1 + \cfrac{3}{z + \ldots}}}}}}} \tag{B.1.19}$$

and truncate the fraction at an appropriate point. In our calculations, we have found it practical to use (B.1.17) for $|z| < 10$ and (B.1.19) otherwise.

Appendix C

The Θ Function

C.1 Proof of (3.3.3)

We claim that, for any trial wavefunction of the form (1.7.3) or (1.8.14),

$$\det(A) \neq 0 \Rightarrow \det(A)\,\mathcal{I}[\Psi_t] = \Theta(k,\varkappa), \tag{3.3.3}$$

where A is the coefficient matrix of the Kohn equations, $\mathcal{I}[\Psi_t] = \langle \Psi_t, \Psi_t \rangle$ and the function, $\Theta(k,\varkappa)$, is independent of τ.

In the following proof, we will write $\Theta = \Theta(k,\tau)$ before explicitly proving the independence of Θ from τ. The proof will not be restricted to specific choices of the correlation functions, $\{\chi_i\}$, so it is sufficient to prove (3.3.3) for the trial wavefunction

$$\Psi_t = (\bar{S} + a_t \bar{C})\,\psi_G + \sum_{i=1}^{M} p_i \chi_i, \tag{C.1.1}$$

which is of the general form used in our Kohn calculations involving explicit

consideration of the target potential. A result of the same form as (3.3.3) then automatically follows for the trial wavefunctions used in our method of models calculations. Henceforth, it will be convenient to consider only the case $M \geq 3$ in (C.1.1). It is straightforward to show that the result (3.3.3) is satisfied for $M < 3$ by explicitly inverting the matrix, A, allowing $\mathcal{I}[\Psi_t]$ to be found. Throughout the proof, we will implicitly make use of the Hermiticity properties (1.7.26), (1.7.27) and (1.7.29).

Applying the Kohn variational principle to (C.1.1) leads to an equation of the form

$$Ax = -b, \tag{C.1.2}$$

where

$$A = \begin{bmatrix} \langle \bar{C}\psi_G, \bar{C}\psi_G \rangle & \langle \bar{C}\psi_G, \chi_1 \rangle & \cdots & \langle \bar{C}\psi_G, \chi_M \rangle \\ \langle \chi_1, \bar{C}\psi_G \rangle & \langle \chi_1, \chi_1 \rangle & \cdots & \langle \chi_1, \chi_M \rangle \\ \vdots & \vdots & \ddots & \vdots \\ \langle \chi_M, \bar{C}\psi_G \rangle & \langle \chi_M, \chi_1 \rangle & \cdots & \langle \chi_M, \chi_M \rangle \end{bmatrix}, \tag{C.1.3}$$

$$b = \begin{bmatrix} \langle \bar{C}\psi_G, \bar{S}\psi_G \rangle \\ \langle \chi_1, \bar{S}\psi_G \rangle \\ \vdots \\ \langle \chi_M, \bar{S}\psi_G \rangle \end{bmatrix}, \tag{C.1.4}$$

$$x = \begin{bmatrix} a_t \\ p_1 \\ \vdots \\ p_M \end{bmatrix}, \tag{C.1.5}$$

together with an equation for $\mathcal{I}[\Psi_t]$ analogous to (1.7.39),

$$\mathcal{I}[\Psi_t] = \langle \bar{S}\psi_G, \bar{S}\psi_G \rangle + a_t \langle \bar{S}\psi_G, \bar{C}\psi_G \rangle + \sum_{j=1}^{M} p_j \langle \bar{S}\psi_G, \chi_j \rangle. \tag{C.1.6}$$

We will denote by $\tilde{A}_{(j)}$ the $(M+1 \times M+1)$ matrix formed by replacing the j^{th} column of A by $-b$. We will denote by $A^{(i)}_{(j)}$ the $(M \times M)$ matrix formed by removing the i^{th} row and j^{th} column of A. The row and column indices of A range from 1 to $M+1$. By assumption, A is nonsingular, so that using (C.1.6) and Cramer's rule, which states that

$$a_t = \frac{\det\left(\tilde{A}_{(1)}\right)}{\det(A)} \tag{C.1.7}$$

and, for $1 < j \leq M$,

$$p_j = \frac{\det\left(\tilde{A}_{(j+1)}\right)}{\det(A)}, \tag{C.1.8}$$

the product, $\det(A)\,\mathcal{I}[\Psi_t]$, can be written

$$\begin{aligned} \Theta(k,\tau) &= \det(A)\,\mathcal{I}[\Psi_t] = \det(A)\,\langle \bar{S}\psi_G, \bar{S}\psi_G \rangle + \det\left(\tilde{A}_{(1)}\right)\langle \bar{S}\psi_G, \bar{C}\psi_G \rangle \\ &+ \sum_{j=1}^{M} \det\left(\tilde{A}_{(j+1)}\right)\langle \bar{S}\psi_G, \chi_j \rangle. \end{aligned} \tag{C.1.9}$$

The Laplace expansion of $\det(A)$ along column 1 of A is

$$\det(A) = \langle \bar{C}\psi_G, \bar{C}\psi_G \rangle \det\left(A^{(1)}_{(1)}\right) + \sum_{i=1}^{M} (-1)^i \langle \bar{C}\psi_G, \chi_i \rangle \det\left(A^{(i+1)}_{(1)}\right), \tag{C.1.10}$$

while the expansion of $\det\left(\tilde{A}_{(j)}\right)$ along column j of $\tilde{A}_{(j)}$ is

$$\det\left(\tilde{A}_{(j)}\right) = (-1)^j \left[\langle \bar{C}\psi_G, \bar{S}\psi_G\rangle \det\left(A^{(1)}_{(j)}\right) + \sum_{i=1}^{M} (-1)^i \langle \bar{S}\psi_G, \chi_i\rangle \det\left(A^{(i+1)}_{(j)}\right)\right]. \tag{C.1.11}$$

Now, it is straightforward to show using (1.7.4) that

$$\begin{aligned} \langle \bar{S}\psi_G, \bar{S}\psi_G\rangle\langle \bar{C}\psi_G, \bar{C}\psi_G\rangle &- \langle \bar{S}\psi_G, \bar{C}\psi_G\rangle\langle \bar{C}\psi_G, \bar{S}\psi_G\rangle \\ = \langle S\psi_G, S\psi_G\rangle\langle C\psi_G, C\psi_G\rangle &- \langle S\psi_G, C\psi_G\rangle\langle C\psi_G, S\psi_G\rangle, \end{aligned} \tag{C.1.12}$$

which is independent of τ. Hence, by noting that $\det\left(A^{(1)}_{(1)}\right)$ is also independent of τ, then defining

$$\begin{aligned} \Theta_0(k,\varkappa) &= [\langle S\psi_G, S\psi_G\rangle\langle C\psi_G, C\psi_G\rangle - \langle S\psi_G, C\psi_G\rangle\langle C\psi_G, S\psi_G\rangle] \\ &\times \det\left(A^{(1)}_{(1)}\right) \end{aligned} \tag{C.1.13}$$

and combining (C.1.9), (C.1.10), (C.1.11) and (C.1.12), we can write

$$\begin{aligned} \Theta(k,\tau) - \Theta_0(k,\varkappa) &= \langle \bar{S}\psi_G, \bar{S}\psi_G\rangle \sum_{i=1}^{M} (-1)^i \langle \bar{C}\psi_G, \chi_i\rangle \det\left(A^{(i+1)}_{(1)}\right) \\ &- \langle \bar{S}\psi_G, \bar{C}\psi_G\rangle \sum_{i=1}^{M} (-1)^i \langle \bar{S}\psi_G, \chi_i\rangle \det\left(A^{(i+1)}_{(1)}\right) \\ &+ \sum_{j=1}^{M} \langle \bar{S}\psi_G, \chi_j\rangle (-1)^{j+1} \left[\langle \bar{C}\psi_G, \bar{S}\psi_G\rangle \det\left(A^{(1)}_{(j+1)}\right)\right. \\ &+ \left.\sum_{i=1}^{M} (-1)^i \langle \bar{S}\psi_G, \chi_i\rangle \det\left(A^{(i+1)}_{(j+1)}\right)\right]. \end{aligned} \tag{C.1.14}$$

It then remains to be shown that the right hand side of (C.1.14) is independent of τ.

Using the fact that, for any square matrix, M, $\det(M) = \det(M^\top)$, together with the fact that A is symmetric, we can deduce that $\det\left(A^{(p)}_{(q)}\right) = \det\left(A^{(q)}_{(p)}\right)$. We can then rewrite (C.1.14) as

$$\begin{aligned}\Theta(k,\tau) - \Theta_0(k,\not{\tau}) &= \left(\sum_{i=1}^{M}(-1)^i \det\left(A^{(i+1)}_{(1)}\right)\times\right.\\ &\quad [\langle\bar{S}\psi_G,\bar{S}\psi_G\rangle\langle\bar{C}\psi_G,\chi_i\rangle -\\ &\quad \langle\bar{S}\psi_G,\bar{C}\psi_G\rangle\langle\bar{S}\psi_G,\chi_i\rangle -\\ &\quad \left.\langle\bar{C}\psi_G,\bar{S}\psi_G\rangle\langle\bar{S}\psi_G,\chi_i\rangle]\right)\\ &\quad + \sum_{i=1}^{M}\sum_{j=1}^{M}(-1)^{i+j+1}\det\left(A^{(i+1)}_{(j+1)}\right)\langle\bar{S}\psi_G,\chi_i\rangle\langle\bar{S}\psi_G,\chi_j\rangle.\end{aligned} \tag{C.1.15}$$

We next define the $(M\times M)$ matrix, $X = A^{(1)}_{(1)}$. Further, we denote by $X^{(i)}_{(j)}$ the $(M-1\times M-1)$ matrix formed by removing the i^{th} row and j^{th} column of X. Further, for $i\neq p$ and $j\neq q$, we denote by $X^{(i,p)}_{(j,q)}$ the $(M-2\times M-2)$ matrix formed by removing the i^{th} and p^{th} rows and j^{th} and q^{th} columns of X. The row and column indices of X range from 1 to M. The elements of X, $X^{(i)}_{(j)}$ and $X^{(i,p)}_{(j,q)}$ are independent of τ. If $i=p$ or $j=q$, we define $X^{(i,p)}_{(j,q)}$ to be the $(M-2\times M-2)$ matrix of zeros. It is easily seen that

$$\det\left(A^{(i+1)}_{(1)}\right) = \sum_{j=1}^{M}(-1)^{j+1}\det\left(X^{(i)}_{(j)}\right)\langle\bar{C}\psi_G,\chi_j\rangle. \tag{C.1.16}$$

Moreover, after careful consideration we have

$$\begin{aligned}\det\left(A^{(i+1)}_{(j+1)}\right) &= \det\left(X^{(i)}_{(j)}\right)\langle\bar{C}\psi_{\mathrm{G}},\bar{C}\psi_{\mathrm{G}}\rangle \\ &+ \left(\sum_{p=1}^{M}\sum_{q=1}^{M}(-1)^{p+q+1+\sigma_{ip}+\sigma_{jq}}\right. \\ &\times \left.\det\left(X^{(i,p)}_{(j,q)}\right)\langle\bar{C}\psi_{\mathrm{G}},\chi_p\rangle\langle\bar{C}\psi_{\mathrm{G}},\chi_q\rangle\right), \end{aligned} \tag{C.1.17}$$

where terms of the form σ_{ab} have the definition

$$\sigma_{ab} = \begin{cases} 0 & (a \geq b) \\ 1 & (a < b) \end{cases}. \tag{C.1.18}$$

Using (C.1.16) and (C.1.17), we rewrite (C.1.15) as

$$\Theta(k,\tau) = \Theta_0(k,\varkappa) + \Theta_1(k,\tau) + \Theta_2(k,\tau), \tag{C.1.19}$$

where

$$\begin{aligned}\Theta_1(k,\tau) = \sum_{i=1}^{M}\sum_{j=1}^{M}(-1)^{i+j+1}\det\left(X^{(i)}_{(j)}\right) &\times \left(\langle\bar{S}\psi_{\mathrm{G}},\bar{S}\psi_{\mathrm{G}}\rangle\langle\bar{C}\psi_{\mathrm{G}},\chi_i\rangle\langle\bar{C}\psi_{\mathrm{G}},\chi_j\rangle\right. \\ &- \langle\bar{S}\psi_{\mathrm{G}},\bar{C}\psi_{\mathrm{G}}\rangle\langle\bar{S}\psi_{\mathrm{G}},\chi_i\rangle\langle\bar{C}\psi_{\mathrm{G}},\chi_j\rangle \\ &- \langle\bar{C}\psi_{\mathrm{G}},\bar{S}\psi_{\mathrm{G}}\rangle\langle\bar{S}\psi_{\mathrm{G}},\chi_i\rangle\langle\bar{C}\psi_{\mathrm{G}},\chi_j\rangle \\ &+ \left.\langle\bar{C}\psi_{\mathrm{G}},\bar{C}\psi_{\mathrm{G}}\rangle\langle\bar{S}\psi_{\mathrm{G}},\chi_i\rangle\langle\bar{S}\psi_{\mathrm{G}},\chi_j\rangle\right)\end{aligned} \tag{C.1.20}$$

and

$$\Theta_2(k,\tau) = \sum_{i=1}^{M}\sum_{j=1}^{M}\sum_{p=1}^{M}\sum_{q=1}^{M}\Bigg((-1)^{i+j+p+q+\sigma_{ip}+\sigma_{jq}}\det\left(X^{(i,p)}_{(j,q)}\right)\times \\ \langle\bar{S}\psi_G,\chi_i\rangle\langle\bar{S}\psi_G,\chi_j\rangle\langle\bar{C}\psi_G,\chi_p\rangle\langle\bar{C}\psi_G,\chi_q\rangle\Bigg). \quad \text{(C.1.21)}$$

We will now show that $\Theta_1(k,\tau)$ and $\Theta_2(k,\tau)$ are each independent of τ.

Considering (C.1.20), since X is symmetric, we note that $\det\left(X^{(i)}_{(j)}\right) = \det\left(X^{(j)}_{(i)}\right)$. Using (1.7.4), when the summation over i and j in (C.1.20) is carried out, a number of terms cancel. After some elementary algebra, we find

$$\begin{aligned}\Theta_1(k,\mathscr{T}) = \sum_{i=1}^{M}\sum_{j=1}^{M}(-1)^{i+j+1}\det\left(X^{(i)}_{(j)}\right) \times \Big(&\langle S\psi_G,S\psi_G\rangle\langle C\psi_G,\chi_i\rangle\langle C\psi_G,\chi_j\rangle \\ &- \langle S\psi_G,C\psi_G\rangle\langle S\psi_G,\chi_i\rangle\langle C\psi_G,\chi_j\rangle \\ &- \langle C\psi_G,S\psi_G\rangle\langle S\psi_G,\chi_i\rangle\langle C\psi_G,\chi_j\rangle \\ &+ \langle C\psi_G,C\psi_G\rangle\langle S\psi_G,\chi_i\rangle\langle S\psi_G,\chi_j\rangle\Big),\end{aligned} \quad \text{(C.1.22)}$$

which is independent of τ. Applying the same method to (C.1.21), with a little work we can write

$$\Theta_2(k,\mathscr{T}) = \sum_{i=1}^{M}\sum_{j=1}^{M}\sum_{p=1}^{M}\sum_{q=1}^{M}\Bigg((-1)^{i+j+p+q+\sigma_{ip}+\sigma_{jq}}\det\left(X^{(i,p)}_{(j,q)}\right)\times \\ \langle S\psi_G,\chi_i\rangle\langle S\psi_G,\chi_j\rangle\langle C\psi_G,\chi_p\rangle\langle C\psi_G,\chi_q\rangle\Bigg), \quad \text{(C.1.23)}$$

which is independent of τ. The cancellation in the summation (C.1.21) arises from the fact that

$$(-1)^{\sigma_{ab}} + (-1)^{\sigma_{ba}} = 0 \qquad (a \neq b)\,. \tag{C.1.24}$$

Finally, combining (C.1.19), (C.1.22) and (C.1.23), we have

$$\Theta\left(k,\mathcal{X}\right) = \Theta_0\left(k,\mathcal{X}\right) + \Theta_1\left(k,\mathcal{X}\right) + \Theta_2\left(k,\mathcal{X}\right), \tag{C.1.25}$$

so that $\Theta = \Theta\left(k,\mathcal{X}\right)$, as required. □

C.2 Extension to the complex Kohn method

In the case of the complex Kohn method, a result similar to (3.3.3) can be derived by a method analogous to that given in the previous section. In fact, we claim

$$\det\left(A'\right) \neq 0 \Rightarrow \det\left(A'\right)\mathcal{I}'\left[\breve{\Psi}_t\right] = -\Theta\left(k,\mathcal{X}\right), \tag{5.4.10}$$

where $\Theta\left(k,\mathcal{X}\right)$ is as in (3.3.3), A' is the coefficient matrix of the complex Kohn equations and $\mathcal{I}'\left[\breve{\Psi}_t\right]$ is as in (5.2.9).

To prove (5.4.10), it is sufficient to consider a trial wavefunction having the same general form as (C.1.1), but for the fact that $\bar{C}$ is replaced by $\bar{T}$ (5.2.2), viz.

$$\breve{\Psi}_t = \left(\bar{S} + a_t'\bar{T}\right)\psi_G + \sum_{i=1}^{M} p_i'\chi_i. \tag{C.2.1}$$

Under these circumstances, the following expression

$$\mathcal{I}'\left[\breve{\Psi}_t\right] = \langle\bar{S}\psi_G, \bar{S}\psi_G\rangle + a_t\langle\bar{S}\psi_G, \bar{T}\psi_G\rangle + \sum_{j=1}^{M} p_j\langle\bar{S}\psi_G, \chi_j\rangle, \tag{C.2.2}$$

is analogous to (5.2.15).

For nonsingular A', we define a function, $\Lambda(k,\tau)$, such that

$$\Lambda(k,\tau) = \det\left(A'\right)\mathcal{I}'\left[\breve{\Psi}_t\right]. \tag{C.2.3}$$

Next, after some manipulation, it is straightforward to show that

$$\begin{aligned}
&\langle\bar{S}\psi_G, \bar{S}\psi_G\rangle\langle\bar{T}^*\psi_G, \bar{T}\psi_G\rangle \quad - \quad \langle\bar{S}\psi_G, \bar{T}\psi_G\rangle\langle\bar{T}^*\psi_G, \bar{S}\psi_G\rangle \\
&= \langle\bar{S}\psi_G, \bar{C}\psi_G\rangle\langle\bar{C}\psi_G, \bar{S}\psi_G\rangle \quad - \quad \langle\bar{S}\psi_G, \bar{S}\psi_G\rangle\langle\bar{C}\psi_G, \bar{C}\psi_G\rangle \\
&= \langle S\psi_G, C\psi_G\rangle\langle C\psi_G, S\psi_G\rangle \quad - \quad \langle S\psi_G, S\psi_G\rangle\langle C\psi_G, C\psi_G\rangle,
\end{aligned} \tag{C.2.4}$$

where we have used (C.1.12). Proceeding in a manner analogous to the previous section and adopting the same notation, using (C.1.13) it is clear that we can then immediately write

$$\Lambda(k,\tau) = -\Theta_0(k,\not{\tau}) + \Lambda_1(k,\tau) + \Lambda_2(k,\tau), \tag{C.2.5}$$

where

$$\Lambda_1(k,\tau) = \sum_{i=1}^{M}\sum_{j=1}^{M}(-1)^{i+j+1}\det\left(X^{(i)}_{(j)}\right) \times \Big(\langle\bar{S}\psi_G,\bar{S}\psi_G\rangle\langle\bar{T}^*\psi_G,\chi_i\rangle\langle\bar{T}^*\psi_G,\chi_j\rangle - \langle\bar{S}\psi_G,\bar{T}\psi_G\rangle\langle\bar{S}\psi_G,\chi_i\rangle\langle\bar{T}^*\psi_G,\chi_j\rangle - \langle\bar{T}^*\psi_G,\bar{S}\psi_G\rangle\langle\bar{S}\psi_G,\chi_i\rangle\langle\bar{T}^*\psi_G,\chi_j\rangle + \langle\bar{T}^*\psi_G,\bar{T}\psi_G\rangle\langle\bar{S}\psi_G,\chi_i\rangle\langle\bar{S}\psi_G,\chi_j\rangle\Big) \tag{C.2.6}$$

and

$$\Lambda_2(k,\tau) = \sum_{i=1}^{M}\sum_{j=1}^{M}\sum_{p=1}^{M}\sum_{q=1}^{M}\Big((-1)^{i+j+p+q+\sigma_{ip}+\sigma_{jq}}\det\left(X^{(i,p)}_{(j,q)}\right)\times \langle\bar{S}\psi_G,\chi_i\rangle\langle\bar{S}\psi_G,\chi_j\rangle\langle\bar{T}^*\psi_G,\chi_p\rangle\langle\bar{T}^*\psi_G,\chi_q\rangle\Big), \tag{C.2.7}$$

$\Lambda_1(k,\tau)$ and $\Lambda_2(k,\tau)$ being analogous to (C.1.20) and (C.1.21), respectively.

Considering first $\Lambda_1(k,\tau)$, it is easily shown that

$$\begin{aligned}
&\langle\bar{S}\psi_G,\bar{S}\psi_G\rangle\langle\bar{T}^*\psi_G,\chi_i\rangle\langle\bar{T}^*\psi_G,\chi_j\rangle - \langle\bar{S}\psi_G,\bar{T}\psi_G\rangle\langle\bar{S}\psi_G,\chi_i\rangle\langle\bar{T}^*\psi_G,\chi_j\rangle\\
-\ &\langle\bar{T}^*\psi_G,\bar{S}\psi_G\rangle\langle\bar{S}\psi_G,\chi_i\rangle\langle\bar{T}^*\psi_G,\chi_j\rangle + \langle\bar{T}^*\psi_G,\bar{T}\psi_G\rangle\langle\bar{S}\psi_G,\chi_i\rangle\langle\bar{S}\psi_G,\chi_j\rangle\\
=\ &\langle\bar{S}\psi_G,\bar{C}\psi_G\rangle\langle\bar{S}\psi_G,\chi_i\rangle\langle\bar{C}\psi_G,\chi_j\rangle - \langle\bar{S}\psi_G,\bar{S}\psi_G\rangle\langle\bar{C}\psi_G,\chi_i\rangle\langle\bar{C}\psi_G,\chi_j\rangle\\
-\ &\langle\bar{C}\psi_G,\bar{C}\psi_G\rangle\langle\bar{S}\psi_G,\chi_i\rangle\langle\bar{S}\psi_G,\chi_j\rangle + \langle\bar{C}\psi_G,\bar{S}\psi_G\rangle\langle\bar{S}\psi_G,\chi_i\rangle\langle\bar{C}\psi_G,\chi_j\rangle\\
+\ &\mathrm{i}\langle\bar{S}\psi_G,\bar{S}\psi_G\rangle\left[\langle\bar{C}\psi_G,\chi_i\rangle\langle\bar{S}\psi_G,\chi_j\rangle - \langle\bar{S}\psi_G,\chi_i\rangle\langle\bar{C}\psi_G,\chi_j\rangle\right].
\end{aligned} \tag{C.2.8}$$

When the summation in (C.2.6) is carried out, it is clear that the final terms in the square brackets in (C.2.8) sum to zero. Using (C.1.20) and (C.1.22), we then have

$$\begin{aligned}\Lambda_1(k,\varkappa) = -\sum_{i=1}^{M}\sum_{j=1}^{M}(-1)^{i+j+1}\det\left(X^{(i)}_{(j)}\right) \times \Big(&\langle S\psi_G, S\psi_G\rangle\langle C\psi_G,\chi_i\rangle\langle C\psi_G,\chi_j\rangle \\ &- \langle S\psi_G, C\psi_G\rangle\langle S\psi_G,\chi_i\rangle\langle C\psi_G,\chi_j\rangle \\ &- \langle C\psi_G, S\psi_G\rangle\langle S\psi_G,\chi_i\rangle\langle C\psi_G,\chi_j\rangle \\ &+ \langle C\psi_G, C\psi_G\rangle\langle S\psi_G,\chi_i\rangle\langle S\psi_G,\chi_j\rangle\Big),\end{aligned} \tag{C.2.9}$$

so that

$$\Lambda_1(k,\varkappa) = -\Theta_1(k,\varkappa). \tag{C.2.10}$$

Next, we consider $\Lambda_2(k,\tau)$. Clearly,

$$\begin{aligned}&\langle\bar{S}\psi_G,\chi_i\rangle\langle\bar{S}\psi_G,\chi_j\rangle\langle\bar{T}^*\psi_G,\chi_p\rangle\langle\bar{T}^*\psi_G,\chi_q\rangle \\ = \;&\langle\bar{S}\psi_G,\chi_i\rangle\langle\bar{S}\psi_G,\chi_j\rangle\langle\bar{S}\psi_G,\chi_p\rangle\langle\bar{S}\psi_G,\chi_q\rangle \\ - \;&\langle\bar{S}\psi_G,\chi_i\rangle\langle\bar{S}\psi_G,\chi_j\rangle\langle\bar{C}\psi_G,\chi_p\rangle\langle\bar{C}\psi_G,\chi_q\rangle \\ + \;&\mathrm{i}\langle\bar{S}\psi_G,\chi_i\rangle\langle\bar{S}\psi_G,\chi_j\rangle\langle\bar{S}\psi_G,\chi_p\rangle\langle\bar{C}\psi_G,\chi_q\rangle \\ + \;&\mathrm{i}\langle\bar{S}\psi_G,\chi_i\rangle\langle\bar{S}\psi_G,\chi_j\rangle\langle\bar{C}\psi_G,\chi_p\rangle\langle\bar{S}\psi_G,\chi_q\rangle.\end{aligned} \tag{C.2.11}$$

Using (C.1.24), we see that the first term in the expansion (C.2.11) does not give an overall contribution to the sum (C.2.7). For the same reason, each of the final two terms in (C.2.11) also sums to zero in (C.2.7). Hence, using (C.1.21) and (C.1.23), we then have

$$\Lambda_2(k,\varkappa) = -\sum_{i=1}^{M}\sum_{j=1}^{M}\sum_{p=1}^{M}\sum_{q=1}^{M}\Bigg((-1)^{i+j+p+q+\sigma_{ip}+\sigma_{jq}}\det\left(X_{(j,q)}^{(i,p)}\right)\times \\ \langle S\psi_G,\chi_i\rangle\langle S\psi_G,\chi_j\rangle\langle C\psi_G,\chi_p\rangle\langle C\psi_G,\chi_q\rangle\Bigg), \quad \text{(C.2.12)}$$

so that

$$\Lambda_2(k,\varkappa) = -\Theta_2(k,\varkappa) \quad \text{(C.2.13)}$$

and, finally

$$\Lambda(k,\varkappa) = \det(A')\,\mathcal{I}'\left[\breve{\Psi}_t\right] = -\Theta(k,\varkappa), \quad \text{(C.2.14)}$$

as required. □

Thus, a relationship analogous to (3.3.3) holds in the complex Kohn method for any trial function of the form (C.2.1).

Appendix D

The $\mathcal{G}$ Function

D.1 Proof of (4.4.26)

For $\Gamma(k)$ and $\mathcal{G}(k)$ as defined in (4.4.15) and (4.4.24) respectively, we claim that

$$\mathcal{G}(k) = \Gamma^2(k). \tag{4.4.26}$$

To prove (4.4.26), inspection of (4.4.24) shows that it is sufficient to prove

$$\mathcal{H} = 0, \tag{D.1.1}$$

where we have defined

$$\mathcal{H} = \left[\tilde{\mathcal{A}}(k) + \mathcal{B}(k)\right]\tilde{\mathcal{A}}(k) + \mathcal{A}(k)\mathcal{C}(k) - \left[2\tilde{\mathcal{A}}(k) + \mathcal{B}(k)\right]\Gamma(k). \tag{D.1.2}$$

APPENDIX D: THE $\mathcal{G}$ FUNCTION

As in appendix C, since the following proof will not be restricted to specific choices of the correlation functions in the Kohn trial function, without loss of generality it is sufficient to prove (D.1.1) for the wavefunction (C.1.1). This trial function is of the general form used in our Kohn calculations involving explicit consideration of the target potential. A result of the same form as (D.1.1) then automatically follows for the trial wavefunctions used in our method of models calculations. Henceforth, it will be convenient to consider only the case $M \geq 3$ in (C.1.1). It is straightforward to show that the result (D.1.1) is satisfied for $M < 3$ by explicitly evaluating expressions for $\tilde{\mathcal{A}}(k)$, $\mathcal{A}(k)$, $\mathcal{B}(k)$, $\mathcal{C}(k)$ and $\Gamma(k)$. Throughout the proof, we will implicitly make use of the Hermiticity properties (1.7.26), (1.7.27) and (1.7.29).

In the case of the trial function (C.1.1), expressions for $\tilde{\mathcal{A}}(k)$ and $\left[\tilde{\mathcal{A}}(k) + \mathcal{B}(k)\right]$ are obtained from (4.4.6) and (4.4.7) by setting $\chi_0 = 0$. This is done only for brevity and does not affect the generality of the proof. We then have

$$\tilde{\mathcal{A}}(k) = \mathcal{P}(k) \langle S\psi_G, C\psi_G \rangle + \sum_{i=1}^{M} \sum_{j=1}^{M} \mathcal{S}_{ij}(k) \langle S\psi_G, \chi_i \rangle \langle C\psi_G, \chi_j \rangle \tag{D.1.3}$$

and

$$\tilde{\mathcal{A}}(k) + \mathcal{B}(k) = -\mathcal{P}(k) \langle C\psi_G, S\psi_G \rangle - \sum_{i=1}^{M} \sum_{j=1}^{M} \mathcal{S}_{ij}(k) \langle C\psi_G, \chi_i \rangle \langle S\psi_G, \chi_j \rangle. \tag{D.1.4}$$

By the same method, from (4.4.3) and (4.4.5) we obtain

$$\begin{aligned}\mathcal{A}(k)\,\mathcal{C}(k) &= \mathcal{P}^2(k)\,\langle S\psi_G, S\psi_G\rangle\langle C\psi_G, C\psi_G\rangle \\ &+ \mathcal{P}(k)\,\langle S\psi_G, S\psi_G\rangle \sum_{i=1}^{M}\sum_{j=1}^{M}\mathcal{S}_{ij}(k)\,\langle C\psi_G, \chi_i\rangle\langle C\psi_G, \chi_j\rangle \\ &+ \mathcal{P}(k)\,\langle C\psi_G, C\psi_G\rangle \sum_{i=1}^{M}\sum_{j=1}^{M}\mathcal{S}_{ij}(k)\,\langle S\psi_G, \chi_i\rangle\langle S\psi_G, \chi_j\rangle \\ &+ \sum_{i=1}^{M}\sum_{j=1}^{M}\sum_{p=1}^{M}\sum_{q=1}^{M}\mathcal{S}_{ij}(k)\,\mathcal{S}_{pq}(k)\,\langle S\psi_G, \chi_i\rangle\langle S\psi_G, \chi_j\rangle\langle C\psi_G, \chi_p\rangle\langle C\psi_G, \chi_q\rangle.\end{aligned} \tag{D.1.5}$$

Next, in the nomenclature of appendix C, we note that

$$\mathcal{P}(k) = \det\left(A^{(1)}_{(1)}\right) = \det(X) \tag{D.1.6}$$

and

$$\mathcal{S}_{ij}(k) = \mathcal{S}_{ji}(k) = (-1)^{i+j+1}\det\left(X^{(i)}_{(j)}\right) = (-1)^{i+j+1}\det\left(X^{(j)}_{(i)}\right). \tag{D.1.7}$$

Combining (D.1.3), (D.1.4) and (D.1.5), as well as using (C.1.13), (C.1.22), (D.1.6) and (D.1.7), after a little work we can write

$$\begin{aligned}&\left[\tilde{\mathcal{A}}(k) + \mathcal{B}(k)\right]\tilde{\mathcal{A}}(k) + \mathcal{A}(k)\,\mathcal{C}(k) = \mathcal{P}(k)\left[\Theta_0(k) + \Theta_1(k)\right] \\ &+ \sum_{i=1}^{M}\sum_{j=1}^{M}\sum_{p=1}^{M}\sum_{q=1}^{M}\mathcal{S}_{ij}(k)\,\mathcal{S}_{pq}(k)\,\langle S\psi_G, \chi_i\rangle\langle S\psi_G, \chi_j\rangle\langle C\psi_G, \chi_p\rangle\langle C\psi_G, \chi_q\rangle \\ &- \sum_{i=1}^{M}\sum_{j=1}^{M}\sum_{p=1}^{M}\sum_{q=1}^{M}\mathcal{S}_{ij}(k)\,\mathcal{S}_{pq}(k)\,\langle S\psi_G, \chi_i\rangle\langle C\psi_G, \chi_j\rangle\langle C\psi_G, \chi_p\rangle\langle S\psi_G, \chi_q\rangle.\end{aligned} \tag{D.1.8}$$

Next, summing (D.1.3) and (D.1.4), we find

$$2\tilde{\mathcal{A}}\left(k\right)+\mathcal{B}\left(k\right)=\mathcal{P}\left(k\right)\tilde{k}, \tag{D.1.9}$$

where we have used (1.7.22), together with the fact that $\mathcal{S}_{ij}\left(k\right)=\mathcal{S}_{ji}\left(k\right)$. Recalling (4.4.15), it is clear that

$$\left[2\tilde{\mathcal{A}}\left(k\right)+\mathcal{B}\left(k\right)\right]\Gamma\left(k\right)=\mathcal{P}\left(k\right)\Theta\left(k\right). \tag{D.1.10}$$

Using (C.1.23), (C.1.25), (D.1.8) and (D.1.10), after some cancellation we can then rewrite (D.1.2) as

$$\mathcal{H}=\sum_{i=1}^{M}\sum_{j=1}^{M}\sum_{p=1}^{M}\sum_{q=1}^{M}\mathcal{T}\left(-1\right)^{i+j+p+q}\left\langle S\psi_{\mathrm{G}},\chi_{i}\right\rangle\left\langle S\psi_{\mathrm{G}},\chi_{j}\right\rangle\left\langle C\psi_{\mathrm{G}},\chi_{p}\right\rangle\left\langle C\psi_{\mathrm{G}},\chi_{q}\right\rangle, \tag{D.1.11}$$

where, using (D.1.6) and (D.1.7), we have defined

$$\begin{aligned}\mathcal{T} &= \det\left(X_{(j)}^{(i)}\right)\det\left(X_{(q)}^{(p)}\right)\\ &- \det\left(X_{(j)}^{(p)}\right)\det\left(X_{(q)}^{(i)}\right)\\ &- \left(-1\right)^{\sigma_{ip}+\sigma_{jq}}\det\left(X\right)\det\left(X_{(j,q)}^{(i,p)}\right).\end{aligned} \tag{D.1.12}$$

If $i=p$ or $j=q$, it follows trivially from the definition of $X_{(j,q)}^{(i,p)}$ given in appendix C that $\mathcal{T}=0$. When $i<p$ and $j<q$, we make use of the following result,

$$\det(X)\det\left(X^{(i,p)}_{(j,q)}\right) = \det\left(X^{(i)}_{(j)}\right)\det\left(X^{(p)}_{(q)}\right) - \det\left(X^{(p)}_{(j)}\right)\det\left(X^{(i)}_{(q)}\right). \tag{D.1.13}$$

Commonly known as the Lewis Carroll identity after its role in Dodgson condensation [98], Fomin and Zelevinsky [99] point out that (D.1.13) was, in fact, proved earlier by Desnanot (see, for example, [100]). It is easily seen to generalise to any $i \neq p$ and $j \neq q$ by multiplying the left hand side of (D.1.13) by a factor of $(-1)^{\sigma_{ip}+\sigma_{jq}}$. Hence, from inspection of (D.1.12) we see that $\mathcal{T}$ is identically zero and, since

$$\mathcal{T} = 0 \Rightarrow \mathcal{H} = 0 \Rightarrow \mathcal{G}(k) = \Gamma^2(k), \tag{D.1.14}$$

the required result (4.4.26) follows. □

References

[1] P. A. M. Dirac, Proc. R. Soc. Lond. A **117**, 610 (1928).

[2] P. A. M. Dirac, Proc. R. Soc. Lond. A **126**, 360 (1930).

[3] P. A. M. Dirac, Proc. Camb. Phil. Soc. **26**, 361 (1930).

[4] C. D. Anderson, Phys. Rev. **43**, 491 (1933).

[5] C. M. Surko, G. F. Gribakin, and S. J. Buckman, J. Phys. B: At. Mol. Opt. Phys. **38**, R57 (2005).

[6] M. Charlton and J. W. Humberston, *Positron Physics* (Cambridge University Press, 2005).

[7] E. Klempt, F. Bradamante, A. Martin, and J.-M. Richard, Phys. Rep. **368**, 119 (2002).

[8] G. Baur et al., Phys. Lett. B **368**, 251 (1996).

[9] M Amoretti et al., Nature **419**, 456 (2002).

[10] E. A. G. Armour, Phys. Rep. **169**, 1 (1988).

[11] E. A. G. Armour and J. W. Humberston, Phys. Rep. **204**, 165 (1991).

[12] H. M. James and A. S. Coolidge, J. Chem. Phys. **1**, 825 (1933).

[13] W. Kohn, Phys. Rev. **74**, 1763 (1948).

[14] C. Schwartz, Ann. Phys., Lpz. **16**, 36 (1961).

[15] R. L. Armstead, Phys. Rev. **171**, 91 (1968).

[16] A. K. Bhatia, A. Temkin, R. J. Drachman, and H. Eiserike, Phys. Rev. A **3**, 1328 (1971).

[17] J. W. Humberston and J. B. G. Wallace, J. Phys. B: At. Mol. Phys. **5**, 1138 (1972).

[18] A. K. Bhatia, A. Temkin, and H. Eiserike, Phys. Rev. A **9**, 219 (1974).

[19] P. Van Reeth and J. W. Humberston, J. Phys. B: At. Mol. Opt. Phys. **28**, L511 (1995).

[20] P. Van Reeth, J. W. Humberston, K. Iwata, R. G. Greaves, and C. M. Surko, J. Phys. B: At. Mol. Opt. Phys. **29**, L465 (1996).

[21] L. Hulthén, K. Fysiogr. Sällsk. Lund **14**, 257 (1944).

[22] H. S. W. Massey and R. O. Ridley, Proc. Phys. Soc. A **69**, 659 (1956).

[23] E. A. G. Armour, J. Phys. B: At. Mol. Phys. **17**, L375 (1984).

[24] R. J. Drachman, J. Phys. B: At. Mol. Phys. **5**, L30 (1972).

[25] G. Laricchia, M. Charlton, C. D. Beling, and T. C. Griffith, J. Phys. B: At. Mol. Phys. **20**, 1865 (1987).

[26] E. A. G. Armour, J. Phys. B: At. Mol. Phys. **18**, 3361 (1985).

[27] E. A. G. Armour and D. J. Baker, J. Phys. B: At. Mol. Phys. **18**, L845 (1985).

[28] E. A. G. Armour and D. J. Baker, J. Phys. B: At. Mol. Phys. **20**, 6105 (1987).

[29] E. A. G. Armour, D. J. Baker, and M. Plummer, J. Phys. B: At. Mol. Opt. Phys. **23**, 3057 (1990).

[30] E. P. Wigner, Phys. Rev. **70**, 606 (1946).

[31] P. G. Burke, I. Mackey, and I. Shimamura, J. Phys. B: At. Mol. Phys. **10**, 2497 (1977).

[32] J. Tennyson, J. Phys. B: At. Mol. Phys. **19**, 4255 (1986).

[33] G. Danby and J. Tennyson, J. Phys. B: At. Mol. Opt. Phys. **23**, 1005 (1990).

[34] T. L. Gibson, J. Phys. B: At. Mol. Opt. Phys. **23**, 767 (1990).

[35] T. L. Gibson, J. Phys. B: At. Mol. Opt. Phys. **25**, 1321 (1992).

[36] J. L. S. Lino, J. S. E. Germano, E. P. da Silva, and M. A. P. Lima, Phys. Rev. A **58**, 3502 (1998).

[37] M. T. do N Varella, C. R. C. de Carvalho, and M. A. P. Lima, Nucl. Instr. and Meth. B **192**, 225 (2002).

[38] J. Schwinger, Phys. Rev. **72**, 742 (1947).

[39] J. Franz and F. A. Gianturco, Nucl. Instr. and Meth. B **247**, 20 (2006).

[40] R. K. Nesbet, Phys. Rev. **175**, 134 (1968).

[41] K. R. Brownstein and W. A. McKinley, Phys. Rev. **170**, 1255 (1968).

[42] I. Shimamura, J. Phys. Soc. Japan **31**, 852 (1971).

[43] K. Takatsuka and T. Fueno, Phys. Rev. A **19**, 1011 (1979).

[44] C. W. McCurdy, T. N. Rescigno, and B. I. Schneider, Phys. Rev. A **36**, 2061 (1987).

[45] B. I. Schneider and T. N. Rescigno, Phys. Rev. A **37**, 3749 (1988).

[46] R. R. Lucchese, Phys. Rev. A **40**, 6879 (1989).

[47] C. Schwartz, Phys. Rev. **124**, 1468 (1961).

[48] D. M. Chase, Phys. Rev. **104**, 838 (1956).

[49] E. S. Chang and A. Temkin, Phys. Rev. Lett. **23**, 399 (1969).

[50] F. H. M. Faisal and A. Temkin, Phys. Rev. Lett. **28**, 203 (1972).

[51] M. Shugard and A. U. Hazi, Phys. Rev. A **12**, 1895 (1975).

[52] M. Born and R. Oppenheimer, Ann. Phys., Lpz. **84**, 457 (1927).

[53] A. Temkin and K. V. Vasadava, Phys. Rev. **160**, 109 (1967).

[54] A. Temkin, K. V. Vasadava, E. S. Chang, and A. Silver, Phys. Rev. **186**, 57 (1969).

[55] N. F. Lane, Rev. Mod. Phys. **52**, 29 (1980).

[56] L. P. Eisenhart, Phys. Rev. **74**, 87 (1948).

[57] B. H. Bransden and C. J. Joachain, *Physics of Atoms and Molecules* (Prentice Hall, 2003).

[58] C. Flammer, *Spheroidal Wave Functions* (Stanford University Press, 1957).

[59] M. Abramowitz and I. A. Stegun, *Handbook of Mathematical Functions with Formulas, Graphs, and Mathematical Tables* (Dover, 1964).

[60] E. A. Hylleraas, Z. Physik **54**, 347 (1929).

[61] F. Jensen, J. Chem. Phys. **110**, 6601 (1999).

[62] L. Wolniewicz, J. Chem. Phys. **103**, 1792 (1995).

[63] Y. N. Demkov, *Variational Principles in the Theory of Collisions* (Pergamon Press, 1963).

[64] N. F. Mott and H. S. W. Massey, *The Theory of Atomic Collisions* (Oxford University Press, 1965).

[65] E. A. G. Armour and D. J. Baker, J. Phys. B: At. Mol. Phys. **19**, L871 (1986).

[66] T. Kato, Prog. Theor. Phys. **6**, 394 (1951).

[67] P. G. Burke, *Potential Scattering in Atomic Physics* (Plenum, 1977).

[68] S. I. Rubinow, Phys. Rev. **98**, 183 (1955).

[69] E. A. G. Armour, A. C. Todd, S. Jonsell, Y. Liu, M. R. Gregory, and M. Plummer, Nucl. Instr. and Meth. B **266**, 363 (2008).

[70] A. C. Todd, Ph.D. thesis, University of Nottingham (2007).

[71] M. Plummer, E. A. G. Armour, A. C. Todd, C. P. Franklin, and J. N. Cooper, Comp. Phys. Comm. **180**, 2410 (2009).

[72] C. P. Franklin, Ph.D. thesis, University of Nottingham (1995).

[73] S. F. Boys and P. Rajagopal, Adv. Quantum Chem. **2**, 1 (1965).

[74] N. C. Handy and S. F. Boys, Theor. Chim. Acta **31**, 195 (1973).

[75] D. C. Clary, Molec. Phys. **34**, 793 (1977).

[76] K. R. Hoffman, M. S. Dababneh, Y.-F. Hsieh, W. E. Kauppila, V. Pol, J. H. Smart, and T. S. Stein, Phys. Rev. A **25**, 1393 (1982).

[77] M. Charlton, T. C. Griffith, G. R. Heyland, and G. L. Wright, J. Phys. B: At. Mol. Phys. **16**, 323 (1983).

[78] R. K. Nesbet, *Variational Methods in Electron-Atom Scattering Theory* (Plenum, 1980).

[79] M. Plummer, *private correspondence* (2009).

[80] J. N. Cooper, E. A. G. Armour, and M. Plummer, J. Phys. A: Math. Theor. **42**, 095207 (2009).

[81] C. W. Chamberlain, Ph.D. thesis, University of Nottingham (2002).

[82] A. Ore and J. L. Powell, Phys. Rev. **75**, 1696 (1949).

[83] http://www.codata.org.

[84] T. Kato, Commun. Pure Appl. Math **10**, 151 (1957).

[85] E. A. G. Armour, *Explicitly Correlated Wavefunctions* (CCP2 Workshop Proceedings), 19 (2006).

[86] L. Spruch and L. Rosenberg, Phys. Rev. **116**, 1034 (1959).

[87] J. N. Cooper, E. A. G. Armour, and M. Plummer, J. Phys. B: At. Mol. Opt. Phys. **41**, 245201 (2008).

[88] P. Van Reeth and J. W. Humberston, J. Phys. B: At. Mol. Opt. Phys. **28**, L23 (1995).

[89] http://www.stfc.ac.uk/about/struc/locs/dl/facs.aspx.

[90] M. Plummer, *private correspondence* (2008).

[91] P. M. Morse, Phys. Rev. **34**, 57 (1929).

[92] M. Born and V. Fock, Z. Physik **51**, 165 (1928).

[93] G. Chen, Phys. Lett. A **326**, 55 (2004).

[94] http://arxiv.org/abs/physics/0206036v1.

[95] H. Feshbach, Ann. Phys., NY **5**, 357 (1958).

[96] G. F. Gribakin and C. M. R. Lee, Phys. Rev. Lett. **97**, 193201 (2006).

[97] E. A. G. Armour, *private correspondence* (2009).

[98] C. L. Dodgson, Proc. R. Soc. Lond. **15**, 150 (1866).

[99] S. Fomin and A. Zelevinsky, Math. Intelligencer **22**, 23 (2000).

[100] T. Muir, *The Theory of Determinants* (Macmillan, 1906).